Lincoln University
Te Whare Wānaka o Aoraki
CHRISTCHURCH•NEW ZEALAND

Lincoln University Digital Thesis

Copyright Statement

The digital copy of this thesis is protected by the Copyright Act 1994 (New Zealand).

This thesis may be consulted by you, provided you comply with the provisions of the Act and the following conditions of use:

- you will use the copy only for the purposes of research or private study
- you will recognise the author's right to be identified as the author of the thesis and due acknowledgement will be made to the author where appropriate
- you will obtain the author's permission before publishing any material from the thesis.

Modelling Bistable Systems: A New Model for Meiosis Initiation in *Saccharomyces cerevisiae* and an Investigation of the Bistable Switch of Meiotic-mitotic Initiation

---

A thesis
submitted in partial fulfilment
of the requirements for the Degree of
Doctor of Philosophy
in Computational Systems Biology

at
Lincoln University
by
Champi Thusangi Wannige

Lincoln University
2014

Abstract of a thesis submitted in partial fulfilment of the requirements for the Degree of Doctor of Philosophy.

Modelling Bistable Systems : A New Model for Meiosis Initiation in *Saccharomyces cerevisiae* and an Investigation of the Bistable Switch of Meiotic-mitotic Initiation

by

Champi Thusangi Wannige

Living cells process diverse information received from the environment and make important decisions to undergo cellular processes such as differentiation, cell growth, division and apoptosis. The complex information processing in cells is carried out by a network of biochemical switches and oscillators similar to those seen in complex electrical circuits. The main objective of systems biology is to acquire a thorough understanding of how the functions and behaviour emerge from the complex networks of interactions and components in biological systems. In this thesis, using the systems biology approaches of mathematical modelling, dynamical system analysis and computational simulations, we investigate one example of a gene regulatory system that exhibits bistable switching behaviour to gain deeper insight into its dynamic aspects.

In the first section of this thesis, we develop a mathematical model for meiosis initiation of the budding yeast, *Saccharomyces cerevisiae*, incorporating the main mitosis initiator and its relationships to the meiosis initiation network. Using this mathematical model, we study meiosis and mitosis initiation dynamics under different extra-cellular nutrient levels. Our ultimate goal is to explore the experimentally-observed initial stage meiotic-mitotic switching behaviour in budding yeast under different nutrient conditions, which has not yet been explained at a gene expression level. We extend an available Boolean model of meiosis initiation, which is more biologically sound with stronger experimental validity than other models, and include all recent findings. We develop the model in an ODE framework that enables us to perform phase plane and bifurcation analyses to obtain deeper insights into the behaviour of the system. Our model accurately and qualitatively predicts the experimentally-

revealed temporal variations in the related proteins under different nutrient conditions as well as diverse mutant studies related to meiosis and mitosis initiation. Further, the model explains the organism-level experimental outputs of mutation studies at the gene expression level. Using model simulations, we clarify the reasoning behind the conflicting experimental observations from two mutation studies carried out using different procedures.

Experimental evidence shows that budding yeast cells can choose between meiosis and mitosis initiation alternatively depending on the available nutrient conditions at the early stage of these two cell division initiation processes. In the second section of this thesis, we use the constructed model to understand this initial phase meiotic-mitotic switching seen in budding yeast cells. In this section, we use dynamical system analysis tools such as phase space analysis, nullcline analysis and bifurcation analysis to explore the model's dynamics under varying nutrient conditions. Using these approaches, we show how meiosis and mitosis initiators form an all-or-none type of bistable switch in response to the available nutrient levels (mainly nitrogen). The transitions to and from the meiosis or mitosis states occur via saddle node bifurcations. This reversible switch helps the optimum usage of available nutrients and explains the mutually exclusive existence of the meiosis and mitosis pathways. Similarly as seen in experiments, temporal analysis of the switch shows that budding yeast cells can transit to mitosis from meiosis initiation throughout all the initial hours of meiosis initiation.

Cellular systems behave robustly against external and internal perturbations. In the third section of this thesis, we investigate the robustness and probable effects on the meiotic-mitotic switch by perturbation of the parameters in the meiosis network. To identify the most sensitive set of parameters, we employ both local and global sensitivity analyses. Based on the global sensitivity analysis results, we find a common group of parameters sensitive in all the main states of the switch. After formulating a mathematical definition for robustness, we perturb this common sensitive group of parameters and study the robustness of meiosis and mitosis initiation against the perturbations at the gene expression level. To examine the effects on the meiotic-mitotic switch by perturbations of the parameters, we perturb the common parameter group and create parameter sets using Latin hypercube sampling. Using these sample parameter sets, we investigate the effects of the most sensitive parameters on the transition from meiosis to mitosis when the nutrient level is varied from a low value to a high value. The robustness analysis carried out at the gene expression level identifies that the state corresponding to the transitions between meiosis and mitosis is less robust against perturbations than the other states. We observe three different types of switches when the

sensitive parameters are perturbed. We categorise them as normal bistable, memory-less and abnormal switches. The robustness of these switches is implied from the observation that the main function of the transition from meiosis to mitosis initiation, when nutrients are increased, is maintained despite perturbation of the most sensitive parameters in all three switch types.

Keywords: *Saccharomyces cerevisiae*, budding yeast, meiosis initiation, mitosis initiation, systems biology, mathematical modelling, ordinary differential equations, parameter estimation, nullcline analysis, phase space analysis, bifurcation analysis, bistable switch, local and global sensitivity analysis, robustness.

Publications and Presentations

Refereed Journal Papers

Wannige C.T., Kulasiri, D. and Samarasinghe, S. 2014. *A nutrient dependent switch explains mutually exclusive existence of meiosis and mitosis initiation in budding yeast*. Journal of Theoretical Biology, 314: 88-101

Wannige C.T., Kulasiri, D. and Samarasinghe, S. *Regulation of meiosis initiation before the commitment point in budding yeast: biology, molecular mechanisms and related mathematical models.* Current Bioinformatics *(Submitted)*

Wannige C.T., Kulasiri, D. and Samarasinghe, S. *The meiotic-mitotic initiation switch in budding yeast maintains its function robustly against sensitive parameter perturbations. (Submitted)*

Book Chapters

Wannige, C. T., Kulasiri, D. and Samarasinghe, S. 2013. *Modelling Stochasticity in Multi-stable and Oscillatory Biological Networks far from Equilibrium*, IN: Network Biology: Theories, Methods and Applications, Nova Science Publishers, New York (Editor: Prof. W.J. Zhang) 163-193 pages.

Conference Presentations

Wannige, C. T., Kulasiri, D. (2013). *Bistability in Cellular Biochemical Systems*, BIT's 4th Annual World DNA and Genome Day-2013, Jinling Convention Centre, Nanjing, China; 054.

Wannige, C. T., Kulasiri, D. (2013). *Bistable Switching in Cellular Decisioning*, Lincoln University Postgraduate Conference-2013, Lincoln University, Canterbury, New Zealand.

Wannige, C. T., Kulasiri, D. (2012). *Modelling Nutritional Dependence of Budding Yeast Cell Division Initiation*, Lincoln University Postgraduate Conference-2012, Lincoln University, Canterbury, New Zealand; 019.

Acknowledgements

First and foremost, I would like to express my sincere gratitude to my principal supervisor, Professor Don Kulasiri, for introducing me to the field of systems biology and providing me with constant inspiration and guidance throughout my PhD journey. His mentoring not only made me an independent researcher but also broadened my view of life.

My special thanks are for my associate supervisor, Professor Sandhya Samarasinghe, for her interesting questions and enthusiastic discussions. These discussions helped me to acquire a detailed level understanding of the fundamental concepts.

Members of the Centre for Advanced Computational Solutions (C-fACS) helped immensely during my PhD studies. My special thanks are for my friends, Jingyi Liang and Yao He, for the stimulating discussions and suggestions at hard times. Their company helped me to go through stressful times. I thank my fellow group members, Yao He, Jingyi Liang, Ranganaathan Jeevabarathie, Dr. Zhou Zhongkun and Dr. Mao Longfei for helpful questions at Wednesday group meetings and especially for the long days we worked together and for all the fun we had together. I have been fortunate to have worked with you all.

I also would like to thank Catriona Cameran for kindly helping me to improve my English writing abilities. Her workshops improved my writing ability significantly.

Finally, I would never have completed the PhD without the encouragement and financial support from my husband and our parents. I am most grateful to my husband, our parents and our sister and brother for their personal support and great patience at all times. This thesis is dedicated to them.

Champi Thusangi Wannige

Lincoln, Canterbury.

2014

Table of Contents

List of Tables

List of Figures

Chapter 1

Introduction to Systems Biology and the Motivation for the Study

"Systems biology is about putting together rather than taking apart, integration rather than reduction. It requires that we develop ways of thinking about integration that are as rigorous as our reductionist programs, but different. It means changing our philosophy, in the full sense of the term" (Noble, 2008).

This chapter starts with an introduction to systems biology and a brief description of its origin, purposes and challenges. We then introduce the field of modelling bistable systems on which this thesis is based. We also introduce the meiotic-mitotic bistable switch, the subject of this study. Further, we provide a detailed discussion about the research questions and the motivations underlying the work in this thesis. At the end of the chapter, an overview of all the chapters comprising this thesis is presented.

1.1 Systems Biology

The ultimate goal of studies of biological systems is to gain a detailed level understanding about how biosystems function even with external and internal perturbations (Kitano, 2001). Modern experimental techniques provide a huge amount of information about the components and their interactions in molecular networks, but fail to provide an understanding of how biological systems work as a whole. Systems biology faces this major challenge by combining experimental information from various sources to understand the functions of biological networks (Boogerd et al., 2007).

Systems biology is defined as an interdisciplinary field of study that aims to understand how the functional properties and behaviour of living systems are brought about by the interactions of their components (Alberghina and Westerhoff, 2007). Using detailed experimental data, systems biology follows a holistic approach and carries out mathematical modelling and computational analysis to understand the underlying principles of biological systems. Accordingly, systems biology uses models to describe the functionalities of biological networks and generalises over various networks in organisms and defines new theories to describe the emerging properties of biological systems (Klipp et al., 2008).

Attempts to gain a systems level understanding of biological systems date back to the 1940s and started with the biological cybernetics proposed by Norbert Wiener (Wiener, 1948). Wiener defined the term cybernetics as the study of control and communication in animals and machines. Since then, many attempts have been made to describe and understand biological systems. Most notably, in 1952, A. L. Hodgkin and A. X. Huxley constructed a mathematical model to explain action potential propagation through the axon of a neuron (Hodgkin and Huxley, 1952). Hodgkin and Huxley received The Nobel Prize for Physiology or Medicine for this work. However, these earlier attempts to describe and analyse biological systems were only at the physiological level because of the lack of knowledge and information about molecular biology. After molecular biology became a data rich field, systems biology today distinguishes itself from previous attempts by connecting a system level theoretical understanding with molecular level knowledge (Palsson, 2006).

There are three major aspects that need to be addressed in systems biology studies (Klipp et al., 2008): (1) Applying experimental high-throughput and whole genome techniques to acquire information about system components, their relationships and system performance;

(2) Understanding network structures and interactions among components using experimental data; (3) Integrating mathematical modelling and computational analysis with experimental data. The work presented in this thesis focuses mainly on the second and third aspects and investigates how the functions of biosystems are brought about by the interacting components of a network using mathematical modelling and analysis.

Mathematical modelling plays a central role in systems biology. Models are used to validate the available knowledge by comparing experimental data with *in-silico* outputs. When differences are found they can be used to expand and revise the model. Models can be iteratively refined, so the model becomes a tool to identify and distinguish the essential characteristics from the non-essential relationships. A well formulated mathematical model would possess a strong predictive capability, which would avoid the high expense required for laboratory experiments and drug discovery studies. Models can even be used to probe system behaviour in ways that would be not possible in a laboratory environment (Gunawardena, 2010; Kitano, 2001). As an example, mathematical modelling and analysis is frequently used to explain complex network behaviour, such as switches and oscillators, in biosystems (Leloup and Goldbeter, 1998; Tóth et al., 2007). This thesis focuses on understanding the decision making process of a biochemical switch using mathematical modelling.

1.2 Modelling Switches in Biosystems

The main purpose of biochemical switches is for decision making in cellular systems. These decisions are made according to the signals received from the extra cellular environment or from its own internal cellular state. Switches convert these graded input signals into all or nothing threshold level outputs. Biochemical switches are the central control units which make the entry decisions into many pathways (Tyson et al., 2011; Yao et al., 2008). Good examples are the switch regulating the entry into apoptosis[1] and the cell division cycle (Figures 2 and 3 in Tyson et. al. (2011)). Switches are used in deciding to create one or several different phenotypes by activating regulatory proteins (Fraser and Kærn, 2009). An example is the switch which regulates the phenotypic choice between the vegetative and

[1] Apoptosis is the process of programmed cell death. In this process, activation of specific proteases and nucleases leads to death that is characterised by chromatin condensation, protein and DNA degradation, loss of the plasma membrane lipid asymmetry and the disintegration of the cell into membrane-bound fragments. Morgan, D., 2006. The Cell Cycle: Principles of Control (Primers in Biology Series).

competent states in *Bacillus subtilis* (Maamar and Dubnau, 2005). Further, switches also decide to progress or not, to some stages in cellular processes, such as at cell cycle checkpoints (Tuck et al., 2013).

Specifically, switches that regulate entry points into pathways, such as at apoptosis, the cell cycle and meiosis are extremely important for living organisms. Malfunction or disregulation of these switches cause complications leading to cancer. Wrong decisions allow defective or abnormal cells to malignantly proliferate, promoting the accumulation of mutated cells in organisms. Mutations usually happen in the genes that decode for proteins associated with the switches, which typically control entry points into pathways. As an example, the loss of Rb function by mutations in the Rb tumour suppressor gene, leads to the malfunction of the Rb/E2F bistable switch which regulates the restriction point[2] in the cell cycle that is identified as a contributor to many human cancers (Nevins, 2001). Therefore, it is extremely important to understand the main regulators, the underlying mechanisms, working conditions and the behaviour of biochemical switches in living organisms. The following issues make the understanding dynamics of biochemical switches difficult: (1) A large number of components (genes, proteins) work together to regulate the main proteins associated with a switch according to a stimulation signal; (2) These components are connected in many different ways to modulate the decision making according to stimulation; (3) A detailed understanding of the switching process requires higher dimensional dynamical systems analysis techniques than the experimentally-available temporal variations of proteins. Therefore, to gain a detailed understanding of biochemical switches, we require a systems biology approach, where mathematical modelling, computational approaches and the experimental literature are used in conjunction.

Systems level study of biochemical switching systems has a long history. The first theoretical biologists who modelled biological interactions as dynamical systems were Alfred Lotka (Lotka, 1924) and Vito Volterra (Volterra and Brelot, 1931). The Lotka - Volterra competition model described the competition between species with multiple steady states. This model consists of non-linear differential equations, which facilitate the application of dynamic systems analysis techniques. However, in the 1930s, the field of cell biology was only beginning and there were no examples of actual biochemical switches (Tyson et al.,

[2] The restriction point is the major regulatory transition at the entry into the cell cycle in G1 of the animal cell cycle. At this point cell becomes committed to the cell cycle, after which extracellular proliferation stimulants are no longer required.

2008). This situation changed with the recognition of the positive and negative feedback control of gene expression (Jacob and Monod, 1961; Umbarger, 1961) and with the discovery of bistability in *lac* operon induction (Novick and Weiner, 1957). After these discoveries, biochemists began to appreciate the importance of switches in molecular cell biology. Further, after 2000, the field of molecular systems biology blossomed and, recently many biochemical switches are being identified. As an example, it is now clearly identified that all the irreversible transitions of the cell cycle are controlled by underlying bistable switches of the main regulatory protein kinases (Verdugo et al., 2013).

This thesis involves the study of meiosis initiation and the initial phase meiotic-mitotic initiation switch[3] in budding yeast, *Saccharomyces cerevisiae*. Understanding meiosis initiation is important since fertility is closely related to meiosis initiation. Dysfunction of the mitotic-meiotic switch may lead to the abnormal proliferation of early germ cells leading to germ cell tumours (GCT); errors in the signalling involved in the meiotic-mitotic switch cause testicular cancer (Jørgensen et al., 2013); dysfunction of the meiotic-mitotic switch causes neoplastic (abnormal growth) conversion of primordial germ cells and the development of germ cell tumours (Adamah et al., 2005). Especially in men, meiotic and mitotic cell divisions are regulated to have a good balance between stem cells and the maturing sperms. If the meiotic-mitotic switch is biased to the meiosis initiation side, the meiotic stem cells would deplete or if it is biased to the mitotic side abnormal cell proliferation would initiate cancer (Kimble, 2011).

However, current understanding of gene expression in human and mammalian meiosis is rudimentary. This is mainly because information about mammalian meiotic gene expression is challenging to acquire because of the experimental intractability of mammalian gonads which create difficulties in obtaining pure germ cell samples when meiosis initiates in the ovary or testis (Li et al., 2010). And even the recently-available reproductive tissues contain both somatic and germ line cells that their microarray profiles record combine results from both somatic and germ line cells (Li et al., 2013). Eukaryotic, unicellular budding yeast cells are easily tractable and synchronously undergo meiosis or mitosis cell divisions according to the nutrients available. Therefore, budding yeast meiosis and mitosis initiation pathways are extensively researched. Budding yeast has also been used successfully as a key modelling organism to explain the switches at the transition points of the mitotic cell cycle (Chen et al.,

[3] Meiotic-mitotic switch: According to extra-cellular initiation signals, budding yeast diploid cells choose between meiotic or mitotic cell division by switching between mitosis and meiosis initiation.

2004; Verdugo et al., 2013). Recent research has characterised most of the meiotic genes in budding yeast, thus yeast serves as an eukaryotic model organism for much meiosis related research (Li et al., 2010; Lodish et al., 2013). Therefore, in this research, we use budding yeast as the model organism to study meiosis initiation and meiotic-mitotic switching.

1.3 Motivation for the Study

Studies in systems biology aim to understand the underlying principles which maintain the key functions of biosystems. The main emphasis of this thesis is to investigate a gene regulatory network which exhibits bistable switching behaviour to gain a detailed understanding in the dynamical features of the network. This study also helps in obtaining valuable insights into the behaviour of the system under diverse internal and external conditions.

This thesis starts with a background study about bistable switches and the mathematical methods used in analysing the gene regulatory networks that exhibit bistable behaviour. The details are presented Chapter 2. The background information provided in this chapter helps with the discussion of the content presented in the following chapters.

We start our journey with a detailed understanding about biology and the molecular mechanisms of our subject network of meiosis and mitosis initiation in budding yeast. Previous molecular cell biology research has mainly focussed on the tight regulation of the meiosis and mitosis initiation processes which occur only under suitable conditions (Kassir et al., 2003). Mathematical models of meiosis and mitosis initiation are being developed to identify the main regulatory mechanisms underlying the tight regulation of initiation processes (Chen et al., 2004; Rubinstein et al., 2007). In spite of this progress, much needs to be understood about meiosis and mitosis both from molecular cell biology research and systems biology studies. To better understand and predict the functionalities of the subject network, we acquire the essential information available by asking the following questions.

a) How do meiosis and mitosis cell divisions initiate and proceed in terms of cellular states and chromosomal states?

b) How does the complex network of regulatory proteins and cellular components control meiosis and mitosis initiation only under the correct conditions in budding yeast?

c) What are the existing models of meiosis and mitosis initiation used to study the underlying mechanisms of functions? Is there any requirement for a new model?

We address these questions by extensively reviewing the available experimental and modelling literature about meiosis and mitosis initiation. Answers to these questions are provided in detail in Chapter 3.

From a modelling literature review, we identify that the available models examine the meiosis initiation network structure, especially the feedback loops, under low nutrient conditions. To date, there are no available models which explore the initial meiotic-mitotic switching behaviour in budding yeast under different nutrient conditions. Therefore, in this study, we explore the initial stage meiotic-mitotic switching dynamics by extending a Boolean model (Rubinstein et al., 2007), which is more biologically sound with stronger experimental validity than the other models, including those of recent findings.

The first objective of this study is to mathematically represent the molecular mechanisms involved in meiosis and mitosis initiation to understand how the network behaves under different conditions to shed light on the typical dynamical behaviour of the network. Using our model, we also aim to understand the conflicting and unclear mutation studies that have been carried out using different experimental approaches, at the gene expression level.

This primary objective is accomplished by constructing a conceptual model and converting the relationships in it into a mathematical model of meiosis initiation, including the mitosis initiator and its relations, with the meiosis initiation network. During the process, we identify the following challenging questions.

(1) What biologically meaningful assumptions would allow us to present the information at a higher level of abstraction that would encapsulate the essential mechanisms of meiosis initiation?

(2) What approach is necessary to estimate the parameters of the mathematical model?

In addressing the above questions, we define a set of assumptions on which we construct a conceptual network of meiosis initiation together with its relations to the mitosis initiator. We then convert the relationships in the conceptual network into a mathematical model of

ordinary differential equations, which facilitates the dynamical analysis required for studying the switching dynamics. We use mass action kinetics to represent the reactions and Hill kinetics to represent the activations, inhibitions and phosphorylations. Since budding yeast is a well-researched organism, experimental parameter ranges for most of the parameters are available. We use these parameter ranges and fine-tune our parameters using the temporal variation of proteins and asking biologically meaningful questions from the model based on experimental mutant studies. The set of assumptions, conceptual model, differential equation set proposed and the parameter values are presented in Chapter 4. After the model is constructed, the following challenging questions are identified.

(3) Do the *in-silico* simulation outputs of the model qualitatively describe the experimental findings of meiosis initiation?

(4) What are the advantages and the limitations of the current model compared with the previous *in-silico* mathematical models?

We validate the results of our simulations with the available experimental gene deletion and mutation studies. After observing that the model results possess a very good agreement with the experimental data, we employ our model to understand the organism level results of mutation studies at the gene expression level. Further, we clarify some conflicting mutation studies by providing a gene expression level understanding of system behaviour under particular mutation conditions. We then carry out an *in-silico* comparison between the available models and highlight the advantages and limitations of the current model. Simulations results and the comparisons of models are provided in Chapter 5.

The second objective of this thesis is inspired by the experimental evidence that yeast cells which decide to initiate meiosis can return to mitosis initiation if the nutrients needed are re-provided. At each time point until the budding yeast cells reach to the commitment point, they can choose between these two alternative cell division pathways according to the nutrients available.

The second objective of this study is to investigate whether the model simulations can explain the meiotic-mitotic initiation switching of yeast cells according to the available nutrient conditions at the gene expression level. We further examine the temporal variation of the switch to understand the reversible switching process through all the early hours of meiosis initiation.

The second objective is addressed using the tools available in dynamical systems analysis. We employ phase space analysis, nullclines and bifurcation analysis to investigate the dynamics of the meiosis initiation network in various dimensions. We aim to understand the budding yeast meiotic-mitotic switch at the gene expression level, which would provide indications for understanding this switching process in higher eukaryotic organisms. We identified the following three challenging questions during the process:

(5) What are the proteins that would show switch like behaviour when the available nutrient level is altered?

(6) How does the switch behave depending on the available nutrient conditions?

Addressing the above questions, we employ phase space analysis and investigate the meiosis initiation dynamics of the main regulatory proteins. We use nullcline analysis to examine the steady state behaviour of the major proteins under different nutrient conditions and identify the proteins that show switch like behaviour (Cdk1/Cln3 and Ime2). Using bifurcation analysis, we investigate how the major regulatory proteins of the switch behave in different nutrient conditions.

(7) How does the switch behaviour between these proteins vary with time starting from the initiation of starvation?

To examine how the meiotic-mitotic switch varies with time, we carry out bifurcation analysis of the switch at different time points and discuss the switch behaviour in different time sections where the switch shows similar behaviour. The details of the work and the major findings in approaching the second objective are presented in Chapter 6. The model constructed and the research findings relating to the first and second objectives are published in a research article in the Journal of Theoretical Biology entitled "Nutrient dependant switch explains mutually exclusive existence of meiosis and mitosis initiation in budding yeast" (Wannige et al., 2014).

The third objective of this thesis is inspired by the typical observation that biochemical systems perform well even with perturbation of the parameters such as at a sudden temperature change. We aim to understand how the subject system would maintain its functionalities against perturbations in the parameters.

The third objective of this thesis involves an investigation of the robustness of meiosis and mitosis initiation against perturbations of the parameters. In particular, whether the meiotic-mitotic initiation switch maintains its transition function between the two pathway initiations against perturbations of the parameters and, further, to study the probable effects on the switch by the perturbations.

This objective is achieved by choosing the most influential parameters of the network, which helps to reduce the complexity associated with the high number of parameters. We aim to predict the effects on the meiotic-mitotic initial switching by perturbations of the sensitive parameters. During the process, we identify the following challenging questions:

(8) What are the parameters that have the most influence on protein expression output levels of the major meiosis and mitosis initiators at meiosis and mitosis initiation?

(9) How does the model investigate the robustness of meiosis and mitosis initiation against perturbations of the most sensitive parameters?

To address the above two questions, we use sensitivity analysis approaches (local and global) and identify the most influential parameters at the protein expression level of the main meiosis (Ime2) and mitosis (Cdk1/Cln3) initiators. We select a set of parameters common to both meiosis and mitosis initiation from the results of the sensitivity studies. We formulate a mathematical definition for biological robustness to study the robustness of the meiosis and mitosis initiation against the various levels of perturbations in the most influential parameters.

(10) How can we use the model to explore the robustness of the meiotic-mitotic switch to perturbation of the most sensitive parameters and to examine the effects on the meiotic-mitotic switch from these perturbations?

To investigate the robustness of the meiotic-mitotic switch, we perturb the most influential set of parameters and create a number of parameter sets and then use them to observe the effects on the switch from the perturbations. More specifically, we are interested in studying how the switch maintains the functionality of the transition to mitosis initiation from meiosis initiation against the perturbations of the most sensitive parameters in a biologically valid range.

1.4 Overview of the Chapters

This thesis comprises eight chapters. In the current chapter, we provide a brief introduction to systems biology, its origins, purposes and challenges. We also briefly introduce the field of mathematical modelling of bistable switches and the meiotic-mitotic bistable switch, the subject of this study. Further, we provide a detailed description of the research questions that led to the motivation for the work described in this thesis.

Chapter 2 provides the background biological and mathematical knowledge useful for the next chapters. We introduce bistable switches in biological systems and discuss the requirements and purposes of bistability. We present several examples of bistable switches in actual biological systems to discuss how these switches are designed for different purposes. We then introduce mathematical modelling of gene regulatory networks, kinetic laws and the techniques used in analysing dynamic systems which exhibit bistable behaviour.

Chapter 3 provides a detailed background of meiosis and mitosis initiation, the molecular components involved and the interactions between them. This chapter also includes a summary of previous efforts to use mathematical modelling for meiosis initiation and highlights the requirement for a new model in this study. In Chapter 4, we construct a conceptual model of budding yeast meiosis initiation including the mitosis initiator and its relation to the meiosis initiation network. This conceptual network depends on a set of assumptions which define the limitations in the usage of the model developed. At the end of this chapter, we convert the relationships in the conceptual model into a set of differential equations using reaction kinetic laws. We also present the set of parameters, their significance and value ranges, which are acquired from the experimental literature. In Chapter 5, we discuss how the constructed mathematical model can be used to understand meiosis initiation at the gene expression level. We compare the *in-silico* results with the experimental gene deletion and mutant analysis results to check whether the model can describe different experimental situations. Further, we employ the model to understand organism level observations at the gene expression level and use it to explain the conflicting observations of mutant analysis. At the end of the chapter, we compare our model results with previous models to check whether our model inherits the advantages, and overcomes the limitations of the previous models.

In Chapter 6, we use the tools of dynamical systems analysis to examine the bistable behaviour of the meiosis and mitosis initiation decision. Using nullcline and bifurcation analysis, we predict that a bistable switch exists between main meiosis (Ime2) and mitosis (Cdk1/Cln3) initiators, which would describe the early stage meiotic-mitotic initiation decision, depending on the available nutrient levels. We further investigate the temporal variation of this switch and provide a detailed level understanding about how the meiosis-decided cells would return back to mitosis initiation if nutrients are re-supplied in the early hours of meiosis.

In Chapter 7, we investigate the robustness of meiosis and mitosis initiation against perturbations in the most sensitive parameters. We use sensitivity analysis approaches to find the set of parameters that is most sensitive and perturb these parameters at different perturbation levels to investigate the robustness of meiosis, mitosis and transition stages. Results from the robustness analysis lead us to investigate the effects of parameter perturbations on the meiotic-mitotic switch. We finish this chapter with the observation that the meiotic-mitotic switch maintains its main function even with perturbations of the most sensitive parameters.

In the final chapter, we present an overall summary and implications, together with the contributions of this thesis and directions for future research.

Chapter 2

Background

"Like a digital computer, information processing within cells is carried out by a complex network of switches and oscillators, but instead of being fabricated from silicon transistors and quartz crystals, the cell's computer is an evolved network of interacting genes and proteins"(Tyson et al., 2008).

The necessary contextual information required for this study is presented in the following two chapters. This chapter is divided into two sections. In the first section, we provide an introduction to bistable switches. We discuss the fundamental bistable switching process using the simple example of cellular apoptosis. Then, using a set of example bistable switches from the literature, we discuss the characteristics and advantages of bistable systems. The second section of this chapter provides the mathematical background useful for modelling. After a brief introduction about modelling gene regulatory networks, we present the issues and challenges in modelling that hinder the construction and simulation of models. We then discuss mass action kinetics and applications of Hill kinetics using examples related to gene regulation and illustrate the use of kinetics in modelling cellular processes. Finally, we discuss how mathematical modelling is used to analyse bistable systems.

2.1 Biological Concepts

2.1.1 Biochemical switches and bistability

Biochemical switches can be memory-less or multi-stable with memory (Figure 2.1). A memory-less switch (Figure 2.1 A) is composed of two stable states and one of these states would be chosen depending on the input signal level. Memory-less switches are typically involved in processes which require reversible transitions between the two stable states and work as signal thresholding components (Wolf and Arkin, 2003). The mechanisms underlying memory-less switches include ultra-sensitivity (Huang and Ferrell, 1996), co-operative activation or inhibition (Arkin and Ross, 1994) and multi-input cascades (Goldbeter and Koshland, 1984). In biosystems, bistable switches are the most commonly found type of multi-stable switches. Bistable switches (Figure 2.1 B) serve mainly in developmental processes such as meiosis and mitosis cell cycles since they are capable of remembering the input stimulation and maintaining the output state even if the input is removed (Yao et al., 2008).

In the following sections, we present some background information about bistable systems since this thesis is based on a biological system that exhibits bistability. A bistable system consists of two stable states separated by an unstable steady state (Figure 2.1 B). Coexistence of two stable steady states under certain input conditions is the hallmark of a bistable system. Depending on initial signal conditions, bistable systems would stabilise at the most stable state or would switch between these stable steady states (Glansdorff and Prigogine, 1971; Vellela and Qian, 2009). If cellular apoptosis of mammals in response to UV radiation is considered as a simple example (Figure 2.2), the two stable states of the apoptosis switch would correspond to the ON and OFF states of the regulatory protein of apoptosis, BAX. The ON state of the BAX protein represents the decision of ‘dying’ and the OFF state represents the decision of ‘not dying / living’.

These ON and OFF states are mutually exclusive with very high (at ON) and very low (at OFF) levels of the BAX protein. The input stress signals are typically conveyed to the system by a protein kinase sensitive to input stimulation. The switch is only turned to the ON stage if the correct threshold signal level is approached. When the input stress level (UV radiation) is low, the apoptosis switch would be at the OFF state (Figure 2.2 A), deciding not to die. At high input stress levels (Figure 2.2 C) the apoptosis switch would be turned to the ON state,

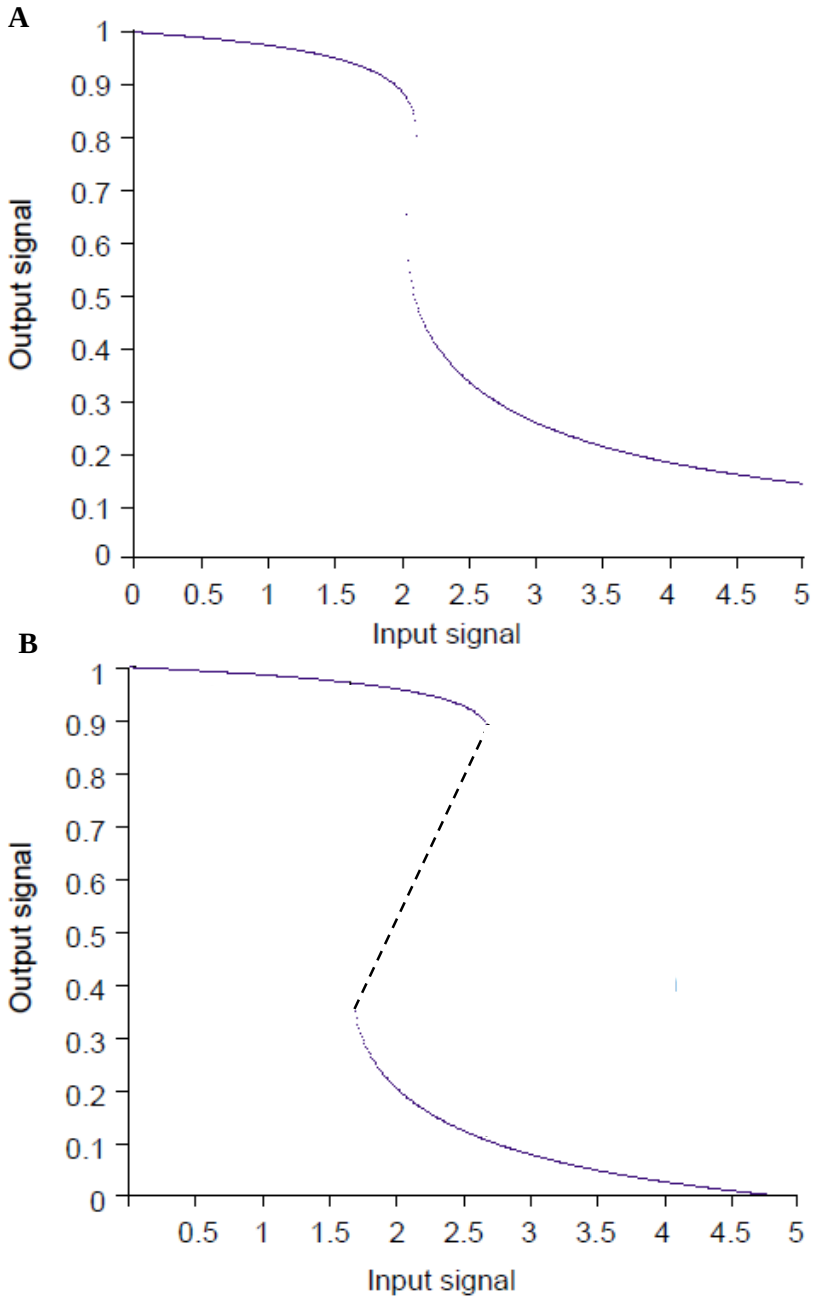

Figure 2.1 An example memory-less switch and a bistable switch. Both (A) memory-less switch and the (B) bistable switch have two stable states. Unstable state is marked with a dashed line. The main difference between bistable and memory-less switch is the overlapped region of the two stable states in the bistable switch, which does not appear in the memory-less switch (Edited and reprinted from (Wolf and Arkin, 2003) with permission from Elsevier).

deciding to die. At mid-stress levels (Figure 2.2 B), some cells would decide to die and some would decide not to die, depending on the initial stress conditions. At this mid-stage, the BAX protein concentration distribution in a set of cells consists of two peaks, one peak corresponds to the number of ON-decided cells and the other peak corresponds to OFF-decided cells. This bimodal distribution is a hallmark of bistability.

2.1.2 Requirements for bistability

In cellular systems, bistability behaviour is exhibited only when certain conditions are met. Three main requirements are essential for a molecular network to exhibit bistability (Ferrell, 2002). The first requirement is a feedback loop, such as a double negative feedback (X inhibits Y and Y inhibits X), positive feedback (X activates Y and Y activates X) or autocatalysis (X works as a catalyst for its own production) (Wolf and Arkin, 2003). However, feedback loops alone will not show bistability if they do not possess the following two features: (1) Bistable systems need some sort of non-linearity within its feedback circuit. Some enzymes in the circuit may respond to their regulators cooperatively by showing ultra-sensitivity to their regulators; and (2) A bistable system must have the two legs of the feedback loop properly balanced. Unbalanced feedback loops, where one of the feedback is stronger or weaker, may show mono-stability (Ferrell, 2002).

2.1.3 Main stages of a bistable switch

In this section, we use as an example, the switch between an activator and inhibitor protein with a double negative feedback loop to discuss the behaviour of the proteins in the main states of a bistable switch (Figure 2.3). The three main stages in this bistable switch are the ON state, the OFF state and the bistability state where the ON and OFF states coexist (Figure 2.3 B). Nullcline[4] analysis can be used to examine the behaviour of the proteins at each state (Fall et al., 2002; Murray, 2002).

The nullcline intersection point of two proteins shows the common steady states of those two proteins. When the nullcline intersection point of the activator and inhibitor protein at the ON state is studied (Figure 2.3 C), the activator protein level is very high and the inhibitor protein is very low, indicating the ON state of the activator protein. The opposite happens at the OFF state (Figure 2.3 E) where the inhibitor level is higher than the activator protein level. In the

[4] Nullcline of a variable is a curve along which the rate of change of the variable is zero.

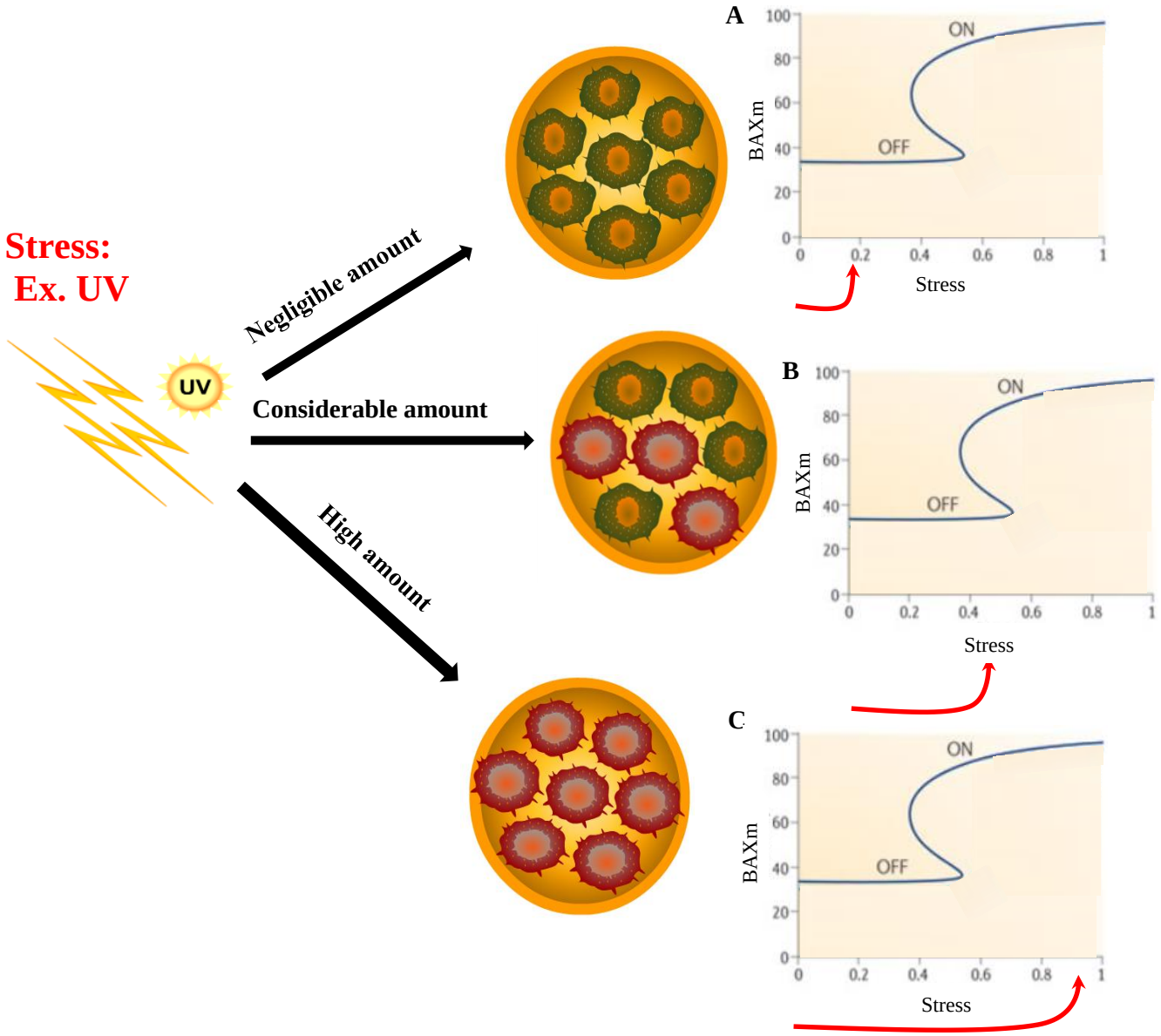

Figure 2.2 Bistable switch controlling apoptosis in mammalian cells. Apoptosis is triggered by activation of BAX proteins in the outer membrane of mitochondria in mammalian cells. The blue curve shows the steady-state concentration of total membrane-bound BAX (BAXm), as a function of stress. The red arrow indicates the corresponding stress level at three stress states: negligible, considerable and high. Red cells represent the cells decided to die and the green cells represent the normal cells. (A) When the stress level is low, the BAXm protein remains in low levels without activating apoptosis. (B) For intermediate levels of stress, the network has two stable steady states: an OFF state with a low level of BAXm and an ON state with a high level of BAXm. (C) High stress levels turn the apoptosis switch to ON state with a high level of BAXm (Tyson et al., 2011).

bistable state (Figure 2.3 D), nullcline analysis shows three solutions or intersection points: two stable solutions and one unstable solution. The two stable solutions correspond to the ON and OFF states. The system would never lie in the intermediate unstable state.

2.1.4 Hysteresis, memory and the irreversibility of a bistable switch

Hysteresis is a feature of a bistable system and is defined as the dependence of the output decision on the history of the stimulation (Murray, 2002). This dependence can be explained by the apoptosis example in Figure 2.2. Consider the following two situations: Situation 1 where the stress level increases from 0 to 0.5; Situation 2, where the stress level increases first from 0 to 0.7 and then suddenly decreases to 0.5. At the end of both situations, the final stress level is similar, at 0.5, but the history differs. In the first situation the cell would stay in the OFF state. In Situation 2, since the stress level first increased, the cell would jump to the ON state and when the stress level decreases, it would remain at the ON state because of the overlapped region of the ON and OFF states. Although the stress levels are similar at the end of Situations 1 and 2, the cell decision differs depending on the history of the stimulation. The strength of the hysteresis depends on the width of the overlapped region of the two stable steady states. Hysteresis is beneficial to systems in avoiding unwanted rapid switching.

The strength of the hysteresis also explains the memory and irreversibility of a bistable switch (Walhout et al., 2012). When the overlapped region of the two steady states decreases, the switch possesses less memory and becomes reversible. Irreversible switches possess high memory and do not have an initial OFF only state, instead they have a long overlapped region of the two steady states; if the threshold stimulation level is increased, the cell would jump to the ON state and the decision would remain at the ON state although the stimulation is removed (Verdugo et al., 2013).

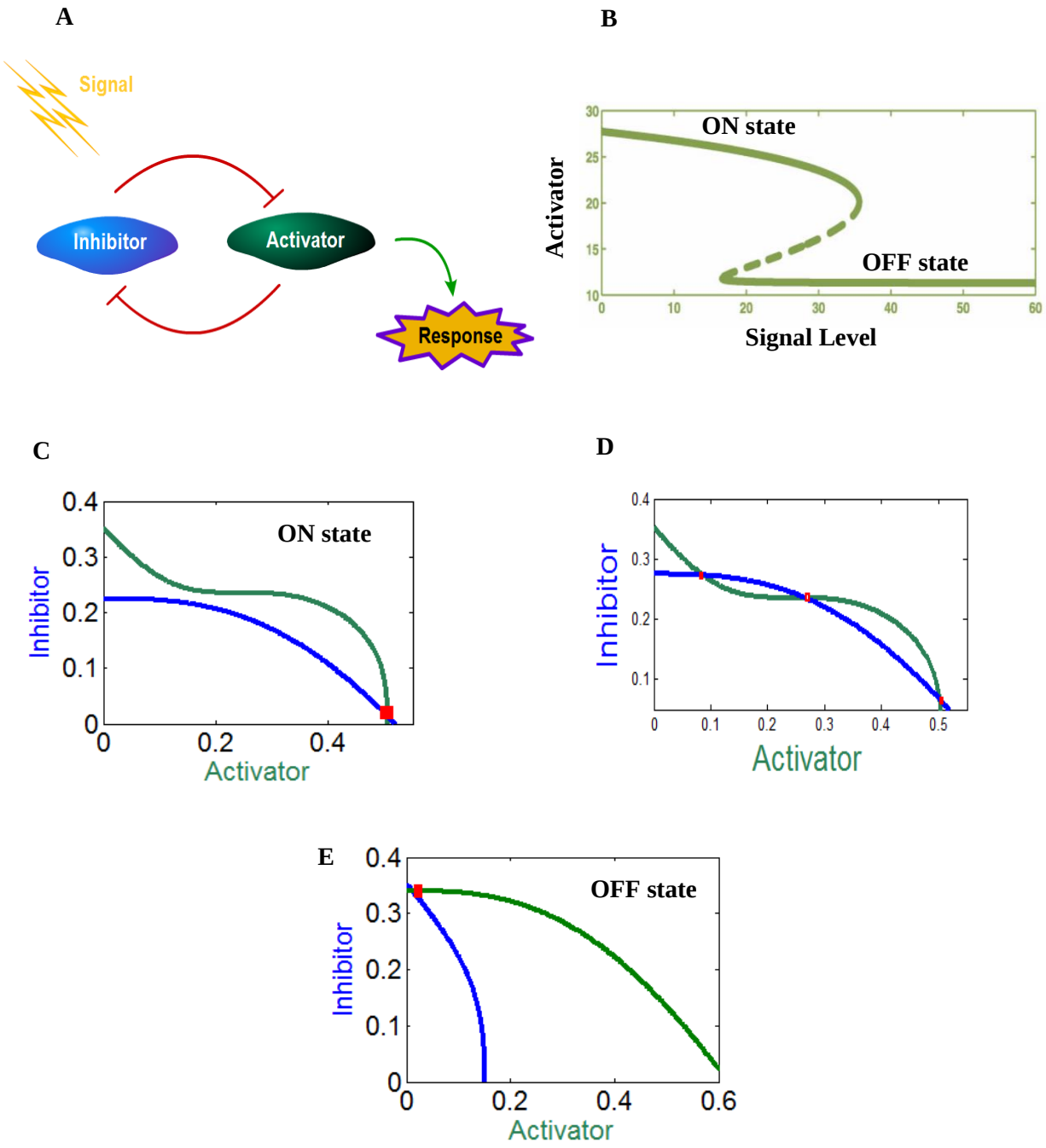

Figure 2.3 A bistable system and its main states. (A) A typical activator inhibitor model of a bistable switch. Double negative feedback loops between activator and inhibitor proteins alter the levels of activator and inhibitor levels. (B) Steady state concentration of the activator protein as a function of signal level. (C) Nullcline plot at the ON state. (D) Nullcline plot at the intermediate state where the ON and OFF states coexist. (E) Nullcline plot at the OFF state.

2.1.5 Bistable systems: advantages and examples

Bistability is a main survival mechanism for many organisms under adverse conditions. One example is the persistence mechanism of the soil bacterium, *Bacillus subtilis*, in harsh nutritional conditions. *Bacillus subtilis* can stay in two phenotypic forms depending on the environmental nutritional conditions (Maamar et al., 2007; Mettetal and van Oudenaarden, 2007). These two phenotypes are called 'vegetative' and 'competent'. When nutrients are deprived, vegetative cells switch to the competent state where cells can uptake DNA and survive. The regulatory protein, ComK's expression pattern is opposite in these two types. The ComK protein expression is at maximum in competent cells and at minimum in vegetative cells. Only cells that express the ComK protein more than at a threshold level can become competent (Figure 1 of Mettetal et. al. (2007) (Mettetal and van Oudenaarden, 2007)). The ComK steady state protein levels comprise a bistable switch with varying regulatory signal level. The ComK protein expression level can be increased either by a regulatory signal or gene expression noise (Figure 2.4 B, E and C, F). The ComK protein circuit (Figure 2.4 D) possesses all the requirements to exhibit bistability including an auto-positive feedback loop which activates ComK expression by itself. In switching between stable states of the ComK bistable switch (Figure 2. 4) and creating either of these phenotypes, *B. subtilis* tries to face the challenges and survive the environmental changes.

Bistable switches regulate the major decision making processes in cellular systems. Bistable switches are employed to decide the progression, or not, into some cellular processes, such as at cell cycle check points. All the mammalian cell cycle checkpoints identified are controlled by bistable switches (Verdugo et al., 2013). For example, we will consider the Rb-E2F switch which underlies the mammalian restriction point[5] (Swat et al., 2004; Yao et al., 2008; Yao et al., 2011). Mammalian cells commit to proliferation or quiescence at the restriction point. Functioning as a bistable switch, Rb-E2F converts graded serum inputs into switch-like E2F responses. The higher E2F levels activate the proteins required for the entire process involved in the activation of DNA replication and regulation of the G1/S transition of the mammalian cell cycle (Nevins, 2001). The Rb-E2F pathway is a complex signalling network (Novak and Tyson, 2004). However, this pathway involves several positive feedback loops which are essential requirements for exhibiting bistability. Together with a simplified ordinary differential equation model and single cell

[5] Restriction point is in the G1 phase of the mammalian cell cycle and at this point, the cell decides whether to become committed to the cell cycle, after which the extracellular proliferation stimulants are no longer required.

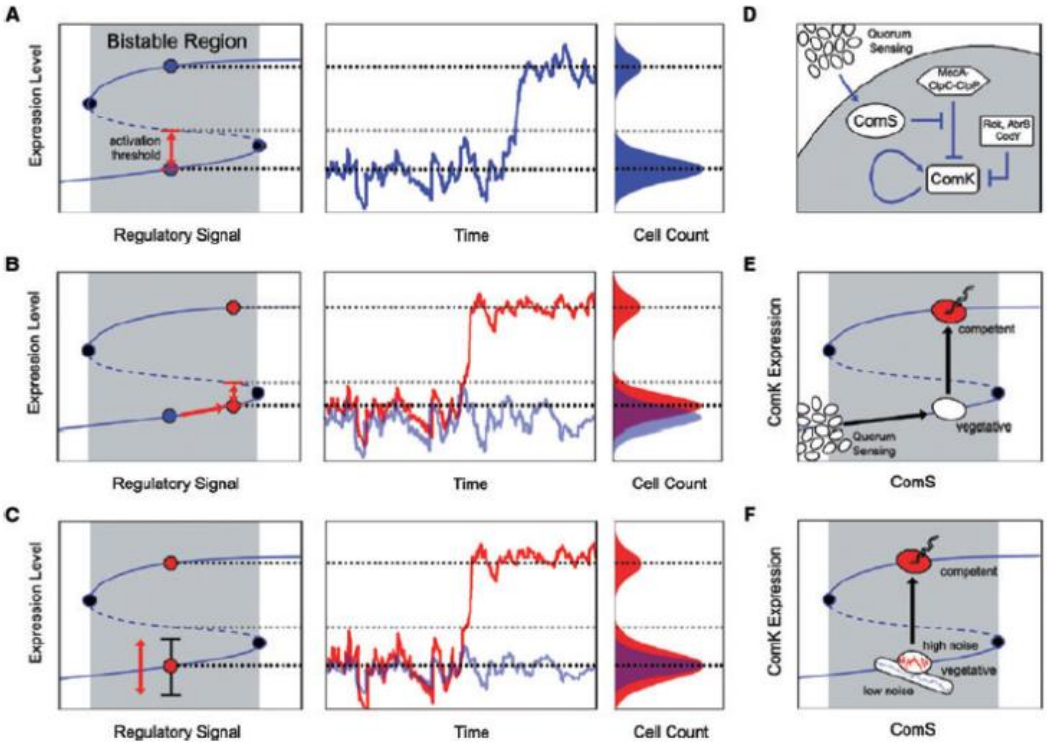

Figure 2.4 Regulation of competence in *B.subtilis*. (A) Steady state diagram, time series plot and population diagram of the ComK expression levels, (B) Response to the increase of the regulatory signal, (C) Response to the increase of the gene expression noise. (D) Competence network of *B.subtilis*. (E) Threshold modulation by quorum sensing. (F) Noise modulation in the development of competence (Adopted from Fraser et. al. (2009) (Fraser and Kærn, 2009), © 2009 The Authors. Journal compilation © 2009 Blackwell Publishing Ltd).

measurements, Yao et. al. show that bistable E2F activation behaviour correlates directly with the ability of a cell to traverse the restriction point, or not, depending on the duration and the concentrations of the serum stimulation (Yao et al., 2011).

Another example of decision making switch controls the frog (*Xenopus*) oocyte's decision for maturation (Ferrell Jr and Machleder, 1998). The oocyte maturation decision is an all or none decision to mature or not (Ferrell, 2002). Frog oocytes are induced to mature by a hormone named progesterone when they complete the first meiotic division and arrest in the metaphase of the second meiosis stage. The *Xenopus* p42 MAPK (Mos-mitogen-activated protein kinase) cascade shown in Figure 2.5 is responsible for this maturation decision (Ferrell, 2002; Ferrell Jr and Machleder, 1998). An oocyte decides to mature when the p42-MAPK level is at a maximum and decides not to mature when the MAPK is at its minimum value. This protein cascade needs to convert a graded triggering stimulus, which is the progesterone input, into a switch like irreversible output of p42 MAPK. This cascade possesses all the requirements for bistability including a positive feedback loop, ultra-sensitivity to dual phosphorylation (Figure 2.5 A) and a balance between the legs of the feedback loop (Ferrell, 2002).

Experimentally, individual oocytes have shown that the decision to mature, or not, by the all or nothing type behaviour of p42 MAPK activity (Figure 2.5 B) (Ferrell Jr and Machleder, 1998). The first row of Figure 2.5 B shows that all the cells decided to mature at high progesterone levels. The second row shows the intermediate state where both maturation-decided and not-decided cells coexist. This bimodal distribution at the intermediate progesterone levels is a hallmark of bistability. The third row shows that all cells have decided not to mature under low progesterone levels. Experiments show that matured oocytes cannot be de-matured by removing the progesterone signal because of the irreversible behaviour of this bistable switch (Ferrell Jr and Machleder, 1998).

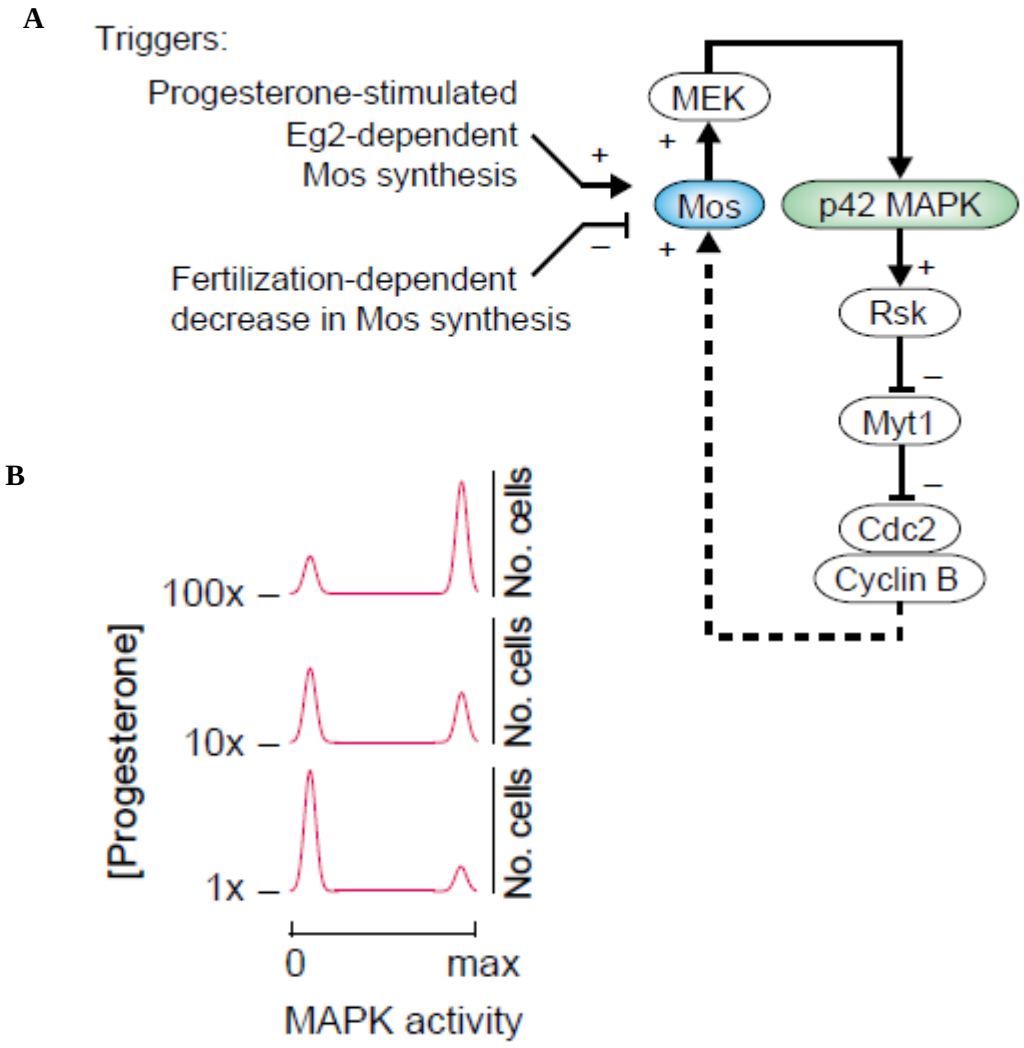

Figure 2.5 Frog (*Xenopus*) oocyte's decision for maturation. (A) The wiring diagram of the *Xenopus* p42 MAPK cascade responsible for oocyte maturation. P42 MAPK is activated by the phosphorylation of MEK, which is activated by the phosphorylation of Mos. P42 MAPK activation stimulates Mos accumulation. The dashed line represents uncertain feedback loops; the line with arrow represents activation; and lines with flat head represent repression. (B) The experimental responses of individual oocytes to progesterone. The responses show all or none type behaviour of the MAPK activity which implies the decision for oocyte maturation. Reprinted from Ferrell et. al. (2002) (Ferrell, 2002; Ferrell Jr and Machleder, 1998), with permission from Elsevier.

2.2 Mathematical Concepts

2.2.1 Mathematical modelling of gene regulatory networks

As mentioned in Chapter 1, mathematical modelling is essentially helpful in understanding the underlying principles of the functions in cellular systems. Four steps are generally followed in modelling cellular genetic networks (Kitano, 2001; Palsson, 2011): (1) network sketch; (2) model design; (3) parameter estimation; and, (4) model validation. Sketching the network of interest is the most important step where all the participating components such as genes, mRNAs and proteins and relationships between them are identified and collected. This needs a good understanding about the biological network of interest and its behaviour in different situations. According to the objectives, the level of detail would vary, but the sketch needs to include all the necessary information required to describe the behaviour of the network of interest. A good sketch resembles a good plan for a building. Most of the biology-related assumptions of the model are identified at this stage. According to our experience, this stage is the most time consuming and errors or neglecting important information at this stage would cause the model to be less reliable and may require more revisions.

The next step, once we have a good sketch, is designing the model. In the model designing phase, a mathematical model is formulated by choosing appropriate modelling methods and kinetics. The main modelling frameworks available and kinetic rate laws are introduced in Sections 2.2.1.2 and 2.2.1.3, respectively. Choosing appropriate methods would depend mainly on the size of the system, the number of participating components, the scale of the temporal behaviour, assumptions and level of details available. Details about the challenges which need to be addressed at this step are given in Section 2.2.1.1. The assumptions made at this stage to address the challenges define the boundaries of the model usage.

After a good representation of the mathematical model is developed, the next step is parameter estimation. Estimation of parameters in a biologically feasible range is difficult in some models because of the unavailability of numerical experimental data values for the parameters. Many methods are proposed in the literature to find parameters in situations where no information is available (Mallavarapu et al., 2009; Xie et al., 2010). For most model organisms, the experimental literature provides ranges in which the parameter values may vary. These parameter ranges are very useful in parameter estimation for developing a real time model that predicts the available experimental data. Using the available experimental

dynamics as the target output, exact parameter values can be estimated within the selected parameter ranges. Software like Copasi (Hoops et al., 2006) uses algorithms such as least square fitting and genetic algorithms for parameter estimation.

Once the parameter values are estimated, model validation is carried out to check whether the model can faithfully predict the desired output under different situations. Gene mutation studies and gene deletion studies can be used for model validation. After these four steps, the model can be used to examine the features of a system, such as bistability.

2.2.1.1 Challenges in mathematical modelling

Modelling is challenging because of some of the features in natural biological systems, such as the existence of multiple temporal and spatial scales, nonlinearity and complexity. Small systems behave very differently from large systems because of some of the system's governing characteristics such as noise.

Systems with a large number of molecules are on a macroscopic scale and, we assume that the system is homogeneous so that we can concentrate on the average particle behaviour rather than individual particles. Changes in the states of a macroscopic system are continuous because we consider the concentrations of the particles participating in the chemical reactions. Conversely, major interest is on the individual particle behaviour in microscopic systems that have a small number of molecules. The dynamics of microscopic systems are governed by stochasticity since the small number of molecules involved. Meososcopic-scaled systems lie between the microscopic and macroscopic scales. The solution of a meososcopic system is assumed to be well mixed, but since the individual particles are considered, the system is stochastic with discrete state changes.

Similar to the behaviour in the aforementioned volume scales, systems show different behaviour in different temporal scales; some biological systems show transient responses while others show steady state behaviour. Computational complexity appears as a result of many components working together with nonlinear, complex relations in biochemical systems. Modelling frameworks need to be selected according to the subject system features.

2.2.1.2 Mathematical modelling frameworks

Boolean networks and differential equation models are the most common types of deterministic modelling frameworks used for macroscopic system analysis. Boolean networks

are based on Boolean logic and do not require exact numeric values for concentrations, expression levels and timings (Walhout et al., 2012). They can be used to examine the qualitative behaviour of a system. Ordinary differential equations, which model the network as a set of coupled chemical reactions, consider the concentrations of molecules as states of a system. These models can be used to look at the detailed, quantitative dynamics of the systems; however, parameter estimation is required using experimental data. Sensitivity analysis and model validations using available gene mutation and gene deletion information would guarantee the accuracy of the parameter values used.

Cellular dynamics are inherently noisy in a small cellular volume especially when the number of molecules involved is low. Deterministic models do not capture the noise effects as they do not consider the uncertainties associated with the parameters (Kulasiri et al., 2008; Rubinstein et al., 2007). Models often ignore the thermodynamic effects, assuming that thermodynamic variables such as temperature and pressure are constant. Cells are open systems that exchange material and energy. Once perturbed, fluctuations drive these open biological systems to self-organised, dissipative structures far from thermodynamic equilibrium, such as fractals and chaos. Therefore, stochastic and thermodynamic theories are equally important in mathematical modelling of biological systems. Stochastic methods need to be followed when low molecular numbers are involved and thermodynamic theories help with understanding the far from thermodynamic equilibrium complex behaviour. Some popular stochastic and thermodynamic theories and methods are presented in Appendix A for the interested reader.

2.2.1.3 Kinetic rate laws

Kinetic rate laws, such as the law of mass action, Michaelis-Menten kinetics, and Hill kinetics are employed to describe the reactions in biological systems (Alon, 2007; Voet et al., 2006). The rate of a reaction can be written as a function of the concentrations of all participating species.

Among the other kinetic laws, the mass action kinetic rate law is the most basic and widely used law, which is valid only for elementary chemical reactions. Michaelis-Menten kinetics are valid for basic enzyme reactions, where substrates are converted to products in the presence of a catalyst. This kinetic law presents the rate of enzymatic reactions in terms of reaction rate and concentration of substrates.

Empirically based Hill kinetics are used to describe ligand receptor interactions and the cooperativity between ligands. Hill kinetics present a relationship for the receptors saturated by ligands as a function of ligand concentrations. Hill functions are frequently used to describe the binding of transcription factor proteins to the promoter region of DNA in inhibition and activation (Angeli et al., 2004) and in modelling phosphorylations (Dushek et al., 2011; Zi et al., 2010), assuming these processes are ligand receptor binding and unbinding reactions.

We present the mass action kinetic rate law in detail and discuss some applications of Hill kinetics since we use these two types of kinetics to describe the reactions in our model. A detailed description of Michaelis-Menten and Hill-type kinetics can be found in (Voet et al., 2006).

Mass action kinetics

The mass action rate law is used to describe the kinetics of elementary reactions that have no reaction intermediates (Palsson, 2011; Voet et al., 2006). Therefore, in an elementary reaction, the participating species advance to the results in a single reaction step with no intermediate products. Let us consider the following elementary monomolecular reaction as an example.

$$A \rightarrow B \qquad (2-1)$$

The mass action kinetic law states that the instantaneous reaction rate of an elementary reaction in a homogeneous medium is proportional to the product of the concentrations of the participating species. According to this law, the rate of the reaction (Equation (2-1)) 'R' can be written in the following form with the concentration of the reactant 'A' and a proportionality constant 'K' called the rate constant.

$$R = KA \qquad (2-2)$$

Using this law, the rate of change of A can be written as the product of the reaction rate and the stoichiometry coefficient of A. Therefore, the rate of change of A can be written as follows.

$$\frac{dA}{dt} = -R = -KA \qquad (2-3)$$

To illustrate the use of mass action kinetics in gene regulation modelling, we consider cellular protein production as an example. We do not present the basic introductory cellular biology related to gene expression in this section, instead, the interested reader is directed to Appendix B and the references cited in that appendix. Proteins are produced by a detailed residue by residue transformation of sequential information in DNA to mRNA to protein. This complex process is simplified here with assumptions. We do not consider the transcription factor involvement in gene regulation. Considering gene transcription, protein translation, mRNA and protein degradation, protein production can be represented by the following set of reaction equations (Equations (2-4) to (2-7)).

$$g \overset{f_m}{\Rightarrow} m + g \qquad (2-4)$$

$$m \overset{d_m}{\Rightarrow} \therefore \qquad (2-5)$$

$$m \overset{f_p}{\Rightarrow} p + m \qquad (2-6)$$

$$p \overset{d_p}{\Rightarrow} \therefore \qquad (2-7)$$

In these equations (Equation (2-4) to 7), 'g', 'm' and 'p' represent a gene, a mRNA and a protein. 'f_m' and 'f_p' are the mRNA transcription rate and protein translation rate, respectively. 'd_m' and 'd_p' are their degradation rates. Using mass action kinetics, rate changes of mRNA m and protein p production from a gene can be given in the following set of differential equations (Equation (2-8) and (2-9)) (Mehta et al., 2008).

$$\frac{dm}{dt} = f_m - d_m m \qquad (2-8)$$

$$\frac{dp}{dt} = f_p m - d_p p \qquad (2-9)$$

Since gene transcription is controlled by the repressors and activators, f_m is always a function of transcription factor concentrations. Equation (2-8) describes the change in the mean

number of mRNA transcription and degradation. Equation (2-9) describes the change in the number of proteins due to protein translation and degradation.

Applications of Hill kinetics

We illustrate the application of the Hill function in gene activation, repression and phosphorylation using simple examples. The derivation of the Hill function is not presented and the interested reader is referred to text books (Alon, 2007; Voet et al., 2006). The Hill function was first introduced to describe the binding of oxygen to haemoglobin by A. V. Hill (Hill, 1910). Since then, Hill kinetics is being used to model processes such as transcriptional activation and repression, assuming these processes are ligand receptor binding and unbinding processes.

When the rate of mRNA 'Y' production is activated by a protein 'X' the Hill function can be used to present the rate of 'Y' production in the following way:

$$R_Y = \frac{\beta X^n}{K^n + X^n} \qquad (2-10)$$

In Equation (2-10), 'β' represents the maximal expression level of 'Y'; 'K' represents the disassociation constant (which is the half maximal reactant concentration) of the activator from the promoter binding site and n represents the Hill coefficient. This equation models the expression of Y in an increasing sigmoidal shape, and we assume that the binding of the activator to the promoter region is enhanced if there are other transcription factors present at other binding sites on the promoter. This phenomenon is called cooperative binding and the Hill coefficient quantifies the degree of cooperativity. In situations where a high Hill coefficient is used to represent strong positive cooperativity, the Y curve modelled would reach its maximum more rapidly than in the situations where a low Hill coefficient is used.

When the mRNA 'Y' production is repressed by a repressor protein 'X' the Hill function can be used to represent the rate of Y production in the following way (2-11):

$$R_Y = \frac{\beta K^n}{K^n + X^n} \qquad (2-11)$$

Similar to Equation (2-10) in (2-11), 'β' represents the maximum expression level of 'Y'; 'K' represents the disassociation constant of the inhibitor from the promoter binding site and 'n' represents the Hill coefficient. The rate of Y production under the repression is modelled as a

decreasing sigmoidal function by this equation. The rapidity of the degradation depends on the cooperativity represented by the Hill coefficient.

Similar to gene activation (Equation (2-10)), phosphorylation has also been modelled using Hill functions, assuming the addition and the removal of the phosphate group as a ligand-receptor binding-unbinding reaction (Angeli et al., 2004; Dushek et al., 2011; Zi et al., 2010).

2.2.2 Analysing models with bistability

Bistability is an attribute of a system. Therefore, modelling the interested biological network accurately is important prior to examining the bistability feature. For discussions in this section, we consider a canonical example reaction system, the Schlogl model, which illustrates bistability with two steady state solutions (Schlögl, 1972). This chemical reaction system consists of three species (‘A’,’B’ and ‘X’) and four reaction channels.

$$A + 2X \underset{k_2}{\overset{k_1}{\leftrightarrow}} 3X \qquad (2-12)$$

$$B \underset{k_4}{\overset{k_3}{\leftrightarrow}} X \qquad (2-13)$$

The concentrations of A and B are fixed, and the system is open with the exchange of chemical materials (Cao et al., 2006). If the concentrations of A and B are equal, the system becomes to equilibrium. When the concentration of A and B are fixed, but different, the system shows two stable steady states as solutions for X (Cao et al., 2006; Vellela and Qian, 2009).

We can write a deterministic model equation for the rate change of X based on the laws of mass action (Wannige et al., 2013). Let the concentrations of A, B and X be represented by 'a', 'b' and 'x', respectively. The corresponding equation is a first order non-linear ordinary differential equation (Equation 3) (Sargsyan, 2005; Vellela and Qian, 2009).

$$\frac{dx}{dt} = k_1\, a\, x^2 - k_2 x^3 + k_3 b - k_4\, x \qquad (2-14)$$

When k_1= 2, k_2 =1, k_3=3, k_4=11, a=3, b=2 , Figure 2.6 B shows the deterministically predicted solutions from Equation (2-14) for different initial conditions.The system possesses

three steady states: X=1, X=2 and X=3. The rate change of X becomes zero at these three X values, which are marked with filled circles in Figure 2.6 A. The solution at X=2 is unstable. Therefore, the system settles on one of the two stable steady states (X=1 or X=3) which is the nearest steady state to the initial condition. This exemplifies a bistable system which has two solutions under similar conditions.

2.2.3 Dynamical systems analysis: phase space diagrams and bifurcation

Phase space analysis is a powerful tool in analysing dynamical systems (Fall et al., 2002; G et al., 2006; Murray, 2002; Strogatz, 2001). A phase plane diagram shows the trajectory of changing states in two variables along the time. The two axis of the phase plane diagram are the two state variables of interest, and the trajectory shows how the values of these two variables change over time. For example, if we consider X_1 and X_2 as variables which change with time, the phase plane diagram is the graph of X_1 versus X_2.The phase plane is a special two-dimensional case of the general n-dimensional phase space (Strogatz, 2001).

Nullcline analysis is frequently used to identify bistable behaviour. Nullclines are the curves on which the rate of change of the variable is zero (Fall et al., 2002; G et al., 2006). In the above example, the nullcline corresponds to the following equation, where the rate of change of X equals zero.

$$\frac{dx}{dt} = k_1\, a\, x^2 - k_2 x^3 + k_3 b - k_4\, x = 0 \qquad (2-15)$$

Nullcline shows the steady states of a system (Murray, 2002; Strogatz, 2001). Since Equation (2-15) is a single variable nullcline of the third degree, the nullcline is not a curve, but has only three points. These three points are indicated in Figure 2.6 A with filled circles. In two-dimensional variable space, the nullclines are curves and the intersection of the nullclines show steady states common to both variables (Figure 2.3). These steady states can be linearly stable or unstable. Small perturbations away from a stable steady state would return to the vicinity of the stable state. At unstable steady states, small perturbations away from the steady state are amplified and the trajectories move away from the unstable state. Bistable

systems are composed of three steady states, in which two are stable and one is unstable. The two stable states correspond to the main two stages of a bistable system and the unstable state separates these two stable states; for example, consider the two stable states in Figure 2.3 C and E which correspond to the ON and OFF stages of the switch, respectively. Figure 2.3 D shows the unstable steady state between these two stable steady states.

Bifurcation diagrams are used to examine how a system's long-term behaviour, such as steady state solutions or periodic orbits change with a selected parameter, which is generally called a bifurcation parameter (Murray, 2002; Strogatz, 2001; Verdugo et al., 2013). As an example, Figure 2.3 B shows how the steady states of an activator protein change with the signal level. In Figure 2.3 B, the number of steady states suddenly changes at the signal level of 17 and 37, from one stable state to three steady states and from three steady states to one, respectively. These two signal levels, where the qualitative behaviour of the system changes abruptly, are called the bifurcation points of the system. At both of these bifurcation points (at signal levels 17 and 37), the system looses or gains two steady states, therefore, these points are called saddle node bifurcation points with the meaning of "node" to a stable steady state and "saddle node" to a unstable steady state (Strogatz, 2001; Verdugo et al., 2013).

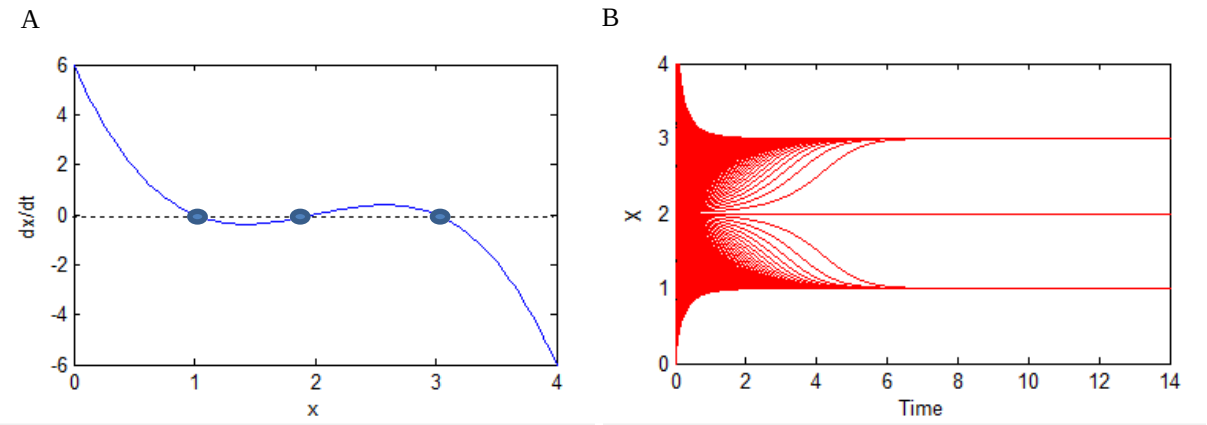

Figure 2.6 (A) Rate change of x against changing X values. The rate change becomes zero at three places (marked with three filled circles), which are the three available solutions. (B) Variation of X with time for different initial conditions of X. In this simulation k_1= 2, k_2 =1, k_3=3, k_4=11, a=3, b=2 (Wannige et al., 2013).

2.2.4 Mathematical definition of biological robustness

Robustness is a property of a biological system that allows the system to maintain its functions despite external or internal perturbations (Kitano, 2004). In many species, the robustness property is evident from the gene expression level to the systematic homeostasis level. Many experiments reveal the roles of robustness in diseases such as cancer and diabetics, which take over the mechanisms that protect the systems to maintain and support these diseases. The available mathematical definition represents robustness 'R' of a system 's' with respect to a function 'a' despite a set of perturbations 'P' as follows (Equation (2-16) and (2-17)) (Kitano, 2007):

$$R_{a,p}^{s} = \int_{P} \psi(p) D_a^s(p) dp \qquad (2-16)$$

Where

$$D_a^s(p) = \begin{cases} 0, & p \in A \subset P \\ f_a(p) / f_a(0), & p \in P|A \end{cases} \qquad (2-17)$$

In this mathematical definition, 'P' is the total perturbation space and 'p' is an instance of perturbation. '$\psi(p)$' represents the probability for perturbation 'p' to occur and ' $D_a^s(p)$'is the evaluation function given in Equation (2-17). In the evaluation function, 'A' represents a set of perturbations where the system failed to maintain the subjected function against perturbation 'p'. Accordingly, $D_a^s(p)$ is zero when the system does not maintain the desired function. In other situations, $D_a^s(p)$ yields the relative viability of a function under perturbation compared to the non-perturbed state. If a system's performance in maintaining a desired functionality is reduced by 40 percent under a certain perturbation, the corresponding $D_a^s(p)$ value equals 0.6.

The above definition of robustness considers only the main concept of maintaining functionality despite diverse perturbations. However, robustness is a broader and more complex concept which requires a mature theory developed after considering factors such as the relationship of robustness with multistabilty, evolvability and fragility (Kitano, 2007).

Chapter 3

Biology of Meiosis and Mitosis Initiation in Budding Yeast and the Requirement for a New Mathematical Model

"Almost all aspects of life are engineered at the molecular level, and without understanding molecules we can only have a very sketchy understanding of life itself" (Crick, 1988).

In this chapter, we first present a general overview of meiosis and mitosis cell division, the essential steps in the division process and the main regulators. We then provide a detailed description of meiosis and mitosis initiation in *Saccharomyces cerevisiae*, mainly the molecular mechanisms and transcriptional cascade, which regulates meiosis and mitosis initiation. We also identify relationships of the mitosis initiator with the meiosis initiation network. The information presented in this chapter would facilitate the discussion of mathematical model development and the simulation results presented in the following four chapters. We conclude this chapter by indicating the requirements of a new model for this research given the mathematical models available of meiosis and mitosis initiation in budding yeast.

3.1 General Overview of Mitosis and Meiosis

Meiosis and mitosis are the two major cell division techniques in organisms. Mitosis, where a cell is replicated into two identical daughter cells, happens in all cells, including somatic and germ cells and is vital for the continuity and growth of cell generation. The meiosis process, in which four unique gametes are produced, only happens in germ cells and is necessary for the production of the sex cells in sexual reproduction (Champion and Hawley, 2002; Vershon and Pierce, 2000).

3.1.1 Cell division in mitosis

In the mitotic cell cycle, cells undergo division to replenish dying cells or for the growth of cell populations, such as in embryo development. Mitosis-type cell division is vital for an organism as cells need to maintain a continuity from one generation to the next and copy hereditary material to the next cell generations (Gupta, 2009). Therefore, the products of mitotic division are identical and represent the mother cell qualitatively and quantitatively. The mitotic cell cycle can be divided into four main stages (Figure 3.1). G1 is a resting phase where cell growth happens, and DNA synthesis takes place in the S phase. G2 is the next resting phase, where the cell is checked for errors in DNA replication and the M phase is the main mitotic cell division phase. This M phase is called the mitosis phase and is where a spindle is formed to divide the replicated DNA into two daughter cells. Mitosis consists of six stages, namely: interface, prophase, metaphase, anaphase and telophase. The cell division steps at each of these six stages are presented in Figure 3.1.

The cell cycle control system consists of checkpoints to detect mistakes and inhibit transitions in a defected cell (Figure 3.1). In animal cells, the G1 checkpoint is also called the restriction check point and it decides whether the cell should delay division, enter a resting stage (G0) or divide according to the cell size and the environmental conditions. If all DNA is not replicated, and the cell is smaller than the required size, the cell cycle will be arrested at the G2 checkpoint without triggering the start of the M phase. The metaphase check point is also called the spindle check point, where the cell is checked for the appropriate number of chromosomes and their alignment. If the cell consists of a larger or smaller number of chromosomes than required, the cell cycle will be arrested leading cell death (Gupta, 2009; Harvey Lodish, 1995).

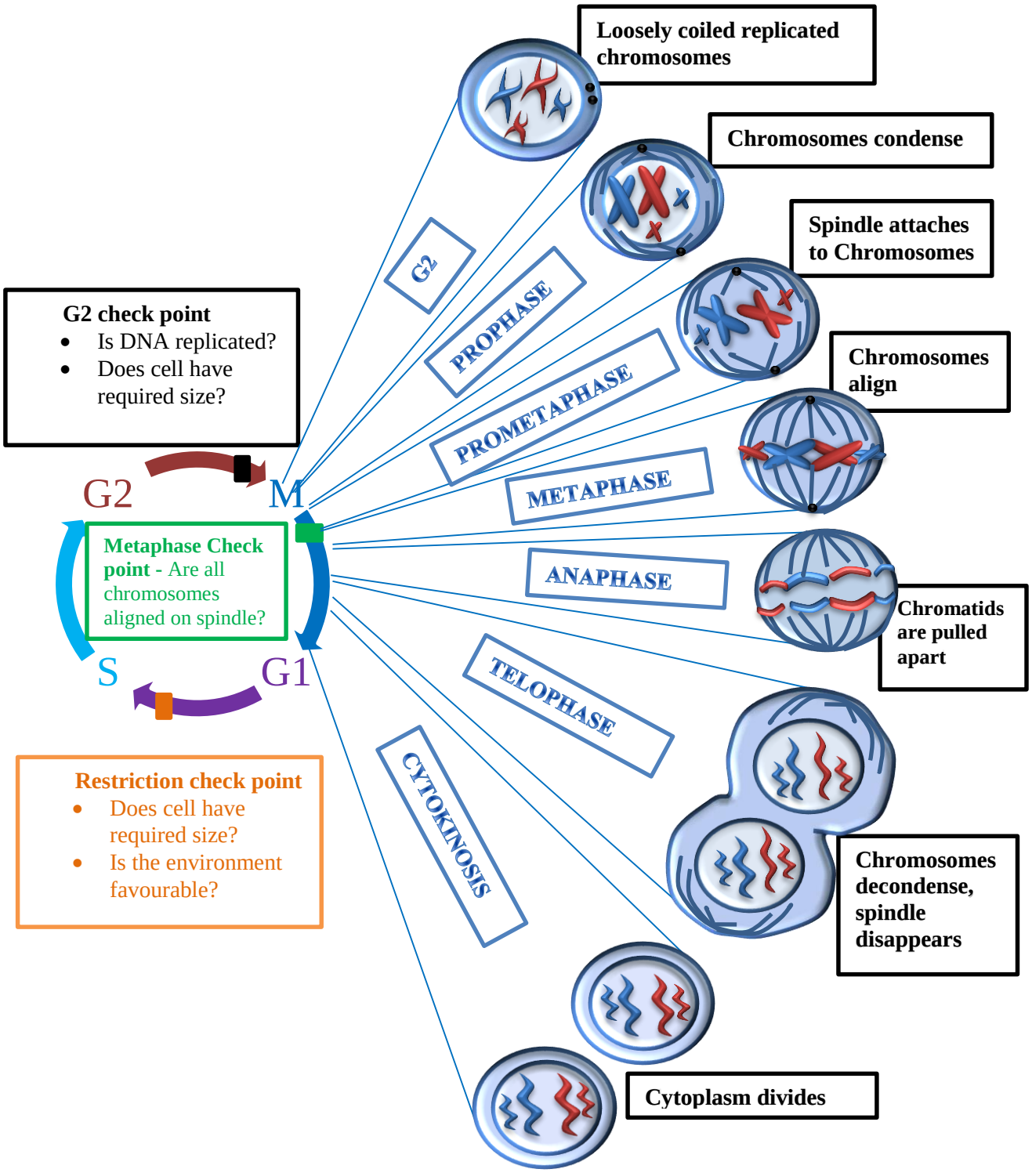

Figure 3.1 The main checkpoints, their regulatory information inputs and the main phases of mitosis. (A) Prophase: spindle fibres appear and chromosomes condense. (B) Metaphase: spindle fibres attach to the centrosome and chromosomes align. (C) Anaphase: sister chromatids move to opposite poles. (D) Telophase: nuclear membrane reforms. Chromosomes de-condense. (E) Cytokineses: cytoplasm divides and the parent cell becomes two daughter cells.

3.1.2 What controls the mitosis cell cycle?

A family of enzymes called, cyclin-dependent kinases (Cdks) act as the independent major controller responsible for the timely activation, and the coordination of the set of proteins that accomplish the cell cycle events (Figure 3.2). These Cdks, which need to function robustly in varying environments and in functional failures, are governed by a network of regulatory subunits and phosphorylations. The activity of Cdks is mainly regulated by cyclins and the oscillating cyclin levels work as a clock, timing and providing only enough time required for cell cycle events. Different stage-specific cyclins control the coordinated execution of the cell cycle events (Graña and Reddy, 1995; Morgan, 1997; Sánchez and Dynlacht, 2005).

The central cell cycle control systems in eukaryotes, including humans and yeasts, are highly conserved and well researched (Figure 3.2). Cyclins can be divided into four classes depending on their functionality at different stages of the cell cycle: G1 cyclins are responsible for the control of cell cycle entry according to environmental factors; G1/S cyclins, S cyclins and M cyclins control the cell cycle events implicated by their names. In budding yeast a single Cdk (Cdk1) regulates the cell cycle while in humans there are four Cdks (Cdk1, Cdk2, Cdk4 and Cdk6) which combine with different cyclins to control the cell cycle.

3.1.3 Cell division in meiosis

Meiosis cell division is a main aspect in the evolution of eukaryotes for two major reasons: meiosis division creates genetic diversity among the gametes and is responsible for maintaining a constant number of chromosomes in each sexually reproducing generation (Gupta, 2009; Lodish et al., 2013). During the meiosis process, chromosomes undergo recombination, shuffling genes to produce unique genetic combinations in each gamete. Two consecutive rounds of divisions, with one round of chromosome replication, create four gametes with half the number of chromosomes of the mother cell. This chromosome number reduction into half during the formation of sex cells ensures that a fused sex cell (zygote) has a similar, constant number of chromosomes as a typical somatic cell (Gupta, 2009). Therefore, the chromosome number reduction at meiosis serves as the mechanism for maintaining a constant chromosome number from one generation to other.

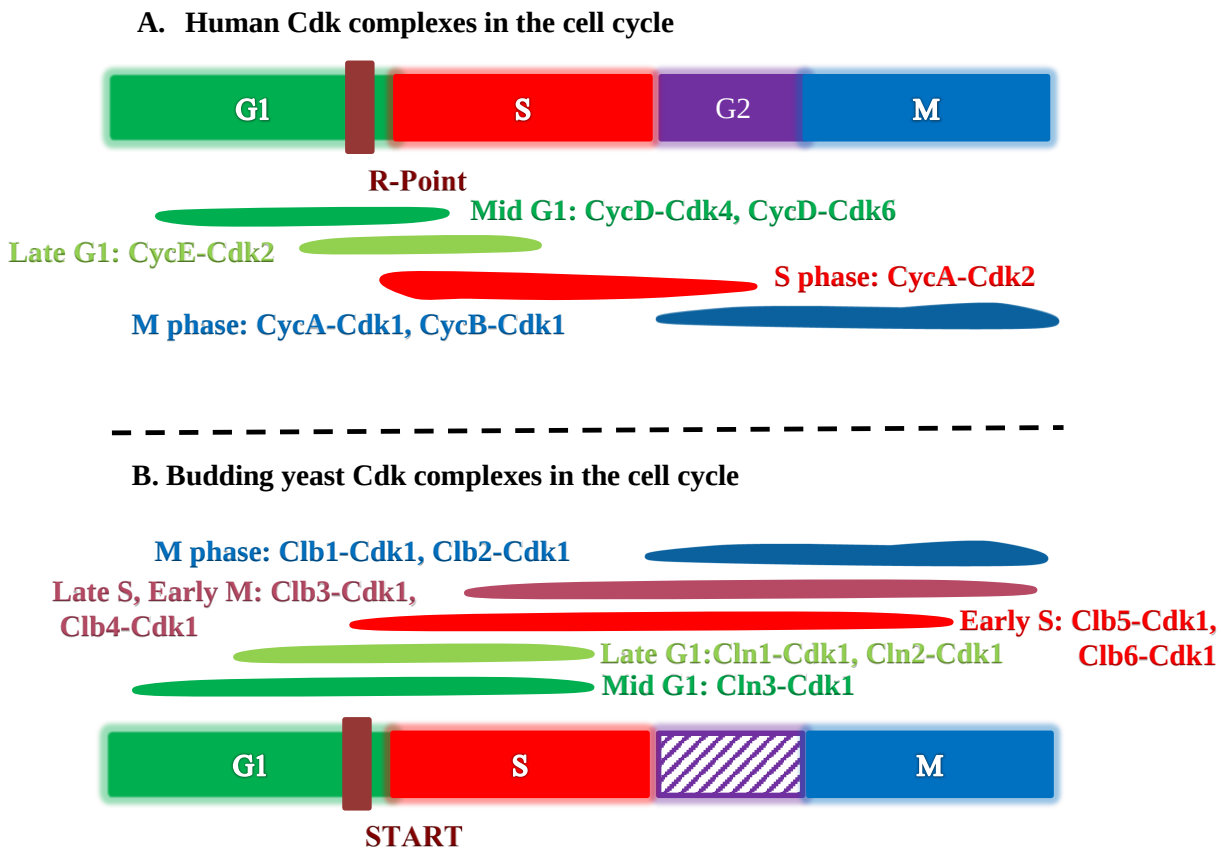

Figure 3.2 Controllers of the cell cycle of human and budding yeast (A) Shows the human cell cycle phases and the controlling cyclin-Cdk complexes. (B) Shows the budding yeast Cdk/cyclins responsible for each phase of the cell cycle. The activity level of the cyclin at each stage is proportional to the width of the stripe representing cyclins (Harvey Lodish, 1995).

Meiosis consists of two rounds of cell division: the first meiotic division (*meiosis I*) and the second meiotic division (*meiosis II*) (Lodish et al., 2013; Morgan, 2006). Cells undergo chromosome replication only once, at interphase prior to *meiosis I*. Both the first and second divisions of meiosis consist of the following four stages (Figure 3.3): prophase, metaphase, anaphase and telophase. During prophase 1 of *meiosis I*, the replicated chromosomes condense and the homologous chromosomes pair with each other. The homologous chromosome pairs then exchange DNA between their adjacent homologous chromatids. The recombined chromosomes align on the equator of the cell at metaphase 1 and spindle fibres attach to the centromere of the chromosomes. At anaphase 1, the chromosomes are pulled apart along the spindle fibre to the opposite ends of the mother cell. At telophase 1, the cell is divided into two daughter cells with the same number of chromosomes as the mother cell. *Meiosis II* is nearly similar to mitosis division but does not include the chromosome replication stage. Each daughter produced at the end of *meiosis I* is independently divided into another two daughters, creating four gametes with half the number of chromosomes as their mother.

3.1.4 Controllers of meiosis cell division

The transcriptional cascade of meiosis initiation and progression comprises several sets of genes, which are expressed sequentially to accomplish the precise and ordered entry and completion of *meiosis I* and *meiosis II* cellular divisions. A special initiation signal can only initiate meiosis under the correct conditions: in humans, meiosis initiation is partially stimulated by retinoic acid (Le Bouffant et al., 2010); in budding yeast, the meiosis initiation signal is nutrient starvation (nitrogen and glucose depletion) (Esposito and Esposito, 1974). These initiation signals stimulate the main meiosis initiators (Ime1[6] in yeast (Kassir et al., 1988) and Stra8 in humans (Le Bouffant et al., 2010)). The initiator proteins then transfer the initiation signal activating the first set of genes on the gene cascade of meiosis. The former set of genes on the cascade are always responsible for activating the later sets of genes and an orderly expression of proteins is required for the completion of the sequential meiotic events (Kurtz and Lindquist, 1984; Smith and Mitchell, 1989).

[6] Notation : Protein names are written in lower case starting with an uppercase letter, and genes and mRNAs are written in upper case.

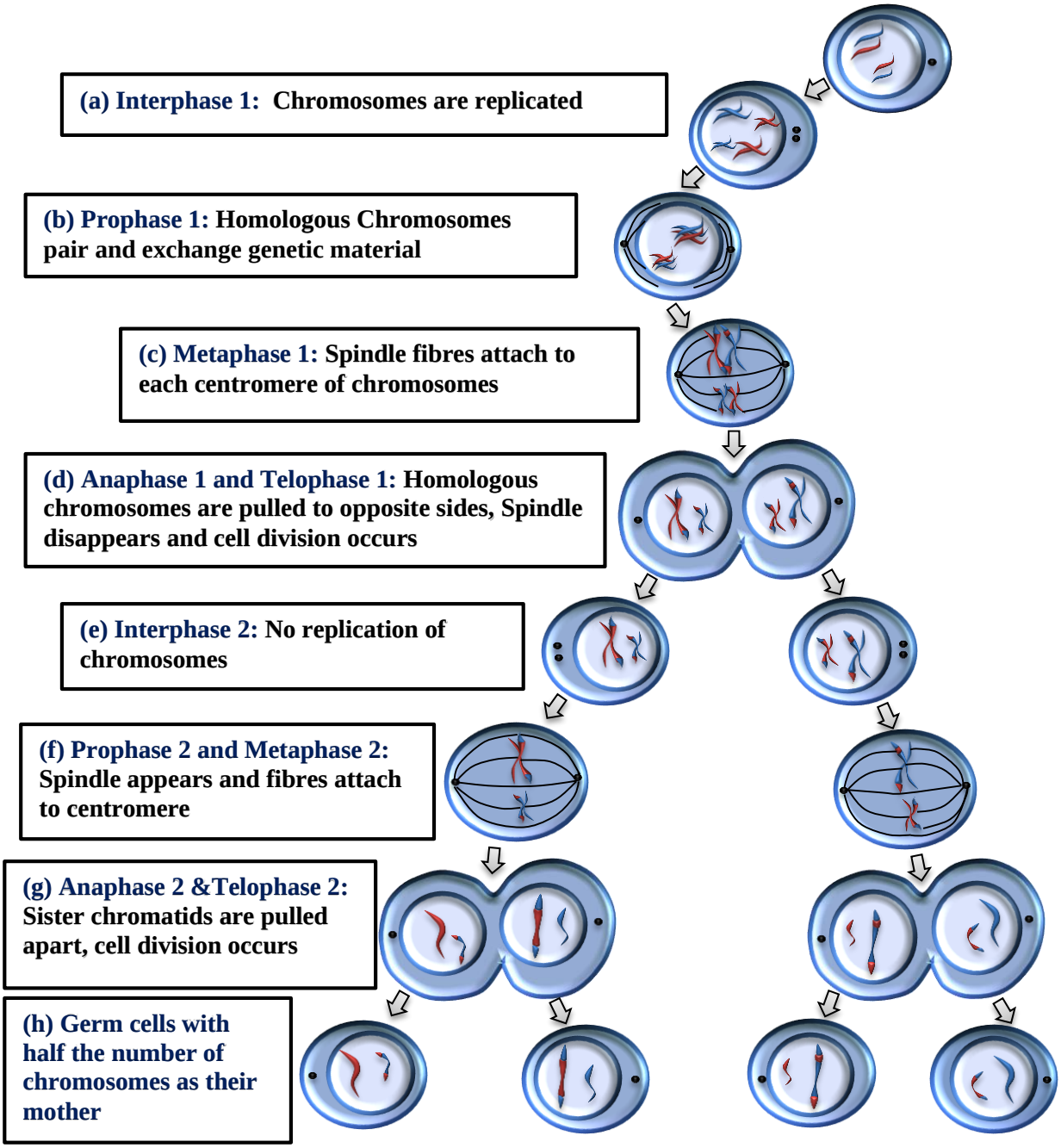

Figure 3.3 Meiosis cell division. For simplicity, two chromosome sets each with maternal and paternal homologs (marked with red and blue, respectively) in the mother cell are considered. Meiosis consists of two rounds of cell divisions: *meiosis I* and *meiosis II*. In the early prophase of *meiosis I*, chromosomes are replicated. Then, chromosomes align with each other and exchange genetic material by crossing over between homologous chromosomes. In metaphase 1, homologous chromosomes line-up along the equator of the cell and spindle fibres attach to the centromere of the chromosomes. In anaphase 1, homologous chromosomes are moved apart from the centromere along the spindle fibres. *Meiosis I* division ends after telophase 1, where cell division occurs. *Meiosis II* starts with interphase 2 without replicating chromosomes and follows similar steps to *meiosis I*, as shown. At the end of two rounds of divisions, four unique gametes are created with half the number of chromosomes as the mother cell (Lodish et al., 2013).

3.1.5 Meiotic-mitotic initiation switch

After being stimulated by extra-cellular initiation signals, germ line cells initiate meiosis by switching from the mitosis cell cycle to meiosis division (mitotic-meiotic switch) (Lodish et al., 2013). Switching from the mitosis cell cycle to meiosis is a major step in the journey from germ line stem cell to differentiated gametes. Proper regulation of the switch from mitosis to meiosis is vital for a germ cell to provide a proper genetic link between generations (Gupta, 2009). The meiosis initiation decision is closely related to fertility, and the correct decision is crucial for embryo and animal development (Eckmann et al., 2004; Lu et al., 2013).

As mentioned in Chapter 1, dysfunction of the mitotic-meiotic switch may lead to abnormal proliferation of early germ cells leading to germ cell tumours (GCT). The meiotic and mitotic cell divisions also need to be regulated for a good balance between stem cells and maturing sperms. If biased to the meiosis initiation side, the meiotic stem cells would deplete or, otherwise, abnormal proliferation would initiate cancer (Kimble, 2011).

3.2 *Saccharomyces cerevisiae* as a Model Organism to Study Meiosis Initiation

The eukaryotic, unicellular budding yeast, *Saccharomyces cerevisiae*, serves as the best model organism for meiosis and mitosis studies mainly because these easily tractable cells undergo meiosis and mitosis synchronously in response to the available nutrients (Roeder, 1995). Therefore, budding yeast remains a well-studied eukaryotic organism in the context of meiosis and mitosis. Most of the genes involved in yeast meiosis and mitosis cell division have been characterised (Morgan, 2006). Genome-wide studies of meiotic and mitotic gene expression (Cho et al., 1998; Li et al., 2010), gene deletion (Deutschbauer et al., 2002) and overexpression mutant studies (Colomina et al., 1999; Gurevich et al., 2010) provide a huge amount of data about these cell division processes.

The information from yeast-based studies provides insights into higher eukaryotic meiosis and mitosis processes. The implications from yeast-based studies are important because meiosis and mitosis cell divisions are analogous in yeast and higher eukaryotes with conserved genes: for example, a study which analysed time series microarray profiles for the meiotic prophase reveals that 129 genes are conserved between humans and budding yeast (Li et al., 2010). Further, some genes in budding yeasts are found to be homologous to human

genes: such as, human CDK2 to yeast IME2 (IME2 shows 58.9% similarity and 37% identity to the human cyclin dependent kinase, CDK2 (Szwarcwort-Cohen et al., 2009)); and human CDC2 to CDK1 in yeast (Ninomiya-Tsuji et al., 1991); in addition, the most upstream budding yeast cyclin Cln3 contains a conserved cyclin box, which is a region of homology that mediates physical interaction with Cdk1 (Miller et al., 2005). Starting from the next section, we provide a detailed description of the biology and molecular mechanisms of meiosis and mitosis initiation in the budding yeast.

3.2.1 Saccharomyces cerevisiae: morphology and life cycle

Budding yeast cells exist in two types, diploid or haploid, for growth and survival (Figure 3.4). Haploid cells have half the number of chromosomes as diploid cells. Haploid cells exist in either of the two mating types, *a* or *alpha* (*α*), which are opposite sexual types. The mating type is determined by the expression of a gene at an active mating type locus (locus is a special location on a gene or in a DNA sequence on a chromosome) called MAT, which is responsible for controlling the sexual behaviour of yeast cells (Strathern et al., 1981). The MAT locus contains either MATa or MAT*α* genes and specifies the two cell types of haploid *a* and haploid α, respectively. Haploid yeast cells can switch between mating types *a* and *α* by rearranging DNA and converting MATa or *α* genes into the opposite type genes. During switching, the genes in the MAT locus are replaced by the genes in either one of two silent locuses, called HML and HMR, which contain transcriptionally inactive *α* specific and *a* specific genetic sequence information (Herskowitz and Oshima, 1981).

As shown in Figure 3.4, the haploid to diploid transition happens by sexual conjugation between haploid gametes of opposite sexual types, a and α. When opposite sexual type cells meet each other, they stop further mitosis cell division and change their shape by growing toward the opposite sexual type cell (Duntze et al., 1970; Levi, 1956). These shape- changed cells are normally fused at their small ends forming a diploid cell. Diploid cells are called MATa/α cells since they are a result of fusion between a and α and contain both MATa and MATα alleles (Herskowitz and Oshima, 1981).

Budding yeast cells have simple nutritional needs. They can survive well in aerobic conditions if supplied with carbon sources such as glucose and acetate, and a nitrogen source such as ammonium sulphate, urea or an amino acid. They may also require a vitamin called biotin and a variety of salts and trace elements (Kavanagh, 2011). Both diploid and haploid

Saccharomyces cerevisiae cells undergo mitosis-type cell division and grow their populations by budding under vegetative conditions with good glucose and nitrogen sources (Herskowitz, 1988). The budding process starts after the mother cell attains a critical cell size. During budding, the DNA is doubled and the daughter cell emerges as a bud from a localised weakened cell wall of the mother cell with exactly the same number of chromosomes as the mother cell (Figure 3.2). Diploid cells undergo meiosis under nutritional stress conditions of nitrogen and glucose starvation (Esposito and Esposito, 1974). During meiosis, diploid cells create four unique stress-resistant haploid spores with half the number of chromosomes as their mother cell. When nitrogen is depleted and glucose is available, diploid cells create elongated cell structures by pseudohyphal growth (Gimeno et al., 1992).

3.3 Mitosis and Meiosis Initiation in Budding Yeast

3.3.1 At which point of the budding yeast cell cycle do meiosis and mitosis start?

The cell cycle of *Saccharomyces cerevisiae* can be divided into three phases (Figure 3.4). These three phases, called G1, S, and M are similar to the phases in the higher eukaryotic cell cycle; however, the G2 phase of the eukaryotic cell cycle cannot be found in the budding yeast cell cycle (Gupta, 2009). *S.cerevisiae* mainly regulates its cell cycle at the G1 phase. At the G1 stage, the regulatory network controls cell cycle progression according to cell size and environmental constraints such as nutritional levels (Forsburg and Nurse, 1991; Gupta, 2009). The G1 phase of the mitotic cell cycle can be further divided into pre-start G1, start and post-start stages. At the pre-start G1 phase, if the nutritional levels and the cell sizes are appropriate, haploid and diploid cells decide to go through a mitosis cell cycle and divide. If a diploid cell is starved for nutrients, it can undergo meiosis, creating four haploid cells (Gupta, 2009).

This study focuses on the meiotic-mitotic initiation stage of diploid budding yeast cells. Diploid cells decide to undergo either mitosis or meiosis at the pre-start G1 phase. At this stage of budding yeast development, the initial decision to undergo meiosis or mitosis is

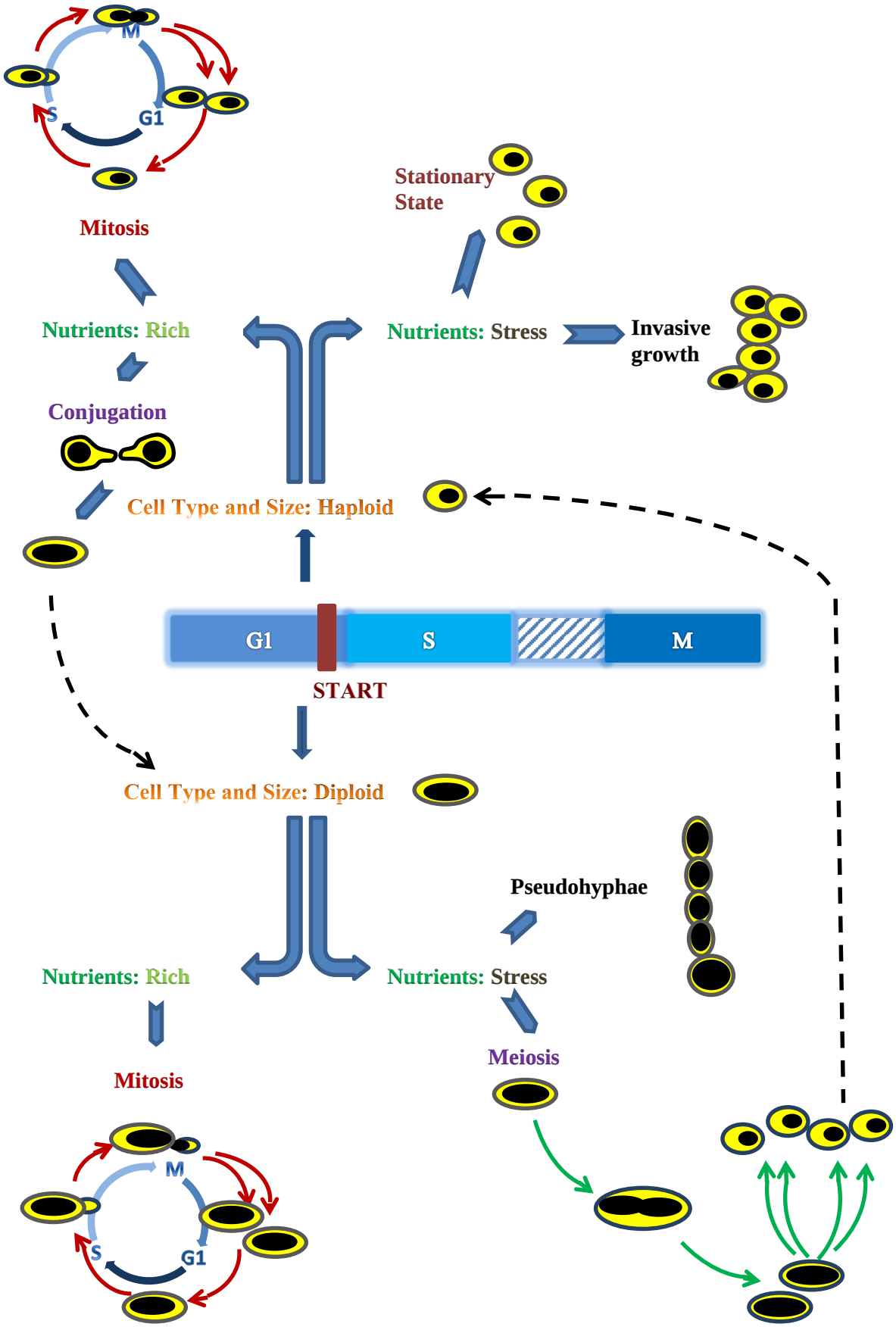

Figure 3.4 Life cycle of budding yeast. Diploid cells are marked with larger black circles inside the yellow circle to represent the high chromosome number. Dashed lines indicate the transition between cell types: haploid and diploid.

reversible and can change according to the available nutrient conditions: meiosis-decided cells would return to mitosis initiation if nutrients are re-supplied and the mitosis-decided cells would then return back to meiosis initiation if the cells are starved (Reviewed in Simchen (2009) (Simchen, 2009)). This reversible switching could take place in meiosis-decided cells until they reach meiotic commitment, which occurs at chromosome segregation before the first division of meiosis (Figure 3.5) (Nachman et al., 2007). The commitment to mitosis occurs at the start checkpoint of mitosis (Simchen, 2009). After the commitment point, the cells irreversibly commit to go forward to the final stage of the process independent of the external nutrients.

3.3.2 The transcriptional cascade responsible for meiosis initiation in budding yeast

3.3.2.1 Meiosis initiation signal and the transcriptional cascade of meiosis

The initiation of meiosis requires specific genetic and nutritional conditions. The cell type genetic signal MATa/α allows only diploid cells to undergo meiosis (Covitz et al., 1991). The nutritional signal for meiosis initiation is nitrogen deprivation and no glucose in a medium with a non-fermentable carbon source such as acetate, which are typically called meiotic conditions (Esposito and Esposito, 1974). Nitrogen and glucose limitation causes the yeast cells to arrest at the G1 phase of the mitotic cell cycle and activate meiosis-specific genes. Non-fermentable carbon sources such as acetate are required because they need to be metabolised through respiration to produce useful energy. The nitrogen signal is transmitted to the meiosis initiation by the cAMP/PKA and TOR pathways (Dennis et al., 1999; Honigberg and Purnapatre, 2003; Matsuura et al., 1990).

The set of genes expressed in meiosis is divided into three categories according to their expression sequence (Figure 3.5). The set of genes expressed initially are called early meiosis specific genes (EMG). The set of genes expressed secondly and thirdly are called the middle and late meiosis-specific genes, MMG and LMG, respectively (Smith et al., 1990). The major regulators of the meiosis initiation in budding yeast are Ime1, a transcriptional activator protein and Ime2, a serine/threonine protein kinase (Initiator of meiosis 1 and 2) (Smith and Mitchell, 1989). Once expressed, Ime1 is responsible for the transcriptional activation of the EMGs (Smith et al., 1990). The transcription of the middle meiosis specific genes mainly depends on Ime2, a kinase that belongs to the early genes and on Ndt80, a kinase expressed

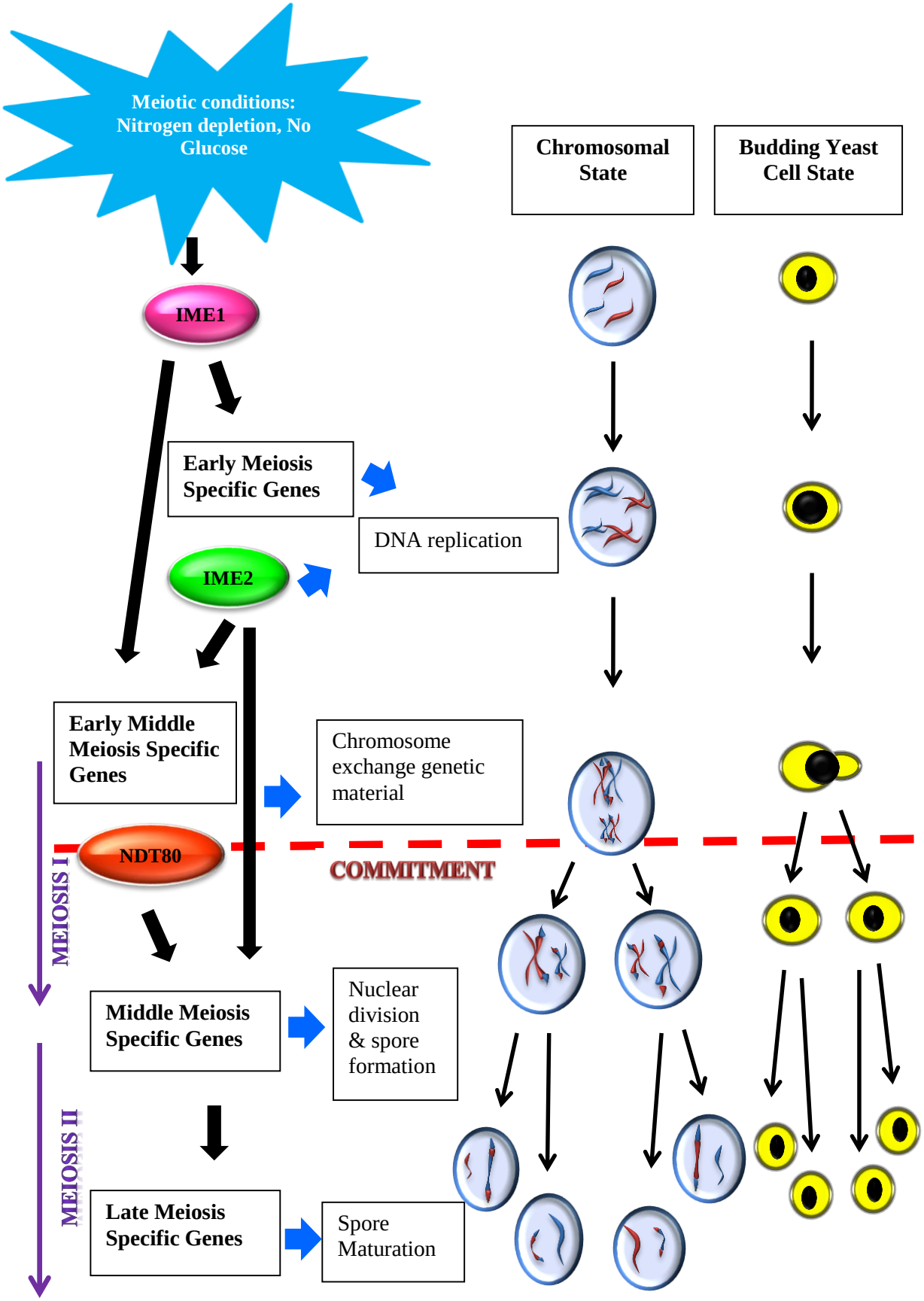

Figure 3.5 Transcriptional cascade regulating meiosis in budding yeast, corresponding chromosomal states and cell states. Upon nutrient deprivation, Ime1 and Ime2 activate the meiotic gene sets, which are then expressed sequentially.

by an early middle gene (Figure 3.5). Transcription of the late genes indirectly depends on Ime1, Ime2 and Ndt80 (Chu and Herskowitz, 1998).

3.3.2.2 Meiosis initiation signals and IME1 expression

Ime1 is the master activator of the transcriptional cascade responsible for meiosis (Figure 3.6). Transcription of IME1 is mainly regulated by two main meiosis initiation signals: a mating-type genetic signal, which allows meiosis to happen only in diploid MATa/α cells and nutrient signals (Smith et al., 1990). This regulation is accomplished by the IME1 regulatory region which is 2.1 kb long and consists of about 10 separate positive and negative elements (Granot et al., 1989; Sagee et al., 1998).

Different signals affect distinct elements of the IME1 5' un-translated region (Figure 3.6) (Sagee et al., 1998). UCS3 and UCS4 repressor elements transfer the cell type genetic signal (MAT) to IME1 transcription. In MATa and MATα haploid cells, IME1 transcription is repressed by the Rme1 DNA binding protein at two sites in the UCS4 element. RME1 expression is repressed in MATa/MATα diploid cells (Covitz et al., 1991; Shimizu et al., 1998), such that when Rme1 is not available, IME1 can be expressed under nutritional stressful conditions. The nitrogen signal transmitted by the cAMP/PKA pathway (Matsuura et al., 1990) is transferred to IME1 through a UCS1 element in the regulatory region (Sagee et al., 1998). UCS1 is a negative element in the regulatory region of IME1 and represses IME1 transcription in the presence of nitrogen. The carbon signal is transferred by UCS1 and by two of the elements of UCS2, namely: UASru and IREu, which function as repressor elements in the presence of glucose (Kahana et al., 2010; Sagee et al., 1998). The protein, Sok2, which is a negative regulator of IREu activity, works as the transmitter of the glucose signal to the IREu element (Sagee et al., 1998; Shenhar and Kassir, 2001). SOK2 gene transcription and its repression activity are controlled by glucose such that Sok2 is not available to repress IME1 during glucose starvation. In the absence of glucose and in the presence of acetate as the sole carbon source, UASru, IREu and UASrm in UCS2 function as activators of IME1 transcription. In the presence of acetate, the activation of IME1 by IREu depends on two zinc finger proteins, Msn2, Msn4, and on Ime1. Msn2, which acts as a positive transcriptional factor, is bound to IREu only in the absence of glucose and Msn2 and Msn4 are localised to the cytoplasm in a glucose medium (Görner et al., 1998; Kahana et al., 2010).

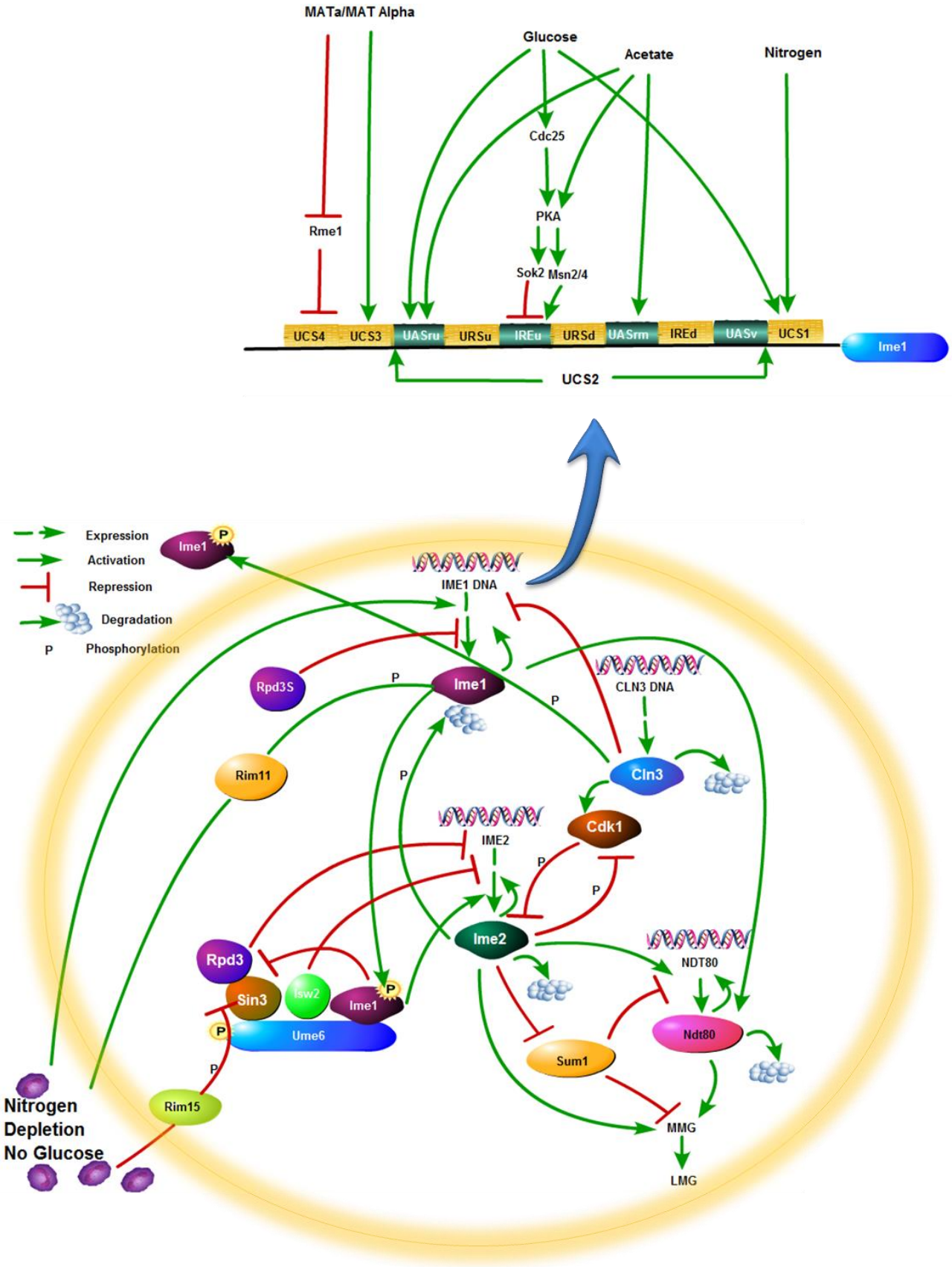

Figure 3.6 A schematic diagram of the meiosis initiation in budding yeast. Meiosis initiates only in diploid cells of budding yeast under nutrient conditions of nitrogen

depletion in acetate medium and with no glucose. The IME1 5' un-translational region (UCS1 to UCS4), drawn at the top left of the figure, controls IME1 expression only under the correct conditions of cell type and nutrients; the cell type signal is controlled by UCS3 and UCS4 elements; the nitrogen signal is transferred by the UCS1 element; the glucose signal is transferred to UASru, IREu and UCS1 elements and the acetate signal is transferred to the UASru, IREu and UASrm elements (Kahana et al., 2010). In the top figure, elements required for activation are marked with white letters and the elements required for repression are marked with black letters. Nutrient depletion activates Ime1 expression and relieves Rpd3/Sin3 repression from EMGs via Rim15 and Rim11. Rising Ime1 levels activate IME2 transcription and help to relieve Rpd3/Sin3 repression. ISW2 removal from the EMG promoters is not clear. Ime2 phosphorylates Ime1 tagging it for degradation by the 26S proteasome. Ime2 inhibits Cdk1/Cln3 functionality and prevents mitosis. Good nitrogen conditions activate Cln3 expression for mitosis initiation. Cdk1s activated by Cln3 initiate the mitosis cell cycle. Meiosis initiation is inhibited during mitosis by Ime2 deactivation by Cdk1 phosphorylation and the transcriptional repression of Ime1 by Cln3; at the same time, the phosphorylated Ime1 by Cln3 is transported out of the nucleus. Ime2 and Ndt80 are the activators of MMG. Sum1 represses transcription of both Ndt80 and MMGs. This Sum1 repression is relieved by Ime2. Further, Sum1 and Ndt80 compete for binding to middle sporulation elements of MMGs even at the auto-regulation of NDT80 allowing more Ndt80 proteins to enhance auto-activation.

The IME1 gene is not transcribed in a vegetative growth medium with glucose and nitrogen by the transcriptional level control, as discussed above. At a basal level of IME1 transcription is observed in growth media with acetate as the sole carbon source (SA-synthetic acetate), but none is observed when glucose is used as the sole carbon source (SD-synthetic dextrose) (Kassir et al., 1988). Nitrogen depletion in the acetate medium (SPM-sporulation medium) initiates IME1 transcription transiently by increasing the number of IME1 mRNA and arresting the G1 phase of the cell cycle (reviewed in Kassir et. al. (2003) (Kassir et al., 2003)). This dependence of IME1 transcription on different nutrients is clearly observed in experiments. As an example, Kahana et. al observed higher IME1 mRNA levels in the sporulation medium compared to synthetic acetate (SA) medium and synthetic dextrose (SD) medium (Figure 3.7) (Kahana et al., 2010). In their experiments, the IME1 open reading frame is expressed from the budding yeast IME1 promoter integrated at the URA3 locus.

Ime1 positively auto-regulates its transcription (Shenhar and Kassir, 2001) (Figure 3.6). Recent research shows that IME1 expression is repressed by the Rpd3S protein complex (Rubinstein et al., 2007). Further, experimental results suggest that nitrogen or cell cycle progression inhibits the translation of IME1 mRNA; however, it is not known how

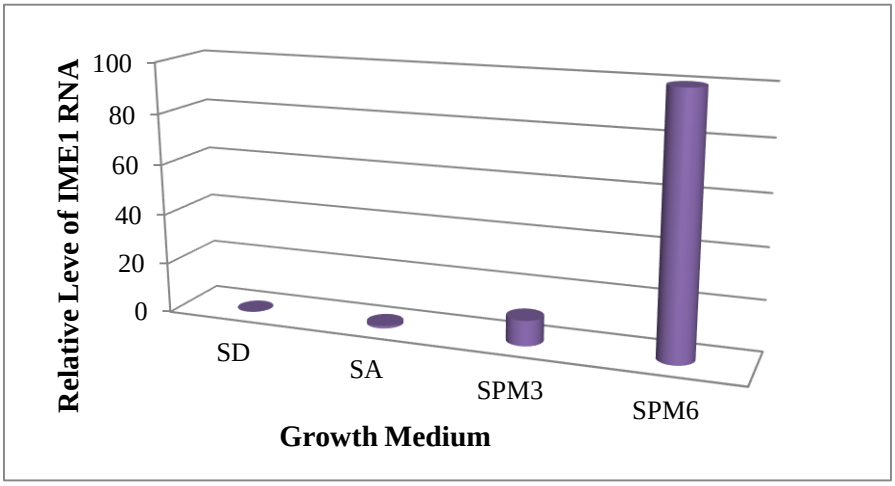

Figure 3.7 Role of nutrients in IME1 transcription. The figure shows the IME1 RNA expression from cells grown in synthetic dextrose (SD) medium (vegetative growth medium with glucose as the sole carbon source), synthetic acetate (SA) medium (growth media with acetate as the sole carbon source), IME1 expression when the SA grown cells were transferred to sporulation medium (SPM) with nitrogen depletion and acetate as the sole carbon source. SPM3 and SPM6 correspond to samples tested at three and six hours after the sporulation, respectively (Data acquired from Kahana et. al. (2010) (Kahana et al., 2010)).

nitrogen or the G1 phase controls the efficiency of translation of IME1 mRNA (Rubinstein et al., 2007; Venkatesh and Workman, 2012).

3.3.2.3 Regulation of early meiosis-specific gene expression

Under vegetative growth conditions, the transcription of early meiosis-specific genes (Figure 3.8 A) is repressed by the recruitment of two repressing complexes. These two repressors are Isw2, which is a chromatin-remodelling complex (Goldmark et al., 2000) and Rpd3, a histone deacetylase (Kadosh and Struhl, 1997). These repressors are recruited to EMG promoters by the DNA binding protein, Ume6 (Ume6 is bound to the URS1 element in the EMG promoters under all growth conditions) (Goldmark et al., 2000). Rpd3 is always present as a complex with Sin3, which is larger than 2 MDa in size (Kasten et al., 1997). Sin3 can recognise DNA binding proteins such as Ume6, and it mediates as a bridge to recruit Rpd3 histone deacetylase (HDAC) to EMG promoters (Kadosh and Struhl, 1997). Rpd3 on the EMG promoters deacetylates histone tails in the nucleosome adjacent to the URS1 elements of the EMG promoters blocking activators and the function of transcription factors (Kadosh and Struhl, 1997). Isw2 also functions in a parallel way to Rpd3/Sin3 (Goldmark et al., 2000).

Under meiotic conditions, EMG repression by Rpd3/Sin3 is relieved by Rim15 and Rim11 kinases, which are inactive in vegetative conditions by the phosphorylations of protein kinase A (PKA) (Pnueli et al., 2004). In meiotic conditions, the kinase active non-phosphorylated Rim15 phosphorylates Ume6 and Sin3 (Figure 3.8 (B-1)). As a result, Ume6 disassociates with Sin3 and removes HDAC (Rpd3) from the EMG promoters. At the same time, the kinase active Rim11 phosphorylates Ime1; this is required to relieve Rpd3 repression and to the interaction of Ime1 with Ume6. In this way, with the meiotic entry signals, Ume6 recruits Ime1 to the promoters of the early meiosis-specific genes. Ime1 is required to relieve Rpd3 repression and transcriptional activation of EMGs (Figure 3.8 (B-2)). The removal of the repression by Isw2 is unclear (Kassir et al., 2003).

3.3.2.4 Meiosis initiator 2 and the antagonism between Ime2 and Cdk1/Cln3

IME2 is one of the EMGs required for the transcription of all meiosis-specific genes (Smith and Mitchell, 1989) . Ime2 positively auto-regulates its transcription by auto-phosphorylation (Bowdish and Mitchell, 1993; Schindler and Winter, 2006). Ime2 accomplishes the correct

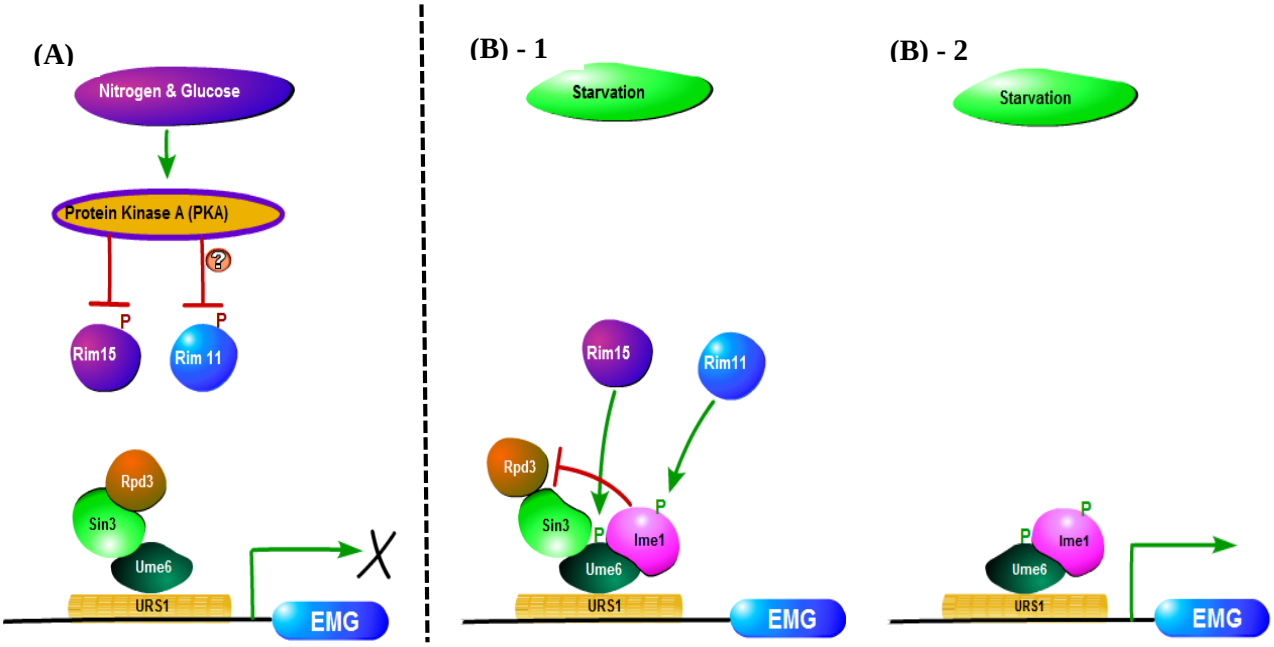

Figure 3.8 Nutrient dependent regulation of early meiosis-specific gene expression. (A) EMGs are repressed by Rpd3/Sin3 under rich nutritional conditions. In the presence of nutrients, PKA inactivates Rim11 and Rim15 protein kinases so that they cannot relieve Rpd3/Sin3 repression. ((B)-1) Rpd3/Sin3 repression is removed under starvation conditions, which do not affect the activity of the Rim11 and Rim15. Therefore, Rim11 and Rim15 phosphorylate Ume6 and Ime1 and remove the repression complex (Rpd3/Sin3) from the EMG promoters under starvation conditions. ((B)-2) When the Rpd3/Sin3 repression is removed, Ime1 activates EMG expression (Honigberg and Purnapatre, 2003; Kassir et al., 2003; Pnueli et al., 2004; Vershon and Pierce, 2000). (Note that the indirect phosphorylation of Rim11 by PKA is represented by a question mark.)

timing and high level transcription of EMGs and MMGs and is responsible for the correct timing of the entry into pre-meiotic DNA replication, meiotic recombination, nuclear division and ascus formation (Foiani et al., 1996). Experiments show that IME2 over-expression bypasses the requirement for Ime1 in transcription of EMGs and sporulation, proposing that Ime2 may act independently in activating the transcription of these meiosis-specific genes (Mitchell et al.,1990). The stability of Ime1 depends on Ime2, because Ime2 phosphorylates Ime1, thereby tagging it for degradation by the 26S proteasome (Guttmann-Raviv et al., 2002).

Many experimental research findings, taken together, show an antagonism between Ime2 and Cdk1/Cln3 (Figure 3.6), which are the main meiosis and mitosis initiators, respectively. On the one hand, functionality of Cdk1 is inhibited by Ime2 since most of the known substrates of Cdk1 are phosphorylated by Ime2, inhibiting cell cycle progression (Holt et al., 2007; Szwarcwort-Cohen et al., 2009); further, Cdk1 phosphorylates and tags Cln3 for degradation (Yaglom et al., 1995). On the other hand, Ime2 functionality is inhibited by Cdk1/Cln3 in the following manner. There are three phosphorylation sites in Ime2 where Cak1 and Cdk1 can bind and phosphorylate Ime2. Cak1 and Cdk1 compete for these three phosphorylation sites in Ime2's regulatory region and the phosphorylation of Ime2 by Cak1 activates Ime2 (Schindler et al., 2003). Therefore, the phosphorylation of Ime2 by Cdk1 inhibits the activity of Ime2 (Gurevich et al., 2010).

3.3.2.5 Ndt80, the transcriptional activator of middle meiosis-specific genes

The transcription of the middle meiotic genes is controlled mainly by two positive regulators: Ndt80 (Chu et al., 1998; Hepworth et al., 1998) and Ime2 (reviewed in Mitchell (1994) (Mitchell, 1994)) (Figure 3.5). Under vegetative conditions, NDT80 transcription is repressed by the Rpd3/Sin3 complex and the transcriptional factor, Sum1 (Figure 3.6). Under meiotic conditions, NDT80 expression depends on two activators, Ime1 and Ime2. Ime1 attaches to Ume6 on the NDT80 promoters and activates the transcription of NDT80 after the removal of Rpd3/Sin3 and Isw2 (reviewed in (Winter, 2012) and (Kassir et al., 2003)). The Sum1 repressor is removed from the middle sporulation elements in two ways. Firstly, Ime2 activates NDT80 by eliminating the repression by Sum1 (Pak and Segall, 2002); secondly, Sum1 and Ndt80 compete for binding to the middle sporulation elements of MMGs even at the auto-regulation of NDT80 allowing more Ndt80 proteins to enhance auto-activation

(Pierce et al., 2003; Xie et al., 1999). Ndt80 binds to the middle sporulation elements of MMGs for the activation of transcription. Further, Ndt80 regulates the transcription of IME2 by binding to the IME2 promoter and this might enhance the transient transcription of IME2 (Hepworth et al., 1998).

3.3.2.6 Returning to mitosis initiation before commitment to meiosis

If nutrition is re-supplied, meiosis-decided cells can return to mitosis growth (RTG) before the meiosis commitment point. The meiosis commitment point resides after DNA replication near the exit of the meiotic prophase, but before entering *meiosis I* division (Figure 3.5) ((Nachman et al., 2007; Simchen, 2009) and reviewed in Winter (2012) (Winter, 2012)). The exit from the meiotic pachytene is closely related to meiotic commitment. (pachytene is one of the stages in meiotic prophase 1 where the homologous chromosomes are connected by the synaptonemal complex (SC). SC disassembly takes place at the exit from pachytene) (reviewed in Winter (2012) (Winter, 2012)). Experiments show that cells in the meiotic pachytene return to mitosis if nutrients are provided (Shuster and Byers, 1989). The effects from the formation of chromosome crossovers at the pachytene are minimised by a distinct pathway during the return to mitosis (Dayani et al., 2011). After cells exit from the meiotic pachytene and enter *meiosis 1*, cells do not return to mitosis division if nutrients are re-supplied.

Production of Ndt80 has been identified as the main event that regulates the pachytene exit and the meiotic commitment point in wild type yeast cells (Winter, 2012). Experiments show that pachytene is blocked in NDT80-mutant cells (Xu et al., 1995) and NDT80 mutants are fully capable of returning to growth after re-feeding (Dayani et al., 2011). The positive auto-regulatory loop of NDT80, and the competition between Sum1 repressor and Ndt80 to attach to middle sporulation genes, would promote the switch-like behaviour of meiotic commitment (Friedlander et al., 2006; Winter, 2012).

3.3.3 Transcriptional cascade responsible for mitosis initiation in budding yeast

To initiate mitosis cell division, a cell should grow to a certain size and requires a vegetative medium with plenty of glucose and nitrogenous compounds. Once these requirements are met in a cell, it initiates mitosis, but this decision would change to meiosis, if the nutrients are depleted before the start checkpoint.

As mentioned previously, cyclin-dependent kinases (Cdks) and cyclins control mitosis initiation and progression in yeasts. In budding yeast, five different kinds of Cdks can be found: CDC28, PHO85, KIN28, SRB10 and CTK1 (Gupta, 2009). Among these Cdks, only CDC28 (also called Cdk1) is involved in the cell division cycle (Figure 3.9). There are also twenty-two cyclins in budding yeast, which can bind to the above mentioned five Cdks. During the G1 phase, three cyclins (Cln1, Cln2 and Cln3) associate with Cdc28 (Cdk1). All these cyclins are required to be inactivated to block the passage through G1 to the S phase at the start check point (Gupta, 2009). However, availability of one of these cyclins can allow progression from G1 to the S phase and mutations in one or two of these genes fail to block the cell cycle. Cdk1/Cln3 is the most upstream activator and its expression is highly regulated by nitrogen and glucose (Gupta, 2009; Jeoung et al., 1998; Morgan, 2006). Under vegetative conditions, Cdk1/Cln3 activates all G1-specific cyclins allowing G1/S transition (Danaie et al., 1999; Morgan, 2006).

Meiosis initiation is inhibited via several mechanisms upon the availability of nutrients under mitotic conditions. Sufficient nitrogen and glucose levels inhibit IME1 transcription (Pnueli et al., 2004). In addition, Cln3 down-regulates IME1 transcription. Cln3 prevents accumulation of the Ime1 protein in the nucleus by phosphorylating and transporting the phosphorylated Ime1 out of the nucleus (Colomina et al., 1999; Kassir et al., 2003). The EMG repression complex (Rpd3/Sin3/Ume6) is not removed by Rim11 and Rim15 because of their inactivation caused by nitrogen and glucose deprivation (Figure 3.5 A). Further, as discussed previously, there exists an antagonism between Ime1 and Cdk1/Cln3.

3.4 What is the Requirement for a New Model Given the Available Mathematical Models for Mitosis and Meiosis Initiation?

A range of mathematical models have been constructed to understand the machinery of the mitosis cell cycle at high nutrient levels (Chen et al., 2000; Chen et al., 2004; Vinod et al., 2011). These studies are helpful for understanding the human cell cycle, since the molecular mechanisms are conserved in both human and yeast cell cycles (Kaizu et al., 2010). The available deterministic models can be categorised into two groups depending on their objectives: (1) cell cycle regulation-focussed models, where the cell cycle is modelled and controlling mechanisms at checkpoints such as START and G1/S are studied by

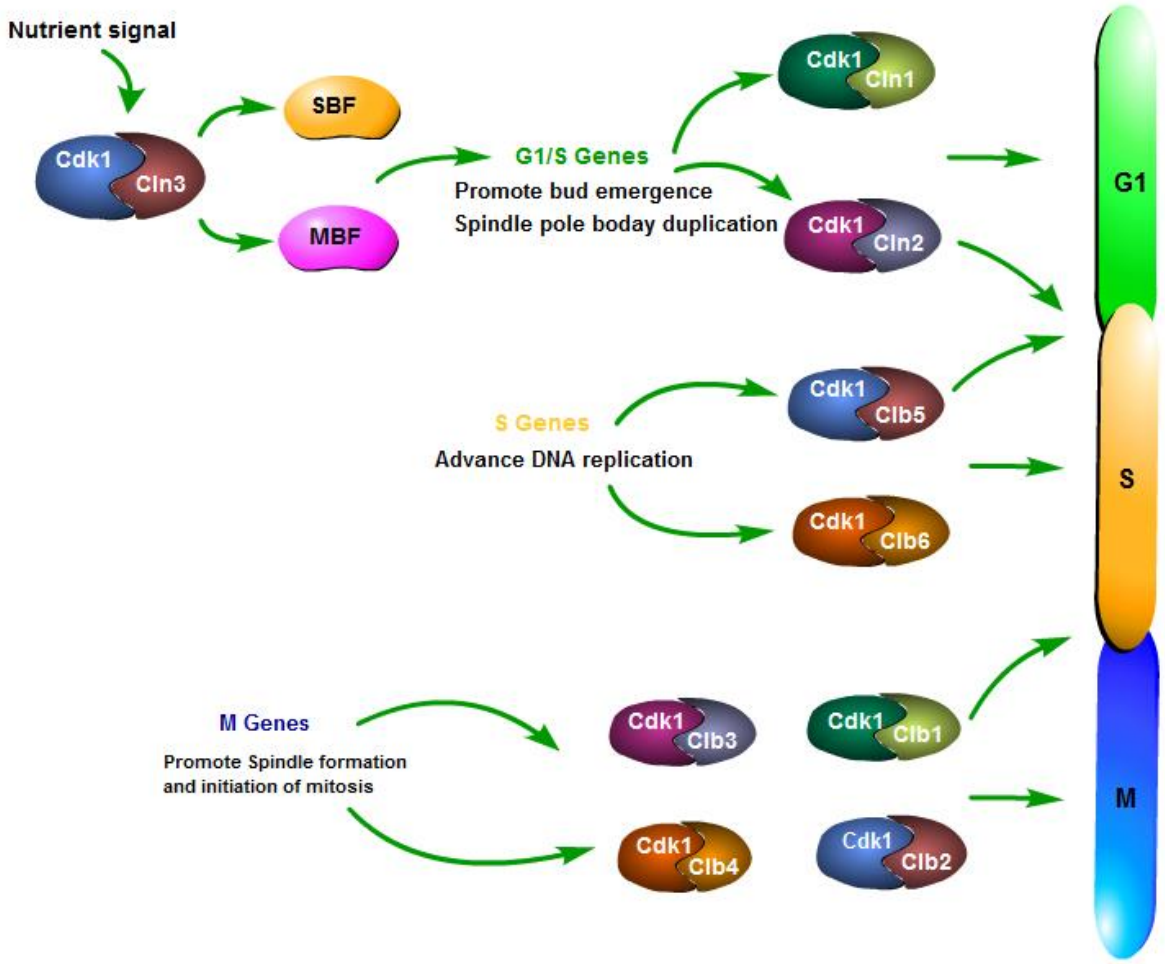

Figure 3.9 Controllers of the budding yeast cell cycle. Nutrient signals activate Cln3 transcription initiating the cell cycle in grown diploid and haploid cells. G1/S genes, S genes and M genes have responsibilities in each phase, some of which are stated in the figure.

model analysis (Barik et al., 2010; Tóth et al., 2007; Verdugo et al., 2013; Vinod et al., 2011); (2) cell cycle temporal, organisation-focused models, which explain the orderly progression of the cell cycle steps by the associated regulators (mainly Cdks and cyclins) periodical activation and inactivation (Chen et al., 2004; Hong et al., 2012; Tyson and Novak, 2008).

We approach the meiosis-mitosis initiation switch from the meiosis-initiation side since two major meiosis initiators (Ime1 and Ime2) have relationships with the most upstream mitosis initiator (Cdk1/Cln3). Therefore, hereafter, we present a comprehensive discussion of the available mathematical models of meiosis initiation in *Saccharomyces cerevisiae*. Comparably there are fewer mathematical models for meiosis than for mitosis. There are few discrete mathematical models (Rubinstein et al., 2007; Shen et al., 2010) and only one recent (constructed in a parallel time to this study) continuous mathematical model (Ray et al., 2013) related with meiosis initiation and progression in budding yeast.

The first meiosis initiation-related mathematical model of budding yeast is an extended Boolean network that includes the main initiator proteins, Ime1 and Ime2, and two hypothetical negative feedback loops (Rubinstein et al., 2007). This model, which is a discrete transition system, represents the initiation process by a graph (Figure 3.10) whose nodes represent RNA or proteins, and the edges denote regulation. This discrete model explains the qualitative behaviour of meiosis initiation including transient and sequential expression patterns of meiotic inducers under nutrient-starved conditions. This model is further used to explore variations in their basic network to identify the negative feedback loops which affect meiosis initiator transcription (Rubinstein et al., 2007). However, this discrete model restricts the protein/RNA expression level to a maximum value of nine, which limits the protein and mRNA expression only to that threshold value, cutting off further expression (Fig. 2A and 3A in Rubinstein et. al. (2007) (Rubinstein et al., 2007)). Further, the weights for each edge are decided without considering the actual mechanisms and do not provide a detailed representation; hence, hindering the accuracy of the prediction of the model.

The major focus of the second available model of yeast meiosis (Shen et al., 2010) is not on the detailed modelling of the meiosis process, but they use yeast meiosis as their modelling system to predict phenotypic consequences from environmental cues or genetic

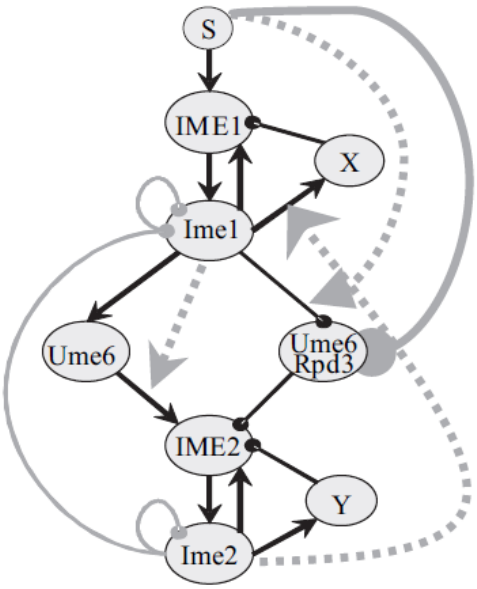

Figure 3.10 The schematic diagram of the extended Boolean network model proposed by Rubinstein et al. (2007) (Rubinstein et al., 2007), describing the relationships between the expression of IME1 and IME2. RNAs are written with capital letters. Solid black Arrows: activation, solid black lines with knob: repression, solid grey lines with a knob: degradation, dotted grey arrows: gating by the conjunction (AND), S: signal that induces meiosis. 'X' and 'Y' are the putative nodes used to shut down transcription of IME1 and IME2. (Adopted from Rubinstein et. al. (2007) (Rubinstein et al., 2007)).

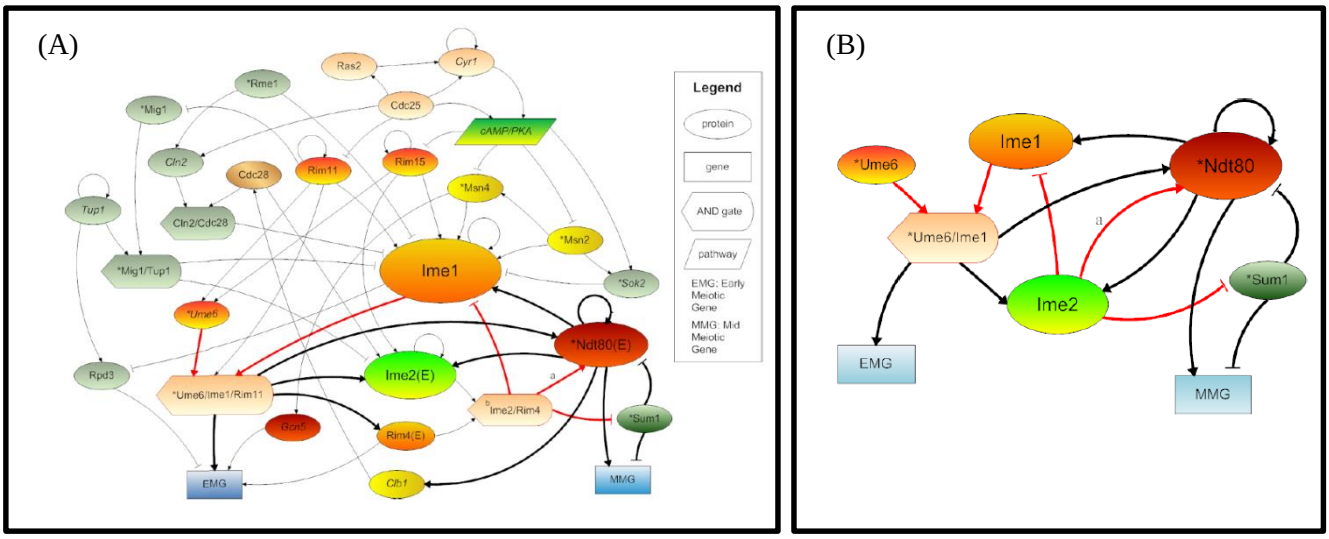

Figure 3.11 (A) The meiosis network developed in (Shen et al., 2010) using experimental evidence. (B) Meiosis network constructed from temporal micro array data and literature. Black colour relations are determined by a method using temporal microarray data. Red colour relations are the added protein-protein interactions because of their experimental importance (Adopted from Shen et. al. (2010) (Shen et al., 2010), Copyright Wei Wang).

perturbations. For this, they first construct a Boolean network using experimental evidence from the meiosis literature (Figure 3.11 A) and examine sporulation efficiency by deleting individual genes. All the genes correlated well with the experimental data, but they found that Rim11 and Ndt80 remained as outliers. Further, by disrupting each feedback loop they found no significant change in meiosis efficiency, thus, confirming that the network is robust to perturbations. Secondly, they exploit a new computational method called UMMI to find the most important regulatory interactions and present a hybrid model (Figure 3.11 B) with both UMMI-selected protein interactions (marked with black in Figure 3.11 B) and added protein interactions that they think are essential for meiosis (marked with red in Figure 3.11 (B)). However, the final proposed network is small that some of the important proteins and relations may be missing; specifically, it does not include the involvement of Rpd3, which is the major EMG repressor; and the disruption of self-activations showed a slight meiosis deficiency, thus, are not included in the model but, auto-regulation of Ime1 and Ime2 are essential for the transient transcription of these genes (Rubinstein et al., 2007).

In 2013, Ray et. al. developed an ordinary differential equation-based mathematical model for yeast sporulation, which is the most recent mathematical model constructed in a similar time to our study (Ray et al., 2013). The mathematical model, which only includes Ime1, Ime2, Rim11, Ume6, Sok2 and the feedback loops between them (Figure 3.12), simulates the orderly and transient dynamics of meiotic initiators. The model is validated using quantitative phenotypes of single gene knockouts. Similarly, as the first Boolean network model, this model also predicts that some feedback loops are essential for the transient expression of meiotic regulators with an auto-positive feedback loop of Ime2 required for its transient expression. The model is an abstract for a real pathway that incorporates only some components and claims that the effects of other molecules are reflected indirectly: the double negative feedback loop between Ime2 and Cdk1/Cln3 and the mutual activation between Ime2 and Ndt80 are both captured by auto-regulation of Ime2; Cdk1/Cln3, Msn2/4, Snf1 are collectively represented by an activation signal. However, some important well researched participants and connections, such as nitrogen involvement in Ime1 expression initiation, Rim15 involvement in Ime2 repression removal and Rpd3/Sin3 in EMG repression, are ignored in this model. The model predicts that Ime1 and Ime2 expression is transient but the maximum level of Ime2 is higher than that of Ime1 contradicting previously published extended Boolean network outputs and experimental

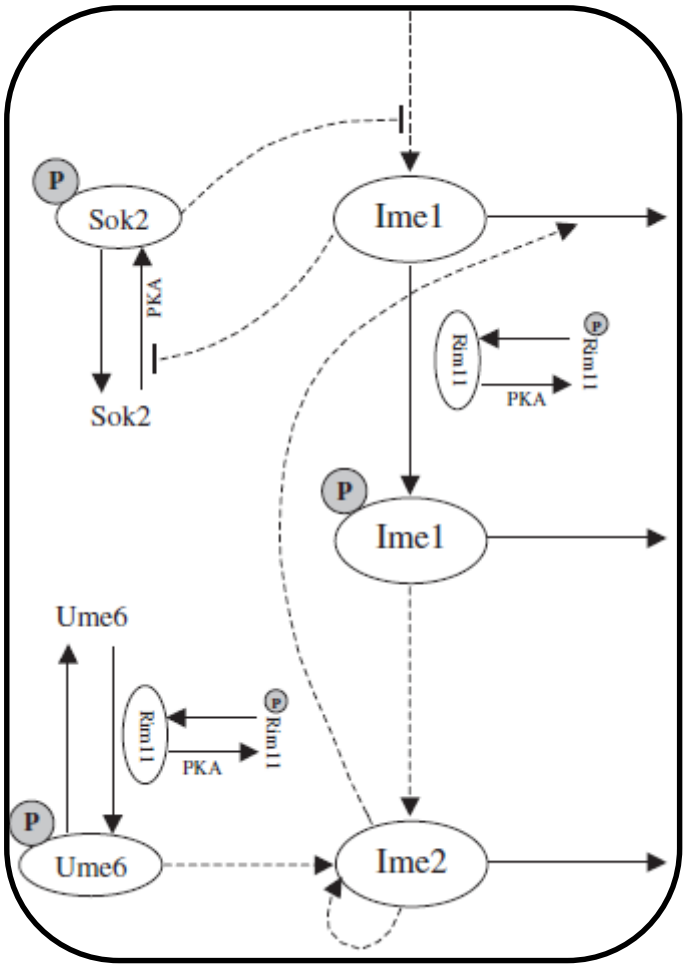

Figure 3.12 A schematic diagram of the meiosis initiation pathway modelled in Ray et. al. (2013) (Ray et al., 2013). Phosphorylated proteins are marked with the letter P. Dashed lines represent regulatory interactions; solid lines represent degradation, phosphorylation. This figure is adopted from Ray et. al. (2013) (Ray et al., 2013), © 2013 Ray et al.; licensee BioMed Central Ltd.

mRNA levels. (Figure 2 of Ray et. al. (2013) (Ray et al., 2013) compared with Fig. 2 of Rubinstein et. al. (2007) (Rubinstein et al., 2007)).

To date, there are no available models which explore the initial meiotic-mitotic switching behaviour in budding yeast under different nutrient conditions. For the purpose of understanding early meiosis-mitosis initiation of budding yeasts at the gene expression level, we develop a detailed model of yeast meiosis initiation extending the available Boolean network model published by Rubinstein et. al. (2007) (Rubinstein et al., 2007). We include the most recent experimental findings into the current model. After the extended Boolean model was published, new experimental studies have been carried out revealing interesting new relationships among the components of the initiation process: specifically, about the relationships of the meiosis initiators with Cdk1/Cln3 (Gurevich et al., 2010; Holt et al., 2007; Szwarcwort-Cohen et al., 2010), negative regulators of IME1 transcription and IME2 transient transcription (Rubinstein et al., 2007). Instead of a discrete Boolean model, we develop a continuous model at a biologically meaningful level of detail using available quantitative experimental data of protein expression, kinetic rates and temporal data. This continuous model facilitates us to undertake complex analyses such as phase space analysis and bifurcation analysis to obtain deeper insights, such as multi-stability, hysteresis and irreversibility. Using this model, which includes both meiosis and mitosis initiators, we explore the initial phase nutrient-dependent meiotic-mitotic switching behaviour in budding yeast, which is not investigated by meiosis models elsewhere to date.

Chapter 4

Biology of Meiosis and Mitosis Initiation into a Mathematical Model

"Perhaps a proper understanding of the complex regulatory networks making up cellular systems like the cell cycle will require a shift from common sense thinking. We might need to move into a strange more abstract world, more readily analysable in terms of mathematics than our present imaginings of cells operating as a microcosm of our everyday world" (Nurse, 2000).

In this chapter, we first sketch a conceptual model of meiosis initiation including the mitosis initiator and its relationship with the meiosis initiation network of budding yeast. This conceptual model is based on the biology presented in Chapter 3. We also present the set of assumptions on which this conceptual model is based. We then convert the relationships in this conceptual network into a mathematical model based on ordinary differential equations. Finally, we discuss how the parameters of the model are estimated, together with the reasoning behind the initial conditions selected.

4.1 Conceptual Model and Assumptions

We develop a conceptual model of budding yeast meiosis and mitosis initiation based on the biological information of yeast meiosis and mitosis, as reviewed in Chapter 3. This conceptual model is an extension of the available Boolean network model (Fig. 1 of Rubinstein et. al. (2007) (Rubinstein et al., 2007)); and we include the mitosis initiator, its relations with meiosis initiators and recent biological findings. The new conceptual model (Figure 4.1) includes the main meiosis initiators (Ime1 and Ime2), the main mitosis initiator (Cdk1/Cln3), the repressor of the EMGs (Rpd3/Sin3) and IME1 (Rpd3S), nutrients and other regulators (nitrogen and Rim15). Upon nitrogen depletion, the transcription of IME1 is transiently induced. Ime1 activates IME2 which, in turn, phosphorylates and tags Ime1 to degradation. IME1 transcription is auto-activated and repressed by Rpd3S and Cln3. Cln3 phosphorylates and transports Ime1 out of the nucleus. IME2, which possesses auto-activation, is repressed by Rpd3/Sin3 and this complex is revealed by the non-phosphorylated Rim15 and Rim11 in the absence of nitrogen. CLN3 expression is activated by nitrogen and Cln3 activates Cdk1 creating the complex, Cdk1/Cln3. The model includes a double negative feedback loop representing the antagonism between Ime2 and Cdk1/Cln3. We use biologically meaningful assumptions to present the information at a higher level of abstraction that encapsulates the essential mechanisms; the rationale for the assumptions as follows:

1. We assume that all the participating reactions take place in a single compartment, as meiosis and mitosis initiation can be considered as nuclear events (Kassir et al., 2003). Most of the transcriptional initiators, including Ime1 and Ime2, are localised to the nucleus of the yeast cell during meiosis initiation (Kominami et al., 1993; Pnueli et al., 2004). Even though the translation of mRNA happens in the cytoplasm and the meiosis related nutritional signals arrive from outside the plasma membrane through the cytoplasm to the nucleus, most of the meiosis related reactions happen inside the nucleus (Kassir et al., 2003). This assumption is the basis for modelling the system as a single compartment and the molecular transport times are ignored.

2. We mainly focus on the nutritional dependence of meiosis and mitosis initiation in grown diploid yeast cells. Therefore, the model is valid only for grown diploid yeast cells and we do not consider the cell type and size control in meiosis and mitosis initiation.

3. Nutrition affecting meiosis and mitosis initiation includes nitrogen, glucose and non-fermentable carbon sources such as acetate. Among the other nutrients, nitrogen plays a major role in meiosis and mitosis initiation regulation (Figure 1 of Kassir et. al. (2003), (Gurevich et al., 2010)). Furthermore, glucose plays a parallel role to nitrogen in meiosis and mitosis initiation (low glucose helps meiosis initiation and high glucose helps mitosis in a similar way to nitrogen) (Parviz and Heideman, 1998; Pnueli et al., 2004). Therefore, we focus only on the effects of nitrogen on meiosis and mitosis initiation; we assume glucose and other nutrients are available in appropriate amounts.

4. Under vegetative conditions the EMGs, including IME2, are repressed by Isw2 and Rpd3/Sin3. As the mechanism of Isw2 removal is not known, we assume that Isw2 is removed from the promoters in a parallel way to Rpd3 (Kassir et al., 2003), so its involvement in repression is not considered in the model.

5. We include the recent research finding of double negative feedback loops between Ime2 and Cdk1/Cln3 to our model, since this relationship would affect the switching dynamics. In one of the negative feedback loops between Ime2 and Cdk1/Cln3, the functionality of Cdk1 is inhibited by Ime2, since probably all known substrates of Cdk1 are phosphorylated by Ime2, inhibiting cell cycle progression (Holt et al., 2007; Szwarcwort-Cohen et al., 2009). Further, Cdk1 phosphorylates and tags Cln3 for degradation (Szwarcwort-Cohen et al., 2010). Since Cdk1 substrates are not included in our model, we assume that Ime2 phosphorylates Cdk1/Cln3 and perturbs its functionality.

6. Ime2 functionality is inhibited in the other negative feedback loop between Ime2 and Cdk1/Cln3; three phosphorylation sites exist in Ime2 where Cak1 and Cdk1 can bind and phosphorylate Ime2. Cak1 phosphorylation activates Ime2. Cdk1 phosphorylates Ime2 at the same sites where Cak1 binds for phosphorylation (Schindler et al., 2003). For simplicity, the involvement of Cak1 is not considered in this model; instead, it is

assumed that Ime2 activates itself and its activity is inhibited by Cdk1 phosphorylation. In this model we ignore the mediator, Ume6 on the EMG promoters and assume direct and simultaneous binding of Rpd3/Sin3 and Ime1 to EMGs.

7. As mentioned in the Chapter 2, upon nitrogen depletion, active Rim15 phosphorylates Ume6 and Sin3 thereby breaking the relationship between the Ume6 and Rpd3/Sin3 complexes. We assume the relief of Rpd3 on EMG promoter is proportional to the amount of active Rim15. Upon transformation to a meiotic medium, RIM15 is not transcribed, and the Rim15 protein gradually disappears (Pnueli et al., 2004). Since RIM15 gene regulation is unclear, we model the active Rim15 protein as a decreasing function from its maximum expression level (decided depending on the available nitrogen level) to a minimum level (Figure 4.3). According to this assumption, at the top level, active Rim15 degrades the Rpd3/Sin3 complex on the EMG promoters. Further, Rim11 phosphorylates Ime1, which then represses the Rpd3/Sin3 complex. For simplicity, we assume that Ime1 directly degrades Rpd3/Sin3. Further, we assume that the degradation of Ime1 also directly depends on Ime2 as Ime2 phosphorylates and tags Ime1 for degradation. We ignore the phosphorylations and de-phosphorylations associated with Rim11, Rim15 and Ime1, which implies that they are faster reactions, and the magnitude of the reaction rates are such that by ignoring these reactions the system dynamics would not change significantly.

8. According to the assumption of nuclear localisation of reactions, we assume that the phosphorylated Ime1 by Cln3 is degraded inside the nucleus rather than its actual transportation out of the nucleus. The Cdk1 expression in budding yeast is constant, and the stability, activity and expression of cyclins are regulated during the cell cycle (Miller and Cross, 2001; Pramila et al., 2002). Therefore, we assume that the amount of active Cdk1/Cln3 depends on Cln3 levels. Further, we assume Cdk1 has a higher level of relative abundance than Cln3.

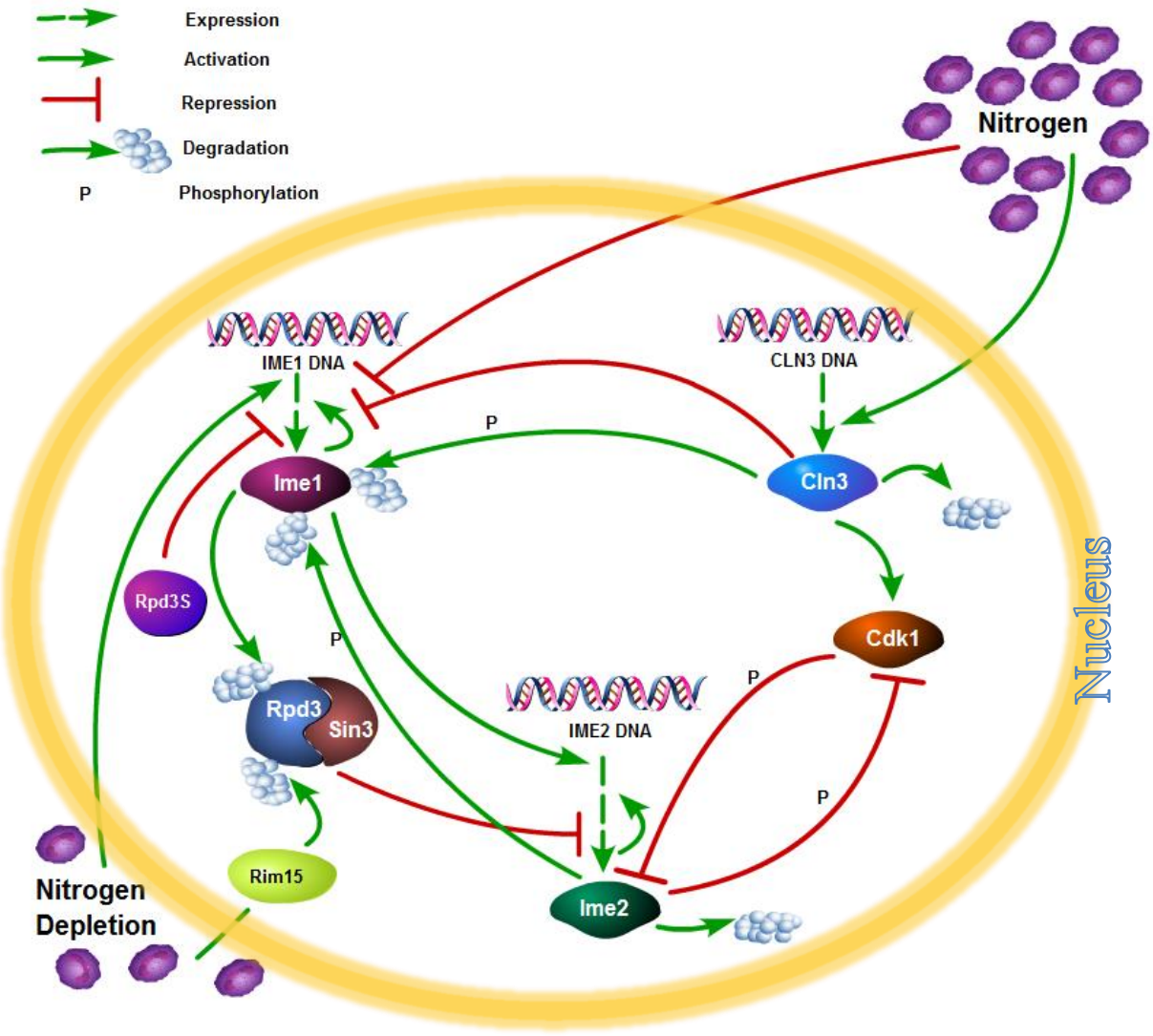

Figure 4.1 Schematic diagram of the model showing the meiosis and mitosis initiation regulatory mechanisms. Nitrogen depletion inhibits mitosis initiation by repressing Cln3 and helps meiosis initiation by activating IME1 expression and relieving Rpd3/Sin3 repression from EMGs via Rim15. Rising Ime1 levels activate IME2 transcription and relieve Rpd3/Sin3 repression. Ime2 activates the further downstream meiotic genes and phosphorylates Ime1, tagging it for degradation. Ime2 inhibits Cdk1/Cln3 functionality and prevents mitosis. Good nitrogen conditions activate the Cln3 expression for mitosis initiation. Cdk1s activated by Cln3 initiate the mitosis cell cycle. Meiosis initiation is inhibited during mitosis by the Ime2 deactivation by Cdk1 phosphorylation and the transcriptional repression of Ime1 by Cln3; at the same time, the Ime1 phosphorylated by Cln3 is transported out of the nucleus which is, instead, modelled as degradation inside the nucleus (Wannige et al., 2014).

4.2 Equations of the Model

Considering the time dependence of each component, the relations in the schematic diagram (Figure 4.1) are converted into a differential equation-based mathematical model to describe the rate of synthesis and degradation.

The protein synthesis rate is modelled as a function of transcription factor concentrations. Although these protein synthesis functions ignore mRNA level information, it is commonly used in systems biology modelling where protein synthesis patterns show similarities to their mRNA expression (Mehta et al., 2008; Novak and Tyson, 2004; Rosenfeld et al., 2005; Süel et al., 2006). We used this approach for protein synthesis functions, considering the similarities between the mRNA and protein expression levels of the meiosis initiators and the negligible nucleo-cytoplasmic transportation delay compared with the meiosis initiation time frame. The typical mRNA transcription time of *S.cerevisiae* is about one minute, including mRNA pre-processing time. The time to translate a protein takes about two minutes, including the nucleo-cytoplasmic transportation delay (Alon, 2007). Comparably, the meiosis initiation time frame is longer and about 20-25 hours (Rubinstein et al., 2007).

Equation (4-1) represents the temporal variation of active Ime1.

$$\frac{dfIme1}{dt} = \alpha_{fIme1} + \beta_{fIme1}\left[\left(\frac{fIme1^{n1}}{{K_{fIme11}}^{n1} + fIme1^{n1}}\right)\left(\frac{K_{N_2}^{n_2}}{K_{N_2}^{n_2} + N_2^{n_2}}\right)\left(\frac{K_{Rpd3SIme1}^{n_{11}}}{K_{Rpd3SIme1}^{n_{11}} + (Rpd3S)^{n_{11}}}\right)\left(\frac{K_{Cdk1/Cln3}^{n_9}}{K_{Cdk1\backslash Cln3}^{n_9} + Cdk1\backslash Cln3^{n_9}}\right)\right] - \gamma_{PIme1Cln3}\left(\frac{Cdk1\backslash Cln3^{n_{10}}}{Cdk1\backslash Cln3^{n_{10}} + K_{PIme1Cdk1\backslash Cln3}^{n_{10}}}\right) - d_{fIme1}(fIme2)(fIme1) \quad (4-1)$$

$$Rpd3S = \left(n_{12} - \left(n_{12}\left(1 - \exp(k(t-6))\right)\right)\right) \quad (4-1.1)$$

The first term (α_{fIme1}) on the right hand side (r.h.s) is the basal synthesis rate of Ime1 when the auto-regulation, nitrogen, Rpd3S and Cln3 repression are not happening. The second term describes the protein synthesis rate as a function of nitrogen, Cln3, Rpd3S and Ime1 transcription factor concentrations. Hill functions are used to model transcriptional activation, repression and phosphorylation, assuming these processes are ligand-receptor binding and unbinding reactions (Angeli et al., 2004; Dushek et al., 2011; Zi et al., 2010). The Rpd3S gene expression is unclear. Therefore, we model the Rpd3S level as a sigmoid increasing

function (Equation 4-1.1 and Figure 4.2) similarly as modelled in the extended Boolean model of meiosis initiation (Rubinstein et al., 2007). To correct the dimensions associated with time, we use a constant $k=1h^{-1}$ in (4 - 1.1). The next term describes the phosphorylation of Ime1 by Cln3 and the transportation of phosphorylated Ime1 out of the nucleus, which is assumed to be degradation. The last term represents the Ime1 protein degradation by itself and with the help of Ime2.

The following equation describes the rate of change of the active Ime2 protein:

$$\frac{dfIme2}{dt} = \alpha_{fIme2} + \beta_{fIme2}\left[\left(\frac{fIme2^{n_3}}{K_{fIme22}^{n_3} + fIme2^{n_3}}\right)\left(\frac{fIme1^{n_4}}{K_{fIme12}^{n_4} + fIme1^{n_4}}\right)\left(\frac{K_{Rpd3/Sin3}^{n_5}}{K_{Rpd3\backslash Sin3}^{n_5} + Rpd3\backslash Sin3^{n_5}}\right)\right] - \gamma_{PIme2}\left(\frac{Cdk1\backslash Cln3^{n_6}}{Cdk1\backslash Cln3^{n_6} + K_p^{n_6}}\right) - d_{fIme2}(fIme2) \quad (4-2)$$

The first term on the r.h.s. of Equation (4-2) is the basal synthesis rate of the Ime2 protein. IME2 expression is repressed by the Rpd3/Sin3 complex and activated by Ime1. IME2 is auto activated similarly as IME1. As it is assumed that the Ume6 is not involved in repression and Ime1 activation, they are directly modelled by using Hill functions in the second term. The third term represents the deactivation of Ime2 by Cdk1/Cln3 phosphorylation by a Hill function. The fourth term represents the normal self-degradation of the Ime2 protein.

The third equation corresponds to the variation of active Cdk1/Cln3 with time:

$$\frac{dCdk1\backslash Cln3}{dt} = \alpha_{Cln3} + \beta_{Cdk1CLn3}\left(\frac{N_2^{n_7}}{K_{N_2Cln3}^{n_7} + {N_2}^{n_7}}\right) - \gamma_{PCdk1Cln3}\left(\frac{fIme2^{n_8}}{K_{PIme2Cdk1}^{n_8} + fIme2^{n8}}\right) - d_{Cln3}(Cdk1\backslash Cln3) \quad (4-3)$$

As the Cdk1 protein is assumed to be constantly abundant and as its activation depends on Cln3, the expression rate of active Cdk1/Cln3 depends only on nitrogen activation. The first term on the r.h.s represents the basal expression rate and the second term models the activation of Cln3 expression by a Hill type function. According to the assumption that Cdk1/Cln3 can be inactivated by the phosphorylation of Ime2, this phosphorylation relationship is modelled with a Hill type function. This phosphorylated Cdk1/Cln3 amount is

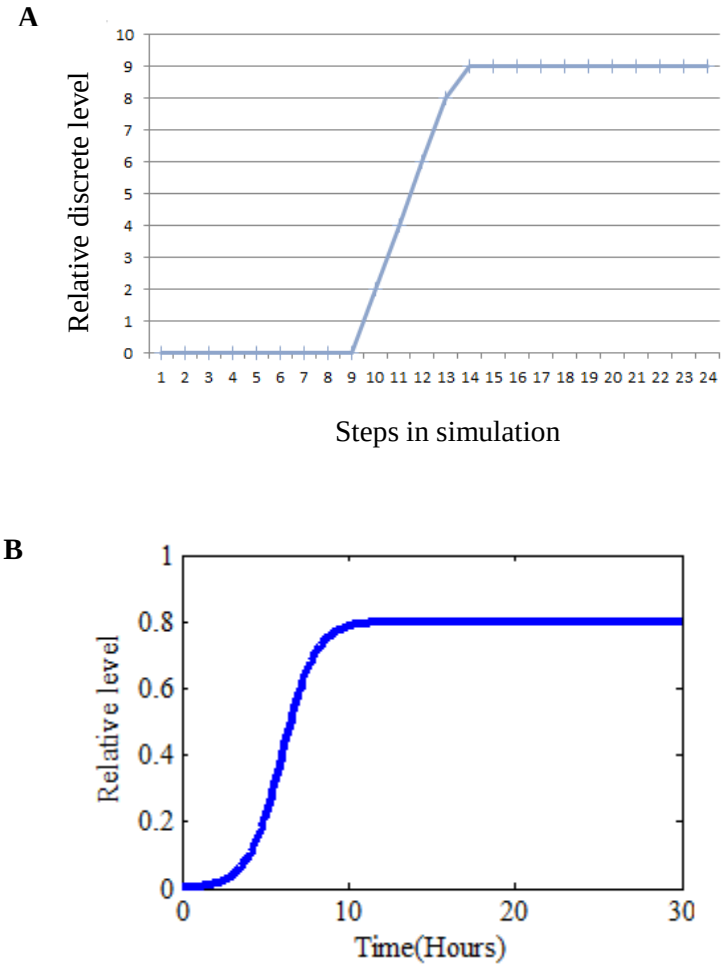

Figure 4.2 Variation of Rpd3S, which is recruited to the IME1 promoter. (A) The variation of Rpd3S modelled by the extended Boolean network. (B) The modelled Rpd3S temporal variation according to Equation (4-1.1).

subtracted as it inactivates Cdk1/Cln3 functionality. The last term represents the self-degradation of Cdk1/Cln3.

The fourth equation describes the temporal variation of the Rpd3/Sin3 complex on the EMG promoter:

$$\frac{dRpd3\backslash Sin3}{dt} = \alpha_{Rpd3Sin3} - d_{Rpd3Sin3}\, fIme1\, Rim15 \qquad (4-4)$$

$$Rim15 = \frac{1}{N_2}\left(\frac{n_{13}}{n_{15} + \exp(k1.6t)} + n_{14}\right) \qquad (4-4.1)$$

The first term on the r.h.s. describes the formation rate of Rpd3/Sin3 complex. As mentioned in Section 4.1, the separation of Rpd3/Sin3 from Ume6 is simplified and we assume that the Rpd3/Sin3 complex is degraded proportional to the amounts of Ime1 and Rim15 available. The Rim15 term represents the related relief of Rpd3/Sin3, which depends on the amount of active Rim15. Since RIM15 gene regulation is unclear, we model the active Rim15 protein as a decreasing function from the maximum expression level (depending on the available nitrogen level) to a minimum (Equation (4-4.1), as shown in Figure 4.3, using the following available facts: Upon transformation to a meiotic medium RIM15 is not transcribed and Rim15 protein degrades and disappears (Figure 4.3 A) (Pnueli et al., 2004); with good nutrients, Rim15 is unavailable as it is inactivated by phosphorylation (Figure 4.3 B). To correct the dimensions associated with time, we use a constant $k=1h^{-1}$ in (4 - 4.1). All parameters in the model and their biological significance are given in Table 4.1.

Table 4.1 . Biological Significance, values and units of parameters, constants and variables of the main model given in the equations 4-1 to 4-4.1. Unit of time is in hours.

Name	Biological Significance	Value	Unit
Parameters			
α_{fIme1}	Basal transcription rate of Ime1	0.0004	nMh^{-1}
α_{fIme2}	Basal transcription rate of Ime2	1.9	nMh^{-1}
α_{Cln3}	Basal transcription rate of Cln3	6.74	nMh^{-1}
$\alpha_{Rpd3Sin3}$	Complex formation rate of Rpd3/Sin3	1.2859	nMh^{-1}
β_{fIme1}	Maximal transcription rate of Ime1	17	nMh^{-1}
β_{fIme2}	Maximal transcription rate of Ime2	40.92	nMh^{-1}
$\beta_{Cdk1\backslash Cln3}$	Maximal transcription rate of Cdk1/Cln3	106.612	nMh^{-1}
K_{fIme11}	Disassociation constant of Ime1 binding to its own promoter	10	nM
K_{N_2}	Disassociation constant of nitrogen binding to IME1 promoter	2.55	nM
d_{fIme1}	Degradation rate of Ime1 protein	0.028	$nM^{-1}h^{-1}$
n_1	Hill coefficient of Ime1 auto regulation	2.8	----
n_2	Hill coefficient of nitrogen repression on IME1 promoter	2.8	----
K_{fIme22}	Disassociation constant of Ime2 binding to its own promoter	40.8	nM
K_{fIme12}	Disassociation constant of Ime1 binding to IME2 promoter	4.65	nM
$K_{Rpd3\backslash Sin3}$	Disassociation constant of Sin3/Rpd3 binding to IME2 promoter	33.0	nM
$K_{Cdk1\backslash Cln3}$	Disassociation constant of Cdk1/Cln3 binding to IME1 promoter	70.325	nM
$K_{Rpd3SIme1}$	Disassociation constant of Rpd3S binding to IME1 promoter	105.3	nM
γ_{PIme2}	Maximal phosphorylation rate of Ime2 by Cdk1/Cln3	20.76	nMh^{-1}
K_p	Dephosphorylation constant of Cdk1/Cln3 from Ime2	80.1408	nM
n_3	Hill coefficient of Ime2 auto regulation	2.06	----
n_4	Hill coefficient of Ime1 activation on IME2 promoter	0.5679	----
n_5	Hill coefficient of Rpd3/Sin3 repression on IME2 promoter	2.8	----
n_6	Hill coefficient of phosphorylation of Ime2 by Cdk1/Cln3	2.803	----
d_{fIme2}	Degradation rate of Ime2 protein	0.149	h^{-1}
K_{N_2Cln3}	Disassociation constant of nitrogen binding to Cln3 promoter	19.4	nM
n_7	Hill coefficient of nitrogen activation on Cln3 promoter	2.85	----
$\gamma_{PCdk1Cln3}$	Maximal phosphorylation rate of Cdk1/Cln3 by Ime2	50.1	nMh^{-1}
$\gamma_{PIme1Cln3}$	Maximal phosphorylation rate of Ime1 by Cdk1/Cln3	1.1384	nMh^{-1}
$K_{PIme2Cdk1}$	Dephosphorylation constant of Ime2 from Cdk1/Cln3	100.987	nM
$K_{PIme1Cdk1\backslash Cln3}$	Dephosphorylation constant of Ime1 by Cdk1/Cln3	125.987	nM
n_8	Hill coefficient of phosphorylation of Cdk1/Cln3 by Ime2	2.8	----
n_9	Hill coefficient of Cdk1/Cln3 repression on IME1 promoter	2.8	----
n_{10}	Hill coefficient of phosphorylation of Ime1 by Cdk1/Cln3	2	----
n_{11}	Hill coefficient of Rpd3S repression on IME1 promoter	2.8	----
n_{12}	Constant related to Rpd3S temporal variation	0.8	----
n_{13}	Constant related to Rim15 temporal variation	37	----
n_{14}	Constant related to Rim15 temporal variation	0.06	----
n_{15}	Constant related to Rim15 temporal variation	0.01	----
d_{Cln3}	Degradation rate of Cdk1/Cln3 protein complex	0.2999	h^{-1}
$d_{Rpd3Sin3}$	Degradation rate of Rpd3/Sin3 protein complex	0.05348	nMh^{-1}
Constants			

$fIme1_o$	Maximum concentration of Ime1 protein	100	nM
$fIme2_o$	Maximum concentration of Ime2 protein	100	nM
N_{2o}	Maximum concentration of Nitrogen	6	nM
$Sin3/Rpd3_o$	Maximum concentration of Sin3/Rpd3 complex	100	nM
$Cdk1/Cln3_o$	Maximum concentration of Cdk1/Cln3 complex	100	nM
$Rpd3S_o$	Maximum concentration of Rpd3S protein	100	nM
$Rim15_o$	Maximum concentration of Rim15 protein	100	nM
k	Constant used for the corrections of dimensions	1	h^{-1}
Variables			
$fIme1$	Concentration of Ime1 protein	----	nM
$fIme2$	Concentration of Ime2 protein	----	nM
$Cdk1\backslash Cln3$	Concentration of Cdk1/Cln3 complex	----	nM
$Rpd3\backslash Sin3$	Concentration of Sin3/Rpd3 complex	----	nM
N_2	Concentration of Nitrogen	----	nM
$Rpd3S$	Concentration of Rpd3S protein	----	nM
$Rim15$	Concentration of Rim15 protein	----	nM

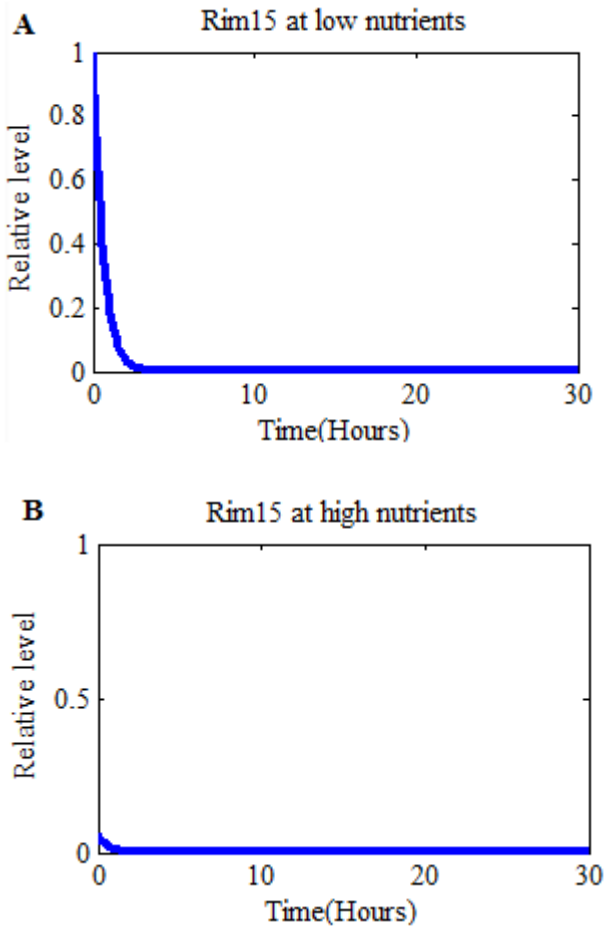

Figure 4.3 The modelled active Rim15 temporal variation according to Equation (4-4.1). (A) Upon transferring to meiotic conditions, Rim15 is active but is not transcribed, therefore the available Rim15 protein amount degrades. (B) With good nutrients, the Rim15 protein is inactivated by phosphorylation, therefore, Rim15 levels are negligible (Wannige et al., 2014).

4.3 The Partially Non-dimensionalised Model

We non-dimensionalised the concentration terms of the model using the total protein levels, as this approach reduces the complexity of our model and the results can easily be compared with the available experimental, relative concentration levels (G et al., 2006). We define this process as partial non-dimensionalisation because only the dimensions of the concentration terms are removed from the model equations. In this partial non-dimensionalisation, a fraction of protein level to the total amount is used instead of the absolute protein values. The protein concentrations are non-dimensionalised using their fractional amount to the maximum value. The defined non-dimensional variables are given in Equation (4-5), and all equations of the non-dimensionalised model are given in Table 4.2. The variable names with the top bar represent the concentration as a fraction of the maximum value. The maximum concentration amounts are represented by a subscript zero.

The non-dimensionalised model was numerically solved using the 'Ode45s' function in Mathlab R2010a (The Mathworks, Natick, MA, and U.S.A).

$$fIme1 = \overline{fIme1}\, fIme1_o \ , \qquad fIme2 = \overline{fIme2}\, fIme2_o \ ,$$
$$Cdk1\backslash Cln3 = \overline{Cdk1\backslash Cln3}\, Cdk1\backslash Cln3_o \ , \ Rpd3\backslash Sin3 = \overline{Rpd3\backslash Sın3}\, Rpd3\backslash Sin3_o$$
$$N_2 = \overline{N_2}\, N_{2o} \ , \ Rpd3S = \overline{Rpd3S}\, Rpd3S_o \ , Rim15 = \overline{Rım15}\, \overline{Rım15_o} \qquad (4\text{ - }5)$$

Table 4.2 The partially non-dimensionalised equations after removing units of concentration.

$$\frac{d\overline{fIme1}}{dt} = \frac{\alpha_{fIme1}}{fIme1_o} + \frac{\beta_{fIme1}}{fIme1_o}\left[\left(\frac{\overline{fIme1}^{n1}}{\left(\frac{K_{fIme11}}{fIme1_o}\right)^{n1} + \overline{fIme1}^{n1}}\right)\left(\frac{K_{N_2}^{n_2}}{K_{N_2}^{n_2} + (N_{2o}\overline{N_2})^{n_2}}\right)\left(\frac{K_{Rpd3SIme1}^{n_{11}}}{K_{Rpd3SIme1}^{n_{11}} + \left(\overline{Rpd3S}\, Rpd3S_o\right)^{n_{11}}}\right)\left(\frac{K_{Cdk1\backslash Cln3}^{n_9}}{K_{Cdk1\backslash Cln3}^{n_9} + \left(Cdk1\backslash Cln3_o\overline{Cdk1\backslash Cln3}\right)^{n_9}}\right)\right]$$

$$- \frac{\gamma_{PIme1Cln3}}{fIme1_o}\left(\frac{\overline{Cdk\backslash Cln3}^{n_{10}}}{\overline{Cdk1\backslash Cln3}^{n_{10}} + \left(\frac{K_{PIme1Cdk1\backslash Cln3}}{Cdk1\backslash Cln3_o}\right)^{n_{10}}}\right) - d_{fIme1}\left(\overline{fIme2}\right)\left(\overline{fIme1}\right)(fIme2_o) \qquad (4-6)$$

$$\frac{d\overline{fIme2}}{dt} = \frac{\alpha_{fIme2}}{fIme2_o} + \frac{\beta_{fIme2}}{fIme2_o}\left[\left(\frac{\overline{fIme2}^{n_3}}{\left(\frac{K_{fIme22}}{fIme2_o}\right)^{n_3} + \overline{fIme2}^{n_3}}\right)\left(\frac{\overline{fIme1}^{n_4}}{\left(\frac{K_{fIme12}}{fIme1_o}\right)^{n_4} + \overline{fIme1}^{n_4}}\right)\left(\frac{K_{Rpd3\backslash Sin3}^{n_5}}{K_{Rpd3\backslash Sin3}^{n_5} + (Rpd3\backslash Sin3_o\,\overline{Rpd3\backslash Sin3})^{n_5}}\right)\right]$$

$$- \frac{\gamma_{PIme2}}{fIme2_o}\left(\frac{\overline{Cdk1\backslash Cln3}^{n_6}}{\overline{Cdk1\backslash Cln3}^{n_6} + \left(\frac{K_{Cdk1\backslash Cln3}}{\overline{Cdk1\backslash Cln3}_o}\right)^{n_6}}\right) - d_{fIme2}\left(\overline{fIme2}\right) \qquad (4-7)$$

$$\frac{d\overline{Cdk1\backslash Cln3}}{dt} = \frac{\alpha_{Cln3}}{Cdk1\backslash Cln3_o} + \frac{\beta_{Cdk1\backslash Cln3}}{Cdk1\backslash Cln3_o}\left(\frac{\bar{N}_2^{n_7}}{\left(\frac{K_{N_{2Cln3}}}{\bar{N}_{2o}}\right)^{n_7} + \bar{N}_2^{n_7}}\right) - \frac{\gamma_{PCdk1Cln3}}{Cdk1\backslash Cln3_o}\left(\frac{\overline{fIme2}^{n_8}}{\left(\frac{K_{PIme2Cdk1}}{fIme2_o}\right)^{n_8} + \overline{fIme2}^{n8}}\right)$$

$$- d_{Cln3}\left(\overline{Cdk1\backslash Cln3}\right) \qquad (4-8)$$

$$\frac{d\overline{Rpd3\backslash Sin3}}{dt} = \frac{\alpha_{Rpd3Sin3}}{Rpd3\backslash Sin3_o} - d_{Rpd3Sin3}\frac{\overline{fIme1}fIme1_o}{\overline{N_2}N_{2o}Rpd3\backslash Sin3_0}\overline{Rim15}Rim15_o \qquad (4-9)$$

Where,

$$Rpd3S = \left(n_{12} - \left(n_{12}\left(1 - \exp(k(t-6))\right)\right)\right)$$

$$Rim15 = \left(\frac{n_{13}}{n_{15} + \exp(k1.6t)} + n_{14}\right)$$

4.4 Parameter Estimation

We use experimentally measured value ranges to determine the specific set of parameters given in Table 4.3. When the whole range of a parameter is unavailable, the available parameter values are allowed to vary fifty times from the highest reference experimental value and one fiftieth from the lowest reference value, to cover experimental error and cellular heterogeneity. Kinetic rates for phosphorylation and complex formation are unavailable. Therefore, we assign ranges that we consider to be realistic so that the output matches the given biological criteria. We assume that these parameter values remain constant during a range of nutrient levels (at both meiosis and mitosis conditions) since kinetics rates are normally affected by temperature and pressure assumed as constants in this work.

We then include the known qualitative features between some parameters, such as protein degradation rates. For example, we consider the fact that Ime2 is an unstable protein and has a higher degradation rate than Ime1. We fine-tune the parameters (Table 4.1) using the trial and error method in a biologically meaningful way according to the following criteria: model produces transient and sequential meiosis initiation signals of its main initiators (Ime1 and Ime2) under nitrogen depletion (In meiosis, nitrogen is input as a constant low level of 0.06); the Cdk1/Cln3 and Rpd3/Sin3 levels are similar to their experimental expression, model captures the qualitative behaviour of the considered mutation studies: Ime1, Ime2, Rim15 deletion, Cln3 overexpression. We validate the model asking biologically meaningful questions based on some qualitative mutant studies (Ime2 copy number variation, Rpd3S mutation) from the model. These mutation studies are discussed in detail in the following chapter.

4.5 Initial Conditions

Typical meiosis initiation conditions include a low basal level of Ime1 and a high level of Rpd3/Sin3 (Rubinstein et al., 2007). The initial and maximum protein concentrations are calculated as follows: the ellipsoidal budding yeast cells have a large diameter of 5-10 μm and a small diameter of 1-7μm (Schaechter, 2011). Assuming the nucleus radius of length as 3.75 μm, width as 2.5 μm and height as 2 μm, volume of an ellipsoid is -

$$V = 4/3 * \pi * \text{radius of length} * \text{radius of width} * \text{radius of height}$$
$$= 7.85 \times 10^{-14} \text{ L} = 7.85 \times 10^{-17} \text{ m}^3.$$

The number of molecules corresponding to 1nM

$$= (7.85 \times 10^{-17} \text{ m}^3) \times (10^{-6} \text{ mole/m}^3) \times (6 \times 10^{23} \text{ molecules/mole})$$
$$= 47.1 \text{ molecules.}$$

The Ime2 protein abundance in a rich medium is 538 molecules per cell (Lu et al., 2006), and this number is assumed to be the basal level of each protein in our model (10-11 nM). As the maximum Ime1 protein expression level is around the relative levels of six and seven (β-gal units: 60 and 70) in Shefer-Vaida et. al. (1995), the maximum protein level chosen is 100 nM, which facilitated us in obtaining a good result presentation. Considering the maximum Ime1 protein expression relative level of 6 (Shefer-Vaida et al., 1995) and, as the experiments revealed that Rpd3/Sin3 is at its maximum activity in the initial stage (Pnueli et al., 2004; Rubinstein et al., 2007), the initial concentration for Rpd3/Sin3 is chosen to be 60 nM (six times larger than the basal level). According to the experimental levels of Cln3 expression (Fig. 7 of Gallego et. al. (1997) (Gallego et al., 1997)), the basal level of Cln3 is also assumed to be a basal level of 10 nM. Later, we non-dimensionalise these concentrations so that the maximum expression level is 1 (corresponds to 100 nM) and the minimum is zero to match with the experiments.

Table 4.3 Initial parameter ranges used for parameter estimation (biological significance of parameters are given in Table 4.1) (Wannige et al., 2014).

Parameter description	Range (in nM and hours)	Source and description
Basal Transcription rate(TR): $\alpha_{fIme1}, \propto_{fIme2}, \propto_{Cln3}$	[2.8e-3 - 7]	Median TR is 7 mRNA/hour in yeast genes and minimum TR is beyond 27 mRNA/h (Pelechano et al., 2010). Basal TR reference value; 7 mRNA/h = 0.14 nM/h (47.1 molecules in 1 nM). Calculating upper and lower limits using 0.14 as reference and allowing 50 times to vary around reference value, range becomes [2.8e-3 - 7].
Maximal transcription rate:$\beta_{fIme1}, \beta_{fIme2}, \beta_{Cln3}$	[0.012 - 218.34]	90% of yeast genes have TRs between 2-30 mRNA/h. Highest transcribed genes have TR of 206 mRNA/h (Pelechano et al., 2010). Reference value for the TR minimum: 30 and maximum:206 mRNA/h. Calculating upper and lower limits using (30 - 206) mRNA/h as reference range and allowing 50 times to vary around reference values, range becomes [0.012 - 218].
Transcriptional factor(TF) disassociation rate from DNA: $K_{fIme11}, K_{N_2}, K_{fIme22}$, $K_{fIme12}, K_{Rpd3\backslash Sin3}$, $K_{Cdk1\backslash Cln3}$, $K_{Rpd3SIme1}$	[0.592 - 138.6]	As more specific data was unavailable, we used the research carried out by J.C.Dorsman et al. (1990)(Dorsman et al., 1990) who determined the disassociation half-time of yeast general TF : GFI. They determined disassociation rates for several DFI-DNA complexes and found that it varied over 70- fold. Range from table III : [0.3 - 70]min directly converting to rate [0.592-138.6]/h
Hill coefficient s: $n_1, n_2, n_3, n_4, n_5, n_6$, $n_7, n_{8,} n_9, n_{10}, n_{11}$	[0 - 2.8]	According to experiments of Hao (2008) (Hao et al., 2008), Hill coefficient for activation of MAP kinases, Kss1 and Fus3 are 1.3 and 2.2 respectively. As other specific data is unavailable, considered the biologically realistic range of [0 - 2.8]
Protein degradation rate: d_{fIme1}, d_{fIme2}	[9.16e-3 - 24.15]	Archana Belle et al. (2006) (Belle et al., 2006) measured the half-life of 3751 proteins and found that half life is log normal distributed with a mean and median of 43 min and Fig 1C shows maximum half-life is beyond 181mins. Therefore the degradation rate/h range was calculated directly by ln(2)/half-life is [9.16e-3 - 24.15].
Protein complex degradation rate: $d_{Rpd3Sin3,} d_{Cdk1Cln3}$	[9.16e-3 - 24.15]	

Chapter 5

Understanding Meiosis and Mitosis Initiation at the Gene Expression Level through the Model

"If we hope to understand biology, instead of looking at one little protein at a time, which is not how biology works, we will need to understand the integration of thousands of proteins in a dynamically changing environment. A computer will be the biologist's number one tool." Craig Venter (Butler, 1999).

In this chapter, we try to understand the meiosis and mitosis initiation of budding yeast at the gene expression level using the model constructed. We simulate meiosis initiation and mitosis initiation at extreme nutrient levels. All predictions and mutation studies are compared with the experimental data. We investigate the roles of some individual components in meiosis initiation by deleting, overexpressing and varying the DNA copy number of those components. We then discuss some organism-level experimental mutant analysis results at the gene expression level using the model's predictions. Further, we clarify the conflicting results of two mutation studies using the model simulations. We compare the results of the constructed model with the available models of meiosis initiation to find the advantages and limitations of each model in predicting meiosis initiation, mitosis initiation and gene deletion mutant analyses.

5.1 Temporal Variation of Proteins during Meiosis and Mitosis Intiation

Meiosis and mitosis initiation are tightly regulated processes which happen only under the correct conditions. In this section, we employ our model to understand meiosis and mitosis initiation at the gene expression level. We first discuss the temporal variations of the main proteins in meiosis initiation.

5.1.1 Meiosis initiation in nitrogen depletion .

Meiosis initiates in nitrogen depletion conditions (Kassir et al., 2003). To initiate meiosis, the nitrogen depletion signal is input to the model in two ways: at a low, constant nitrogen level and a decreasing sigmoid function around the low nitrogen level. We present the results corresponding to the low, constant nitrogen level (0.06) in Figure 5.1 and similar results were observed to the other input type. The resulting Ime1 and Ime2 expressions are transient and sequential, as expected, and transient expressions of initiators are vital for the efficient entry into the meiosis developmental pathway (Rubinstein et al., 2007; Shefer-Vaida et al., 1995). The Ime1 protein peaks during six to nine hours and the active Ime2 protein peaks during 15-17 hours, delaying by three to four hours than the pure Ime2 peak expression by the phosphorylations of Cdk1/Cln3. Ime2 expression without post-translational modifications peaks at around 11-13 hours (Nachman et al., 2007; Shefer-Vaida et al., 1995). These protein synthesis patterns show similarities to their experimental mRNA expression (Fig. 2 (b) of Rubinstein et. al. (2007) and (Shefer-Vaida et al., 1995; Sherman et al., 1993)).

5.1.2 The behaviour of Cdk1/Cln3 and Rpd3/Sin3

The modelled Cdk1/Cln3 levels reside in low levels under meiotic conditions (Figure 5.1). These low levels are required for arresting the G1 phase of the yeast cell cycle (Gallego et al., 1997; Gupta, 2009). In contrast, Cdk1/Cln3 levels are high under mitotic conditions (Gupta, 2009). When the nitrogen levels are varied from high to low values in our model, the resulting patterns of Cdk1/Cln3 expression are consistent with their experimental patterns of expression (Gallego et al., 1997). We compare experimentally-measured Cln3 with the modelled Cdk1/Cln3, as we assume that Cdk1s are abundant to form Cdk1/Cln3 complex thereby representing the available Cln3 levels.

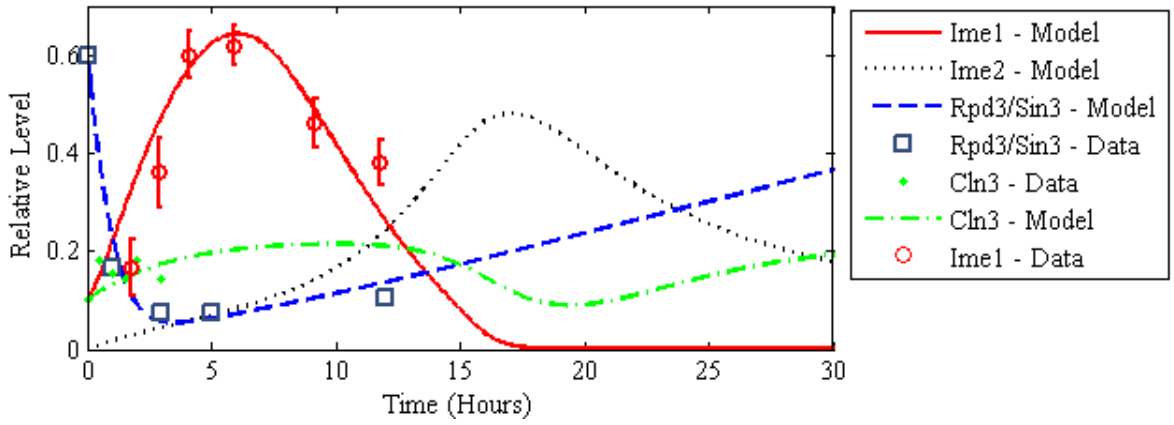

Figure 5.1 The modelled meiosis initiation related protein variation in the sporulation medium (SPM). The circles and their error bars represent the scaled data from the Ime1 protein expression patterns measured in beta-galactose (β gal) units from Shefer-Vaida et. al. (1995) (Shefer-Vaida et al., 1995). The filled circles represent the scaled data from Fig. 7 B of Gallego et. al. (1997) (Gallego et al., 1997). The squares represent the scaled data from Fig. 2 D of Pnueli et. al. (2004) (Pnueli et al., 2004). Initial conditions for the model were within the normal range under which meiosis initiation occurs: 0.1 for Ime1 and 0.6 for the Rpd3/Sin3 concentration, constant level of 0.06 for nitrogen concentration, 0.1 for Cln3 and 0 for the other proteins (Wannige et al., 2014).

Rpd3/Sin3 occupies and represses the EMG promoters including IME2, under non-meiotic conditions (Pnueli et al., 2004). Our model's results for the Rpd3/Sin3 complex show a sudden decrease in its concentration during the initial stage of meiosis (Figure 5.1). This trough during 12-15 hours is related to the Ime2 peak, which is an EMG representative. In fact, the relief of IME2 repression (induced by Rpd3/Sin3) increases the histone acetylation and Ime2 expression, which are consequences of this decrease of Rpd3/Sin3. The slight increment in the Rpd3/Sin3 complex at later meiotic stage correlates to the re-association of the Rpd3/Sin3 complex on IME2 promoters to repress IME2 expression (Pnueli et al., 2004).

5.1.3 Mitosis-type division initiation in rich nitrogen conditions

The model predicts that meiosis initiator (Ime1 and Ime2) levels are low and mitosis initiator (Cdk1/Cln3) levels are high in rich nitrogen levels (Figure 5.2). These results are consistent with the experimental results; a low basal level of Ime1 exists, and Ime2 is absent in the nucleus during vegetative conditions (Sagee et al., 1998). The Cln3 expression prediction of our model agrees with the experimental results of Gallego et. al. (1997). The Rpd3/Sin3 complex on the promoters shows a high value in our model output. This is reasonable because a high amount of Rpd3/Sin3 resides on IME2 promoters to repress IME2 expression under rich nitrogen conditions.

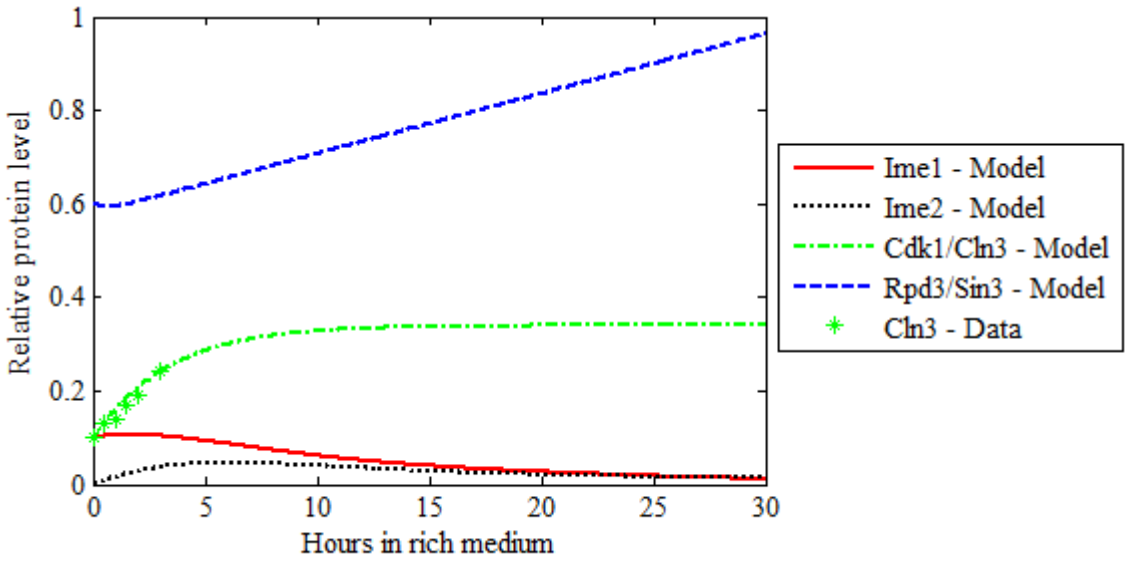

Figure 5.2 The behaviour of proteins at high nitrogen concentration (at a level of 1). The meiosis initiator levels are low and the mitosis initiator level is high. Stars represent the scaled Cln3 expression data from Fig. 7 B of Gallego et. al. (1997) (Gallego et al., 1997) . Initial conditions other than nitrogen were set as stated in Figure 5.1.

5.2 Understanding Mutation Studies using the Model

5.2.1 Basic mutant studies

We also check whether our model could reproduce the available basic mutant studies. Experiments show that the deletion of Ime2 from the budding yeast cells results in a non-transient, increased expression of the Ime1 protein. This increment in Ime1 reflects that the Ime2 related degradation of Ime1 does not take place because of the unavailability of the Ime2 protein. Our model also produces a non-transient expression pattern of Ime1 when the Ime2 related terms are removed from the model equation corresponding to Ime1 (Equation (4-1)) (Figure 5.3 A). We also delete the Ime1-, Rim11- and Rim15-related terms from our model and observe that the results agree well with the corresponding experiments. The deletion of Ime1, Rim11 and Rim15 are discussed in detail later in this chapter (Section 5.3.3), when we compare our model results with the other available models.

Experiments further show a quadratic trend in the maximum Ime1 level when the IME1 copy number is altered from one copy to five copies. We also change the Ime1 copy number according to the experiments (Gurevich et al., 2010). During simulations, the IME1 copy number is multiplied by the Ime1 expression terms of basal transcription level and maximal transcription level in the model equation corresponding to Ime1 (Equation (4-1)). Further, we set the initial conditions similar to previous experiments (from Figure 3 B, first row of Gurevich et. al. (2010)). Results show a quadratic trend in the maximum Ime1 level to the copy number (Figure 5.3 B) with a good agreement to the corresponding experiments (Gurevich et al., 2010).

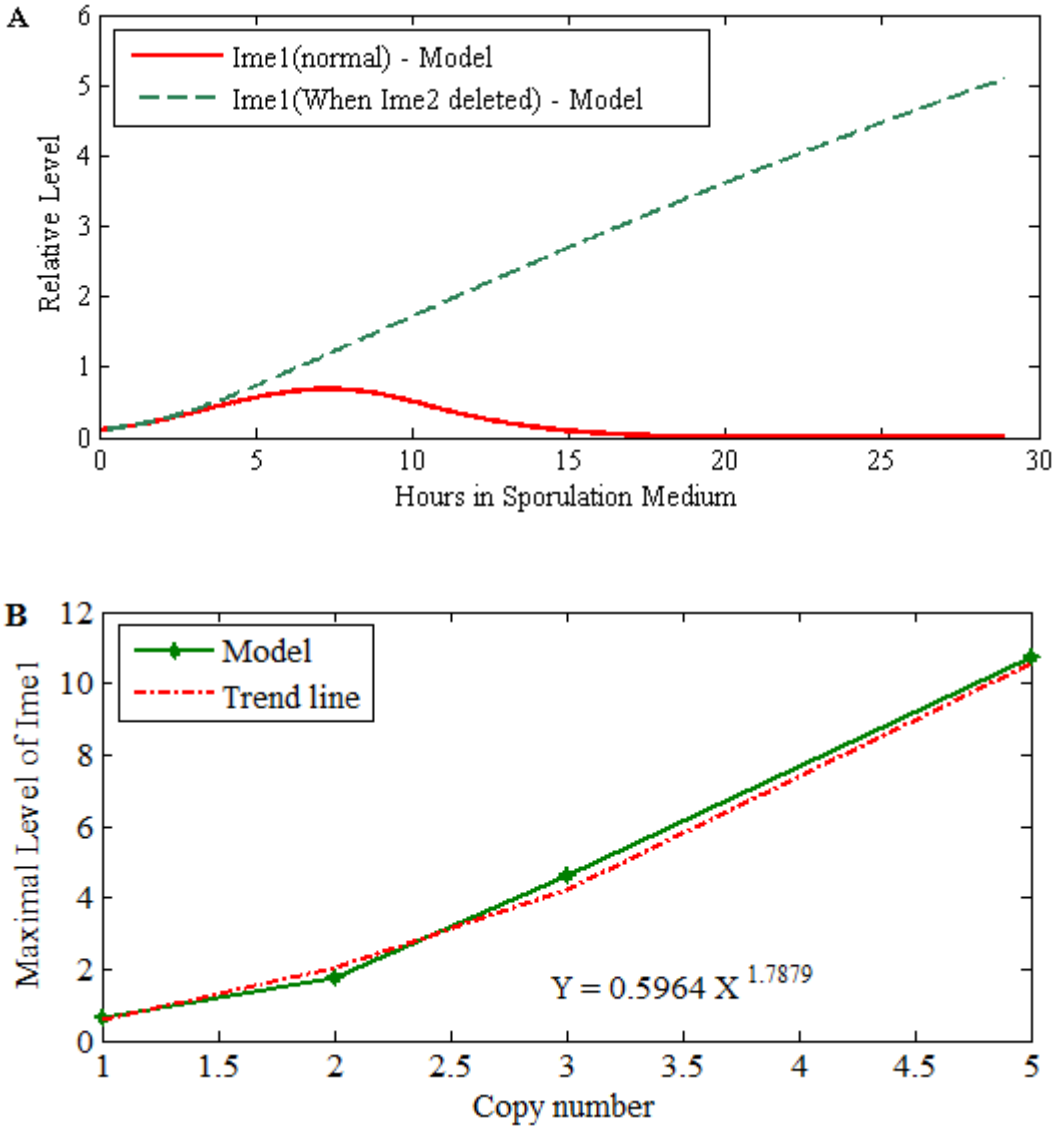

Figure 5.3 Predicted Ime2 deletion mutant and IME1 copy number variation. (A) Deletion of Ime2 results in an increase in the Ime1 protein level. During the simulation, all Ime2 terms from the model were removed and the initial conditions for the other proteins were set as given in Figure 5.1. SPM refers to sporulation medium. (B) When the IME1 copy number is changed, the maximum level of Ime1 and the IME1 copy number approximately fit to a quadratic trend. Green line connects the four calculated Ime1 maximum values from the *in-silico* mutation analysis. The equation of the trend line which is calculated using the least square fitting method is given inside the figure.

5.2.2 Model explains organism level results of mutant analysis at the gene expression level

We employ the model to understand the organism-level results produced from experimental mutation studies. The first mutant study involves phosphorylations associated with the Ime2 protein by Cdk1/Cln3. The Ime2 protein, which is activated by Cak1, possesses three potential phosphorylation sites where Cdk1 can bind and phosphorylate. When these three phosphorylation sites are blocked (Ime2-3SA), it showed a reduction in the number of budding cells compared to wild type cells, and the nitrogen depletion caused a more rapid and efficient G1 arrest than the wild type (Szwarcwort-Cohen et al., 2010). Further, the mutant cells initiated the meiotic S phase at approximately four hours pre-maturely. These results suggest that the Ime2-3SA protein was activated pre-maturely initiating the DNA replication.

To test the effects of the mutations on the Cdk1 phosphorylation sites on Ime2, we remove the term associated with Cdk1/Cln3 phosphorylations on Ime2 from our model equation of Ime1 protein (Equation (4-1)). The protein levels of the mutant and the normal system predicted by the model are given in Figure 5.4. The removal of phosphorylation results in increased levels of the Ime2 protein in the initial hours. The premature Ime2 protein expression prediction by the model, which is approximately three hours, explains the experimental observation of rapid G1 arrest and premature meiotic S-phase initiation. Since MMGs and LMGs are activated by EMGs, it is conceivable that the expression patterns of MMGs and LMGs follow EMGs such as Ime2. However, it is observed from experiments that MMGs and LMGs are not expressed during the initial hours, similar to EMGs, until a time point after which the expression follows the EMG pattern (compare EMG and MMG expression before six hours in Figure 3 A of Gurevich et. al. (2010) (Gurevich et al., 2010)). Our model's prediction of the post-translational (via phosphorylation) reduction of Ime2 levels during the initial hours would not activate the MMGs and LMGs in the initial hours, matching with the experimental results in Figure 3A of Gurevich et. al. (2010). The experimental Ime2 protein expression by beta-gal assays provides a measure of Ime2 protein expression before post-translational modifications (marked by filled circles in Figure 5.4). Accordingly, when the post-translational modification of phosphorylations is removed, the model output matches the Ime2 expression data.

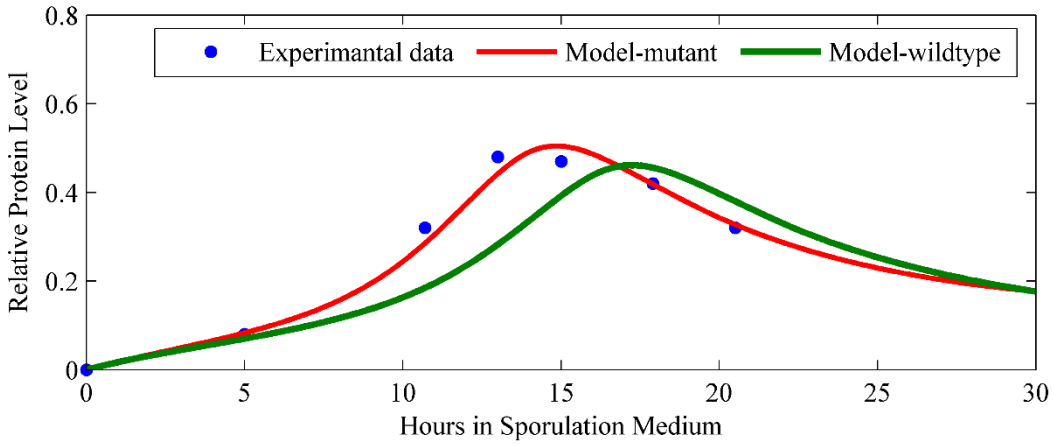

Figure 5.4 The post-translational modification removal in Ime2. The model output when the post-translational phosphorylations are removed (continuous line) shows higher Ime2 protein levels than for the wild type (dashed line) in the initial hours. The experimental data of Ime2 expression measured by yellow fluorescent protein (YFP) levels (Filled circles represent the scaled data from several trajectories of Ime2 protein in Figure 2 A of Nachman et. al. (2007) (Nachman et al., 2007)) match the predicted mutant behaviour since the post-translational modifications are removed during mutant analysis. Initial conditions for the model were within the normal range under which meiosis initiation occurs: 0.1 for Ime1 and 0.6 for the Rpd3/Sin3 concentration, 0.06 for nitrogen concentration, 0.1 for Cln3 and 0 for the other proteins (Wannige et al., 2014).

5.2.3 Model clarifies the conflicting results of two mutation studies which use different methods for Cln3 overexpression

The model accurately explains and clarifies Cdk1/Cln3 overexpression-related mutant studies carried out experimentally. Cdk1/Cln3 related repression on Ime1 and Ime2 (Figure 5.5) has been experimentally tested in two different ways: overexpressing Cln3 by the IME2 promoter, and overexpressing Cln3 using a tetracycline regulatable system. The experimental results indicate that these two ways have overexpressed Cln3 at two different concentration levels, since the former experiment caused only a two hour delay in entering pre-meiotic DNA replication while the latter even caused a doubling of the number of cells (driving cells to mitosis initiation) and arrested a high percentage of cells with 4c DNA content, presumably by higher Cln3 overexpression, compared to the former experiment. (Fig. 6 B and Fig 2 of Colomina et. al. (1999)). To simulate the first study of Cln3 overexpression, we overexpressed Cln3 from the IME2 promoter by replacing the expression terms of Cln3 with Ime2 (Figure 5.5 B) (The first two expression terms of the Equation (4-3) are replaced with the first two terms of the Equation (4-2)), and the results match the experiments (Gurevich et al., 2010). Secondly, when we overexpress Cln3 at very high levels (12 times higher than the usual expression in meiotic conditions, the value 12 is used because it is sufficiently large enough to reproduce the experimental results), we observe a decrease in Ime1 levels relative to the normal levels (Figure 5.5 A) that agree with the experiments (Colomina et al., 1999). This clarifies that the two different resulting levels of Ime1 from Cln3 overexpression are simply because of the methods used in overexpression, that cause overexpression of Cln3 at two different levels.

However, overexpression of Cln3 in these two experiments has resulted in conflicting Ime1 levels: the former experiment results in higher Ime1 levels than the normal level; and the latter produces lower Ime1 levels than the normal level. We interpret these conflicting results using the simulations as follows: when the relations between these three proteins (Ime1, Ime2 and Cln3) are considered, it can be seen that Ime1 is repressed in two different ways: Cln3 inhibits Ime2 and Ime2 tags Ime1 for degradation; Cln3 directly represses IME1 transcription, and transports Ime1 out of the nucleus after phosphorylation by Cln3. According to the model simulations, it can be understood that the reasoning behind the resulting higher Ime2 levels in Figure 5.5 B is because of the moderate overexpression of Cln3 in the former experiment, which inhibits Ime2 levels allowing more Ime1 to exist; the direct inhibition of Ime1 by Cln3 may be very low and masked in this experiment.

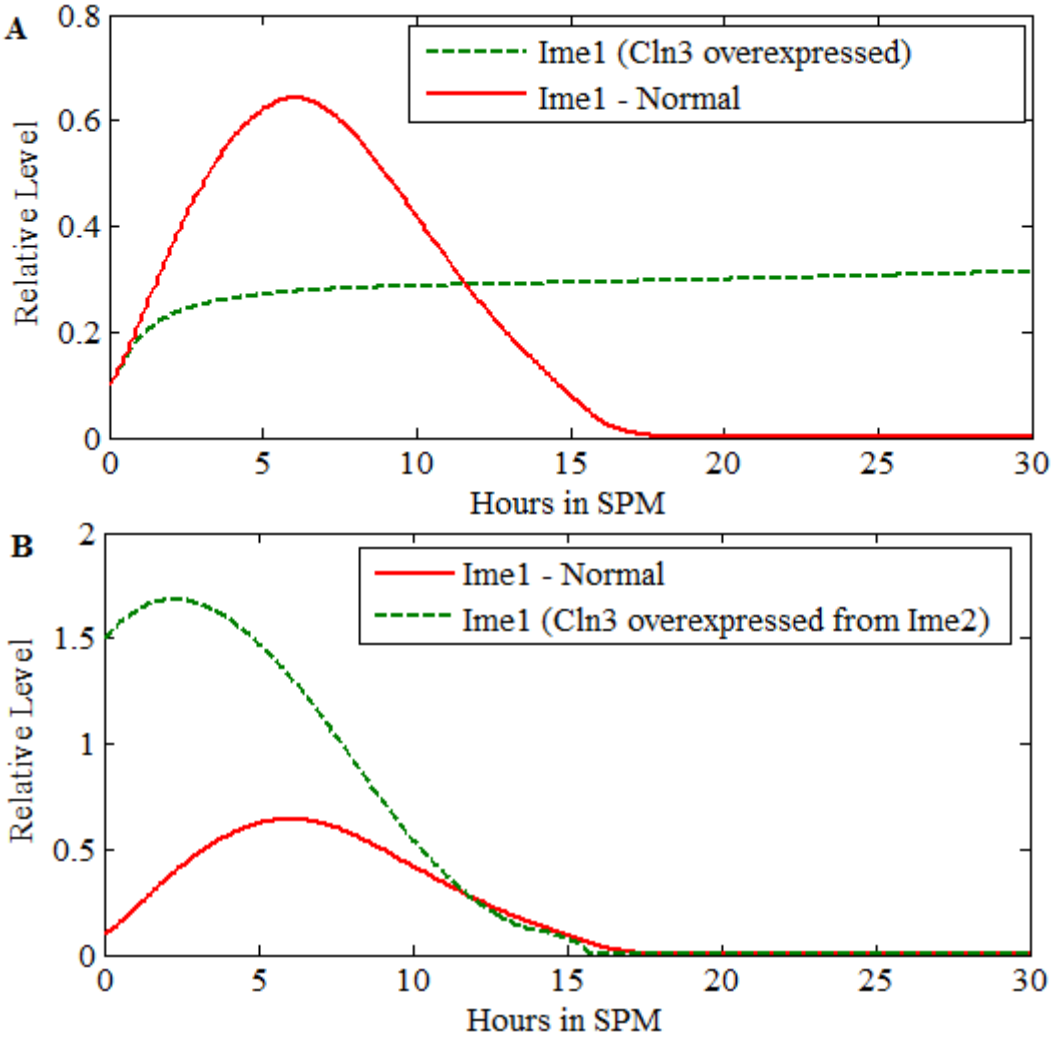

Figure 5.5 Predicted mutant analysis results. (A) When Cln3 is overexpressed twelve times more than the normal meiotic Cln3 expression the model shows low Ime1 levels compared with the normal expression of Ime1. The first two terms of Equation (4-3) of the model were multiplied by twelve to impose the overexpression of twelve times. (B) Ime1 expression when Cln3 is overexpressed from IME2 promoter. The first two expression terms of the Equation (4-3) were replaced with the first two terms of the Equation (4-2) (Wannige et al., 2014).

The reasoning behind the resulted lower Ime2 levels in Figure 5.5 A is because of the extremely high overexpression of Cln3 in the latter experiment, which transcriptionally inhibits the Ime1 level. Further, the increased Cln3 can phosphorylate and transport the phosphorylated Ime1 out of the nucleus. The increased Ime1 amount because of the inhibition of Ime2, which did not tag Ime1 proteins for degradation, may be carried out of the nucleus after phosphorylation by the high amount of Cln3.

5.3 Model Comparison with the Available Models: Extended Boolean Network Model and Abstract Model of Meiosis Initiation

In this study, we compare our model results with previous models to find whether our new model inherits the advantages and overcomes the limitations of the available models. We compare meiosis initiation in our model with the extended Boolean network model published by Rubinstein et. al. (2007) (Rubinstein et al., 2007), and with the abstract model of meiosis initiation published by Ray et. al. (2013) (Ray et al., 2013). For *in-silico* studies of the Rubinstein's model, we use the dRNA (Discrete Regulatory Network Analyser, v2.1) software provided by Rubinstein (personal communication 21st February 2012). For the Ray's model, we use their differential equation set (in the methods section of Ray et. al. (2013)) and solve them using Mathlab. A detailed description of these two models is given in Appendix C.

5.3.1 Meiosis initiation prediction

In Figure 5.6, we present the meiosis initiation prediction of all three models. We present and compare only the common proteins in the three models. Depending on the focus of each study, the initiation signal for each model differs: the initiation signal in Rubinstein's model (Rubinstein et al., 2007) is nutrient depletion, nitrogen depletion is the meiosis initiation signal in our model, and the phosphorylated Sok2 depletion mediated by glucose depletion is the initiation signal for Ray's model (Ray et al., 2013).

All three models predict that the expression of meiosis initiators, Ime1 and Ime2, are transient and sequential (Figure 5.6). Similarly, as in the experimental results (Fig. 2 of Rubinstein et. al. (2007) (Rubinstein et al., 2007)), the Ime1 peak time precedes that of Ime2 in all three

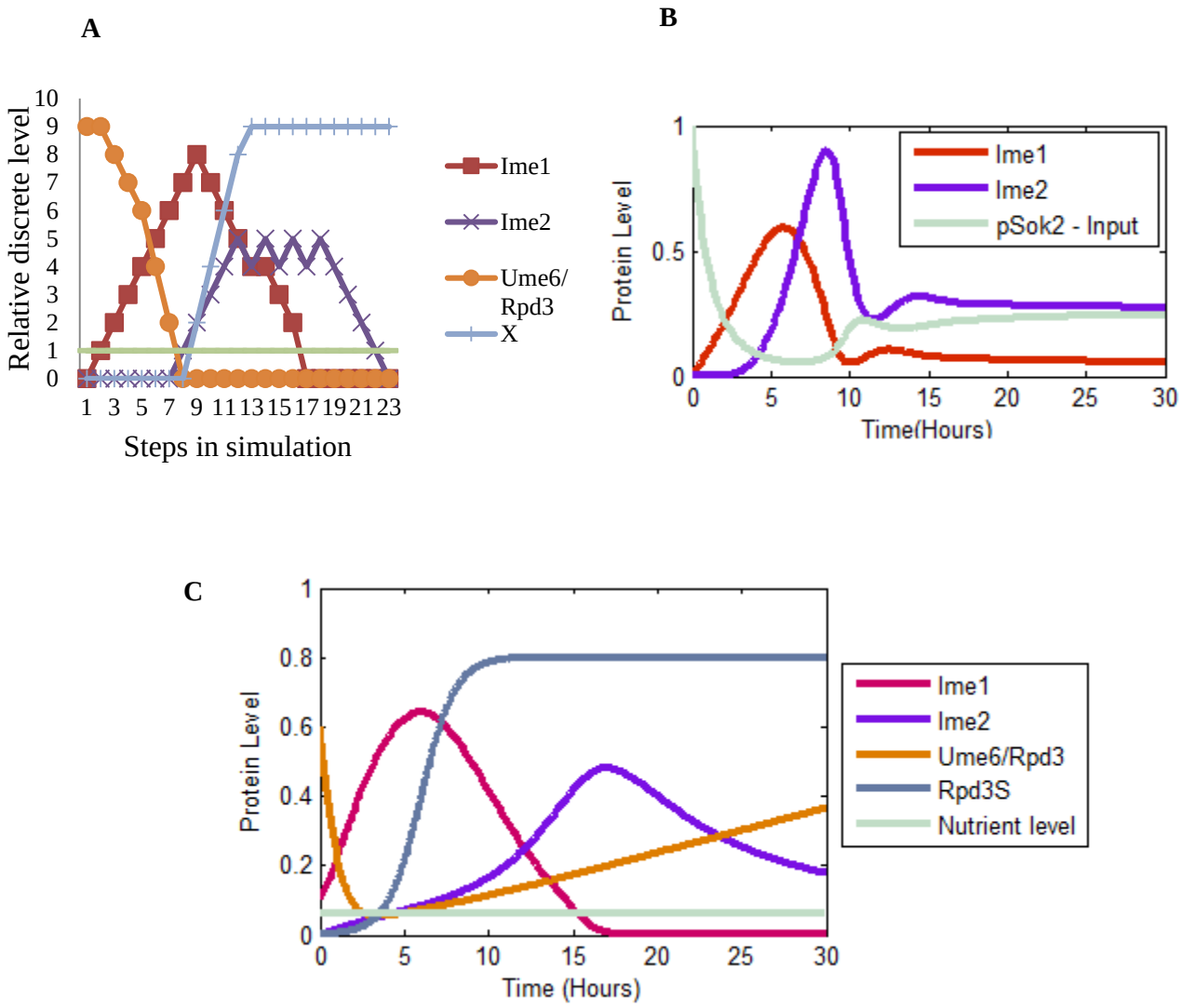

Figure 5.6 Meiosis initiation predicted by three models. (A) Rubinstein's model (Rubinstein et al., 2007) prediction of meiosis initiation. S corresponds to the nutrients. We use dRNA software and set the initial conditions in the model as follows: Ime1: 0, IME1: 1, Ime2: 0, IME2: 0, Ume6/Rpd3: 9, S: 1. (B) Ime1 and Ime2 protein expression predicted by the model of Ray et. al. (2013) (Ray et al., 2013). In Ray's model, the initial conditions are pSok2: 1, other variables: 0. (C) For the meiosis initiation in our model, the initial conditions are Ime1: 0.1, Ime2: 0, Rpd3/Sin3: 0.6, Cdk1/Cln3: 0.1, nitrogen: 0.06.

predictions. These predictions indicate that the mechanisms used in modelling the nutrient effects on Ime1 and Ime2 expression work successfully in the three models. The predictions of the peak time for the Ime1 and Ime2 proteins differ in the three models. According to experiments, the peak time of Ime1 expression is around six to nine hours in sporulation medium (Guttmann-Raviv et al., 2002; Shefer-Vaida et al., 1995) and Ime2 is around 10-12 hours in SPM (Nachman et al., 2007; Rubinstein et al., 2007). The variation of the peak time among the models is partly because some models also include post-translational modifications that may alter the peak time. Specifically, in our model (Figure 5.6 C), we draw the free Ime2 protein after the post-translational phosphorylations by Cdk1/Cln3 which alters the peak time of Ime2 by three to four hours. The experimental expression data do not include these post-translational modifications. Only Ray's model (Figure 5.6 B) predicts that the peak Ime2 expression is higher than the peak Ime1 level, which contradicts with the associated experiments; where the experimental peak IME1 mRNA expression level is higher than the peak IME2 mRNA expression (Fig.2 B of Rubinstein et. al. (2007)).

Further, there is a small bump after the first peak in both Ime1 and Ime2 protein predictions in Ray's model (Ray et al., 2013) which is not observed in the experiments (Figure 5.6 B). According to our observations, this may be because of the bump after the peak Ime2 protein which affects Ime1 variation since Ime1 degradation depends on Ime2; we observed that this small bump disappears from the Ime1 variation pattern when Ime2 is deleted from the model (Figure 5.8 C). The results of Rubinstein's (1997) model (Figure 5.6 A) show that the Ume6/Rpd3 complex on the promoters approaches zero and remains at zero, while our model predicts that it increases after the sudden reduction, agreeing with the experiments. In experiments (Fig. 2 D in Pnueli et. al. (2004) (Pnueli et al., 2004)), the Ume6/Rpd3 complex suddenly decreases upon meiotic conditions (during the first one to three hours) because of the removal of Rpd3/Sin3 from EMGs; then it increases because of the reloading of the Rpd3/Sin3 to EMG promoters to block the Ime2 expression required for the transient expression pattern of Ime2. This comparison shows that despite the different initiating signals and associated mechanisms used, the three models faithfully describe the transient and sequential meiosis initiation pattern with slight differences, as discussed above. Our new model predicts meiosis initiation protein expression both quantitatively and temporally better agreeing with available experimental data than the other two models.

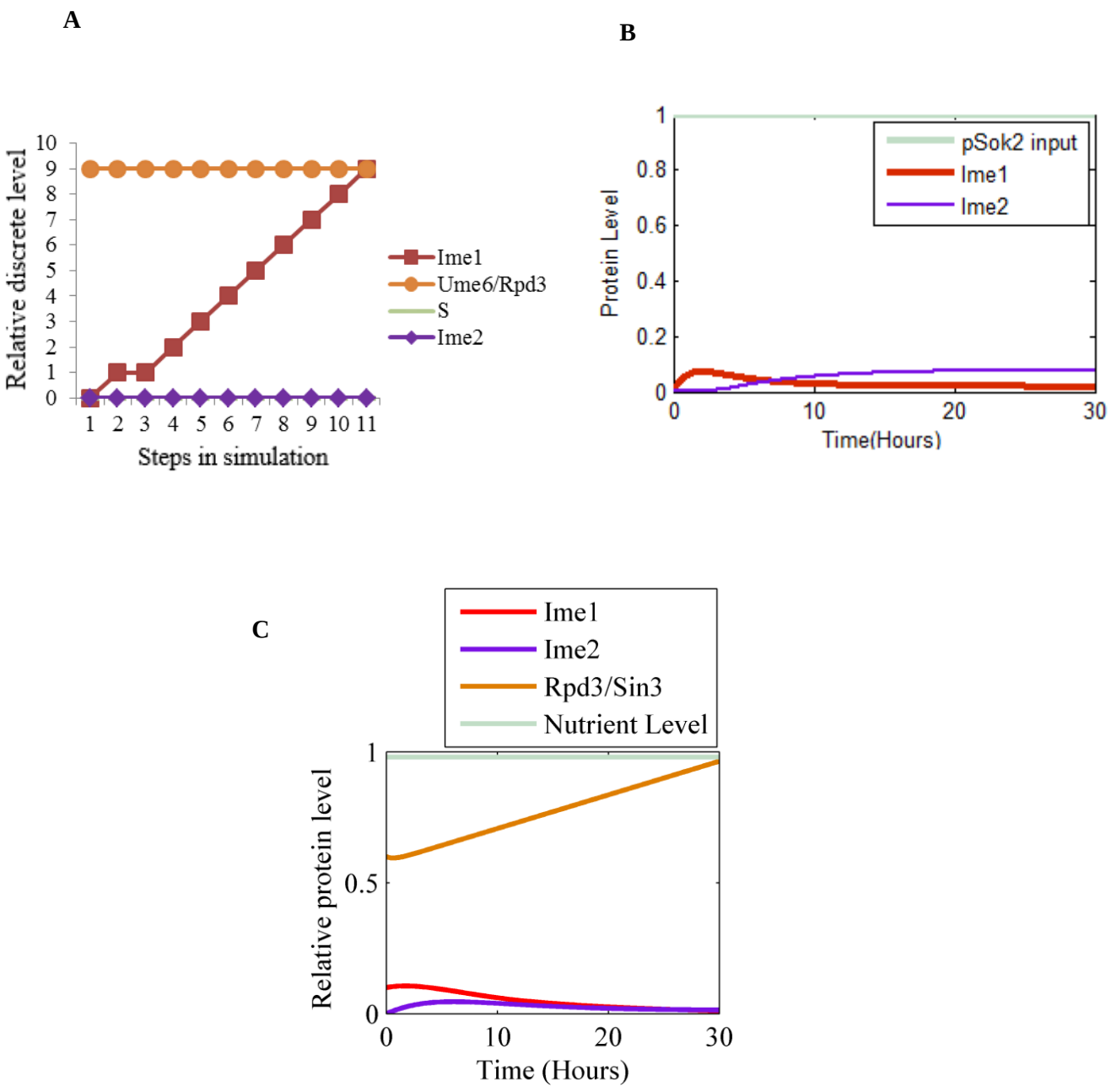

Figure 5.7 Mitosis initiation predicted by three models. (A) Rubinstein's model's (Rubinstein et al., 2007) prediction of mitosis initiation. S corresponds to the nutrients. Initial conditions are as follows: Ime1: 0, IME1: 1, Ime2: 0, IME2: 0, Ume6/Rpd3: 9, S: 0. (B) Ray's (2013) model output of meiosis initiation. In Ray's model, the initial conditions are pSok2: kept continuously at 1, other variables: 0 (C) Current model prediction of mitosis initiation is Ime1: 0.1, Ime2: 0, Rpd3/Sin3: 0.6, Cdk1/Cln3: 0.1, nitrogen: 0.98. Only protein expressions involved in mitosis initiation that are common to at least two models are displayed.

5.3.2 Comparison of Mitosis initiation

We employed Rubinstein's (1997) and Ray's (2013) models to look at how the meiosis initiation is inhibited in the presence of nutrients and compared the results of the three models.

All models (Figure 5.7) predict that Ime2 levels are low under high nutrient levels which implies that meiosis is inhibited, agreeing with experiments (Guttmann-Raviv et al., 2002). The expression of Ime2 in vegetative cultures is toxic (Guttmann-Raviv et al., 2002). Only the extended Boolean network (Figure 5.7 A) shows high Ime1 levels with high nutrients and this contradicts with the experiments which show that a low basal level of Ime1 exists, and Ime2 is absent in the nucleus under vegetative conditions (Sagee et al., 1998). This may be because this model focuses only on meiosis initiation, thus, it does not include the relationships of Ime1 repressions and inactivations happening under high nutrient levels. Of all three models, only our model incorporates the biological relationships of mitosis initiation and shows that the Ime1 level is low under high nutrients, as expected (Figure 5.7 C).

Ray's (2013) model (Figure 5.7 B) also shows low Ime1 levels, because Ime1 synthesis in their model depends only on phosphorylated Sok2 (pSok2), which acts as an input for the model, and we keep the pSok2 level at 1 to input mitosis initiation to the model and this imposes maximum repression on Ime1 synthesis (see Schematic and equations in page 12 of Ray et. al. (2013)) (Ray et al., 2013). The Rpd3/Ume6 complex resides in high levels, in the predictions by Rubinstein's (1997) model and our model in mitosis initiation, helping to repress Ime2 expression. Further, our model shows a slight increase in the Ume6/Rpd3 levels, which is resulted by the basal synthesis term of Rpd3/Sin3 used in modelling; however, the extended Boolean model is capped at level 9, which might be the reason for not showing this increase.

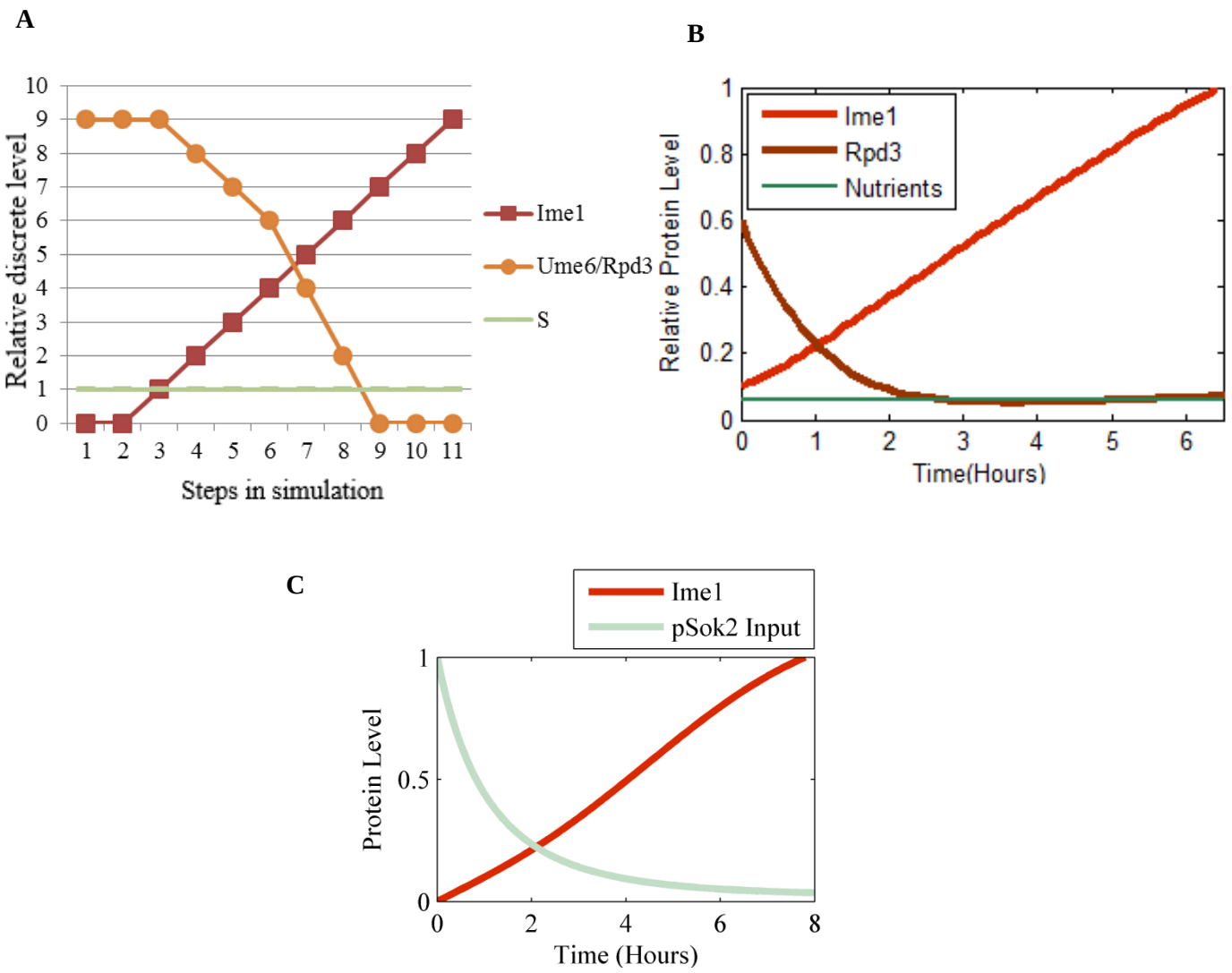

Figure 5.8 Model outputs when the Ime2 protein is deleted from the model. (A) Extended Boolean network model (Rubinstein et al., 2007) prediction of Ime2 deletion. S corresponds to the nutrients. (B) Our model prediction of Ime2 deletion. (C) Ray et. al. (2013) model's prediction of Ime1 and Ime2 (Ray et al., 2013). While carrying out these experiments, the Ime2 related terms are removed from the three models and initial conditions are set as in meiosis initiation.

5.3.3 Comparison of gene deletion mutant analyses

5.3.3.1 Ime2 deletion

Ime2 helps the transient expression of Ime1 by phosphorylating Ime1 and tagging phosphorylated Ime1 for degradation by the 26S proteasome. In experiments, deletion of Ime2 has created a 21-fold increase in Gal4-Ime1 levels.

When we employ our model to look at the Ime1 variation in Ime2-deleted cells (Figure 5.8 B), we notice a non-transient sudden increase in Ime1 without a reduction during the meiosis initiation time period, consistent with experiments (Guttmann-Raviv et al., 2002). We also observed that these increased Ime1 proteins decrease after reaching to a maximum level long after 30 hours. The Boolean network model (Figure 5.8 A) also produces similar increasing Ime1 levels when Ime2 is deleted from the system. The reduction of Ume6/Rpd3 levels is more rapid in our model than the extended Boolean model, since the Ume6/Rpd3 level in our model, at typical meiosis initiation levels, rapidly decreases, consistent with the experiments (Fig.2 D in Pnueli et. al. (2004)). Ray's model (Figure 5.8 C) also predicts higher Ime1 levels reflecting Ime2 inhibition removal agreeing with the corresponding experiments. Taken together, the three models have captured the mechanisms of the Ime2 related inhibition on the Ime1 protein.

5.3.3.2 Rim15 deletion

We can examine the effects of removing Rim15 only from our model (Figure 5.9 A) and the extended Boolean network model (Figure 5.9 B) because Ray's model does not include Rim15 related mechanisms. When the Rim15 effect on Ume6/Rpd3 is removed, both models show meiosis initiation, but our model shows late and lower Ime2 expression and higher Ume6/Rpd3 levels than the extended Boolean model. These higher Ume6/Rpd3 levels on EMG promoters reflect the experimental fact that Rim15 kinase helps to dissociate Rpd3 and Ume6 under nitrogen deprivation. Further, the experiments of RIM15 deletion showed that Rpd3 occupies the promoters of EMGs and its dissociation from EMGs was prevented in cells transferred to the sporulation medium (Pnueli et al., 2004). The later Ime2 initiation shows Rim15's unavailability to remove Rpd3 repression at the initial stages reflecting its pattern of availability; Rim15 levels gradually disappear in SPM since the

A

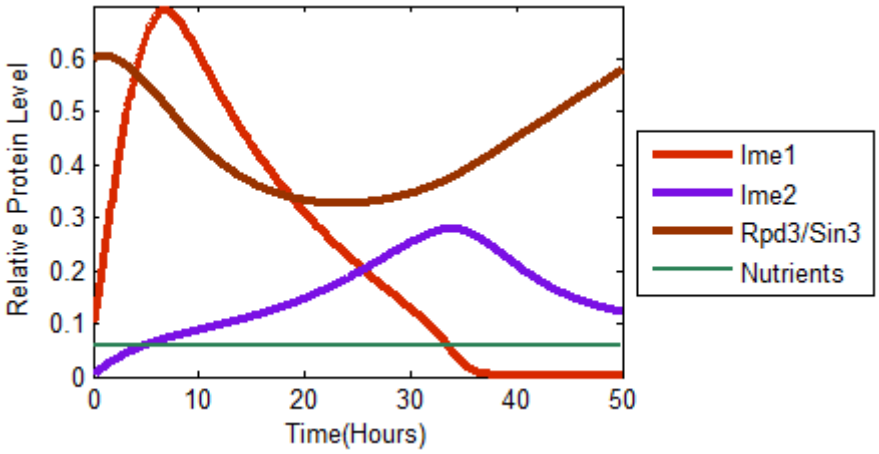

B

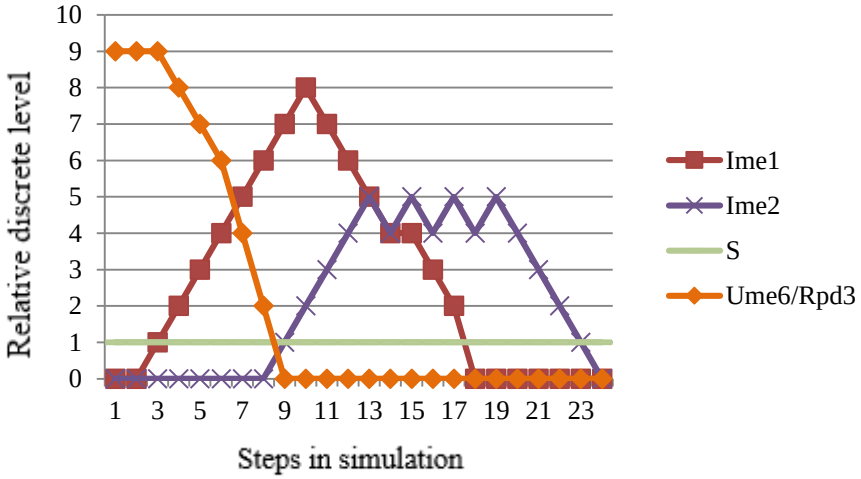

Figure 5.9 Two model outputs when the effect of the Rim15 protein is removed from models. (A) Current model prediction of Rim15 deletion from the model. (B) Deletion of RIM15 from the extended Boolean network model (Rubinstein et al., 2007). S corresponds to the nutrients.

RIM15 gene is not transcribed upon transferring to meiotic conditions and the Rim15 protein gradually disappears (Vidan and Mitchell, 1997). The Ime2 gene is expressed in mutant cells despite Rim15 deletion since Rim11 also helps to remove the Rpd3 repression and promotes Ime2 activation in meiotic conditions and this is verified by the experiments which show that Rim15-deleted cells show only a slight sporulation deficiency (Pnueli et al., 2004).

5.3.3.3. Rim11 deletion

We compare these models to examine the effects of Rim11 deletion. Our model shows that even if Ime1 is expressed, Ime2 is not expressed when the effect of Rim11 is eliminated from the model (Figure 5.10 A); To imply the Rim11 removal, we remove Ime1 terms from the Rpd3/Sin3 equation, which corresponds to the Rim11 effects on Rpd3/Sin3, according to our assumptions. Rim11 involvement is essential to remove the repression by Rpd3/Sin3 and for the activation of IME2 rather than Rim15. This is evident from the fact that sporulation was deficient in RIM11-deleted mutants (Bowdish et al., 1994), while spore formation was slightly deficient in RIM15-deleted cells. Higher Ime1 levels are observed because the Ime2 levels are low, which phosphorylate and tag Ime1 for degradation. Ray's model (2013) also shows similar results (Figure 5.10 B) when Rim11 is deleted: Ime2 is unavailable and Ime1 levels show high values reflecting the Ime2-related degradation of Ime1.

However, the extended Boolean network outputs show a mixture of transient and abnormal results for Rim11 deletion in the model for different input patterns (Rubinstein et al., 2007). The Rim11 effect is removed by eliminating the AND edge from S to the edge starting from Ime1 to Ume6. When we input a similar input pattern as our model to the Boolean network model, it results in transient Ime1 and Ime2 initiation under starved conditions; experiments show that sporulation is deficient in Rim11 deletion in starved conditions. As a percentage, Rubinstein et. al. (2007) observed transient expression in 56.8% from 81 different initial vectors when the Rim11 effect is removed by eliminating the AND edge even in the presence of nutrients (Table 2 of Rubinstein et. al. (2007)).

5.3.3.4 Ime1 deletion

We remove all the terms associated with Ime1 from all three models to study the effects from Ime1 removal. All three models predict that Ime2 is not initiated and remains at low levels if the Ime1 gene is deleted. Ime1 activates Ime2 after the Sin3/Rpd3 complex is removed from the IME2 promoters. Once Ime1 is deleted in the experiments, these Ime1 mutants arrested in

A

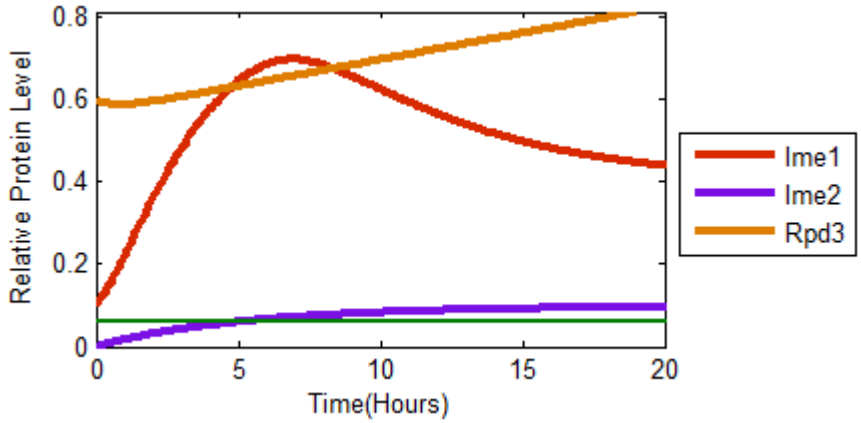

B

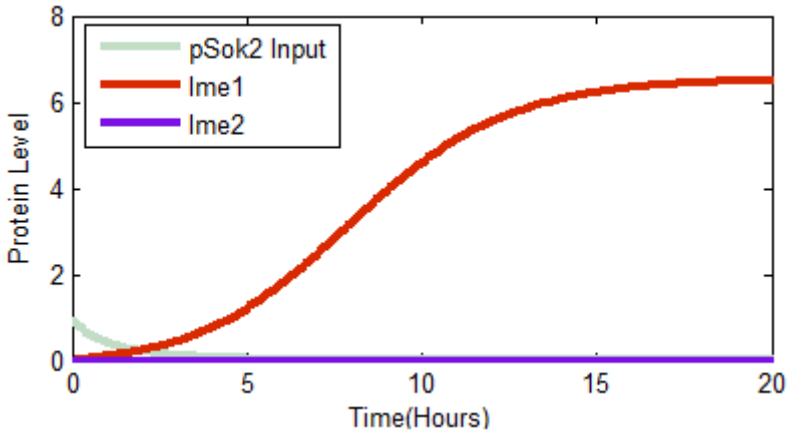

Figure 5.10 Two model outputs when the effect of the Rim11 protein is removed from the models. (A) Current model prediction of Rim11 deletion. (B) Prediction of Ray's (Ray et al., 2013) model when all the Rim11 terms are removed from the model equations.

meiosis prior to the initiation of pre-meiotic DNA synthesis (Foiani et al., 1996).

5.4 Summary and Conclusions

Living cells decide to undergo different cell division pathways according to the available nutrient conditions. Regulated entry into cell division pathways is essential for controlled cell proliferation. Wrong decisions to enter into cell division pathways at unfavourable input signal levels are costly. The two main cell division initiations, meiosis and mitosis, are tightly controlled processes and occur only under the correct conditions. This tight regulation is accomplished by gene cascades consisting of transcriptional and translational regulators of the meiosis and mitosis initiators.

In Chapters 4 and 5, we develop a mathematical model for meiosis initiation in budding yeast, including the mitosis initiator, and investigate the tight regulation of meiosis, mitosis initiation and their dynamics at the gene expression level. The important property of the model, which distinguishes it from previous models, is the inclusion of the mitosis initiator and its relations to the meiosis initiation network. The mitosis initiator affects meiosis initiation in many ways, but mainly to inhibit mitosis initiation during meiosis and vice-versa. Recently, many experimental investigations have revealed important relationships between meiosis and mitosis initiators. We include all the relations between meiosis and mitosis initiators to investigate the tight regulation of the initiation of these two processes under different nutrient levels. This inclusion also allows us to investigate these two process initiation under a range of nutrient conditions. Further, we non-dimensionalised the concentration terms of our model equations so the results are easy to compare with the available relative protein levels. The main conclusions from the model simulations and comparisons are summarised below.

The model can simulate the transient and sequential expression pattern of the main meiosis initiators (Ime1 and Ime2) at low nitrogen levels with a good agreement to the relative experimental protein levels. Other helping protein expression also matches well with the corresponding experimental relative levels. Under rich nitrogen conditions, simulations produce high mitosis initiator (Cdk1/Cln3) levels and negligible meiosis initiator levels, implying mitosis initiation. The *in-silico* gene deletion experiments reproduce the gene expression patterns similar to those seen in experiments. Our model could explain all the

available basic mutant studies related to the deletion of key genes and gene copy number variations.

The model is used to understand the organism-level results of mutant analysis at the gene expression level. When the post-translational modification of phosphorylation is removed from the differential equation corresponding to Ime2 expression, the model predicted a premature Ime2 expression. This premature Ime2 protein expression prediction, which is approximately three hours, explains the experimental observation of the rapid G1 arrest and pre-mature meiotic S-phase initiation in this mutation condition. We also identify from this mutation study that post-translational modifications of Ime2 are the reasons behind the experimental observation which showed that further down-stream EMG activated-MMGs and LMGs are not expressed during the initial hours similar to EMGs, until a time point after which the expression followed the EMG pattern.

Further, our model accurately and qualitatively clarifies two mutant studies carried out using different experimental methods. Specifically, the model reproduces the Cdk1/Cln3-related repression on Ime1 and Ime2 (Figure 5.5) which was experimentally tested by two different ways: overexpressing Cln3 by the me2 promoter (Gurevich et al., 2010) and overexpressing Cln3 using a tetracycline regulatory system (Colomina et al., 1999). We identify that these two ways have overexpressed Cln3 at two different concentration levels and our model reproduces these two experimental observations. This verifies that the observed differences in the outputs of the mutation study are because of the methods used to overexpress Cdk1/Cln3. Further, we clearly interpreted that the reasoning behind the conflicting Ime1 levels from the two overexpression experiments is because of the activation of two different pathways of Ime1 repression. In the former experiment, the increment in Ime1 is because of the Cln3 inhibition of Ime2 levels, which allows more Ime1 to exist; the direct inhibition of Ime1 by Cln3 may be very low and masked in this experiment. In the latter experiment, the resulting lower Ime2 levels in Figure 5.5 A are because of the extremely high overexpression of Cln3 in the latter experiment which transcriptionally inhibits the Ime1 protein level. Further, the increased Cln3 levels can phosphorylate and transport the phosphorylated Ime1 out of the nucleus.

An *in-silico* comparison of the available two meiosis initiation models with the constructed model allowed us to check whether our model inherits the advantages and overcomes the limitations. During *in-silico* comparisons, we only compared the common proteins among the

three models. Among the many similarities in the predictions, we also observed some differences. The main difference we observed in the comparisons of meiosis initiation was the higher peak value of Ime2 than Ime1 in Ray's model (Ray et al., 2013) which was opposite in the other two models' predictions. We identified that this is mainly because of the parameters associated with the input signal level and the Ime2 expression in Ray's model (2013). The second main difference is associated with Rubinstein's model (1997) prediction at rich nutrient levels. We observed that Ime1 is expressed in high amounts under rich nutrient conditions in Rubinstein's model (Rubinstein et al., 2007). Again, our model explained that this increment in Ime1 is because this model does not include the mechanisms between meiosis and mitosis initiators that inhibit one another under opposite nutrient conditions. We also observed some differences in the outputs when we delete Rim11 and Rim15 from the models, which we could explain using the simulations of the current model.

Taken together, *in-silico* comparisons show that all three models describe the meiosis initiation qualitatively; therefore, they have captured the main regulatory mechanisms of meiosis initiation. We observed differences in the predictions mainly because of the level of detail considered and the mechanisms captured, depending on the focus of modelling. The current model and Rubinstein's model include more biological relationships than Ray's (2013) abstract model. The comparisons between the current model and Rubenstein's model verified that our attempt to extend the Boolean network model was successful because the current model inherited all the advantages and represented the meiosis initiation process in a more detailed level using real biological parameter value ranges.

Chapter 6

Dynamical Analysis of Meiosis Initiation and the Meiotic-Mitotic Switch

"To understand cells as dynamic systems, mathematical tools are needed to fill the gap between molecular interactions and physiological consequences"(Tyson, 2007).

In this chapter, we employ dynamical systems analysis to understand the dynamics of the meiosis initiation network. We use phase space analysis to study how the main meiosis and mitosis initiators behave during meiosis initiation. We then employ nullcline analysis to study how the steady states of the proteins behave with varying nutrient levels. After observing the existence of a switch between the main meiosis and mitosis initiator proteins from the nullcine analysis, we employ bifurcation analysis and study the nutritional dependence of the switch. We also examine how the transitions happen between the two main steady states of the switch. Further, we investigate how this switch behaves along the time axis since experiments have shown that this switching is observed during all the initial hours of meiosis initiation.

6.1 Phase Space Analysis of Meiosis and Mitosis Initiators

As discussed in Chapter 2, phase space analysis is a useful tool to analyse the dynamics of variables in the state space. In this section, we employ phase space analysis to study the dynamical behaviour of meiosis and mitosis initiator variables during meiosis initiation. Since we have three major initiator proteins (Ime1, Ime2, Cdk1/Cln3), we have three different pairs of proteins. We plot the phase plane diagram of each of these protein pairs and then discuss how these main protein kinases work together to initiate meiosis.

The phase plane diagram of the Ime1 versus Ime2 (Figure 6.1 A) looks like a triangle under meiosis initiation conditions. The two vertices of this triangular phase plane plot correspond to the Ime1 and Ime2 peaks. The expression pattern of meiosis initiators is transient and sequential. The transient behaviour is reflected by the acute angles of the two vertices in the triangular phase portrait. The sequential behaviour, which is the appearance of the Ime2 peak after the Ime1 peak, is indicated by the distance between the two vertices representing the Ime1 and Ime2 peaks. The initial meiosis initiation conditions for Ime1 and Ime2 are 0.1 and zero, respectively. The trajectory of the phase space starts from these values and eventually reaches zero, as expected. When the initial conditions are altered, as shown in Figure 6.1 B, the triangular shape of the trajectories remains the same. This reflects that the meiosis initiators are expressed in a transient and sequential pattern despite the initial condition changes and agree with previous experiments (Gurevich et al., 2010; Rubinstein et al., 2007).

The phase portrait between Ime2 and Cln3 (Figure 6.1 C) shows that the Cln3 level remains at low levels (between 0.1 and 0.25) while Ime2 is transiently expressed. The loop shape of the trajectory resembles the trough in the Cdk1/Cln3 temporal variation, which can be seen at Ime2 peak time (Figure 5.1). The initial Ime2 and Cdk1/Cln3 conditions are 0 and 0.1, respectively. Starting from these initial conditions, the trajectory reaches low Ime2 and Cln3 levels at the end. The initial condition variations shown in Figure 6.1 D do not change the pattern of the phase portrait and eventually, they reach low Ime2 and Cdk1/Cln3 values. The phase plane diagram between Ime1 and Cdk1/Cln3 (Figure 6.1 E) also shows that Cdk1/Cln3 levels remain at low levels while Ime1 has a peak at the middle of its expression. The initial condition changes in Ime1 and Cdk1/Cln3 (Figure 6.1 F) do not affect the pattern of the Ime1 and Cdk1/Cln3 trajectory.

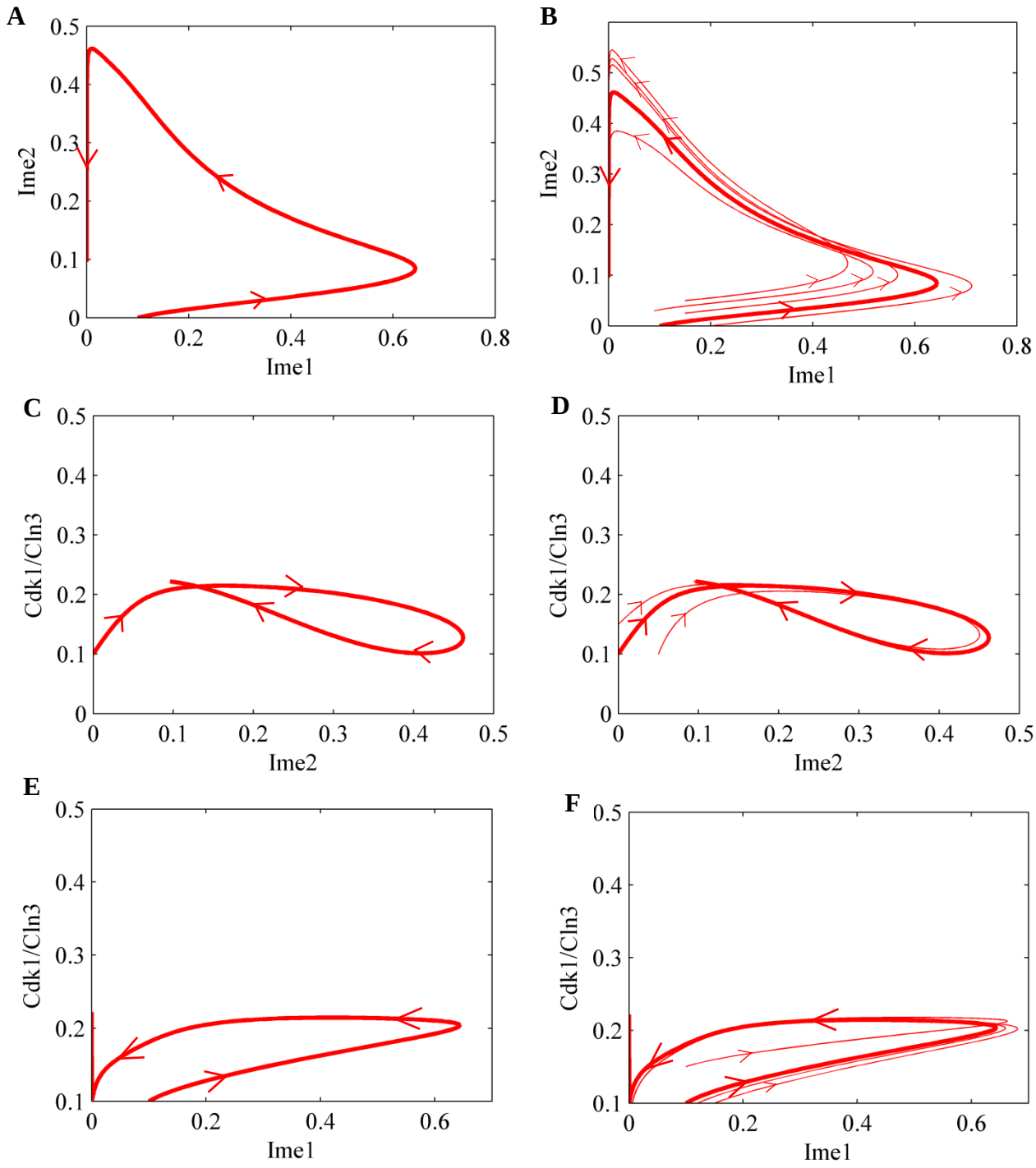

Figure 6.1 2-d projections of the phase space analysis of meiosis initiators, Ime1 and Ime2 and mitosis initiator, Cdk1/Cln3. (A) Phase portrait of Ime2 versus Ime1. (B) Phase portraits of Ime2 versus Ime1 when the initial conditions are changed. (C) Phase portrait of Cdk1/Cln3 versus Ime2. (D) Phase portraits of Cdk1/Cln3 versus Ime2 when the initial conditions are changed. (E) Phase portrait of Cdk1/Cln3 versus Ime1. (F) Phase portraits of Cdk1/Cln3 versus Ime1 when the initial conditions are changed.

6.2 Nullcline Analysis and the Switch between Meiosis and Mitosis Initiators

Nullcline analysis is frequently used in bistable system analysis (Ferrell, 2008; Tóth et al., 2007). With the main intention of studying the steady state behaviour of meiosis and mitosis initiators, we examine the global (we use the term global to represent the model with all the proteins) steady states in our model by equating the rate changes of all the equations of proteins to zero and did not find any common stable steady state (Here, we use the fixed parameter values given in Table 4.1 and use XPPAUT software to find fixed points (Ermentrout, 2012)). This is reasonable because the temporal variations of Ime1, Ime2 and Rpd3/Sin3 are transient and do not have long term common steady states.

To study a subset of the variables' steady states regardless of the other variables' temporal changes, the equation set of a system is normally reduced to a less (mostly two) dimensional model of the proteins of interest (Tóth et al., 2007; Toth Attila, 2004); the other variables, except the variables of interest, are assumed to be in pseudo steady states in this method. However, we cannot reduce the equations in a meaningful manner because of the nature of the relations between the variables. For example, we do not have any Sin3/Rpd3 involvement in the right-hand side of Equations (4-1) or (4-4). Further, we have time dependent terms in Equations (4-1) and (4-4) which correspond to Ime1 and Sin3/Rpd3, respectively. In this situation, we divided the temporal variation into time sections (time sections are of six hours which are sufficient to capture the different behaviour of the temporal variation of proteins) and employed nullcline analysis at each time section, assuming other variables, except the interested variables, stay at their average values. At each time section, we study each pair of variable's balance curves throughout a range of nutritional conditions, starting from a low value and going to a very high value. To show the different behaviour observed in the nullclines of variable pairs, we present the nullcline diagrams in the nitrogen conditions which show different types of behaviour in one of the considered time sections (twelve to eighteen hours) in Figure 6.2.

At all time sections (from 0 hours to 18 hours), the nullcline analysis between meiosis (Ime2) and mitosis (Cdk1/Cln3) inducers shows a single steady state under nitrogen-starved conditions, which may correspond to the meiosis state (in the first raw of Figure 6.2 A and Figure 6.3 A). The meiosis initiator (Ime2) level of this steady state is higher than the mitosis initiator (Cdk1/Cln3) level.

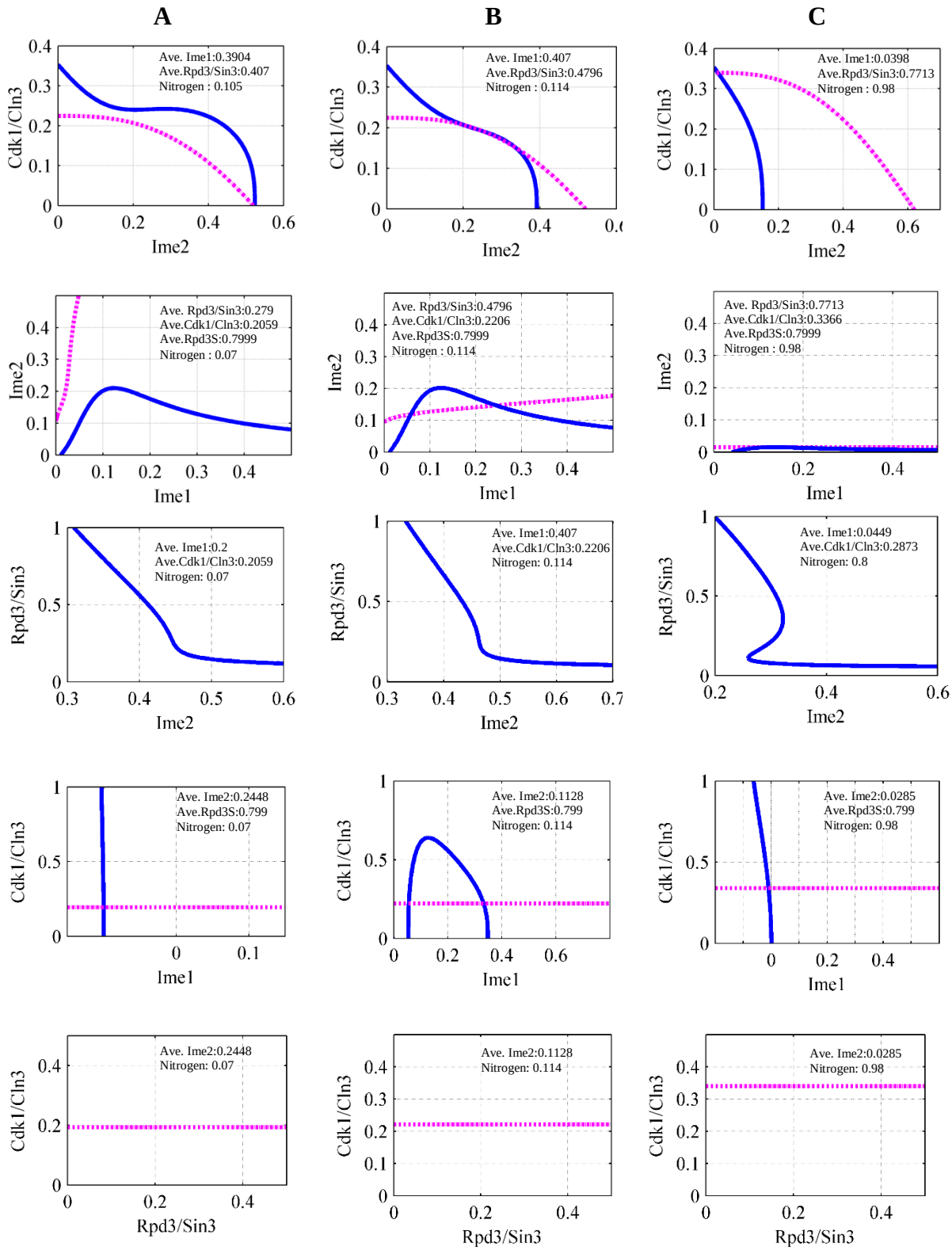

Figure 6.2 Nullcline analysis of variable pairs during 12-18 hours. Nitrogen level is varied in a range (from 0.03 to 1) and in this figure, we plot the nullcline behaviour only in the nitrogen conditions which shows different types of behaviour. X and Y axis titles of each plot represent the considered variable names. Nullcline corresponding to the Y axis variable is marked with a dashed line. Average protein levels and nitrogen conditions for each figure is given inside each figure. Ave. refers to average in the legend.

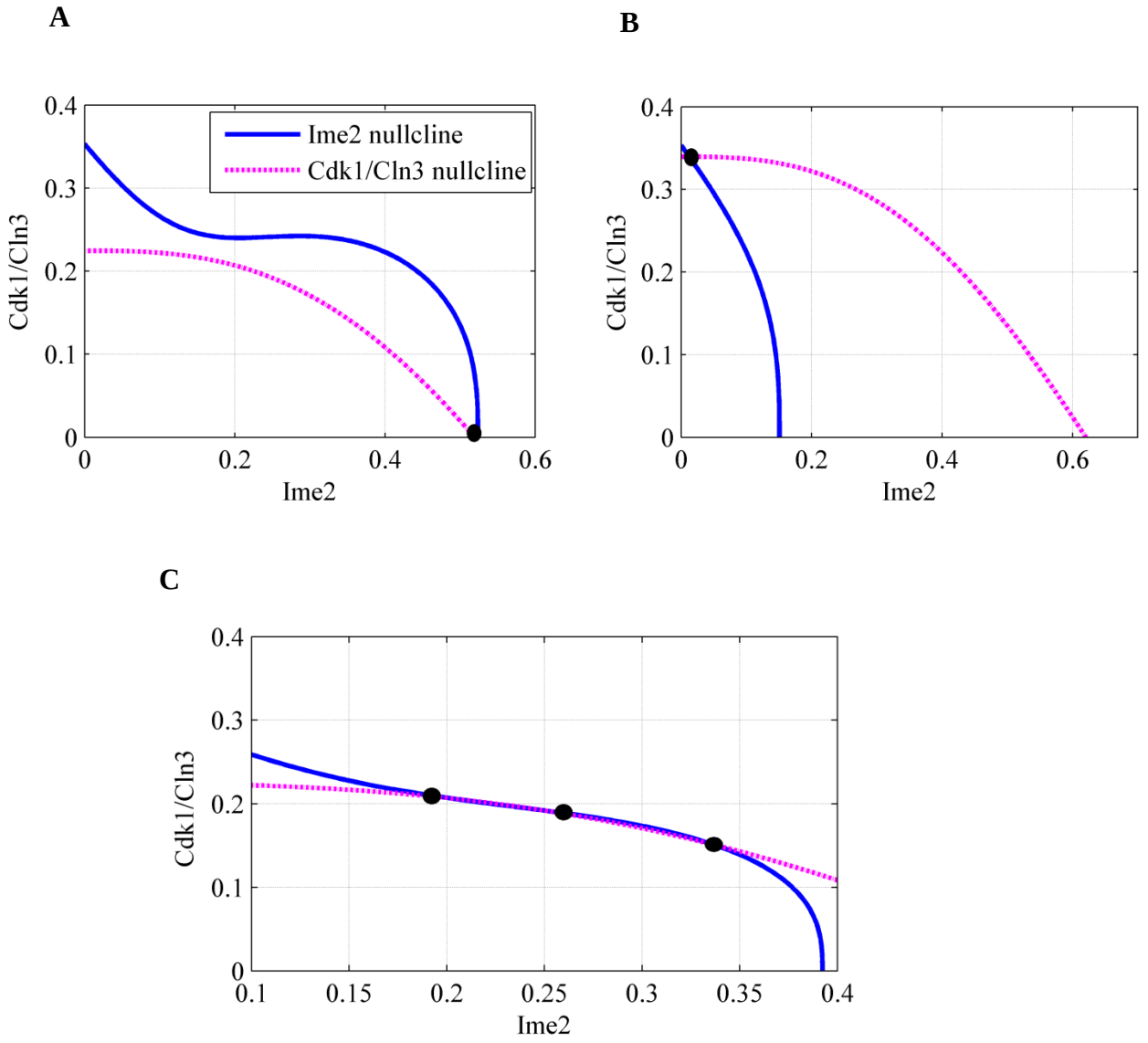

Figure 6.3 Nullcline analysis between meiosis (Ime2) and mitosis (Cdk1/Cln3) inducers at the six hour time section around Ime2 maximum. (A) Balance curves under meiosis initiation conditions (at nitrogen level of 0.07). Average values of other proteins: Ime1 - 0.0440, Rpd3/Sin3 – 0.3453 (B) Balance curves under mitosis initiation conditions (at nitrogen level of 0.98). Average values of other proteins: Ime1 - 0.0857, Rpd3/Sin3 – 0.6569 and (C) Balance curves at the transition from meiosis to mitosis (at nitrogen level of 0.083) Average values of other proteins: Ime1 - 0.1975, Rpd3/Sin3 – 0.4549.

When the nutritional conditions are further increased from the lowest level, we observe three intersection points (steady states) in the same variable pair (in the first row of Figures 6.2 B and 6.3 C). Further, the higher nutritional levels show a single steady state, which may correspond to the mitosis state, where the mitosis inducer levels are higher than the meiosis inducer levels (in the first row of Figures 6.2 C and 6.3 B). An enlarged version of the nullcline analysis between Ime2 and Cdk1/Cln3 at the six hour time section around Ime2 maximum time (Hereafter, we use this time section because Ime2 can be considered as fully expressed during this time period and Ime2 increases or decreases rapidly outside this time period, thus a steady state is most probable during this time period) is also shown in Figure 6.3. None of the other variable pairs show this type of switch-like steady states. Variable pairs with Rpd3/Sin3 do not show nullclines for Rpd3/Sin3, because there is no Rpd3/Sin3 term in the right hand side of Equation 4-4.

To further study the local stability (by local stability we mean the persistence of stable steady states in Ime2 and Cdk1/Cln3 despite the variations in the other two proteins (Ime1 and Rpd3/Sin3), global model refers to the whole model with all the equations and local refers to the two equations of Cdk1/Cln3 and Ime2 considering other proteins stay at average levels in a considered time period) of Ime2 and Cdk1/Cln3 steady states inside the time sections, we study the effect of the levels of Ime1 and Rpd3/Sin3 on the steady states of Ime2 and Cdk1/Cln3. For this purpose, we consider the six hour time section around the Ime2 peak value where the Ime2 protein can be considered as fully expressed. During this time period, we study the effects on our balance curves of interest (Ime2 and Cdk1/Cln3) by the values (mainly at peak Ime2 time, average values around the peak and at arbitrary time points) of Ime1 and Rpd3/Sin3 (Figures 6.4, 6.5 and 6.6).

Using the average Ime1 and Rpd3/Sin3 values of the selected time sections (the time sections selected are given in Figures 6.4, 6.5 and 6.6) as the pseudo steady states of Ime1 and Rpd3/Sin3, we examine the other two proteins' nullcline behaviour. We also consider the peak time and arbitrary time points near the peak Ime2 time and study how Ime1 and Rpd3/Sin3 values at those time points affect the Cdk1/Cln3 and Ime2 nullcline behaviour. The Ime2 balance curve does not change over its entire shape, but the curvature changes for the different Ime1 and Rpd3/Sin3 average values (Figure 6.4). However, a steady state corresponding to meiosis is found at the intersection of nullclines for the average value pairs and arbitrary time points. This intersection point has a gradual variation in its Ime2 value for

changing Ime1 and Rpd3/Sin3 levels. However, the shape of the Cdk1/Cln3 balance curve does not change for the average values of Ime1 and Rpd3/Sin3, because the Cdk1/Cln3 nullcline equation does not include any Ime1 and Rpd3/Sin3 variables.

We repeated the aforementioned procedure with the nitrogen level (0.083), where we found three steady states. The results (Figure 6.6) show that there exist three intersection points regardless of Ime1 and Rpd3/Sin3 variations. This nitrogen level is more unstable than the other two levels since it is the transition state, where the steady states can easily jump either to meiosis or mitosis states when the nitrogen level is altered. Further, at higher nitrogen levels (Figure 6.5), we found one nullcline intersection point, corresponding to mitosis initiation despite the changes in Ime1 and Rpd3/Sin3 variation.

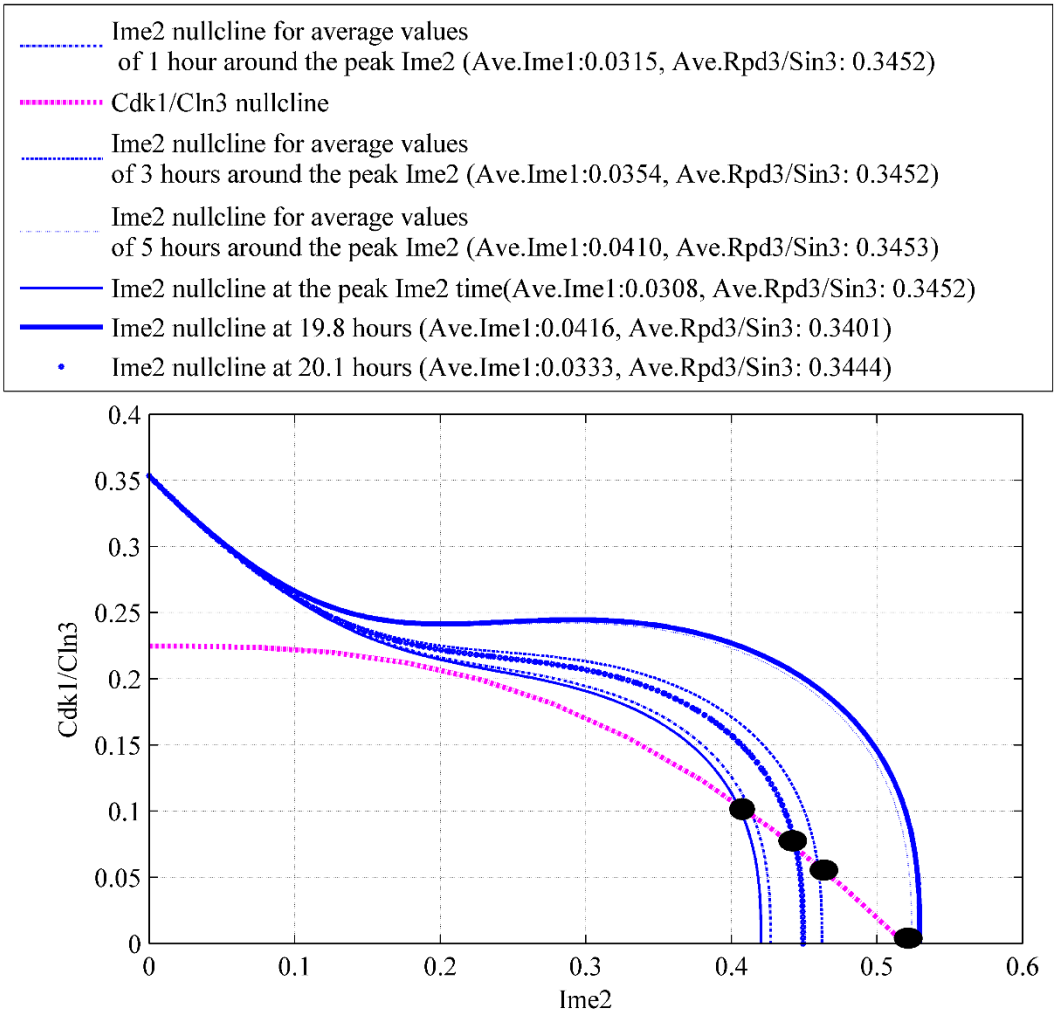

Figure 6.4 The effect of different steady state levels of Ime1 and Rpd3/Sin3 on the nullcline intersection points. Nullcline plots for low nitrogen conditions (0.07). Nullcline plots of Ime2 are shown in blue and the nullcline plots of Cdk1/Cln3 are drawn in pink. Ave. refers to average in the legend.

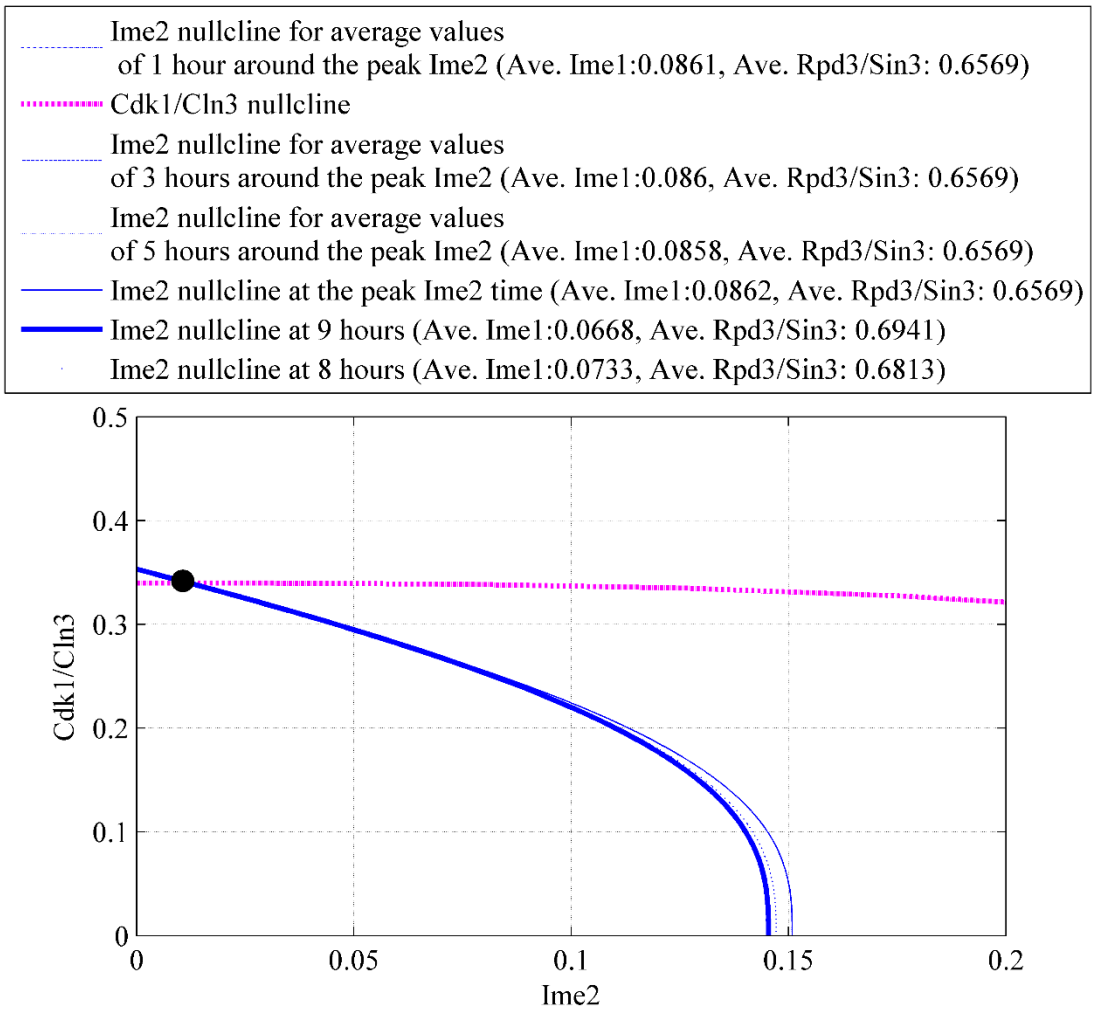

Figure 6.5 The effect of different steady state levels of Ime1 and Rpd3/Sin3 on the nullcline intersection points. One intersection point is found at higher nitrogen conditions (0.98). Nullcline plots of Ime2 are shown in blue and the nullcline plots of Cdk1/Cln3 are drawn in pink. Ave. refers to average in the legend.

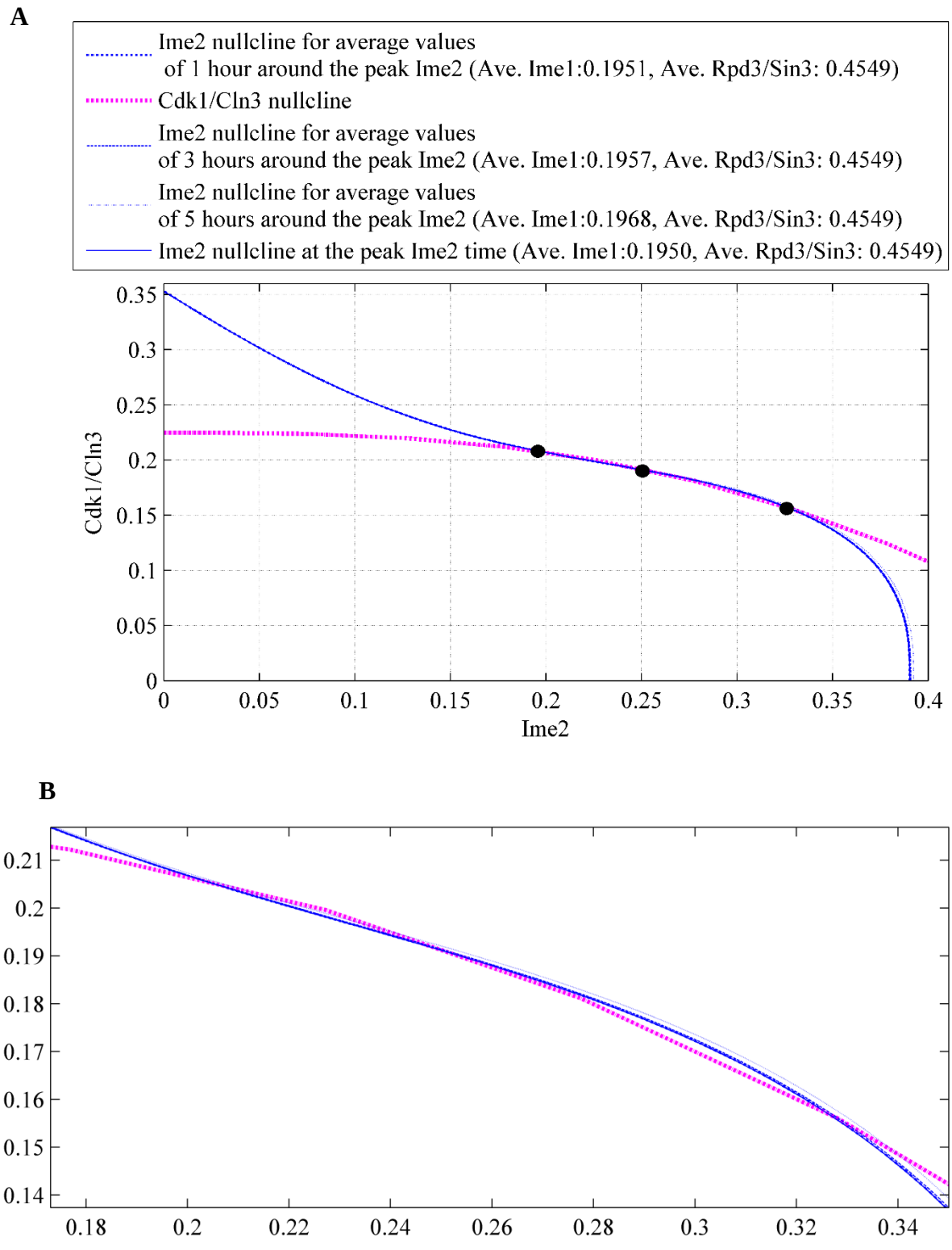

Figure 6.6 The effect of different steady state levels of Ime1 and Rpd3/Sin3 on the nullcline intersection points. Nullcline plots for nitrogen condition (0.083) with three intersection points. Nullcline plots of Ime2 are shown in blue and the nullcline plots of Cdk1/Cln3 are drawn in pink. Ave. refers to average in the legend.

Despite the Ime1 and Rpd3/Sin3 variations, we found one steady state corresponding to meiosis at low nitrogen levels and another steady state corresponding to mitosis at high nitrogen levels and three steady states at an intermediate low nitrogen level corresponding to the transition. We conclude that the existence of the bistable switch in Ime2 or Cdk1/Cln3 is not affected by supporting protein (Ime1 and Rpd3/Sin3) variations.

6.3 Nutritional Dependence of the Switch between Meiosis and Mitosis

We use bifurcation analysis to examine meiosis and mitosis initiator behaviour for the whole range of nitrogen conditions, assuming Ime1 and Sin3/Rpd3 remain at steady state levels. These steady state levels of Ime1 and Rpd3/Sin3 are assumed to be the mean values corresponding to time segment of length two hours, which includes the maximum meiosis initiator (Ime2) level. This time segment is chosen because it is the most probable Ime2 steady state as the Ime2 level decreases or increases outside this time interval (Figure 5.1). We conducted the bifurcation analysis of the meiosis and mitosis initiators considering the nitrogen level as the bifurcation parameter (Figures 6.7 and 6.8).

The observed bistable switch shows that meiosis initiates only under limited nitrogen conditions, matching previous experiments (Kassir et al., 2003). Both Ime2 and Cdk1/Cln3 show two steady states corresponding to meiosis and mitosis stages separated by one unstable steady state, which are the key characteristics of a bistable switch (Ferrell, 2002; Morgan, 2006). We observed that the gap between the threshold steady states of meiosis and mitosis initiation is around 0.1, equivalent to 10 nM, which would be sufficient for the mutually exclusive initiation of these two processes.

6.4 Transition between Meiosis and Mitosis

The transition from mitosis to meiosis initiation is predicted to happen between a low nitrogen level of 0.08 and 0.09, well under the maximum nitrogen level of 1. This is consistent with the experimental facts that meiosis initiates in nutrient deprivation and further, Ime2 expression in vegetative cultures is toxic (Guttmann-Raviv et al., 2002). We notice a saddle node bifurcation from the bistable state to the meiosis state when the nitrogen level is decreased from the transition region. The saddle node bifurcation appears again at the transition to the mitosis state.

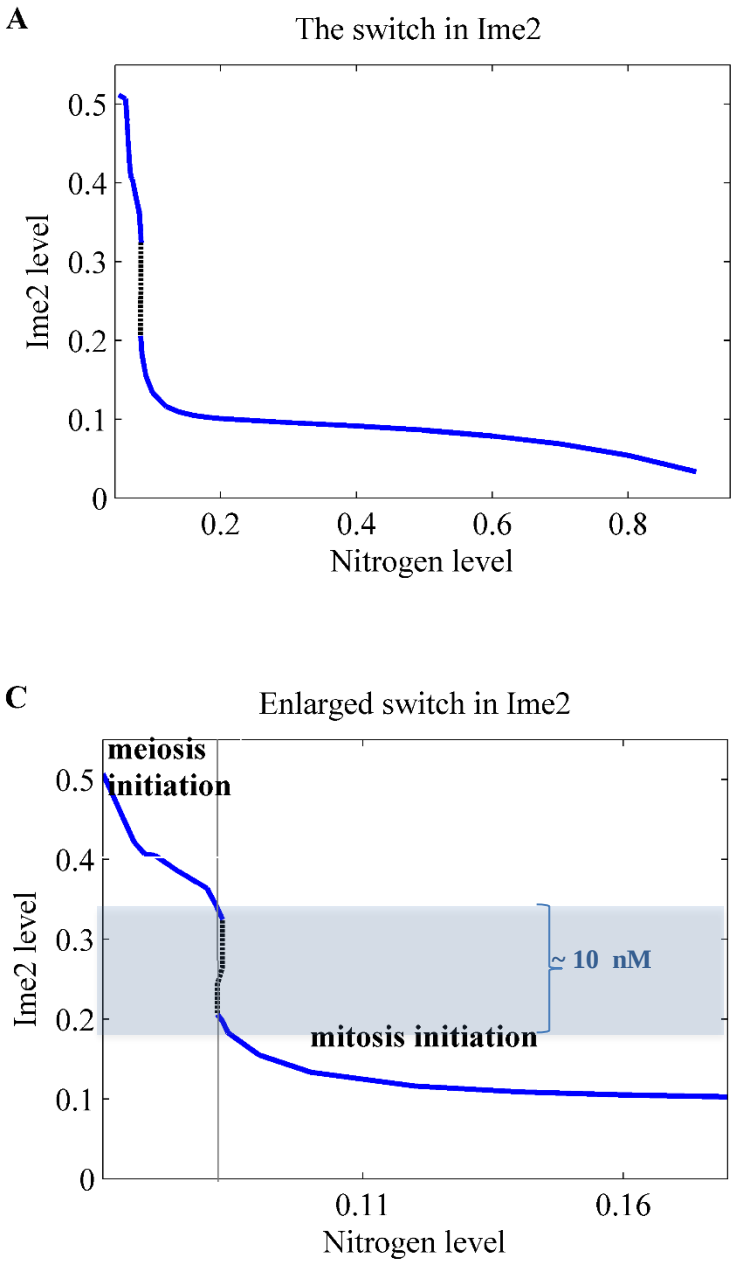

Figure 6.7 Bifurcation diagram Ime2 considering the relative nitrogen level as the bifurcation parameter. XPPAUT software is used to find the stable and unstable steady states when nitrogen varies and Mathlab software is used to draw the diagrams. Stable steady states are bold, and the unstable steady states are drawn with dashed lines. (A) The nutritional dependence of the Ime2 switch. (B) The enlarged switch in Ime2.

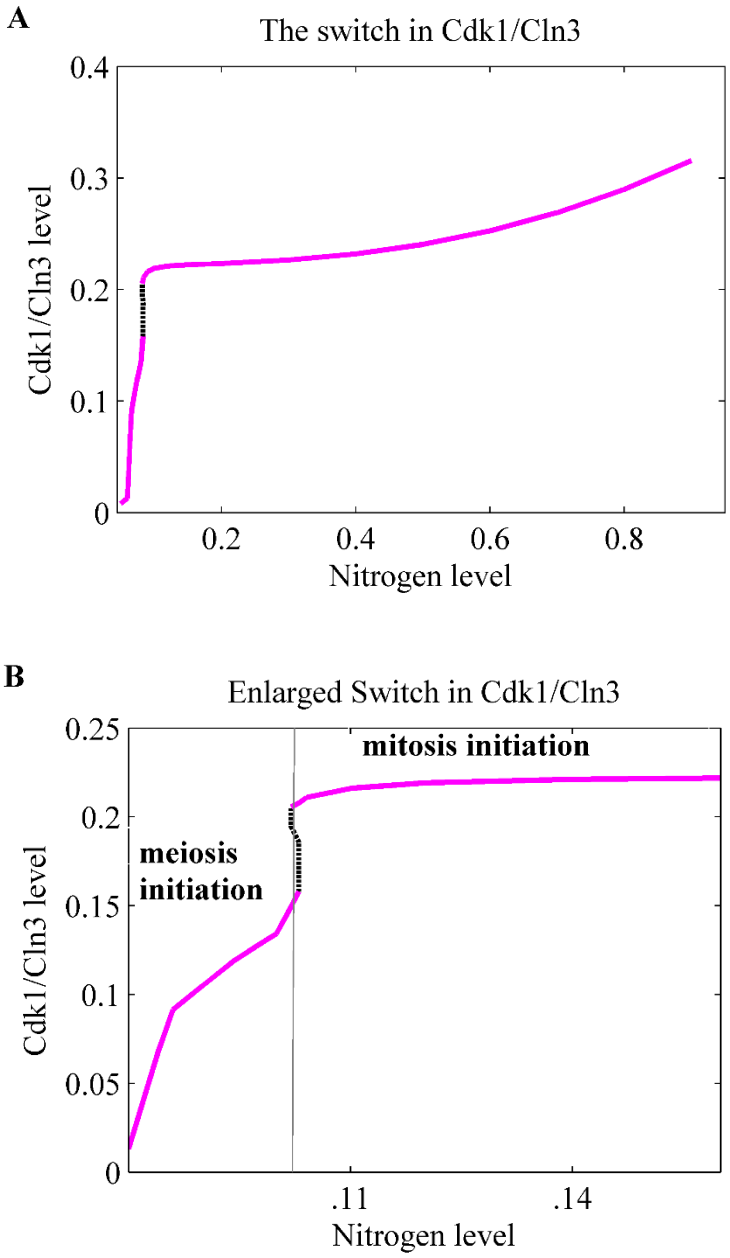

Figure 6.8 Bifurcation diagram of Cdk1/Cln3 considering the relative nitrogen level as the bifurcation parameter. XPPAUT software is used to find the stable and unstable steady states when nitrogen varies and Mathlab software is used to draw the diagrams. Stable steady states are bold, and the unstable steady states are drawn with dashed lines. (A) The nutritional dependence of Cdk1/Cln3 switch. (B) The enlarged switch in Cdk1/Cln3.

This observed nutrient dependent switch is reversible since the transition period is extremely narrow. Because of this reversibility, a cell which has decided to undergo meiosis (because of nutrient stress conditions) would change its decision if the nutrient conditions change to favour mitosis initiation. In fact, previous experiments reveal that budding yeast cells can choose between meiosis or mitosis initiation according to the available nutrients until an irreversible point called the 'commitment point'(Simchen, 2009). Such flexible decision making is required for the optimum use of nutrients for the survival of the organism.

6.5 Temporal Dependence of the Meiotic-mitotic Switch

In the previous section, we studied the bistable switch at the time period corresponding to the Ime2 peak time. In experiments, this switching behaviour is observed during all the initial hours from starvation initiation (at 0 hours) until the meiosis-decided cells are committed to meiosis at the commitment point (Winter, 2012). To investigate the switching behaviour in the initial hours, we study the temporal variation of the bistable switch from zero to 24 hours. For better presentation of the temporal behaviour of the switch, we show the switch in the following five time regions, where we observe the consistent behaviour of the switch (Figures 6.9 and 6.10): between 0 – 0.5 hours, 0.5 - 6 hours, 6 - 12 hours, 12 – 18 hours, 18 – 24 hours. We assume that Ime1 and Rpd3/Sin3 stay at their average values in each time section.

Figures 6.9 A and 6.10 A show that the switches stay in the mitosis state during the first 30 minutes. This mitosis state at meiosis initiation conditions appears as a consequence of the initial conditions used in the simulation of meiosis initiation. Typically, in experiments, the initial conditions for meiosis initiation correspond to a mitosis stage with high Rpd3/Sin3 levels and low basal levels of meiosis initiators. This mitosis state during the first 30 minutes is consistent with the experimental fact that the yeast cells are easily reversible to mitosis initiation in the very early hours of meiosis initiation (Simchen, 2009).

During the time between 0.5-18 hours (Figures 6.9 and 6.10 B, C and D), the switch between meiosis and mitosis initiators shows the typical bistable behaviour with two steady states representing meiosis and mitosis. The two steady states are separated by an unstable steady state. Once the nitrogen level is increased, the switch transits from the meiosis state to the mitosis state. The nitrogen level at the transition stage lies at very low levels, between 0.18 and 0.12 agreeing with the experimental fact that meiosis initiates only in very low nitrogen

levels. When the three switches in the above mentioned time period are examined, the gap between the steady states corresponding to meiosis and mitosis remains constant; the gap between the two steady states of the Cdk1/Cln3 switch is around 6 nM and the gap between the two steady states of the Ime2 switch is between 10 nM. Similar gap values are found at the maximum Ime2 time, as shown in Figures 6.7 and 6.8. This constant gap value explains the mutually exclusive existence of meiosis and mitosis pathway initiations.

The switch shows only the mitosis state in the later hours of meiosis initiation (Figure 6.9 E and 6.10 E). This appears when Ime2 decreases to zero, while Rpd3/Sin3 increases and Ime1 remains around zero during these later hours (Figure 5.1). In these later hours, yeast cells have already passed the commitment point; therefore, this mitotic state shown by the switch is out of the valid period of the bistable switch. The switch between Ime2 and Cln3 explains the early meiotic-mitotic switching in budding yeast cells only until the commitment point for meiosis. The time at which the commitment happens depends on the yeast strain and the experimental conditions (Nachman et al., 2007). Therefore, we consider the molecular biological detail that Ndt80/Sum1 switch underlies the commitment point (Simchen, 2009). NDT80 expression is activated by Ime2; Ndt80 becomes fully active by maximising at the same peak time as Ime2 (Gurevich et al., 2010)) (Compare the plots corresponding to NDT80 and IME2 in Figure 3 of Gurevich et. al. (2010)). Therefore, when Ime2 decreases after maximising during the later hours, the Ndt80/Sum1 switch has already decided on to commit to meiosis. Therefore, the mitotic state shown by the switch at the later hours lies out of the valid region for the bistable switch.

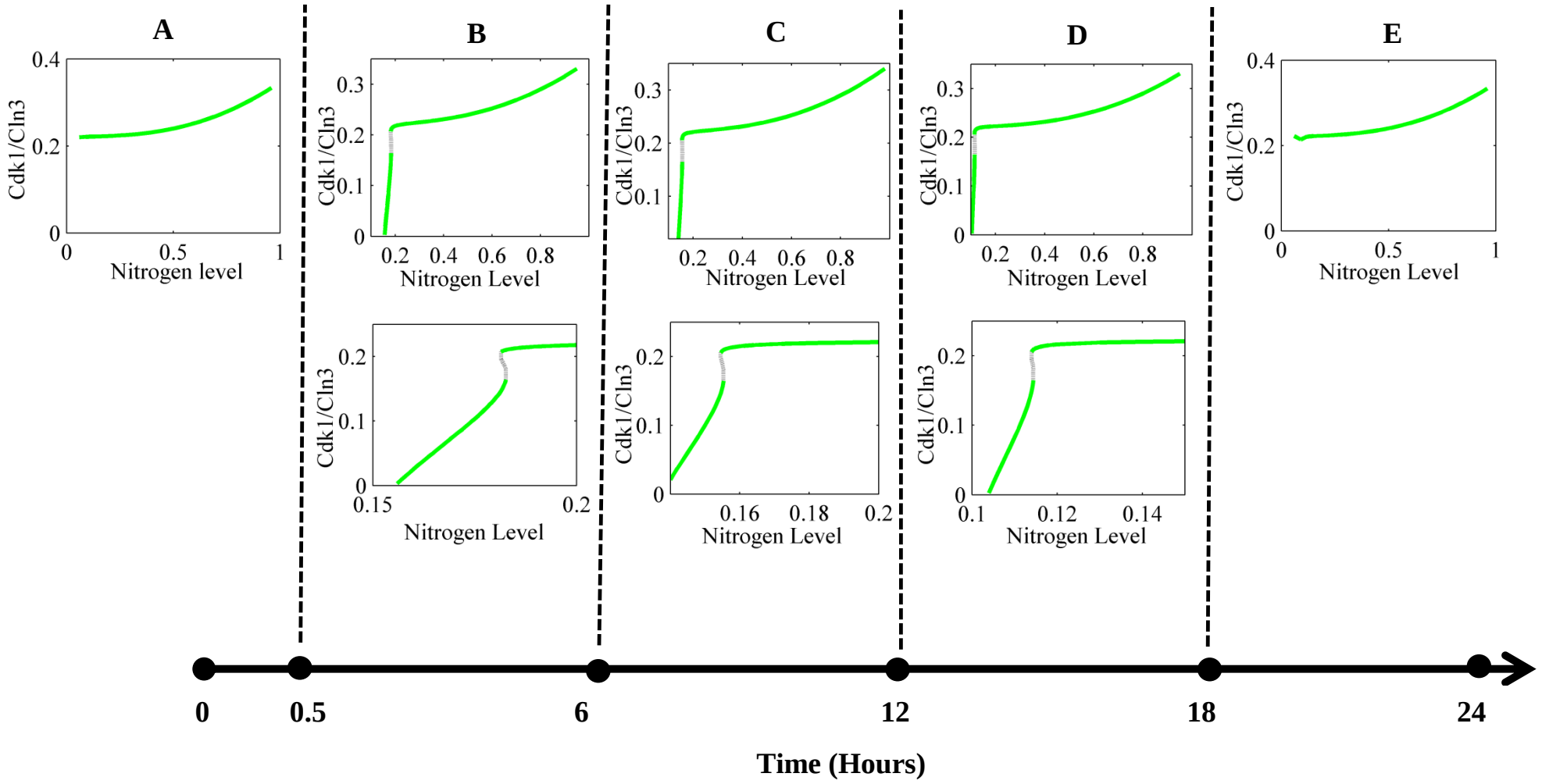

Figure 6.9 Temporal variation in the Cdk1/Cln3 switch. At each time section, one switch is drawn to represent the switch behaviour, which is consistent at each time point in the time section considered. (A) The switch behaviour in the first 30 minutes after the starvation initiation. Similarly, (B), (C), (D), (E) show the switch behaviour between 0.5-6 hours,6-12 hours, 12-18 hours, 18-24 hours after the starvation initiation, respectively. Switches shown in the second row are enlarged versions of the switches in the first row. XPPAUT software is used to find the stable and unstable steady states when nitrogen varies and Mathlab software is used to draw the diagrams.

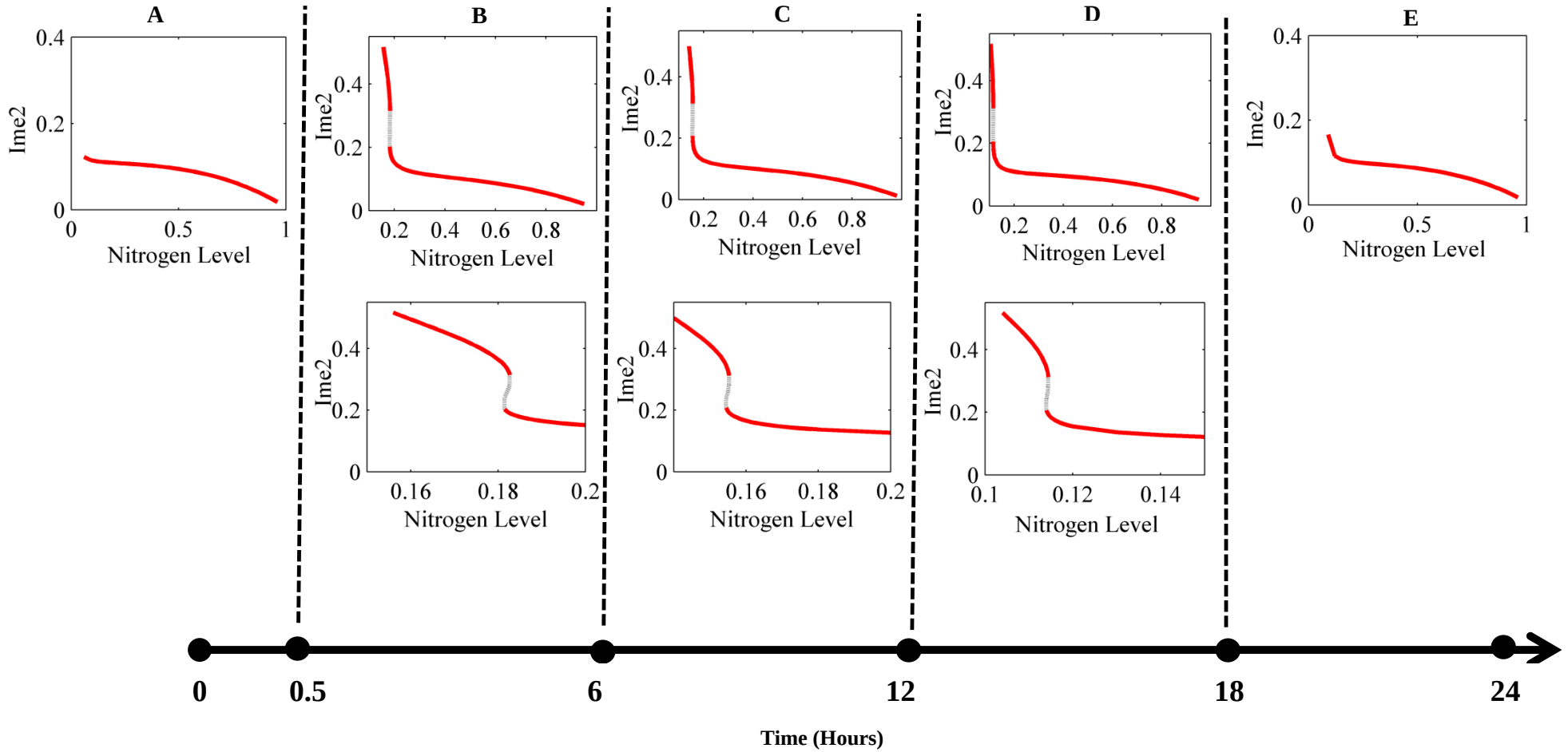

Figure 6.10 Temporal variation in the Ime2 switch. At each time section, one switch is drawn to represent the switch behaviour, which is consistent at each time point in the time section considered. (A) The switch behaviour in the first 30 minutes after the starvation initiation. Similarly, (B), (C), (D), (E) show the switch behaviour between 0.5-6 hours,6-12 hours, 12-18 hours, 18-24 hours after the starvation initiation, respectively. Switches shown in the second row are enlarged versions of the switches in the first row. XPPAUT software is used to find the stable and unstable steady states when nitrogen varies and Mathlab software is used to draw the diagrams.

6.6 Summary and Conclusions

One of the goals of systems biology is to understand how the functions are brought about by the interacting components of biochemical networks. It is of interest to understand how budding yeast cells alternatively choose between meiosis or mitosis initiation until commitment, depending on the available nutrient conditions. In this chapter, we examine our model using dynamical system analysis tools to understand the early stage meiotic-mitotic switching process seen in budding yeast diploid cells. Main conclusions are presented below.

Phase space analysis between the main meiosis and mitosis initiators explains the expression patterns of the main initiators among each other. Specifically, phase plane analysis between meiosis and mitosis initiators shows a transient and sequential initiation pattern of meiosis initiators that is essential for the correct activation of the further downstream proteins of meiosis initiation. From nullcline analysis, we identify that a switch exists between the main meiosis and mitosis initiators that would explain the early stage meiotic-mitotic switching behaviour seen in budding yeast diploid cells. From the bifurcation analysis studies using nutrients as the bifurcation parameter, we explain the nutrient dependent switching behaviour of the main meiosis and mitosis initiators.

The predicted switch in the meiosis initiator is turned on to the meiosis initiation state when the nitrogen is starved, as shown by experiments (Fig. 1 of Kassir et. al. (2003)); and, the switch in mitosis initiator is turned on at abundant nutrient levels which also agrees with the experiments (Gallego et al., 1997). Our modelled switch explains the mutually exclusive existence of these two developmental processes by the substantial gap (unstable steady state) between the threshold levels of the two stable states. The predicted switch is reversible so that once the meiosis switch is turned on by nutritional stress it would change its decision to mitosis initiation if high levels of nutrients are provided. This is experimentally evident by the observation of the return to growth (mitosis) in meiosis-decided cells if exposed to nutrients before they reach the meiotic commitment point. A similar reversible behaviour, according to available nutrients, is observed in mitosis-decided cells until they reach the mitotic commitment point (Simchen, 2009).

Temporal analysis of the switch explained that the cells which decided on meiosis initiation can return back to mitosis initiation if the nutrients are increased from the lowest level during all the initial hours of meiosis initiation. This agrees well with nutrient re-feeding experiments which showed that the cells could return to mitosis initiation during starvation initiation until

the commitment point. Further, this temporal analysis predicted that it is easier for the cells to return to mitosis during the first half hour of meiosis initiation.

The mutually exclusive existence of meiosis and mitosis requires a bistable switch in its initiators with a substantial gap between the two stable steady states. The requirements for a bistable switch include a feedback loop, either double negative or positive, in which the two legs of the feedback loop are properly balanced. It was initially suggested that Cln3 repression on Ime1 would help to explain the incompatibility of meiosis and mitosis (Colomina et al., 1999). However, our model does not show a bistable switch between Ime1 and Cln3 by nullcline analysis, but shows a bistable switch only between Ime2 and Cln3. This is possible since the negative cross talk between Ime1 and Cln3 is uni-directional and it is experimentally revealed that meiosis is robust under decreased or increased levels of IME1 RNA(Gurevich et al., 2010).

In summary, we show that meiosis and mitosis initiators create bistable switches with two alternative stable states corresponding to the mitosis and meiosis states. The transition to and from each state happens via a small region where the two steady states coexist. The cell would transit from meiosis to mitosis or vice versa from a saddle node bifurcation. Due to the narrow region of coexistence of the two steady states, the proposed switch is reversible which helps the optimal usage of available nutrients. Once a cell decides to undergo meiosis under stress nutrients, if the nutrients are additionally provided, the cell would return to growth (mitosis initiation) and vice-versa until they reach the commitment point, as shown in the experiments (Simchen, 2009).

The nutritional dependence of yeast cell division decision can be considered as a survival strategy of an organism. In fact, meiosis produces unique gametes which may survive harsh nutritional conditions. Mitosis type cell division creates identical cell copies for the continuation of the cell generation. The reversible switch between these two processes would allow the cells to choose between these two types of cell divisions for the optimal usage of available nutrients for the survival and growth of the organism.

Chapter 7

Sensitivity Analysis and the Robustness of Meiosis and Mitosis Initiation

"Robustness and sensitivity are two sides of the same coin" (Klipp et al., 2008).

In this chapter, we investigate the robustness of meiosis and mitosis initiation against perturbations of the most sensitive parameters. We also study the behaviour of the meiotic-mitotic switch under perturbations by the most sensitive parameters. In the first section of this chapter, we identify the most influential parameters for the output protein levels of the meiosis and mitosis initiators by employing both local sensitivity analysis (LSA) and global sensitivity analysis (GSA). Based on the GSA results, we find a common set of parameters sensitive in all the three main nutrient-driven states (meiosis, mitosis and transition). We simultaneously perturb this set of parameters and study the robustness of meiosis, mitosis and transition stages at the gene expression level. We also study the behaviour of the switch under the most sensitive parameter perturbations. We categorise the resulting switches from the perturbations of the most sensitive parameters into three groups: normal bistable switch, memory-less, and bistable switch with abnormalities. We also study whether the main functionality of the meiotic-mitotic switch is preserved in these three types of switches despite the perturbations. Finally, we provide the probable reasons for the observed memory-less and abnormal switches by studying the corresponding parameter ranges of the most sensitive parameters.

7.1 Sensitive Parameters from Local Sensitivity Analysis

In this section, our main scope is to identify the most sensitive parameters of meiosis and mitosis initiation. It is important to study the role of each parameter on the output of an *in-silico* biological system that contains a large number of parameters. Sensitivity analysis is used to study the output sensitivity of a system with respect to a change in a set of parameters (Morbidelli and Wu, 2005; Xie et al., 2010). Sensitivity analysis helps to identify inputs which cause significant changes to the output, providing hints to the identity of the most influential mechanisms involved. This helps to counter errors in modelling and increases our understanding about the structure of the model. From the available methods, we first use local sensitivity analysis (LSA) where a single parameter is altered to check the effect of that on the output.

In meiosis initiation, our main interest is on the transient expression of meiosis initiators with sufficient protein levels of the main meiosis (Ime1, Ime2) initiators. According to the molecular biology relationships and the results discussed in Section 3.3, Ime2 and Cdk1/Cln3 concentrations play major roles in meiosis and mitosis initiation; therefore, we select the peak values of Ime2 and Cdk1/Cln3 as significant measures to monitor the system under different parameter changes.

In this model we perturb the set of parameters given in the Table 7.1, which includes all the parameters of the main model apart from the parameters used for non-dimensionalisation and the constants used to generate the Rim15 temporal variation. We perturb one parameter at a time by ±30% from the standard value and examine the peak values of Ime2 and Cdk1/Cln3. Standard variation (Equation (7-1)) is used as the measure to calculate the normalised significance of the changed parameter (Morbidelli and Wu, 2005).

$$\text{Standard variation} = \frac{C^{\max}_{(-30\%\text{ of standard})} - C^{\max}_{(+30\%\text{ of standard})} \;/\; C^{\max}_{\text{standard}}}{P_{(-30\%\text{ of standard})} - P_{(+30\%\text{ of standard})} \;/\; P_{\text{standard}}} \qquad (7-1)$$

where P_{standard} is the parameter value corresponding to the standard condition and $C^{\max}_{\text{standard}}$ is the maximum concentration value of the variable of interest, employing standard parameter values. $P_{(-30\%\text{ of standard})}$ represents the parameter value reduced by 30% from the standard value and $C^{\max}_{(-30\%\text{ of standard})}$ represents the corresponding peak output concentration using parameters reduced by 30% from the standard value. Similarly, $P_{(+30\%\text{ of standard})}$ represents the parameter values increased by 30% from the standard value and $C^{\max}_{(+30\%\text{ of standard})}$ represents the corresponding peak output concentration.

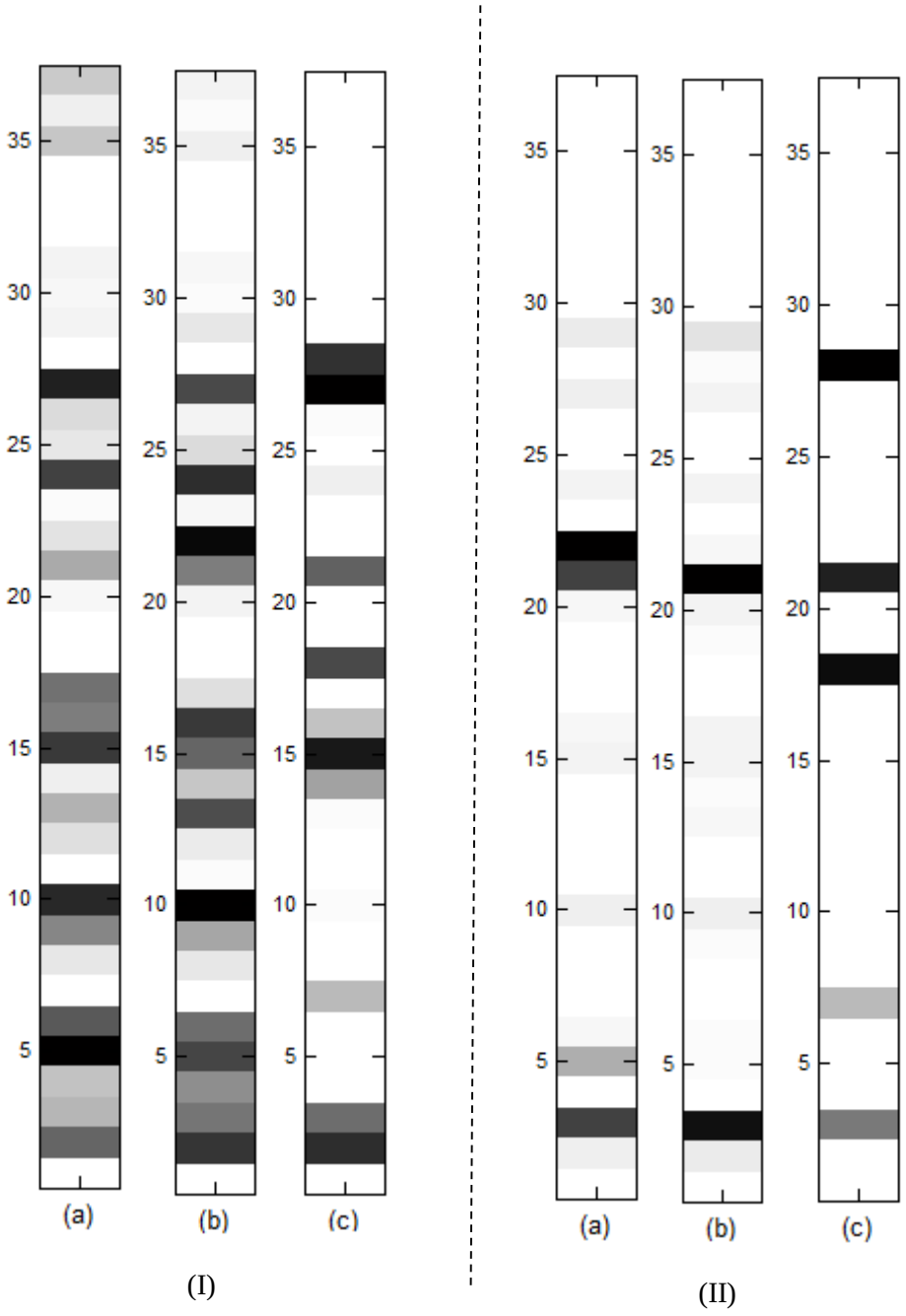

Figure 7.1 Local sensitivity analysis of the model. (I) The local sensitivity analysis based on the peak concentration of Ime2; and, (II) shows the sensitivity based on the peak concentration of the Cdk1/Cln3. (a) Corresponds to meiosis initiation at low nitrogen level (0.06) (b) Corresponds to transition stage at nitrogen level of 0.083 (c) Corresponds to mitosis initiation at high nitrogen levels (0.98). Standard parameter values, their definition and the index are given in the Table 7.1. The dark colour in the heat map indicates higher sensitivity and the lighter colour indicates the lower values of the sensitivity.

Table 7.1 Parameters, their significance and index values

Index	Name	Biological Significance
1	α_{fIme1}	Basal transcription rate of Ime1
2	α_{fIme2}	Basal transcription rate of Ime2
3	α_{Cln3}	Basal transcription rate of Cln3
4	$\alpha_{Rpd3Sin3}$	Complex formation rate of Rpd3/Sin3
5	β_{fIme1}	Maximum transcription rate of Ime1
6	β_{fIme2}	Maximum transcription rate of Ime2
7	$\beta_{Cdk1\backslash Cln3}$	Maximum transcription rate of Cdk1/Cln3
8	n_1	Hill coefficient of Ime1 auto regulation
9	K_{fIme11}	Disassociation constant of Ime1 binding to its own promoter
10	K_{fIme22}	Disassociation constant of Ime2 binding to its own promoter
11	K_{N_2}	Disassociation constant of nitrogen binding to IME1 promoter
12	K_{fIme12}	Disassociation constant of Ime1 binding to IME2 promoter
13	$K_{Rpd3\backslash Sin3}$	Disassociation constant of Sin3/Rpd3 binding to IME2 promoter
14	γ_{PIme2}	Maximum phosphorylation rate of Ime2 by Cdk1/Cln3
15	K_p	Dephosphorylation constant of Cdk1/Cln3 from Ime2
16	d_{fIme2}	Degradation rate of Ime2 protein
17	d_{fIme1}	Degradation rate of Ime1 protein
18	K_{N_2Cln3}	Disassociation constant of nitrogen binding to Cln3 promoter
19	$\gamma_{PCdk1Cln3}$	Maximum phosphorylation rate of Cdk1/Cln3 by Ime2
20	$K_{PIme2Cdk1}$	Dephosphorylation constant of Ime2 from Cdk1/Cln3
21	d_{Cln3}	Degradation rate of Cdk1/Cln3 protein complex
22	$d_{Rpd3Sin3}$	Degradation rate of Rpd3/Sin3 protein complex
23	n_2	Hill coefficient of nitrogen repression on IME1 promoter
24	n_3	Hill coefficient of Ime2 auto regulation
25	n_4	Hill coefficient of Ime1 activation on IME2 promoter
26	n_5	Hill coefficient of Rpd3/Sin3 repression on IME2 promoter
27	n_6	Hill coefficient of phosphorylation of Ime2 by Cdk1/Cln3
28	n_7	Hill coefficient of nitrogen activation on Cln3 promoter
29	n_8	Hill coefficient of phosphorylation of Cdk1/Cln3 by Ime2
30	$K_{Cdk1\backslash Cln3}$	Disassociation constant of Cdk1/Cln3 binding to IME1 promoter
31	n_9	Hill coefficient of Cdk1/Cln3 repression on IME1 promoter
32	$\gamma_{PIme1Cln3}$	Maximum phosphorylation rate of Ime1 by Cdk1/Cln3
33	n_{10}	Hill coefficient of phosphorylation of Ime1 by Cdk1/Cln3
34	$K_{PIme1Cdk1\backslash Cln3}$	Dephosphorylation constant of Ime1 by Cdk1/Cln3
35	$K_{Rpd3SIme1}$	Disassociation constant of Rpd3S binding to IME1 promoter
36	n_{11}	Hill coefficient of Rpd3S repression on IME1 promoter
37	n_{12}	Constant related with Rpd3S temporal variation

Table 7.2 Fifteen most sensitive parameters with a local sensitivity of more than 1, selected from the local sensitivity analysis (parameter definitions are given in Table 7.1)

Parameter	Index	Parameter	Index
α_{fIme2}	2	d_{fIme2}	16
α_{Cln3}	3	K_{N_2Cln3}	18
$\alpha_{Rpd3Sin3}$	4	d_{Cln3}	21
β_{fIme1}	5	$d_{Rpd3Sin3}$	22
β_{fIme2}	6	n_3	24
K_{fIme22}	10	n_6	27
$K_{Rpd3\backslash Sin3}$	13	n_7	28
K_p	15		

We analyse the system at each of the three different states by changing the nitrogen level: meiosis-only at the nitrogen level of 0.06; mitosis-only at the nitrogen level of 0.98; bistable transition stage at nitrogen level of 0.083.The results obtained from the local sensitivity analysis are given in Figure 7.1. In these heat maps, darker colours show higher sensitivity. The fifteen most sensitive parameters of meiosis and mitosis initiation, which have standard variation values of more than 1, are given in Table 7.2, together with their indices.

7.2 Biological Implications from the most Sensitive Parameters Revealed by Local Sensitivity Analysis

In this section, we categorise the 15 most sensitive parameters (Table 7.2) into six groups and discuss the possible reasoning behind the sensitivity of these parameters in the biological context of meiosis and mitosis initiation. We considered six categories as follows: synthesis rates (α_{fIme2} , α_{Cln3} , $\alpha_{Rpd3Sin3}$, β_{fIme1} , β_{fIme2}) ; degradation rates (d_{fIme2} , d_{Cln3} , $d_{Rpd3Sin3}$) ; Ime2 positive auto-regulation (K_{fIme22} , n_3) ; Rpd3/Sin3 repression on Ime2 ($K_{Rpd3\backslash Sin3}$); phosphorylation of Ime2 by Cdk1/Cln3 (K_p , n_6); Cln3 activation by nitrogen (K_{N_2Cln3} , n_7).

Protein homeostasis requires a well-controlled balance between protein synthesis and degradation. Experiments reveal that protein synthesis and degradation rates are most influential for some biological system outputs: the protein synthesis rate is found to be the predominant regulator of protein expression during differentiation (Kristensen et al., 2013), protein synthesis and degradation rates account for the differential responses of neurons to spaced and massed training protocols (Naqib et al., 2011). Our LSA results indicate that the protein synthesis and degradation terms have the most influence for the output from meiosis and mitosis initiator levels. Similar results were observed for the sensitivity analysis of the previous theoretical model of meiosis initiation (Ray et al., 2013). Our first sensitive parameter group possesses synthesis terms for almost all proteins, with only the degradation term of Ime1 missing. When Ime1 degradation during meiosis initiation is considered, the Ime2 protein plays a major role in phosphorylating Ime1 and tagging it for degradation: experiments show that the Ime2 deletion mutation results in a non-transient increase in the Ime1 protein (Guttmann-Raviv et al., 2002). The Ime2 related degradation of Ime1 is represented in our model by an Ime2 term that is included to Ime1 degradation term. Since Ime2 plays a major role in Ime1 degradation, the sensitivity of Ime2 degradation and the synthesis terms would represent the sensitivity of the missing Ime1 degradation.

The second category comprises two terms from the Hill function which represents the Ime2 positive auto-regulation. The Ime2 positive auto-regulation amplifies its own expression to ensure that EMGs are sufficiently expressed (Bowdish and Mitchell, 1993). When nitrogen depletion activates IME1 expression, rising Ime1 protein levels activate IME2 expression; however, cells with low levels of Ime1 have shown faithful sporulation (Bowdish and Mitchell, 1993). Furthermore, the modulation of the IME1 copy number had no deleterious effects on sporulation (Gurevich et al., 2010). Experiments suggest that Ime2 self-stimulation would create sufficient Ime2, if a cell makes enough Ime1 to stimulate IME2 expression (Bowdish and Mitchell, 1993). Therefore, Ime2 auto-regulation plays an important role in maintaining Ime2 protein levels at sufficient levels; this may be the reason behind the sensitivity shown on Ime2 auto-regulation in Ime2 expression.

The sensitivity of the Rpd3/Sin3 repression on Ime2 expression is obvious since Rpd3 is a histone deacetylase complex, which is required to be transiently removed from the IME2 promoters for histone acetylation at meiosis initiation. The fifth category is related with the phosphorylation of Ime2 by Cdk1/Cln3. Ime2 possesses three Cdk1 phosphorylation sites in its regulatory region and experiments with mutations in these sites showed an approximate four hour premature entry into the meiotic S phase and high Ime1 levels (because the lack of Ime2 reduces Ime1 degradation) (Gurevich et al., 2010). These experiments suggest that the phosphorylation of Ime2 by Cdk1/Cln3, which is identified as sensitive from our analysis, affects Ime2 homeostasis.

The last category is related with the nitrogen-related repression of Cln3. CLN3 expression is controlled mainly by nutrients. Cln3 production is reduced by transcriptional repression, translational repression and degradation upon nitrogen depletion (Colomina et al., 1999; Gallego et al., 1997; Parviz and Heideman, 1998). The identification of the nitrogen related terms as sensitive is conceivable, because these nutrient-related terms directly affect the level of Cln3 expression.

7.3 Group Effects of the Most Sensitive Parameters of Local Sensitivity by Global Sensitivity Analysis

In this section, we employ global sensitivity analysis to study the group effects of the most sensitive parameter set on system behaviour. Global sensitivity analysis is normally used to study the variations in outputs caused by a group of parameters when they are altered simultaneously. Global sensitivity analysis is more appropriate for theoretical sensitivity

analysis of biological systems since real kinetic rate constants vary simultaneously under different environments (Rand, 2008).

The most sensitive parameters selected from the local sensitivity analysis (Table 7.2) are varied simultaneously over a range to study their global effects on the system discussed. Considering the typical parameter variation ranges of biological systems, the range of a selected parameter is selected as ± 30% from the standard value (Kilfoil et al., 2009). We randomly generate 3000 vectors of 15 parameters in the given range using Latin hypercube sampling (LHS) since LHS guarantees that individual parameter ranges are covered evenly. We input these 3000 parameter sets into our model keeping the other parameters at their standard values. The output is checked for normal behaviour: in meiosis initiation, we check whether the output is transient and whether the maximum value of Ime2 is in the typical range (±30% from standard value); in mitosis initiation, we check whether the meiosis initiator levels are less than the typical values (+30% from standard value) and whether the mitosis initiator's maximum value is in the typical range (±30% from standard value). The outputs not in these normal ranges are considered as non-behaviour. For each parameter we calculate and compare the cumulative distributions of behaviour and non-behaviour sets. The resulting cumulative frequency distributions of behaviour and non-behaviour sets for each parameter are given in Appendix D. The statistical differences between behaviour and non-behaviour sets calculated by the Kolmogorov-Smirnov (KS) test are used to identify parameter's global sensitivity index (Stephens, 1970). The least P-valued (resulting from the KS test) parameter is the most sensitive and other parameters' sensitivity index decreases with the increasing P value (Appendix D). This procedure was repeated for the three nitrogen conditions (meiosis, mitosis and transition) and the resulting global sensitivity indexes are given in Figure 7.2.

7.4 Implications from the Global Sensitivity Analyisis

7.4.1 Biological implications from local (LSA) and global (GSA) sensitivity ranks

We compare the LSA and GSA ranks in Figure 7.2 to examine the differences between the individual effects and group effects on the output by the most sensitive parameters. The similarly ranked parameters of the LSA and GSA lie along the diagonal line in Figure 7.2 (a), (b) and (c). Many parameters lie closer to the diagonal line of the three states in Figure 7.2 implying that most of the parameters have similar group and individual impacts on the output.

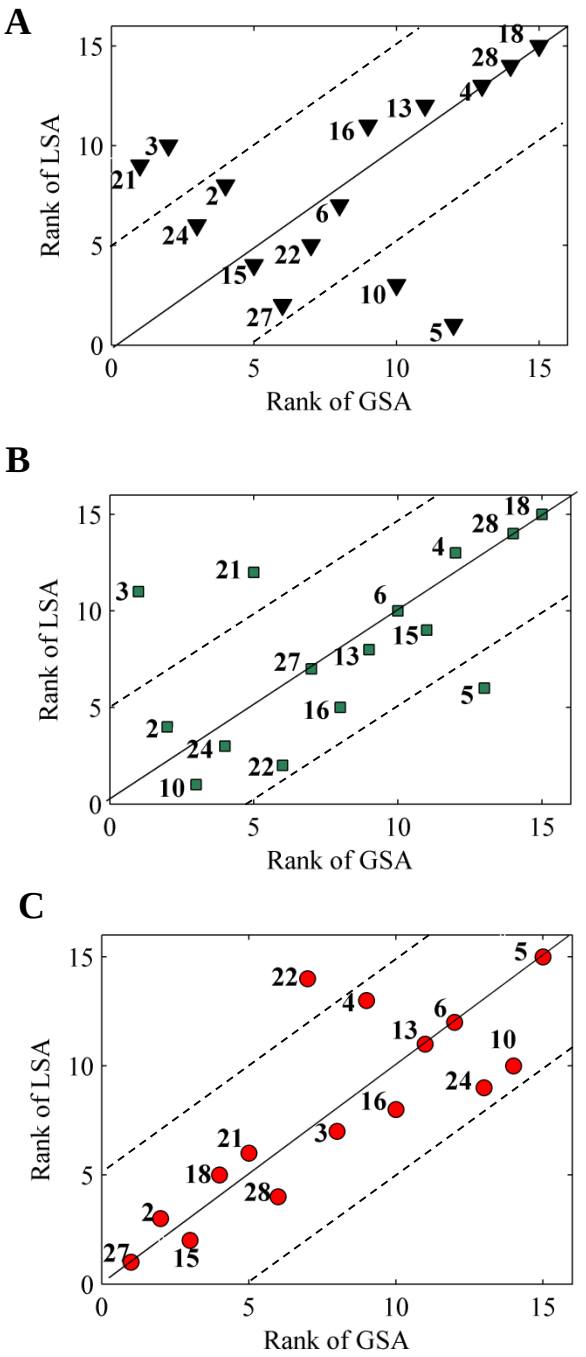

Figure 7.2 Global and local sensitivity analysis results of different states at different nitrogen levels: (A) meiois-only state at the nitrogen level of 0.06. (B) transition state at the nitrogen level of 0.083. (C) mitosis-only state at the nitrogen level of 0.98. Refer to Table 4.1 for definitions of the indices. The most sensitive parameter has the lowest rank (the lowest rank starts from 1), and the global or local sensitivity decreases when the rank increases.

To find the variables which scored significantly different rank from two analyses, we drew two diagonal lines of the distance of the five ranks around the central diagonal line (marked with a dashed line in Figure 7.2). Five ranks are selected because this number sufficiently distinguished the parameters which lie near the diagonal line from the other parameters. The set of parameters which lie outside these two dashed lines are significantly different in LSA and GSA ranks.

This set with significantly different ranks of LSA and GSA consists of five parameters, of which two of them, ($\boldsymbol{\beta_{fIme1}}, \boldsymbol{K_{fIme22}}$), show high GSA and low LSA ranks; and three of them, ($\boldsymbol{\alpha_{Cln3}}, \boldsymbol{d_{Cln3}}, \boldsymbol{d_{Rpd3Sin3}}$), show low GSA and high LSA ranks. The first group, ($\boldsymbol{\beta_{fIme1}}, \boldsymbol{K_{fIme22}}$), shows a high GSA rank and a low LSA rank which means this group has lower global sensitivity than individual local sensitivity. This implies that these two variables can cause a lesser effect on the system behaviour while working in a group. This is conceivable, since these two variables, which are related with IME1 expression and Ime2 positive auto-regulation, have direct effects on the Ime2 expression level. Ime2 requires sufficient Ime1 to activate IME2 initial expression and Ime2 positive auto-regulation amplifies Ime2 levels to produce adequate Ime2 levels for the downstream protein activation. Less global effects of these two variables imply the importance of the cooperation between the mechanisms of IME1 activation and Ime2 auto-regulation on IME2 expression rather than their individual effects. The second group consists of Cdk1/Cln3 expression, degradation-related parameters and a parameter related to the degradation of Rpd3 and shows a low GSA rank implying that the effects from perturbations in these proteins are increased when working as a group rather than individually.

7.4.2 Common parameters to the three states: meiosis, transition and mitosis

We examine the first eight sensitive parameters of GSA in the three states: meiosis, transition and mitosis (Figure 7.3) to identify the common sensitive parameters. The results show that five of the eight most sensitive parameters in each nutrient condition are common to all three nutrient conditions.

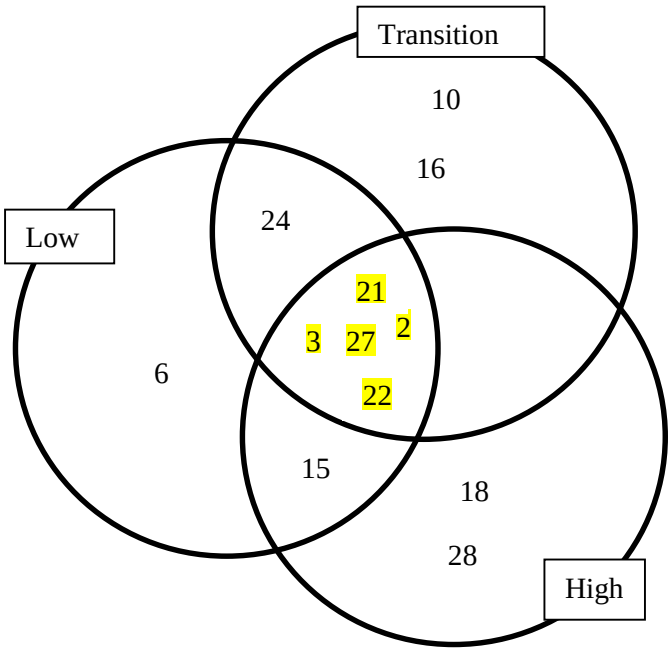

Figure 7.3 The eight most sensitive parameters of the global sensitivity analysis at each three nitrogen conditions. The three circles represent the three nutrient conditions at meiosis, mitosis and transition. The set of common parameters to the three states are marked with yellow. Parameters are represented by the index numbers given in Table 7.1.

This implies that this common parameter set may play a major role in the meiotic-mitotic switch during nutrient-based transitions. Four of these five parameters belong, specifically, either to meiosis initiator Ime2 or mitosis initiator Cln3 regulation only: basal transcription rate of Ime2, hill coefficient of the Ime2 phosphorylation by Cdk1/Cln3, basal transcription rate of Cln3 and degradation rate of Cln3. This is conceivable since they are the major initiators of meiosis and mitosis. The remaining parameter is the degradation rate of Ime2 inhibitor, Rpd3, which is essentially removed from IME2 promoter for histone acetylation.

7.5 Robustness of Meiosis, Mitosis and Transition Stages at the Gene Expression Level

In this section, we investigate the robustness of maintaining meiosis, mitosis and transition states at the gene expression level despite perturbations in the most sensitive parameters. We first present the criteria we use to measure the function and performance of our system. Secondly, we define a mathematical formulation to investigate the robustness and use this definition to study the robustness of meiosis and mitosis initiation under perturbations of the most sensitive parameters.

7.5.1 Defining the criteria to check the functionalities of meiosis initiation, mitosis initiation and transition

At each of the three stages, (meiosis, mitosis and transition) we check whether the meiosis and mitosis initiator proteins behave as expected against parameter perturbations. In the first stage (meiosis), we measure the main functionality of meiosis initiation by observing the following features from the protein expression levels: the expressions of the main meiosis initiators need to be transient and sequential; the mitosis initiator level needs to stay at low values (less than +30 percent from the standard value). To check the sequential expression of Ime2 after Ime1, we check whether the peak time of Ime2 precedes that of the Ime1 protein. To check the transient peak like shape of the Ime1 and Ime2 protein expressions, we first check whether Ime1 and Ime2 peak values lie within ±30 percent from their standard values (This is to check whether these proteins reach the threshold values required). Specifically, maintenance of the Ime2 threshold value is important since the downstream proteins activated by Ime2 respond to Ime2 levels in a threshold mode. We also check whether these protein expressions reach the peak value transiently or by continuous increment. We check this by observing whether the protein expression has an increment and a reduction instead of a single increment which would peak at the maximum Ime1or Ime2 level (for this, we use the ‘diff’

function in Mathlab to count the number of increments in the matrix of protein levels and check whether all the protein values increase continuously). Under a particular instance of perturbation, if the protein expressions of meiosis and mitosis initiators meet the above criteria, we consider that the system behaves robustly in meeting the required performance level in that instance.

Under mitosis initiation conditions (second stage), we check the functionality of the system by inspecting the required higher threshold value of the mitosis initiator (Cdk1/Cln3) and the lower meiosis initiator levels. For this, we first check whether the mitosis initiator's peak value is higher than that of the meiosis initiators. We then check whether the mitosis initiator levels have reached the threshold region by examining whether the peak Cdk1/Cln3 level lies between ±30 percent from the standard peak value. We also check whether the Ime1 and Ime2 peak values are lower than +30 percent from their standard peak values. Once all the above criteria are met, we consider that the function of mitosis initiation is preserved in the instance considered.

We define the criteria to check the functionality at the transition stage (third stage) based on the gene expression pattern under standard conditions. Protein levels predicted under standard conditions in the transition stage show meiosis initiator proteins are expressed transiently and sequentially having lower threshold values than in the meiosis stage at a low nitrogen level. Mitosis initiator level also shows higher values than in the meiosis stage under low nitrogen levels. Following the same methods that we used when inspecting the functionality of meiosis initiation, we check whether Ime1 and Ime2 are expressed transiently and sequentially in reaching the required threshold peak levels. We also check whether the mitosis initiator protein level reaches the corresponding threshold level of ±30 percent from the standard value. If the above criteria are met at an instance of a certain perturbation level, we consider that the protein expression pattern possesses the requirements to preserve the functionality at the transition stage.

7.5.2 Robustness of meiosis initiation, mitosis initiation and transition stages

To quantify the robustness at each meiosis, mitosis and transition stage, we perturb the set of the five most sensitive parameters in several parameter perturbation regimes: standard values ±10%, standard values ±20%, standard values ±30%, standard values ±40% and standard values ±50%. For an individual parameter regime at each stage, we generate 2000 sample

vectors of the most sensitive parameters. In order to make sure that the individual parameter ranges are evenly covered, and to ensure that the generated vectors represent the real variability of the parameter regime considered, we use Latin hypercube sampling to generate the parameter vectors of the most sensitive parameters (McKay et al., 1979).

Once the parameter vectors for each perturbation regime are generated, we run the simulation using each parameter vector in each of the three stages: meiosis at the nitrogen level of 0.06, mitosis at the nitrogen level of 0.98 and transition at the nitrogen level of 0.084. We keep the other parameter values constant at the same values as in standard conditions. Using one parameter vector at a time under meiosis initiation conditions, we check whether the gene expression pattern satisfies the criteria, defined in Section 7.6, to maintain the desired meiosis initiation functionalities. Similarly, we perturb the system at mitosis and the transition stage and check whether the system maintains its functionalities. We record the performance level (Equation 7-2) (probability of maintaining functionality) at each individual perturbation regime in all three stages using the following measure. Table 7.3 shows the performance levels (V_i) for the three stages of meiosis, mitosis and transition.

$$Performance\ Level(V_i) = \frac{Number\ of\ sample\ vectors\ where\ functionality\ is\ maintained}{Number\ of\ all\ sample\ vectors} \quad (7\text{-}2)$$

The results (Table 7.3) show that performance levels (V_i) in the meiosis and mitosis states are barely affected by the parameter perturbations at ±10% from the standard values. The performance level at all the three stages (meiosis, mitosis and transition) decreases with increasing perturbation levels. These results indicate the high robustness of meiosis and mitosis initiation against the presence of low levels of perturbations in the key kinetic parameters of the model.

Table 7.3 Probability of maintaining functionalities at meiosis, mitosis and transition based on the criterion defined in Section 7.6. V_i indicates how often a cell can perform as expected to initiate meiosis, mitosis or transition against perturbations in the most sensitive parameters.

Parameter Range	Performance level(V_i) at three main stages		
	Meiosis	Transition	Mitosis
Standard Values ±10%	0.9735	0.5745	0.9795
Standard Values ±20%	0.745	0.269	0.8435
Standard Values ±30%	0.5605	0.167	0.74
Standard Values ±40%	0.44	0.104	0.6705
Standard Values ±50%	0.383	0.054	0.6195

7.5.3 Mathematical definition of robustness for this model

In this analysis, we do not use the primitive mathematical definition of robustness presented in Equation 2-16 because of the binary nature of the outputs produced from our functionality assessment. We have binary outputs from our functionality assessment rather than the continuous performance levels assumed in Equation 2-16. For example, in a successful meiosis initiation situation, we have one as the output and, in a situation where meiosis did not initiate successfully, we have zero as the output. Therefore, we define the following measure (Equation 7-3) to check the robustness of meiosis initiation, mitosis initiation and the transition under diverse parameter perturbations.

$$R = \frac{\sum_i \left(\sum_j \Delta p_j\right) * V_i}{\sum_i \sum_j \Delta p_{ij}} \qquad (7-3)$$

In this equation, 'R' represents the robustness. 'i' represents the number of perturbation levels and 'j' represents the number of parameters perturbed. 'Δp_j' represents the full range of the jth parameter perturbed. 'V_i' is used to input the performance level under i^{th} perturbation level, as defined in Equation 7-2.

According to the mathematical measure for robustness presented in Equation 7-3, we calculate the robustness at the three states: meiosis, mitosis and transition. The results (Figure 7.4) show that the meiosis and mitosis initiation stages are more robust to parameter perturbations than the transition stage. This low robustness at the transition stage may be related to the narrowness of this region in the meiotic-mitotic switch.

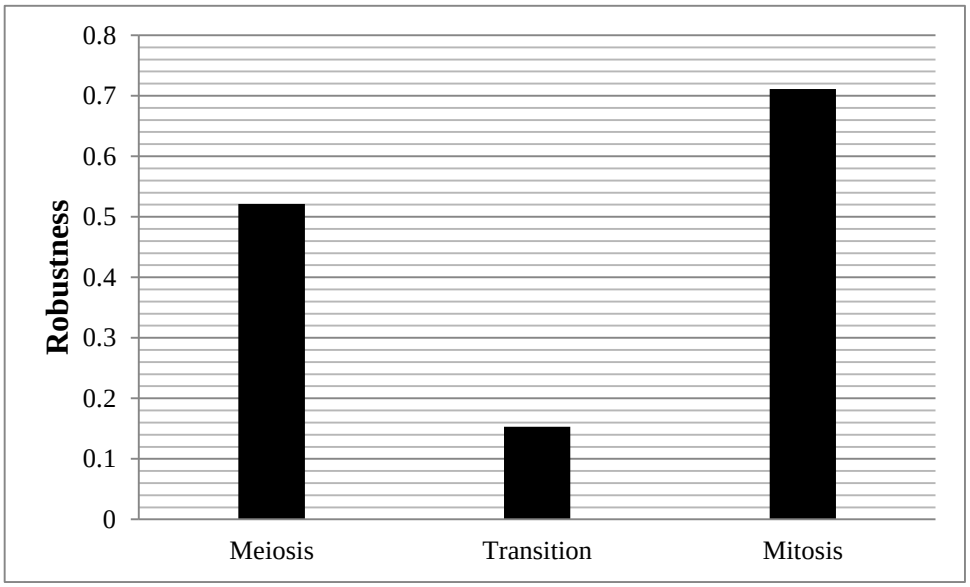

Figure 7.4 Robustness of the main three stages of meiosis, transition and mitosis at the gene expression level. The robustness values are calculated using the defined robustness measure in Equation (7-3).

7.6 Effects of Common Parameter Perturbations on the Meiotic-mitotic Switch

The resulting low, robust values at the transition stage in Section 7.6 leads to the question of what would happen to the meiotic-mitotic switch under perturbations of the most sensitive parameters. In this section, we examine the effects on the meiotic-mitotic switch by perturbations of the most sensitive five parameters common to the three states of meiosis, mitosis and transition. Since this set of five parameters is common to meiosis, mitosis and transition stages, they may play a major role in the meiotic- mitotic switch. For this, we perturb the five common parameters, as discussed in the above section (α_{fIme2}, α_{Cln3}, d_{Cln3} ,$d_{Rpd3Sin3}$,n_6), within ±30% from their standard parameter values and generate 75 random parameter sets using Latin hypercube sampling. We examine the behaviour of the switch at each parameter set and present the results in Table 7.4.

As can be seen from Table 7.4, we observe three main types of switches (Figure 7.5): normal bistable, memory-less and bistable switch with abnormalities. The memory-less switch does not have a bistable state (where the meiosis and mitosis states coexist). The abnormal switch does not have a meiosis-only state and shows a wider transition region. Differences in the transition region of these three types of switches indicate the lower robustness observed in the previous section (Figure 7.4). We observe that all three types of switches transit from the meiosis to the mitosis stage when the nitrogen level is increased from its minimum level (Figure 7.5). This preserved characteristic of transitioning to mitosis when nutrients are provided is the main functionality of the meiotic-mitotic switch. This observation implies that even with parameter perturbations, budding yeast cells are robust to transit to mitosis initiation when the nutrients are provided.

The bistable transition region in the normal meiotic-mitotic switch is, in fact, very narrow. This narrow transition region allows reversible switching between meiosis and mitosis. Transitions in memory-less switches are always reversible. However, in the abnormal switches, we see that the bistable transition region is broader than in the normal switch. This is probably a consequence of dissemination of effects from the most sensitive parameter perturbations to preserve the main functionality of transition to mitosis. This bistable transition region is a consequence of the double negative feedback loops between Ime2 and Cdk1/Cln3 which typically help with the adaptation to perturbations (Yi et al., 2000).

Table 7.4 Observed switch types and their percentages when the most sensitive, common parameter set is perturbed. We use 75 random parameter sets of the five parameters, generated by Latin hypercube sampling, within ±30 percent of the standard parameter values.

Observed Switch Type	**Percentage**
Normal bistable meiotic-mitotic switch with meiosis only, bistable and mitosis-only states (Figure 7.5 A, B).	24%
Memory-less switch with no bistable state (Figure 7.5 C, D).	38.6%
Bistable switch with abnormalities: meiosis-only state is missing and the bistable transition region is broader (Figure 7.5 E, F).	37.3%

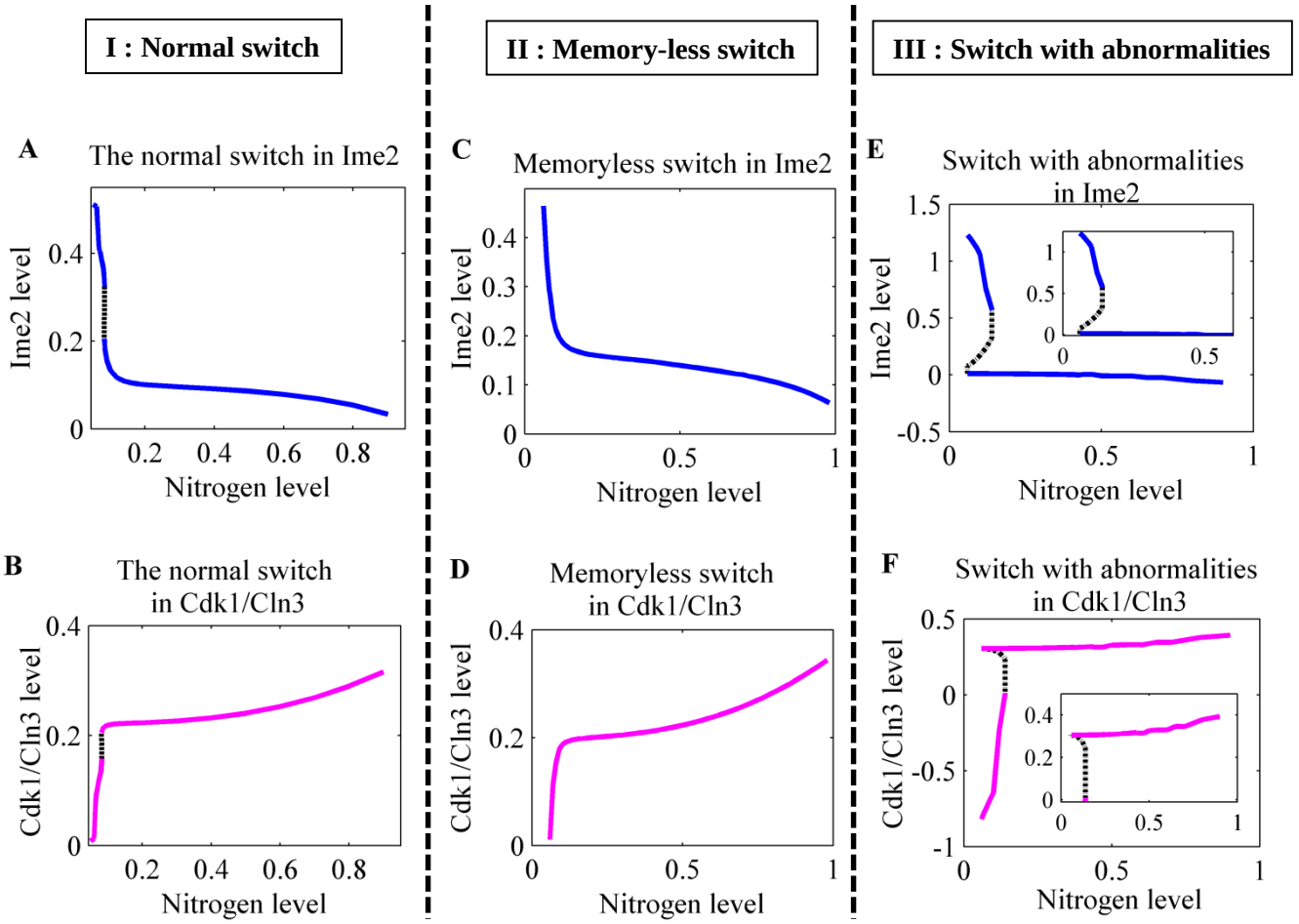

Figure 7.5 The three types of switches observed when the most sensitive common parameters of the three states (meiosis, mitosis and transition) are perturbed simultaneously. (I) The first column shows the normal switch. A and B correspond to the normal switch observed in Ime2 and Cdk1/Cln3, respectively. (II) The second column shows the memory-less switch. C and D correspond to the memory-less switch observed in Ime2 and Cdk1/Cln3, respectively. (III) The third column shows the switch with abnormalities. E and F correspond to the switch with abnormalities observed in Ime2 and Cdk1/Cln3. The inset plots in E and F show the sections of the corresponding switches having positive values and the sections with negative values are ignored as negative protein levels do not exist in a real system.

To study the parameter ranges of each switch type, we draw each sensitive parameter's value range (Figure 7.6) for each of the three switch types. We compare these parameter ranges with the full parameter range of ±30 percent from the standard parameter value.

When the parameter ranges of the abnormal bistable switch are considered (Figure 7.6), α_{Cln3} shows discrete high values and d_{Cln3}, α_{fIme2} show lower values. Taken together, these three parameter variations explain the reason for the abnormalities observed: the missing meiosis-only state and the lower Ime2 state which represent the mitotic state at low nutrients, with higher Cdk1/Cln3 values observed at low nitrogen levels.

The high synthesis rate and lower degradation rate of Cln3 would produce more Cln3. Higher Cln3 levels inhibit meiosis initiation by several mechanisms: Cln3 represses IME1 translation and transcription, Cdk1/Cln3 phosphorylates Ime1and the phosphorylated Ime1 is transported out of the nucleus and Cdk1/Cln3 inactivates Ime2 by phosphorylation. This inhibition of meiosis at lower nutrients is further facilitated by the lower Ime2 synthesis rate. Consequently, these parameter sets produce abnormal switches with the meiosis-only state missing because of high Cln3 values at low nutrients. Skipping the meiosis-only state, the switch starts from the bistable region where the meiosis and mitosis states coexist.

The parameter ranges of the memory-less switch do not provide hints for a good explanation for the missing bistable state where the meiosis and mitosis states coexist. Several requirements are essential to show bistability: a feedback loop (the double negative feedback loop between Ime2 and Cdk1/Cln3 in this system), a kind of non-linearity within the feedback loop and two properly balanced legs of the feedback loop. The most probable reason for the observation of a memory-less switch without the bistable region may be the unbalanced levels of Ime2 and Cdk1/Cln3 produced by the perturbations in the most sensitive parameters.

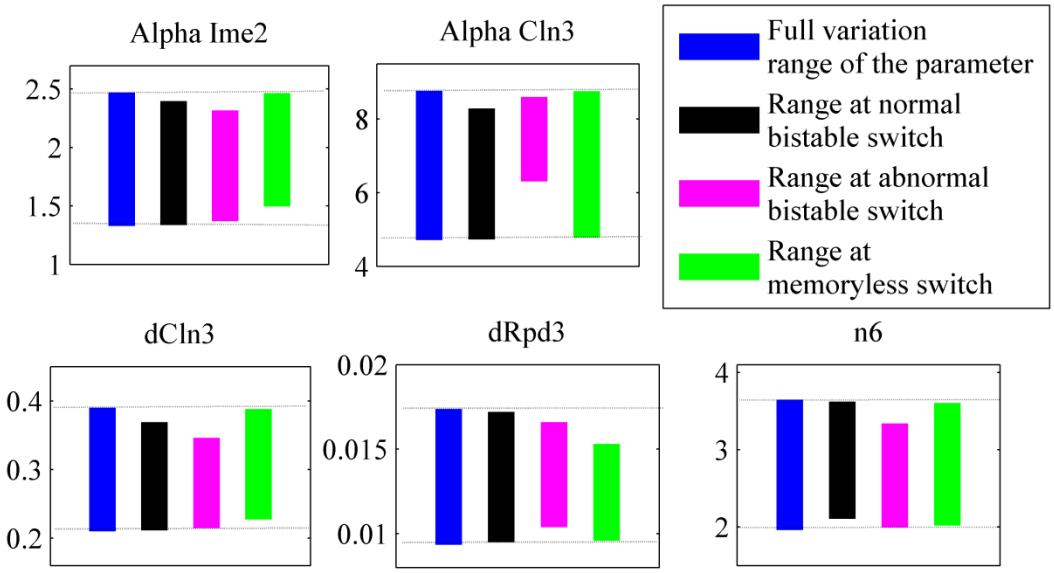

Figure 7.6 Value ranges of the five sensitive parameters in the three types of switches. The full parameter variation range is between ± 30 percent from the standard parameter value. The dashed two lines in each plot indicate the maximum and minimum values of the full parameter variation range which lies between ±30 percent from the standard parameter value.

7.7 Summary and Conclusions

Living cells typically function under varying environmental conditions with abundant uncertainties. As a consequence of these different environmental conditions, real time cell populations show heterogeneity and function under a range of parameter values. Kinetic parameter values are mainly affected by temperature and pressure changes in the cellular environment. However, living systems have evolved to maintain their main functionalities robustly even in these varying environments robustly.

In this chapter, we investigate the robustness of meiosis and mitosis initiation against perturbations of the most influential parameters at the gene expression level. We also examine whether the meiotic-mitotic initiation switch can maintain its functionality robustly against perturbations of the most influential parameters. The main conclusions are summarised below.

We first identify the most influential parameters on the output protein levels of the meiosis (Ime2) and mitosis (Cdk1/Cln3) initiators. By employing local sensitivity analysis (LSA), we identify a set of parameters which can cause the most influential, individual effects on the output initiator levels. The most sensitive parameter set consists of a group of synthesis rates (α_{fIme2} , α_{Cln3} , $\alpha_{Rpd3Sin3}$, β_{fIme1} , β_{fIme2}) and degradation rates (d_{fIme2} , d_{Cln3} , $d_{Rpd3Sin3}$), which are frequently found to be sensitive in experiments. Some parameters related to Ime2 positive auto-regulation (K_{fIme22},n_3) are also very sensitive, and this is conceivable because Ime2 positive auto-regulation plays a major role in Ime2 expression even in situations where the Ime1 level, which activates Ime2 expression, is low. The other sensitive parameters are related to Rpd3/Sin3 repression on Ime2 ($K_{Rpd3\backslash Sin3}$), phosphorylation of Ime2 by Cdk1/Cln3 (K_p , n_6) and Cln3 activation by nitrogen (K_{N_2Cln3} , n_7), all of which play major roles in the expression of the main meiosis and mitosis initiators.

Secondly, we employ global sensitivity analysis (GSA) on the above set of parameters selected from LSA and identify the parameters which can mostly influence the output initiator levels as a group. Comparison of the results from GSA and LSA showed that most of the parameters have similar sensitivities as individuals or as a group. The other parameter set with significantly different ranks of LSA and GSA consists of five parameters from which two of them, (β_{fIme1}, K_{fIme22}), shows high GSA and low LSA ranks; and three of them, (α_{Cln3}, d_{Cln3}, $d_{Rpd3Sin3}$), shows low GSA and high LSA ranks. The lower global sensitivity of the first group, (β_{fIme1}, K_{fIme22}), implies that these two variables have a lower influence while working in a group. These two variables directly regulate the Ime2 expression level. Ime2

requires sufficient Ime1 to activate IME2 initial expression and IME2 positive auto-regulation to amplify Ime2 levels to produce adequate Ime2 levels for the activation of further downstream genes.

By comparing the first eight most sensitive parameters from the GSA results in all three stages (meiosis, mitosis and transition), we identify that the five of the eight parameters are common to the three main stages. Identification of common parameters implies that this set may play a major role in the meiotic-mitotic switch during nutrient-based transitions. Further, four out of five parameters of this set belong specifically, either to meiosis initiator (Ime2) or mitosis initiator (Cln3) regulation only. A robustness analysis of meiosis and mitosis initiation against the perturbations of the common sensitive set of parameters revealed that the robustness of maintaining meiosis initiation, transition and mitosis initiation at the gene expression levels decrease with the increasing perturbation levels of the parameters. Further, the robustness of maintaining the transition stage was lower than at the other two stages.

We successfully investigate whether the meiotic-mitotic switch can maintain its functionality against the perturbations in the common set of parameters, using a set of parameter vectors generated using Latin hypercube sampling. This analysis resulted in three main types of switches: normal bistable, memory-less and abnormal switches. Differences in the transition region of these three types of the switches indicate the lower robustness of the transition state observed in Section 7.5. The main preserved functionality in all of the switches against the perturbations was the transition from the meiosis state to the mitosis state when the nutrient level is increased from its lowest value. This implies that the meiotic-mitotic initiation switch can robustly maintain its main functionality even with perturbations in the most sensitive parameters.

Chapter 8

Conclusions and Future Directions

"Follow the evidence to where it leads, even if the conclusion is uncomfortable"(Steven, 2009).

The central theme of this thesis is to employ the knowledge of mathematics to model and understand biological systems which exhibit bistable behaviour. The main objective is to develop a mathematical model to understand the initial meiotic-mitotic switching of budding yeast at the gene expression level as observed from experiments. Depending on the level of detail in the system and the research questions asked, we use a deterministic approach to model the meiosis initiation biological network. Analytical approaches are used to understand the system dynamics under parameter perturbations. The simulation results show that these deterministic and analytical approaches can be successfully used to understand and predict interesting behaviour for this biological system and useful to gain novel insights. Starting from the next section, we provide a brief overview of what we have achieved; the contributions from these achievements and future directions that can be followed from the current developments.

8.1 General Overview

The focus of this research is to develop a deterministic model of meiosis initiation incorporating the recently elucidated relationships of the mitosis initiator with the meiosis initiation network of budding yeast. The main purposes of this model are: (1) to integrate and verify the biological knowledge of the relations between meiosis and mitosis initiators in budding yeast; (2) to increase our confidence in understanding meiosis initiation at the gene expression level by checking the agreement between *in-silico* results and *in-vitro* data; (3) to employ the model to understand the initial meiotic-mitotic switching in budding yeast which depends on the available nutrients; (4) to investigate the robustness of meiosis and mitosis initiation to parameter perturbations; and, (5) to predict the effects of parameter perturbations on the initial stage meiotic-mitotic switch.

The initial step in the development of the model was identifying the meiosis initiation network of budding yeast. The biological facts of transcriptional and translational regulation of the main regulators (meiosis initiators: Ime1 and Ime2, mitosis initiators: Cdk1/Cln3) of the network were identified using the experimental literature, where western blotting and quantitative PCR (polymerase chain reaction) measurements were mainly used (Chapter 3). The relations between the main regulators of the network were also identified using gene deletion and mutation studies stated in the literature. After a careful interpretation, we constructed a conceptual network in a biologically meaningful level of detail based on a number of assumptions (Chapter 4). This conceptual network includes all the essential regulators, their regulatory mechanisms and relations between the main regulators. We converted all the information in the conceptual network into an ordinary differential equation model using mass action kinetics and Hill kinetics. Our detailed model includes four differential equations and forty parameters. During parameter estimation, we found biological value ranges of the most of parameters from the experimental literature. We fine-tuned the parameter values using the regulatory gene expression data from the experimental literature.

The constructed model was then thoroughly validated using gene deletion and mutation related studies in the experimental literature (Chapter 5). The validation process increased our confidence about the model predictions under different situations such as the varied nutrient levels and mutation situations. We summarise the main findings we found during the model validation process as follows: (1) the model simulates the expression pattern of the main regulators of meiosis and mitosis initiation at correspondingly extreme nutrient levels, with a good agreement to the experimental data. The model reproduces the transient and sequential

expression pattern of the main meiosis initiators at low nutrient levels. At high nutrient levels, the model predicts mitosis initiation with higher mitosis initiator levels and very low meiosis initiator levels; (2) the model is used to understand the roles of some individual components in meiosis initiation by deleting, overexpressing and varying the DNA copy number of those components. Specifically, the model reproduces and explains the Cdk1/Cln3-related repression on Ime1 and Ime2 (Figure 5.5) which produced contradictory results for Ime1 expression when experimentally tested two different ways: overexpressing Cln3 by IME2 promoter (Gurevich et al., 2010) resulted in higher Ime1 levels than the standard value, and overexpressing Cln3 using a tetracycline regulatory system (Colomina et al., 1999) resulted lower Ime1 levels than the standard. Our model shows that these two different output levels of Ime1 is because of the different Cln3 overexpression mechanisms used in these experiments; (3) the model explains some organism-level experimental mutant analysis results at the gene expression level. The model clarified the reason behind the premature initiation of the meiotic S phase when all the three phosphorylation sites of Ime2, where Cdk1/Cln3 can bind, are blocked. When all the terms related to these phosphorylation sites are removed, our model shows premature Ime2 protein expression, which explains the observed premature S phase entry and the rapid G1 arrest of the mutant cells; (4) the model inherits the advantages and overcome the limitations of the available models. The current model explains meiosis initiation more quantitatively accurately than the other two models and includes more biological relations than the other two models. Further, the current model explains meiosis and mitosis initiation under different nutrient levels more accurately since it includes all the relationships between mitosis initiator and meiosis initiation network.

Our second focus was to employ the model to understand the early stage meiotic-mitotic switching of budding yeast, which was experimentally observed when the nutrient levels are altered in yeast cells (Chapter 6). For this, we employed dynamical systems analysis methods and we summarise the main findings as follows: (1) phase space analysis of the model explains the transient and sequential expression pattern of meiosis initiators (Ime1 and Ime2); (2) nullcline analysis and bifurcation analysis of the main meiosis (Ime2) and mitosis (Cdk1/Cln3) initiators show a bistable switch, which includes two steady states corresponding to meiosis and mitosis states. Further, this bistable switch includes a narrow region where the transition happens from meiosis to mitosis when the nutrients are increased from the lowest value. This switch explains the early phase meiotic-mitotic switching observed in budding yeast and agrees well with the experimental observations that this switching is reversible and the transition happens soon after the nutrients are increased from the lowest value. The switch

transits from meiosis to mitosis state when the nutrients are increased and vice-versa via the saddle node bifurcation; (3) in addition, this bistable switch is observed at each time point between 0.5 hours to 18 hours agreeing with previous experiments. Experiments showed that budding yeast cells which initiated meiosis can return back to mitosis initiation reversibly if nutrients are re-supplied during the period from starvation initiation until they reach the meiotic commitment point. Further, our model shows that the system is already at the mitosis state in the very initial hours (0-0.5 hours) after the starvation initiation, and this explains why the yeast cells can be returned to mitosis easily in the very early hours. This mitosis-only state appears because of the initial conditions for meiosis initiation, which are protein levels corresponding to the mitosis state (high level of Rpd3, the IME2 repressor).

The third focus of this research was to investigate the robustness of meiosis, mitosis and the transition stages against the most sensitive parameter perturbations at the gene expression level (Chapter 7). We also examined the effects on the meiotic-mitotic switch by these most sensitive parameter perturbations. We applied sensitivity analysis approaches to identify the most sensitive parameters which affect the main meiosis (Ime2) and mitosis initiator (Cdk1/Cln3) protein levels. We also defined a mathematical formulation to measure the robustness at the three stages of meiosis, mitosis and transition. The main results observed are summarised below: (1) the local sensitivity analysis, which was used to identify the individual effects of parameters on the output, revealed that the system is more sensitive to the parameters that are related to the homeostasis of proteins. Many experimental studies of biological systems have also confirmed this sensitivity of protein synthesis and degradation rates (Kristensen et al., 2013). Further, LSA revealed that the Ime2 expression is sensitive to the Ime2 auto-regulation related proteins. Experiments also have shown that the self-regulation of IME2 is very important for Ime2 expression because self-regulation creates sufficient Ime2 if the cell creates enough Ime1 to stimulate the expression of IME2;
(2) global sensitivity analysis of the most sensitive set of parameters revealed that five of the eight most sensitive parameters were common to all three states of meiosis, mitosis and transition. Four out of these five parameters belong to either meiosis initiator Ime2 or to the mitosis initiator Cdk1/Cln3 regulation; (3) the robustness of the gene expression patterns of meiosis, mitosis and transition states against simultaneous perturbations of the five common set of parameters revealed that the meiosis and mitosis stages were more robust than the transition state. This was conceivable since the transition state was limited to a narrow region of nutrients; and, (4) when the meiotic-mitotic switch was perturbed with the simultaneous perturbations of these five common parameters, three main switch types were observed: a

normal bistable switch, a memory-less switch with no bistable region and a switch with abnormalities (no meiosis-only stage, transition region is broader). However, in all these three switch types, the main functionality of the transition to mitosis state when the nutrients are increased form the lowest value is preserved. This indicates the robustness of maintaining the main functionality of the meiotic-mitotic switch against the most sensitive parameter perturbations.

8.2 Contributions

- Expands our understanding of meiosis initiation while mitosis is inhibited, and vice-versa, at the gene expression level by building and validating a model incorporating all the relationships of the mitosis initiator with the meiosis initiation network. The unique features of the current model compared with previous studies are that: (1) the model incorporates the regulation of both meiosis (Ime1, Ime2) and mitosis (Cdk1/Cln3) initiators; (2) the model is investigated under a range of nutrient conditions; and (3) the concentration terms of the model equations are non-dimensionalised so the results are easily comparable with the available relative protein levels.

- Provides a fundamental level and a detailed understanding about the nutrient based, initial phase meiotic-mitotic reversible switching observed in budding yeast diploid cells. The switch explains the mutually exclusive existence of these two developmental processes by a substantial gap (unstable steady state) between the threshold levels of the two stable states corresponding to meiosis and mitosis. Temporal analysis of the switch predicts that budding yeast cells are easily reversible to mitosis, from meiosis initiation, if nutrients are re-supplied during the initial hours after the starvation initiation.

- Model simulations explain the organism-level results of mutant analysis at the gene expression level. Further, the model clarified the conflicting mutant analysis results observed from experiments.

- Identifies the set of parameters which has the most influential individual effects on the meiosis and mitosis initiators through the LSA approach. We also analyse the biological significance of these sensitive parameters.

- Identifies the set of parameters common for all the three states of meiosis, mitosis and transition which has the most influential group effects by applying the GSA approach.

- Formulates a mathematical expression for the robustness of each of the three states (meiosis, mitosis and transition) against the perturbations of the most sensitive common set of parameters. Using this mathematical formulation, we identify that the transition stage is less robust than the meiosis and mitosis stages.

- Investigates the effects of the perturbations in the most sensitive common set of parameters on the meiotic-mitotic switch. This investigation reveals that the main functionality of the meiotic-mitotic switch, which is the switching from meiosis to mitosis when the nutrients are re-supplied from the lowest value, is preserved against perturbations of the most sensitive parameters.

8.3 Future Directions

While the constructed model has helped us to understand the key mechanisms of meiosis initiation and explained the early phase meiotic-mitotic switching, some open questions still remain to be investigated. In this section, we discuss some future directions in which to extend and improve the model presented in this thesis.

1. The current model only explains meiosis initiation in the very early stage before the commitment point. How do the components of meiotic and mitotic initiation collaborate at the commitment point of meiosis? Meiosis or mitosis initiation-decided cells can initially return to the opposite type of cell division, if the initiation signal is reversed favouring the other type of cell division initiation. However, after the commitment point, cells dedicate to finish the decided cell division without depending on the initial signal variations. It is hypothesised that Ndt80/Sum1 switch would accomplish the meiotic commitment point (Winter, 2012). Current mathematical models need to be expanded to understand how the components of the system work together to achieve the irreversible commitment. This would expand our understanding of how the early phase meiotic-mitotic switch is taken over by the switch regulating the commitment point.

2. All the available models (Ray et al., 2013; Rubinstein et al., 2007; Wannige et al., 2014) include subsets of meiotic components and show transient and sequential

expression of the main meiosis initiators. What is the minimal model of meiosis initiation in budding yeast (minimal model is defined as a hypothetical molecular network with a minimum number of genes, proteins and interactions necessary to initiate meiosis in nutrient starved conditions)? Mathematical modelling that incorporates wise conceptual insights into biological data is required to identify the minimally required components of meiosis initiation in budding yeast.

3. The current model assumes that the participating reactions happen in a single compartment. However, proteins are localised to different compartments such as the nucleus and the cytoplasm during meiosis initiation: as examples, Cdk1/ Cln3 phosphorylates Ime1 and transports the phosphorylated Ime1 out of the nucleus (Colomina et al., 1999); meiosis-related proteins, including Ime1 and Ime2, are localised to nucleus during meiosis initiation (Kominami et al., 1993). How does the meiosis initiation process manage the time required for protein localisations between different compartments? Integration of compartments into the current model would facilitate understanding the roles of protein localisation inside and outside the nucleus during meiosis initiation.

4. The model constructed is valid only for grown diploid budding yeast cells and ignores cell type and size control mechanisms. The mechanisms for the transcriptional regulation of IME1 by the mating type related genetic signals can be included in the current model to study how meiosis is restricted to diploid cells. Yeast cell growth and mitosis cell division are tightly coupled and Cln3 levels control the growth in budding yeast cells (Morgan, 2006). How do yeast cells control the cell size during meiotic-mitotic switching? Expanding the current model by including the mechanisms for controlling the cell size would provide a more detailed model which would be useful to examine how yeast cells maintain their size during the meiosis initiation.

5. Some assumptions of the current model are made mainly due to the lack of experimental data from the literature: The mechanisms for the regulation of RIM15 and RPD3S are not clear. Further, the mechanism of the Isw2 complex removal from the IME2 promoters is still unknown. Therefore, the current model assumes that the Isw2 complex is removed from the Ime2 promoters in a parallel way to Rpd3/Sin3. Further, the temporal variation of Rim15 and Rpd3 are modelled using time dependent functions in the current model. Experimental investigation of these mechanisms would

describe the meiosis initiation in more detail and explain EMGs tight repression removal during meiosis initiation.

6. The current model shows that the bistable switch in Ime2 and Cdk1/Cln3 underlies the meiotic-mitotic decision. The cross talk procedures between meiosis and mitosis initiator proteins considered in the model are as follows: Cdk1/Cln3 represses IME1 and Cdk1/Cln3 phosphorylates Ime1 and sequesters the phosphorylated Ime1 out of the nucleus (Colomina et al., 1999); Cln3 protein expression is down-regulated by translational, transcriptional repression and degradation upon nitrogen deprivation (Gallego et al., 1997); an antagonism exists between Ime2 and Cdk1/Cln3 (Gurevich et al., 2010). What are the other meiosis/mitosis specific proteins which have cross talks between meiosis and the mitosis initiation pathways? Experimental research focussed more on how the meiosis and mitosis initiators work together in returning to the other type of cell division initiation is lacking and more research would clarify how this initial meiosis-mitosis initiation switch is designed to optimise the nutrient usage minimising the cost of wrong decision making.

7. Research on budding yeast mitosis cell cycle has helped extensively in the understanding of human cell cycle regulation. What useful information from budding yeast meiosis initiation research can be used to understand human meiosis initiation? What are the relations between the key conserved genes of meiosis initiation in multicellular organisms and budding yeast? Meiosis initiation is conserved among yeast and other eukaryotes (Li et al., 2010; Manning et al., 2002). Much information on the molecular level control of meiosis initiation has been elucidated in budding yeast over the last few decades. How does this information relate to the meiosis initiation of other organisms? More research, focussed specifically on conserved genes, is required to relate these molecular level details to other organisms that have similar evolutionary conserved components; a good example is the functional analysis of the homology between yeast Ime2 and human Cdk2 (Szwarcwort-Cohen et al., 2009).

8. The current model only addresses the nitrogen-related regulation of meiosis initiation. Glucose-related mechanisms are not included in the current model since glucose also plays a parallel role as nitrogen in meiosis initiation. However, including glucose and other nutrient related control mechanisms into the current model would be useful to study the meiosis initiation in a wide range of nutrient conditions.

9. While examining the robustness and the effects on the meiotic-mitotic switch by the parameter perturbations, we only consider the most sensitive common parameter set, assuming that these parameters together would impose the most influence on the system output. However, the perturbations in other parameters which have close relations with the most sensitive parameters would sometimes impose more influence on the output. Therefore, this analysis can be expanded by including more parameters into the current five parameter set by choosing candidate parameters that have close relations with the most sensitive common parameter set. Although computationally difficult, it is also better to analyse the effects on the meiotic-mitotic switch and robustness by perturbing all parameters simultaneously. This is because most parameters are perturbed simultaneously in real situations, like a sudden temperature change. Further, we assume that the perturbations occur in equal probability in the simulations. Since perturbations do not occur with equal probability in real systems, it is important to investigate situations where such perturbations would occur according to the normal distribution (the 'lhsnorm' function in Mathlab can be used to generate a Latin hypercube sample from normal distribution).

10. It is evident from the experiments that stochasticity influences the transitions in bistable systems. Therefore, it is important to investigate the stochasticity properties of the meiosis initiation system. After identifying intrinsic and extrinsic noise origins and consequences, one can select a suitable stochastic approach such as chemical Langevin equations (CLE), Ito stochastic differential equations or the Gillespie stochastic simulation algorithm to investigate the stochastic effects of this bistable system.

8.4 Conclusions

Cellular biological systems are amazingly complex with trillions of cells containing evolutionary-selected networks of many biochemical interactions. Despite this complexity, biosystems maintain a smooth functionality even with external and internal perturbations. Moreover, evolution works by making changes to these systems and selecting the best mechanisms that help survival. For decades, evolution has converged these systems again and again into a set of cellular network elements that obey general design principles. In aid to understand the functionality of these cellular systems, current advances in experimental technology provides detailed and comprehensive information about these networks of biochemical interactions. This huge amount of *in-vivo* data alone cannot describe how cellular processes are functioning. Mathematical modelling and computational simulation approaches have shown enormous potential in understanding the underlying principles of these biological processes. In this thesis, we demonstrate how mathematical modelling approaches, using kinetic equations of biological reactions, can be employed to model and understand biosystems exhibiting bistable behaviour.

This research focuses on a specific example of a system which exhibits bistability behaviour and provides a detailed understanding about the corresponding decision making point. Many exciting and challenging biological phenomena still remain unexplained. We believe that the piece of work described in this thesis would inspire many biologists and mathematicians to take the challenge of interdisciplinary work and use integrative holistic approaches to understand the principles behind the inherent simplicity of biological systems.

Appendix A

Stochastic Modelling Approaches and Far from Equilibrium Theories

A.1 Why Stochastic Modelling?

Bio-molecular systems are inherently stochastic mainly because of the small copy numbers and the infrequent reactions. Modelling provides insights into these systems to see how they cope with the molecular noise in different ways, whether they amplify noise or suppress or use it to change states. Deterministic approaches assume that the reactions occur frequently and with plenty of reaction molecules freely available. In a practical situation, some of the participating reactants may decay to zero while others do not; or all the reactions may not occur at the same speed and, usually, the results may depend on the slowest reaction in a chemical reaction system. In deterministic modelling, the mean is normally the average of the system; however, the interest is on the fluctuations around the mean in a real system. At the same time, the bistability and the stabilisation in deterministically unstable states are impossible to predict deterministically (Ullah and Wolkenhauer, 2010). Thus, stochastic methods are essential for modelling bio-molecular reaction systems.

A.2 Stochastic Modelling Approaches

Several different approaches can be found in the literature to describe the evolution of a biochemical system.

A.2.1 Chemical master equation

The chemical master equation (CME) is the most exact and basic equation to predict the evolution of a well stirred biochemical reaction system (to allow each molecule pair to collide with each other in equal probability). CME has a firm, microphysical basis, considering the inevitable effects of molecular level randomness (Gillespie, 1977; Gillespie, 2002). CME describes how the state of a biochemical system changes probabilistically with time.

A state of a system 'X(t)' is defined as the set of the number of each species ($X_1(t),X_2(t),....X_n(t)$) in the system at a certain time. The answer to the question of "What is the probability of the system falling into state 'n' at time 't+dt', '(P(n,t+dt))'?" initiates the

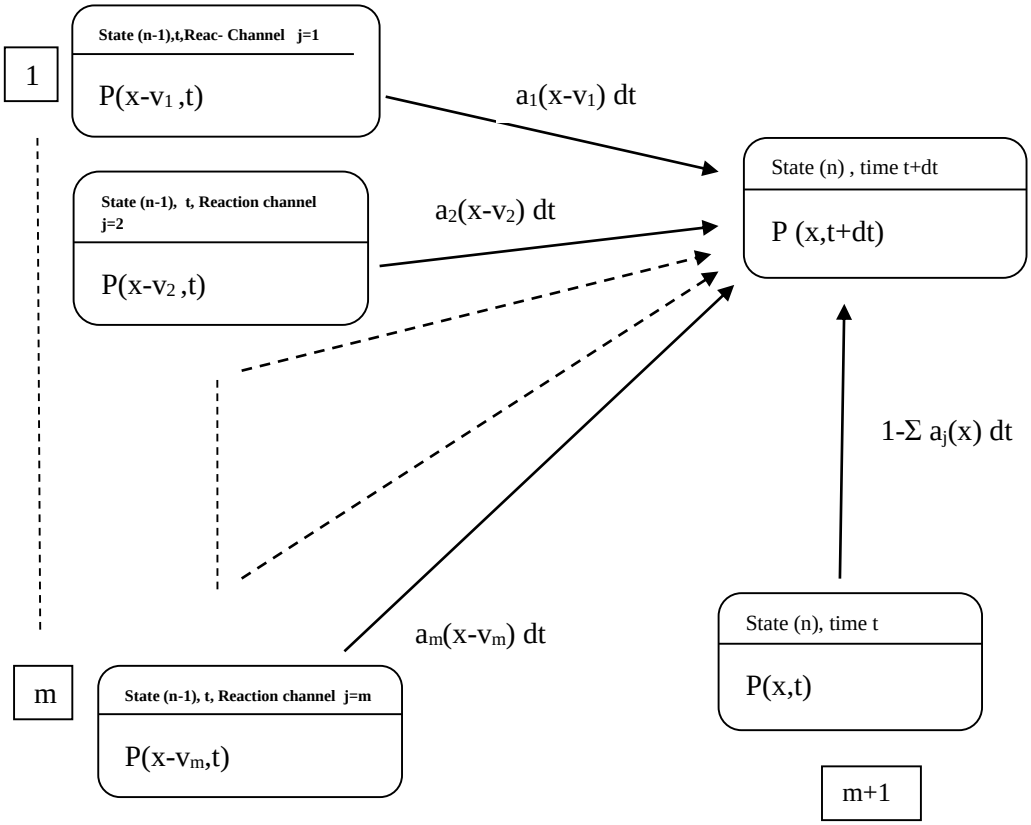

Figure A.1: Probable state transitions for the state 'n' at time 't+dt'. There are 'm+1' number of ways to become to the state 'n' from any other state.

chemical master equation. At time ‘t’ , the system may be in the same state ‘n’ or in another state. In the latter case, a chemical reaction may take the system from the other state to state ‘n’. If it is assumed that there are ‘m’ reaction channels there are ‘m+1’ ways to become state ‘n’ from other states, as shown in Figure A.1.

If '$a_j(X(t))$' is the propensity function which describes the tendency for one reaction type ‘j’ can happen, '$a_j(X(t))dt$' gives the probability that one reaction of type ‘j’ will occur in the system in the next infinitesimal time interval '(t,t+dt)'.

If the change in the number of molecules of type ‘i’ produced by the reaction channel ‘j’ is given by ‘v_{ij}’, the probability of the system falling into the state ‘n’ at time 't+dt (P(n,t+dt))' can be written simply as,

$$P(x,t+dt) = \sum_{j=1}^{m} a_j(x-v_j)P(x-v_j,t)dt + \left[1 - \sum_{j=1}^{m} a_j(x)\,dt\right] \mathrm{P(x,t)}$$

For a vanishingly short 'dt’ the above equation can be rearranged as the chemical master equation (Gillespie, 1977; Nguyen, 2009).

$$\frac{dP(x,t)}{dt} = \sum_{j=1}^{m} a_j\,(x-v_j)P(x-v_j,t) - \sum_{j=1}^{m} a_j(x)P(x,t)$$

CME is a state function where an ordinary differential equation is written for each and every state. When the number of states of a system increases, it is impractical to solve the set of master equations analytically or numerically (Ullah and Wolkenhauer, 2010). A better alternative is Gillespie's algorithm or the stochastic simulation algorithm (SSA), which provides a way to make exact numerical calculations in a stochastic framework without dealing with the master equation directly.

A.2.2 Gillespie's algorithm

Gillespie's stochastic simulation algorithm uses a Monte Carlo procedure to numerically evaluate the time evolution of a chemical reaction system. Two main questions, “When will the next reaction occur?” and “What kind of reaction will it be?” are answered at each repeating step in the algorithm. This process is repeated until one species become extinct or the desired time elapses (Gillespie, 1976; Gillespie, 1977).

D.T. Gillespie (Gillespie, 1977) has given a detailed probabilistic description of how to generate solutions to the above two questions at each repetition. The answer to both the above questions can also be obtained by the memory-less property of the Markov process (Ullah and Wolkenhauer, 2010).

- **When will the next reaction occur?**

If Markov process N(t) is in state n at time 't' and '$T_j(n)$' is the waiting time in state 'n' until the reaction 'R_j'takes the system to a different state 'n+s_j'and if '$a_j(n)$' is the propensity on the state 'n',

The probability that an 'R_j reaction will not occur in the next time interval of length 't' is given by (Ullah and Wolkenhauer, 2010),

$$Pr\left[T_j(n) > t\right] = exp(-a_j(n)t)$$

If $a_o(n) = \Sigma\, a_j(n)$, the time '$T_0(n)$' until the next reaction taking the process away from state 'n' (i.e. the time interval '$T_o\,(n)$' that no reaction will occur) is given by,

$$Pr[T_0(n) > t] = exp(-a_0\,(n)t)$$

To draw a random pair of 'τ' (time for the next reaction) and 'μ' (type of the reaction), a unit interval uniform random number generator is used and if 'r_1'is a unit interval uniform random number, equating 'r_1'to the above probability,

$$r_1 = exp(-a_0(n)\ t)$$

thus,

$$\tau\ = \left(\frac{1}{a_0(n)}\right) ln\left(\frac{1}{r_1}\right)$$

The answer for the first question 'When will the next reaction occur?' is given by the above equation.

- **What kind of reaction will it be?**

If the index of the next reaction occurring in state 'n' is ‘J(n)’, the probability of the index ‘J(n)’ taking the value μ can be given by (Ullah and Wolkenhauer, 2010),

$$Pr(J(n) = \mu) = \frac{a_{\mu}(n)}{a_0(n)}$$

To draw a random ‘μ’ value, a unit interval uniform random number generator is used and if ‘r_2’ is a unit interval uniform random number,

$$r_2 = \frac{a_{\mu}(n)}{a_0(n)}$$

‘μ’ will be the integer for which,

$$\sum_{\nu=1}^{\mu-1} a_\nu < r_2\, a_0 \leq \sum_{\nu=1}^{\mu} a_\nu$$

With these random values for ‘μ’ and ‘τ’ the SSA is given by D.T. Gillespie (see Figure A.2),

Using the Gillespie’s algorithm, coupled chemical reactions can be simulated and the behaviour of the particle numbers and mean concentrations can be observed (Figure A.3).

The Gillespie's algorithm is an good, alternative way to the master equation in that it numerically calculates the time evolution of coupled chemical reactions, and is physically and mathematically well-grounded, being equivalent to the master equation (Gillespie, 1977). However, Gillespie’s direct method discussed above (‘μ’ and ‘τ’ are generated directly) has a high computational cost as the speed of the simulation depends on the number of species. If the number of species is high, higher random numbers are needed to be generated.

In the last few years, many improvements to Gillespie's original algorithm have been made to improve the computational efficiency of the method. Gillespie (Gillespie, 1976) introduced the first reaction-based method which generates a “tentative reaction time” for each reaction to occur if no other reactions occurred first. A minimum tentative reaction time from all the reactions is considered as ‘τ’ and, corresponding, ‘μ’ is considered as the reaction number for the next step of the algorithm. Gillespie’s direct method and first reaction-based method are equivalent although the calculation of ‘μ’ and ‘τ’ are different (Gibson and Bruck, 2000; Gillespie, 1976). The next

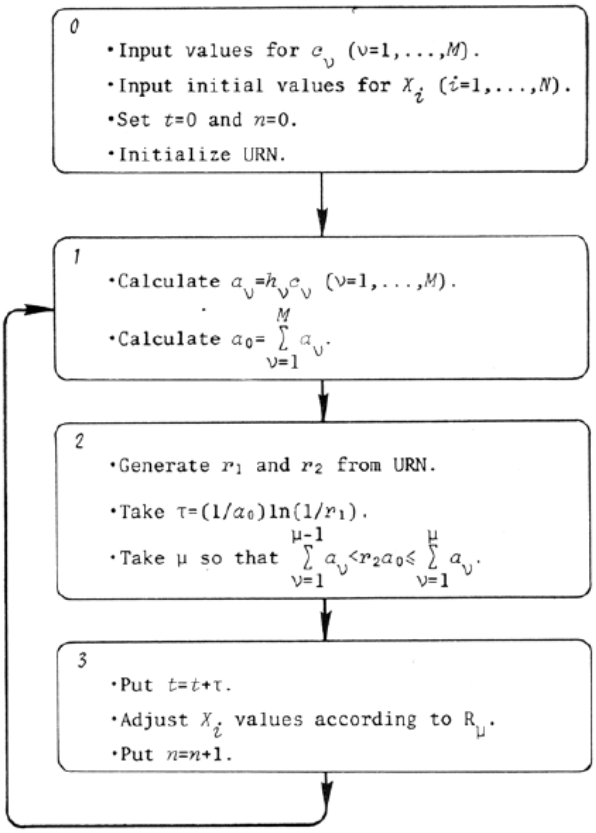

Figure A.2 : Gillespie's algorithm (Adopted from (Gillespie, 1977))

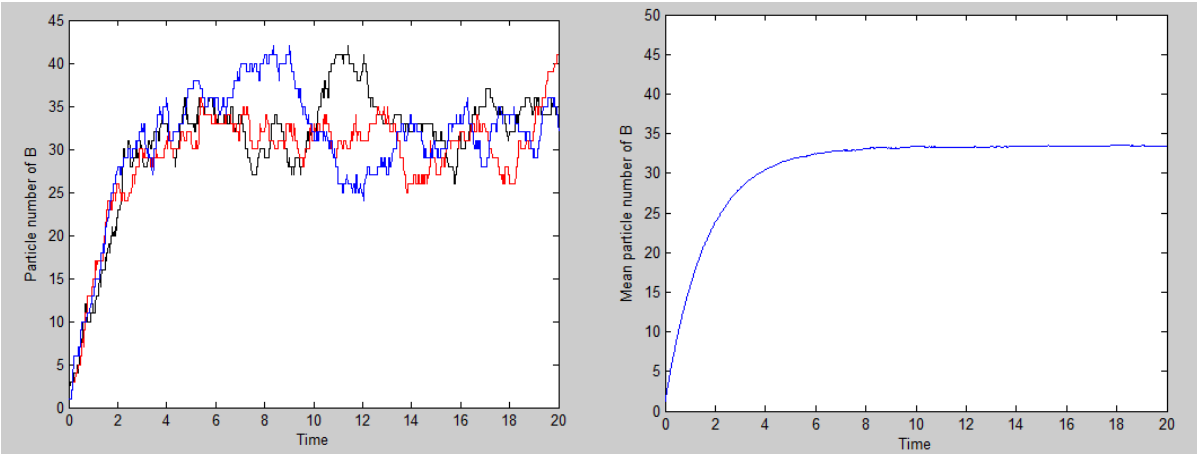

Figure A.3: Gillespie algorithm outputs. Three realisations for the particle number of B (left), and mean number of B particles for 1000 realisations (right), for the $A \leftrightarrow B$ coupled reaction with the initial condition of number of A particles to 50 and B equals zero.

reaction-based method was introduced with the intention of efficient recalculation of propensity and 'τ'. Other efficient, exact methods found in the literature are the optimised direct method (Cao et al., 2004) and the sorting direct method (McCollum et al., 2006).

Later, Gillespie et. al. (2001) and (2003) (Gillespie, 2001; Gillespie and Petzold, 2003) introduced some approximate procedures such as explicit and implicit τ- leaping methods, with good simulation speed but with some acceptable accuracy losses. A brief history of SSA implementation is given by Mario P.K in Figure A.4(Mario, 2007).

A.2.3 Chemical Langevin equation [CLE]

The chemical Langevin equation approximates the jump Markov process as defined by the CME by a continuous Markov process (Gillespie, 2000; Gillespie, 2002; Nguyen, 2009). CLE considers a fixed 'τ' (the time interval until the next reaction), which is a variable in the stochastic simulation algorithm. In this time interval, all the reactions that would have occurred are fired simultaneously. The Langevin equation is given by,

$$X(t+\tau) = X(t) + \tau \sum_{j=1}^{m} v_j \, a_j\big(X(t)\big) + \sqrt{\tau} \sum_{j=1}^{m} v_j \sqrt{a_j X(t)}\, N_j(0,1)$$

$$\frac{dX(t)}{dt} = \sum_{j=1}^{m} v_j \, a_j\big(X(t)\big) + \sum_{j=1}^{m} v_j \sqrt{a_j X(t)}\, dW_j(t)$$

This equation is called the white noise form of the CLE, because of the white noise term of $dW_j(t) = \lim_{n\to\infty} N_j\,(0,1)$

Tau 'τ' defines the special circumstances under which the above approximate equation is valid. The requirements are that the 'τ' to be (Gillespie, 2002):

1. Small enough that none of the propensity functions 'a_j' changes in a macroscopically noticeable way during 'τ', to consider 'a_j (x(t))' constant over the time period 't,t+τ'.

2. Large enough that each reaction channel '$R_{j'x}$' fires many more times than once during time period 'τ'.

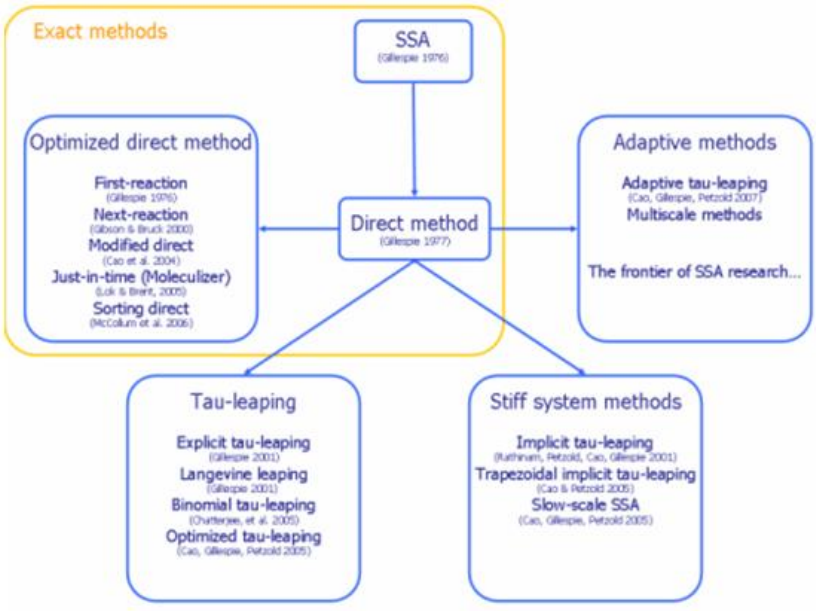

Figure A.4: A brief history of SSA developments (Adopted from (Mario, 2007)). Exact methods are marked with a yellow curve.

When modelling stochasticity, this equation is considered as a stochastic differential equation (SDE) and noise is added to the deterministic part as follows (van Oudenaarden and Pedraza, 2005):

$$\frac{dX(t)}{dt} = \underbrace{\sum_{j=1}^{m} v_j\, a_j\big(X(t)\big)}_{\text{Deterministic term}} + \underbrace{\sum_{j=1}^{m} v_j \sqrt{a_j X(t)}\, dW_j(t)}_{\text{Additive White noise term}}$$

A.2.4 Fokker-planck equation

The chemical master equation gives the probability to be in the state n at time 't', 'p(n,t)' only for the integer values of the state 'n'. The Fokker-Planck equation is defined supposing the propensity '$a_j(n)$' is a smooth function for the real values of 'n'.

Consider the Master equation

$$\frac{\partial P(x,t)}{\partial t} = \sum_{j=1}^{m} a_j\,\big(x - v_j\big)P\big(x - v_j, t\big) - \sum_{j=1}^{m} a_j(x)P(x,t)$$

Each $1 \le j \le m$, introduces a new function, $F_j(x,t) = a_j(x)P(x,t)$, and CME can be written as,

$$\frac{\partial P(x,t)}{\partial t} = \sum_{j=1}^{m} F_j\,\big(x - v_j\,, t\big) - \sum_{j=1}^{m} F_j(x,t)$$

By carrying out a Taylor expansion around the vector x, ignoring terms of order three and higher, the Fokker-Planck equation(FPE) can be written as a partial differential equation,

$$\frac{\partial P(x,t)}{\partial t} = \sum_{j=1}^{m}\left[-\sum_{i=1}^{m} v_{ij}\,\frac{\partial\, F_j(x,t)}{\partial x_i} + \frac{1}{2}\sum_{i=1}^{n}\sum_{k=1}^{n} v_{ij}\, v_{kj}\,\frac{\partial^2 F_j(x,t)}{\partial x_i \partial x_k}\right]$$

As a partial differential equation, the Fokker-Planck equation provides scientists with potential computational advantages to numerically simulate the systems better than with the CME (Gillespie, 2002). Sensitivity analysis and the bifurcation theory tools are applicable to the Fokker-Planck equation allowing easier analysis (Nguyen, 2009). However, the FPE becomes impossible to solve numerically, even with a low number of species.

A.3 Far from Equilibrium Theories

A.3.1 Thermodynamics of biochemical reaction systems

Thermodynamics is the science of energy conversion involving heat and other forms of energy-like mechanical work, which is mainly applicable to systems in equilibrium (Qian and Beard, 2005). Experimental reproducibility is the primary and fundamental requirement in thermodynamics; it is one of the important branches of physics that is applied to biochemistry.

If we consider a thermodynamic system as the region of the universe under study, everything in the universe except the system is known as the surroundings. A boundary separates the system from the surroundings. Thermodynamic systems can be classified into three types, as open systems, closed systems and isolated systems. In open systems, mass flow, work and heat are allowed to transfer through the boundary, while, in closed systems, work and heat only are allowed to cross through. In isolated systems, mass flow, work or heat are not allowed to cross through the boundary. There are four types of boundaries: fixed, movable, real and imaginary. For closed systems, the boundaries are real while the boundaries are imaginary for open systems.

Living systems are open to heat, work and material exchange (Qian and Beard, 2005). Thus, living biochemical systems are considered as open systems with imaginary boundaries. Spontaneous processes in thermodynamics can proceed without any outside involvement. In a reversible process, a system can change in such a way that the system and the surrounding can be put back into their original state by reversing the process. Keizer J. (1987) (Keizer, 1987) describes a reversible process as a movie that can be rewound. All real processes are spontaneous and irreversible. At thermodynamic equilibrium, the properties of the system do not change with the time macroscopically; however, there may be some stationary fluctuations in a statistical sense. A system at thermodynamic equilibrium is said to be in detailed balance when every process is balanced in detail by its opposing process (Qian, 2007).

An open system approaches a non-equilibrium steady state after a sufficiently long time compared to its relaxation time (Qian and Beard, 2005). This non-equilibrium steady state (NESS) is also known as a stationary non-equilibrium state or dissipative structure. These dissipative structures with non-equilibrium steady states can be described by suitable external principles in non-equilibrium thermodynamics.

- **Entropy of a thermodynamic system**

Entropy is a measure of the randomness or orderliness of a thermodynamic system. It is usually defined as the ratio of heat delivered to the temperature at which it is delivered. It is related to the various modes of motion in molecules such as translational, vibrational and rotational motion. Ludwig Boltzmann described the concept of entropy on the molecular level using microstates, which are motions of a sample of molecules at a particular instant in time by the following equation:

$$S = k \ln W$$

W is the number of microstates and k is the Boltzmann Constant. When the temperature, or the number of particles, or the volume is increased in a system, the number of microstates is increased and entropy is increased as a consequence. All spontaneous processes tend towards equilibrium, which is the maximum disorder with maximum entropy. For all reversible processes, the entropy change of the system and the surrounding remains a constant. Entropy increases in an irreversible process. Therefore, total entropy never decreases but remains constant or increases. Entropy maximises at the equilibrium, which is the most general condition of equilibrium (Thron, 1997).

- **Gibb's free energy**

Gibb's free energy is a thermodynamic quantity which is used frequently to measure the energy associated with a chemical reaction that can be used to work. Gibb's free energy becomes zero (at constant temperature and pressure), when entropy maximises at the equilibrium. When G is related to chemical equilibrium, if the equilibrium constant for a couple of reactions is K_{eq}, the standard Gibbs free energy difference ΔG^o is defined as,

$$\Delta G^o = -RT \ln K_{eq}$$

And, for non-standard conditions ΔG, if the reaction quotient is Q for a couple of chemical reactions,

$$\Delta G = \Delta G^o + RT \ln Q$$

At equilibrium, ΔG becomes zero as Q becomes equal to K_{eq}. For spontaneous processes, ΔG becomes negative. Therefore, ΔG is used to decide whether a process is spontaneous.

- **Chemical potential of a substance**

The extent of a system's internal energy change by adding some amount of a pure substance is defined by the substance's chemical potential, μ. If the internal energy of the system is U, the chemical potential (μ_i) of the i^{th} substance is defined as,

$$\mu_i = \left(\frac{\partial U}{\partial n_i}\right)_{s,v}$$

Gibb's free energy can be formulated as a function of chemical potentials and molar numbers as,

$$G = \sum \mu_i n_i$$

At equilibrium, when temperature and pressure is constant,

$$\Delta G = \sum \mu_i \, dn_i = 0$$

However, as the chemical potential 'μ' is normally a difficult quantity to determine, a related quantity, activity is frequently used. The activity of the i^{th} substance 'a_i'is defined by,

$$a_i = e^{(\mu_i - \mu_{io})/RT}$$

where 'μ_{io} ' is the chemical potential of the i^{th} substance in the standard state, 'R' is the Gas constant and 'T' is the temperature. Thus,

$$RT \ln a_i = \mu_i - \mu_{io}$$

Therefore, the general expression for equilibrium in terms of activities is given by,

$$\sum (RT \ln a_i + \mu_{io}) \, dn_i = 0$$

- **Chemical affinity**

Chemical affinity refers to the force that causes chemical reactions. It is the electronic property by which dissimilar chemical species are capable of forming chemical compounds. Chemical affinity can also refer to the tendency of an atom or compound to combine by chemical reaction with atoms or compounds of unlike composition (Yao et al., 2011). Chemical affinity is considered as zero at equilibrium.

In thermodynamics, if we consider a mixture of chemical species with the possibility of chemical reaction, affinity A is defined by,

$$A = -\left(\frac{\partial G}{\partial \varepsilon}\right)_{P,T}$$

Where G is the Gibb's free energy and ε is the extent of reaction at constant pressure and temperature.

In 1954, IIya Prigogine and Defay (Yao et al., 2011) defined chemical affinity as a function of the increments in uncompensated heat of reaction 'dQ' and reaction progress variable 'dε'.

$$A = \frac{dQ}{d\varepsilon}$$

This definition is useful for quantifying the factors responsible both for the state of equilibrium systems and for changes of state in non-equilibrium systems.

A.3.2 Theoretical developments of modelling fluctuations in biochemical reaction systems

- **Lars Onsager's theories on modelling fluctuations**

Lars Onsager was the first to develop theories in the field of fluctuations in equilibrium and near equilibrium systems. The Onsager theory (Keizer, 1987; Onsager and Machlup, 1953; Yao et al., 2008) describes the molecular fluctuations for extensive variables like internal energy and volume, which depend on the extent or the size of the system. The Onsager principle defines linear laws for irreversible processes in an equilibrium ensemble stating that the average time derivative of an extensive variable is linearly related to the average deviations of the conjugate intensive variables from their equilibrium values. It describes the linear relaxation of the averages of extensive variables to their equilibrium value.

If extensive variable 'n' deviates from equilibrium state from an amount of 'a ($a = n - n^e$)', the time derivative of 'a_i' according to linear regression law,

$$d\overline{a_j}/_{dt} = \sum_k L_{jk}\,\overline{X_k}$$

By defining $'\overline{X_K}'$ force in terms of the conjugate intensive thermodynamic variables,

$$\bar{X}_k = \sum_l S_{kl}\overline{a}_l$$

Thus, the differential equation with extensive variables becomes,

$$d\bar{a}_j/_{dt} = \sum_j H_{ij}\,\bar{a}_l$$

where $H_{\mathrm{ij}} = \sum_k L_{kj}\,S_{kl}$

'H' is relaxation matrix governing the return of the average values to the equilibrium. As a real system in ensemble will not exhibit this exponential relaxation due to molecular fluctuations, Onsager's regression hypothesis for fluctuations was introduced. Onsager's original theory provided a partial picture of the dynamics of the systems indicating only the average time dependence of the extensive variables. If fluctuations are given by $= a(t) - \bar{a}$

Onsager's regression hypothesis for fluctuations is given by,

$$\frac{d\delta a}{dt} = H\delta a + \tilde{f}$$

where '$\tilde{f}$' is a random term. Considering the Onsager theory and the above equation, a Langevin type equation can be found for 'a(t)',

$$\frac{da}{dt} = Ha + \tilde{f}$$

$'\widetilde{f}'$ is a random term which is the multivariate white noise and the stochastic process is an Ornstein-Uhlenbeck process. For white noise,

$$< \widetilde{f}_i(t) > = 0$$
$$< \widetilde{f}_i(t)\widetilde{f}_j(t) > \gamma_{ij}(\bar{n})\delta(t - t')$$

where γ satisfies the fluctuation dissipation theorem. $H\sigma + \sigma H^T = -\gamma$ with the σ the equilibrium co-variance matrix, $\sigma = < aa^T >$.

This fluctuation dissipation theorem shows that the strength 'γ' of random terms in the time derivatives of extensive variables is determined by relaxation matrix 'H' and the co-variance matrix sigma (σ).

The Onsager theory, which includes the effects of the fluctuations, is linear and applicable for all states of matter, having limited use only in the neighbourhood of equilibrium.

- **Keizer's general, mechanistic theory on modelling fluctuations**

J. Keizer in 1987 (Keizer, 1987; Kulasiri, 2011), developed a general theory, which provided a mathematical description at the thermodynamic level of molecule number fluctuations due to chemical reactions, for large system volumes. For his above mentioned mechanistic statistical theory of non-equilibrium thermodynamics, he introduced his ansetz (Keizer, 1987) for the probability of a transition from a given set of molecule numbers 'n' at time 't' to another set 'n' at 't+dt', and cooperated mainly with the Fokker-Planck Equation, Ornstein-Uhlenbeck process, and stochastic differential equations. The theory is valid only for contracted descriptions where individual systems contain a large number of molecules. The theory is summarised below.

A homogeneous macroscopic system of N chemical species is considered, and it is assumed that the species can react with each other through any number of elementary chemical reactions, distinguished by the index, k. The molecule number of each species is represented by n_j. The chemical reactions can be given by the following equation,

$$(n_{k1}^{+}, n_{k2}^{+}, \dots \dots n_{kN}^{+}) \leftrightarrow (n_{k1}^{-}, n_{k2}^{-}, \dots \dots n_{kN}^{-})$$

The changes in '*n'* due to the reaction 'k' are defined as $\omega_k = n_k^{+} - n_k^{-}$. The rate expressions can be written as,

$$V_k^{\pm} = \Omega_k \, exp\left[\sum_j n_{kj}^{\pm} \, \mu_j \, / K_B T\right]$$

Consider that there are systematic sources or sinks for each chemical species. In a time interval of '*dt'*, these systematic effects will cause a change in 'n' of the form $dn_s = S(n,t)dt$. 'S (n, t)' is a column vector of the rates of sources or sinks.

Using the above terms, the theory can be stated by the following equations. Keizer has shown that his ansetz gives rise to a simple stochastic diffusion process. He has shown that for a large system the conditionally averaged molecule numbers '$\bar{n}$', satisfies,

$$\frac{d\bar{n}_i}{dt} = \sum_k \omega_{ki}\,\Omega_k \left\{ exp\left[\sum_j n_{kj}^{+}\ \mu_j(\bar{n})/K_B T\right] - exp\left[\sum_j n_{kj}^{-}\ \mu_j(\bar{n})\right]\right\} + S_i\ (\bar{n}, t)$$

$$\equiv\ R_i(n, t)$$

He found that the conditional fluctuations $\delta n_j\ (t) \equiv (n_j - \ \bar{n_j})$ satisfy a Fokker-Planck equation that implies the conditional fluctuation is a time-dependent Ornstein-Uhlenbeck process. This process satisfies the following stochastic differential equation,

$$\frac{d\delta n_i}{dt} = \ H_{ij}(\bar{n},\ t)\delta n_j + \tilde{f}$$

where, $\quad H_{ij}(\bar{n}, t) \equiv \frac{\partial\ R_i(\bar{n},t)}{\partial \bar{n_j}}$

and

$$< \tilde{f}_i(t) > = 0$$

$$< \tilde{f}_i(t)\tilde{f}_j(t) >\ \gamma_{ij}(\bar{n})\delta(t - t')$$

with,

$$\gamma_{ij}(\bar{n}) = \sum_k \omega_{ki}\,\Omega_k\omega_{kj}\ \left\{ exp\left[\sum_j n_{kj}^{+}\ \mu_j(\bar{n})/K_B T\right] + exp\left[\sum_j n_{kj}^{-}\ \mu_j(\bar{n})/K_B T\right]\right\}$$

The above set of equations provides a general mechanistic statistical theory of fluctuations of molecular numbers around the mean. Further, Keizer claims that the Onsager theory can be considered as a special case of equilibrium with Keizer's general theory (Keizer, 1987). It can be shown that the results of the stochastic chemical reactions simulated by the other stochastic approaches such as Gillespie's algorithm coincides with the results of Keizer's general theory (Kulasiri, 2011). The results of an application of the theory and Gillespie's algorithm are given in Figure A.5. As a mechanistic statistical theory of irreversible processes, comparably, this theory is advantageous in predicting molecular fluctuations with less computational cost and with more thermodynamic insights.

- **Prigogine's work on modelling fluctuation far from equilibrium**

Prigogine also introduced theories related to fluctuations in non-equilibrium thermodynamic systems. He showed that the non-equilibrium, irreversible processes may lead to a new type of dynamic state of matter called "dissipative structures" (Prigogine, 1978). Prigogine looked at the positive functions of the state variables, which vanish at a steady state, and are generally called Lyapunov functions. He identified (Nicolis and Prigogine, 1971; Prigogine, 1978) that $\delta^2 S$ (S refers entropy) is a Lyapunov function in the neighbourhood of equilibrium independent of the boundary conditions. He showed that the macroscopic description is sufficient for a large system near equilibrium, because of the existence of the above Lypanov function verify damping of all fluctuations.

He further extended the theory of fluctuations to non-linear systems far from equilibrium (Nicolis and Prigogine, 1971), using a phase space theory of fluctuations starting from the Boltzmann equation. Using this equation, he studied the behaviour of the system in the limit of small fluctuations in a local equilibrium regime. The introduced equation for small fluctuations has appeared contradictory when applying it to a system which is slightly beyond a state of marginal stability. However, he has not analysed the behaviour of large fluctuations of macroscopic size (Nicolis and Prigogine, 1971). He also worked on a Lyapunov function which can be used to extrapolate the stability property away from equilibrium by using a non-unitary transformation (Prigogine, 1978). His transformation theory allows introducing non-unitary equations of motion that display irreversibility.

J. Keizer in 1979, identified that this attempt of using local equilibrium entropy as a central principle far from equilibrium failed (Keizer, 1979) because, mathematically, the Lyapunov theorem provides only a sufficient condition for stability. Using the theory of molecular fluctuations, Keizer has attacked on the problem of thermodynamic functions away from equilibrium differently, as discussed in the previous section (Keizer, 1987).

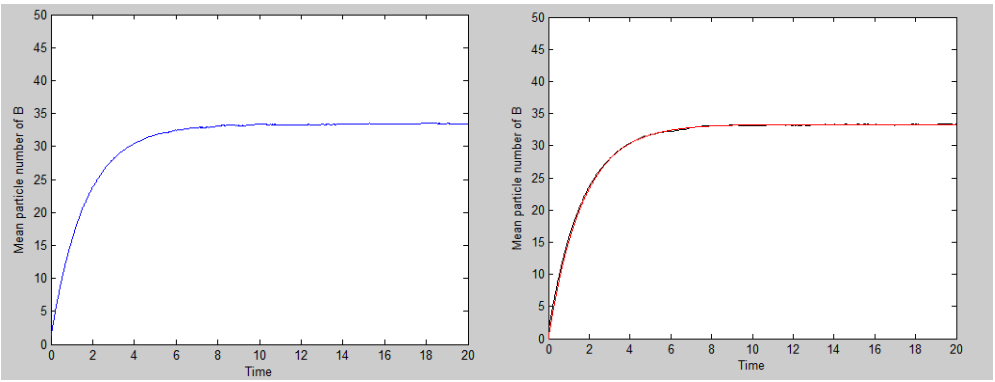

Figure A.5 : Comparison of the results of Keizer's theory and Gillespie's algorithm. Mean number of B particles for 1000 realisations (left) using Gillespie's algorithm (blue), for the $A \leftrightarrow B$ coupled reaction with the initial conditions of number of A particles to 50 and B equals zero. The r.h.s. graphs shows Keizer's theory results (red) on top of the Gillespie algorithm simulation results for the same initial conditions.

- **Qian Hong's theories on fluctuations**

Qian Hong also worked on the thermodynamics of biochemical systems in living systems far from equilibrium (Qian and Beard, 2005; Qian et al., 2002). He pointed out that living systems are open to energy and material exchanges with their surrounding and, after a sufficiently long time compared with its relaxation time, an open system approaches a non-equilibrium steady state (NESS) or dissipative structure (Qian, 2006; Qian, 2007). The kinetics of macroscopic non-linear biochemical reaction systems far from equilibrium can be in NESS or can execute oscillations about a fixed mean (Qian and Qian, 2000; Qian et al., 2002). Qian has generalised the concepts in equilibrium thermodynamics enthalpy, entropy and Gibb's free energy of biochemical reaction systems to non-equilibrium settings of a NESS. Further, he established the energy conservation and second law for NESS in biochemical networks. Identifying that Keizer's theory of fluctuations is general, he has also specifically defined fluctuations of concentrations for NESS. Furthermore, Qian worked on the non-equilibrium thermodynamics and non-linear kinetics of cellular signalling switches and bistable chemical systems (Qian and Reluga, 2005; Qian et al., 2009; Vellela and Qian, 2009).

- **John Ross's work on thermodynamics and fluctuations far from equilibrium**

In 2010, John Ross et al. introduced theories for thermodynamics and fluctuations both far from and near equilibrium systems. They developed mesoscopic formulations, using an approach based on the master equation for probability distributions. They focussed on processes leading to, and in, non-equilibrium stationary states, systems with multiple stationary states, and about relative stability of such states. They established measurable thermodynamic state functions having simple relations to the concept of work. These state functions depend on the irreversible processes which provide necessary and sufficient conditions for the stability or instability of systems. Their theory is substantiated by some experiments (Ross and Berry, 2008; Ross and Villaverde, 2010).

- **Johan Paulsson's theories on noise modelling**

Johan Paulsson has worked in the area of theoretical modelling of stochastic gene expression. He introduced an equation summing up the noise in gene networks, unifying and extending both mathematical and biological perspectives (Paulsson, 2004; Paulsson, 2005). The equation is summarised below.

If the probabilities of having n_1 and n_2 molecules per cell of chemical species X_1 and X_2 can be given by the following events,

$$n_1 \xrightarrow{R_1^+(n_1)} {n_1}_-^+ 1 \; and \; n_2 \xrightarrow{R_2^+(n_1,n_2)} {n_2}_-^+ 1$$

Then, by using the omega (Ω) expansion (Qu et al., 2003), where the first and second terms reproduce the macroscopic rate equations and the fluctuation dissipation theorem, the equation for stationary fluctuations around a stable fixed point is written as,

$$\frac{\sigma_2^2}{< n_2 >^2} = \frac{1}{< n_2 > \; H_{22}} + \frac{\sigma_1^2}{< n_1 >^2} \frac{H_{21}^2}{H_{22}^2} \frac{H_{22}/\tau_2}{H_{11}/\tau_1 + \; H_{22}/\tau_2}$$

where, σ_1 is the standard deviation, $<n_i>$ is for averages, τ_i for average life times, and H_{ij} is given by,

$$H_{ij} = \frac{\partial \ln(R_i^-/R_i^+)}{\partial \ln(n_j)}$$

This measures how the balance between production and elimination of X_i is affected by X_j. He pointed out that the basic principles of noise associated with the central dogma, auto-repression, replication and transcription can be understood by the above equation. He further claimed that this equation can be extended to any chemical system; thus, providing a basis for a stochastic biochemical system theory. However, this equation doesn't incorporate the thermodynamics of living biochemical reaction systems.

In summarising the work done on concentration fluctuations in biochemical reaction systems far away from equilibrium, it can be concluded that Joel Keizer (Keizer, 1987) developed the most general, mechanistic theory for large systems. Onsager's theory, which was the first theory on fluctuations, is applicable only to systems near equilibrium. Prigogine introduced the theory of fluctuations to non-linear systems far from equilibrium using a phase space theory of fluctuations, but in the limit of small fluctuations in a local equilibrium regime. Qian Hong also worked on the thermodynamics of the biochemical systems in living systems far from equilibrium, especially for the systems in non-equilibrium steady states (NESS) or for systems oscillating about a fixed mean. John Ross et al. developed mesoscopic formulations for thermodynamics and fluctuations for both far from and near equilibrium based on the Master equation for probability distributions. However, this mesoscopic approach is not as detailed as a statistical, mechanical analysis based on averages over mechanical motions, related to probability distributions and macroscopic chemical rates (Ross and Villaverde, 2010).

Appendix B

Gene Expression in Cells

B.1 The Building Blocks of Life: Cells and Genes

Despite changes at their macroscopic level, all organisms have strong similarities at their microscopic molecular level. Cells are the basic structural and functional units of all organisms. Cells work together to accomplish the tasks required for living. All living cells can be categorised into two broad classifications as prokaryotic or eukaryotic cells. Eukaryotic cells are more complex and significantly different from prokaryotic cells, because eukaryotic cells have membrane-bound organelles specified for certain metabolic activities. Complex compartmentalisation cannot be seen in prokaryotic cells.

Proteins and genes can be identified as the most important components in cells. A network of proteins accomplishes every process in a cell. Genes carry the necessary information to specify and create the proteins required for cell functions. The concept of gene was developed from the theory of evolution by Charles Darwin and Mendel's experimental work about the inheritance of peas. Genes are composed of deoxyribonucleic acid (DNA) strands. DNA is called the central molecule of life because DNA is the carrier of the hereditary information that controls the characteristics of an organism. DNA is formed as two intertwined helices (Figure B.1). Genetic information coded in the gene is released as a protein by a process called gene expression.

B.1.1 Gene expression and the central dogma of molecular biology

Protein production is an important and regulated process, because proteins are the main functional units in all cellular processes. All the necessary information required to create a protein is stored in a gene. Whenever a protein creation signal is released, the corresponding gene transcribes a RNA strand which is then translated into a protein. This protein creation process from the information coded in genes is called gene expression.

The detailed residue by residue transformation of sequential information in DNA to mRNA and to protein, but not the reverse, is called the central dogma of molecular biology (Figure B.2). The central dogma is very important as it is the major inherited information retrieval method in organisms.

In eukaryotes, the synthesis of RNA happens inside the nucleus with the help of RNA polymerase, an enzyme that can produce RNA. During transcription, RNA polymerase moves

along the DNA separating it into its two strands and creating matching RNA nucleotides that are paired with complementary DNA bases. The created RNA is then modified into a mRNA and transported from the nucleus to the cytoplasm where translation occurs. The delay imposed by the transportation of mRNA to the cytoplasm is called nucleo-cytoplasmic transportation delay. The nucleo-cytoplasmic transportation delay varies from one second to one hour from single cellular organisms like yeasts to multicellular organisms like humans. In prokaryotes, these two processes happen in the same place due to the lack of compartmentalisation. All the information for protein production is not required all the time; therefore, information retrieval is highly regulated by several mechanisms.

B.1.2 Regulation of gene expression

The characteristics of each cell are determined by its active protein composition. Gene expression is a tightly regulated process which determines the type and amount of various proteins in a cell. The regulation of gene expression can be divided into transcriptional and post-transcriptional control (Black, 2003; Lackner and Bähler, 2008; Rosenfeld et al., 2005). The transcriptional regulation of gene expression can be identified as the main control point which decides both the protein type and the amount of proteins produced. Other regulatory control mechanisms are degradation and post-translational modifications.

Translational control decides which set of proteins are translated via alternative splicing. During the alternative splicing process, the coding RNA chunks are reconnected in different ways to produce different proteins. The mRNA and protein concentration are controlled by degradation. Post-translational modifications such as phosphorylation decide protein activity.

B.1.3 Mechanisms of transcriptional control and cooperativity

The special region of a gene's DNA that codes for protein is called the coding region and the rest is called the regulatory or non-coding region. The regulatory region contains all the gene regulation-related DNA sequences. Transcriptional control can switch on, or off, gene expression by binding or unbinding regulatory proteins to this regulatory region. Therefore, transcriptional control can be considered as the main operating point of gene expression.

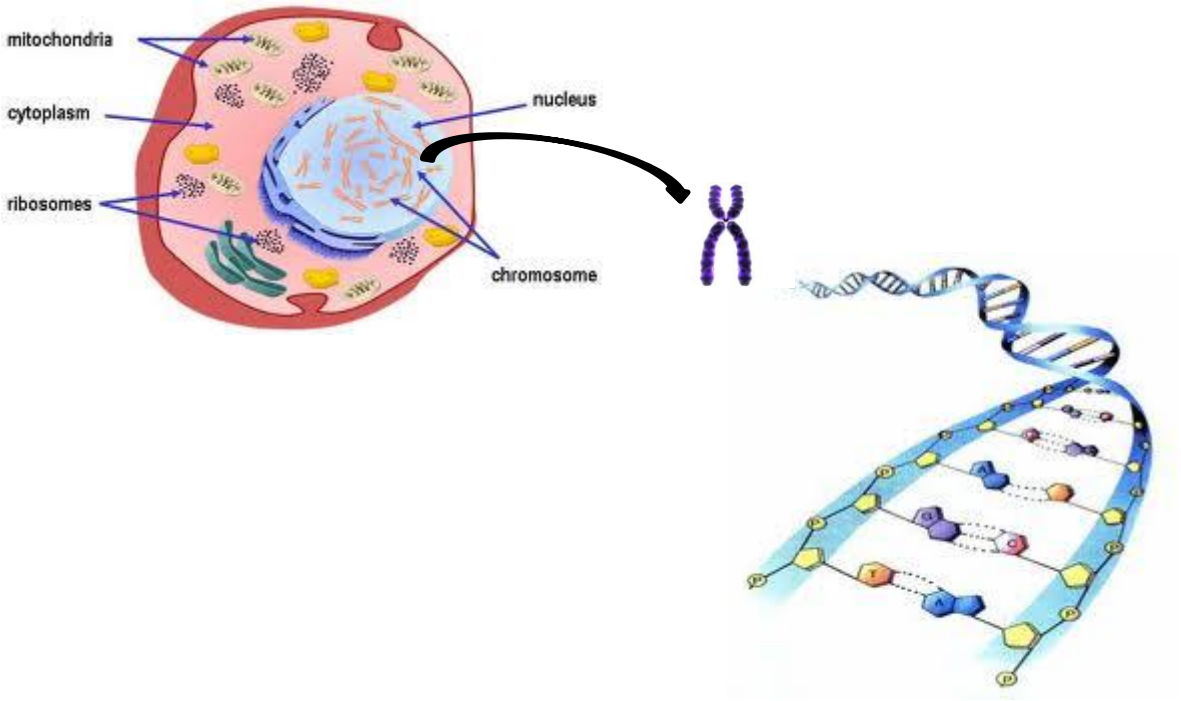

Figure B.1: Chromosomes reside in the nucleus. Chromosomes are made from DNA and short sections of DNA are called genes.

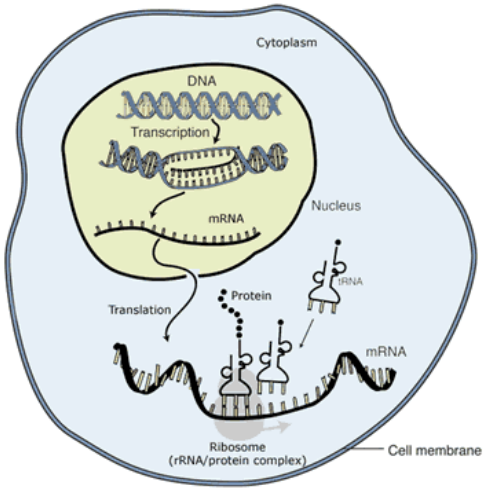

Image adapted from: National Human Genome Research Institute.

Figure B.2: Central dogma in molecular biology. The information retrieval from a gene to create a gene but not reverse is called central dogma of molecular biology. DNA is transcribed into an mRNA in the nucleus and it is translated into a protein in the cytoplasm (Adopted from National Human Genome Research Institute).

Transcriptional control is mainly undertaken through transcriptional factor recruitment. Transcription factors are proteins that can bind to a specific gene segment called an ‘operator ’ in a regulatory region and control the corresponding gene’s expression. There are two types of transcription factors, activators and repressors. Activators can promote gene expression by supporting RNA polymerase attachment to a specific DNA segment called a ‘promoter’. Repressors can block the attachment of RNA polymerase. Normally, the promoter and the operator reside upstream of the coding region facilitating the transcriptional control (Harvey Lodish, 1995).

Co-operative binding occurs when there is more than one binding site in operation for the transcription factors. If the binding of one transcription factor for a binding site increases the affinity of another transcription factor to another site, that operator exhibits positive cooperativity. In contrast, if the attachment of one transcription factor reduces the affinity for another site, the operator exhibits negative cooperativity. If the transcription factors bind to the operator sites independently, the binding is called non-cooperative. Transcription factors are also proteins expressed by genes. In other words, genes are controlled by their products. The collection of DNA, RNA and proteins that interact via feedback loops and work with other substances of the cell and control cell’s DNA expression indirectly is called a gene regulatory network.

B.1.4 Feedbacks and nonlinear dynamics in gene regulatory networks

Frequently, feedback control can be found in gene regulatory networks. Feedback regulation alters the activity or production rate of cellular components. Feedback loops can be classified as positive or negative feedback loops. A positive feedback loop can accelerate a process and generate a positive net gain around the loop. In gene regulation, transcription factors may promote its own gene regulation creating a positive feedback loop. Conversely, negative feedback loops slow the process and generate a negative net gain around the loop. Repressor inhibition of its own gene can be considered as an example of a negative feedback loop in gene regulation. Other feedback mechanisms can be identified as activation and deactivation by phosphorylation.

Feedback loops in many biological circuits show complex nonlinear dynamics such as oscillations, multistability, chaos and fractals. For example, circadian rhythms, which are connected with an individual’s sleep-wake cycle, are generated by a gene regulatory network that communicates through positive and negative feedback loops.

Appendix C

Meiosis Initiation Mathematical Models Used for Comparisons

C.1 Extended Boolean Network of Meiosis Initiation

This extended Boolean network has ten expression levels (0 to 9) rather than two (0 and 1) levels in conventional Boolean networks. This network includes the main initiator proteins, Ime1 and Ime2, and two hypothetical negative feedback loops to shut down the transcription of IME1 and IME2, Ume6 and Rpd3 proteins (Rubinstein et al., 2007). This model, which is a discrete transition system, represents the initiation process by a graph (Figure C.1) whose nodes represent RNA or proteins, and the edges denote regulation. Logical AND operation is introduced to describe the conjunctive conditional dependence between functions, namely the activity of a regulator is enabled only if some other regulator in the system is active.

The positive and negative edges have weights of +1 and -1 respectively. For self degradation loops, Ime1 has a weight of -1 and Ime2 has a weight of -2. The conditional dependence in all cases is positive. The initial vector has state 1 for the IME1 mRNA, state 0 for Ime1, Ime2 proteins and IME2 mRNA, state 9 for Ume6/Rpd3; consequently, Ume6, X and Y are in state 0.The current state of the system is represented by a vector of RNA and protein levels (each expression level is an integer between 0 and 9) associated with the nodes. This discrete model explains the qualitative behaviour of meiosis initiation including transient and sequential expression patterns of meiotic inducers under nutrient-starved conditions. This model is further used to explore variations in their basic network to identify the negative feedback loops which affect meiosis initiator transcription (Rubinstein et al., 2007). More details are available in Rubinstein et. al. (2007).

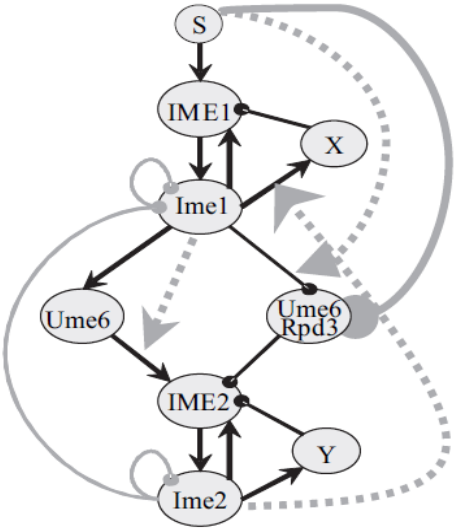

Figure C.1 The schematic diagram of the extended Boolean network model proposed by Rubinstein et al. (2007) (Rubinstein et al., 2007), describing the relationships between the expression of IME1 and IME2. RNAs are written with capital letters. Solid black Arrows: activation, solid black lines with knob: repression, solid grey lines with a knob: degradation, dotted grey arrows: gating by the conjunction (AND), S: signal that induces meiosis. 'X' and 'Y' are the putative nodes used to shut down transcription of IME1 and IME2. (Adopted from Rubinstein et. al. (2007)). This figure which also appears in the Section 3.4 is repeated in this appendix to compare with the other model (Ray et al., 2013) .

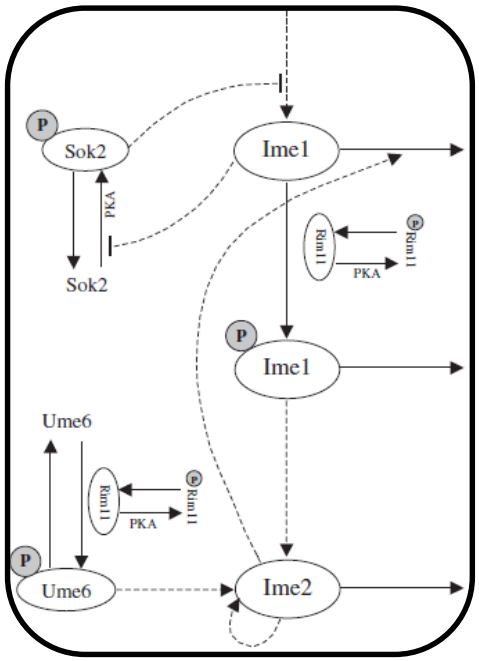

Figure C.2 A schematic diagram of the meiosis initiation pathway modelled in Ray et. al. (2013) (Ray et al., 2013). Phosphorylated proteins are marked with the letter P. Dashed lines represent regulatory interactions; solid lines represent degradation, phosphorylation. This figure which also appears in the Section 3.4 is repeated in this appendix to compare with the other model (Rubinstein et al., 2007). This figure is adopted from Ray et. al. (2013) (Ray et al., 2013), © 2013 Ray et al.; licensee BioMed Central Ltd.

C.2 The Mathematical Model of Meiosis Initiation Developed by Ray et. al. (2013)

In 2013, Ray et. al. developed an ordinary differential equation-based mathematical model for yeast sporulation (Ray et al., 2013). This mathematical model includes Ime1, Ime2, Rim11, Ume6, Sok2 and the feedback loops between them (Figure C.2). The model is an abstract for a real pathway that incorporates only some components and claims that the effects of other molecules are reflected indirectly: the double negative feedback loop between Ime2 and Cdk1/Cln3 and the mutual activation between Ime2 and Ndt80 are both captured by auto-regulation of Ime2; Cdk1/Cln3, Msn2/4, Snf1 are collectively represented by an activation signal.

This model consists of six differential equations based on mass action and hill type kinetics as given in the Figure C.3. These six equations represent six proteins in either phosphorylated or non-phosphorylated form. The variables in this model are dimensionless and represent the relative protein levels within the range of zero and one. The differential equations include terms describing protein synthesis, degradation, phosphorylation dephosphorylation, regulatory activation and repression. The parameters of this model, some of which are based on the experimental parameter values are given in the Table C.1. Initial conditions are set as following: All variables except for pSOK2 are set to zero and pSOK2 level is given the maximum level of 1 as the initial condition.

$$\frac{dRim11}{dt} = u_{rim11} \cdot (1 - Rim11) - p_{rim11} \cdot Rim11 \quad (1)$$

$$\frac{dpUme6}{dt} = p_{ume6} \cdot Rim11 \cdot (1 - pUme6) - u_{ume6} \cdot pUme6 \quad (2)$$

$$\frac{dpSok2}{dt} = p_{sok2} \cdot \frac{c_{sok2}}{c_{sok2} + \mathrm{Ime1}} \cdot (1 - pSok2) - u_{sok2} \cdot pSok2 \quad (3)$$

$$\frac{d\mathrm{Ime1}}{dt} = s_{ime1} \cdot \frac{c_{ime1}}{c_{ime1} + pSok2} - p_{ime1} \cdot Rim11 \cdot \mathrm{Ime1} - d_{ime1} \cdot \mathrm{Ime1} - d'_{ime1} \cdot \mathrm{Ime2} \cdot \frac{\mathrm{Ime1}}{c_1 + \mathrm{Ime1}} \quad (4)$$

$$\frac{dp\mathrm{Ime1}}{dt} = p_{ime1} \cdot Rim11 \cdot \mathrm{Ime1} - d_{pime1} \cdot p\mathrm{Ime1} \quad (5)$$

$$\frac{d\mathrm{Ime2}}{dt} = s_{ime2} \cdot pUme6 \cdot p\mathrm{Ime1} + s'_{ime2} \cdot \frac{\mathrm{Ime2}^5}{c_2{}^5 + \mathrm{Ime2}^5} - d_{ime2} \cdot \frac{\mathrm{Ime2}}{c_3 + \mathrm{Ime2}} \quad (6)$$

Figure C.3 Differential equations of the mathematical model of Ray et. al. (2013). This figure is adopted from Ray et. al. (2013) (Ray et al., 2013), © 2013 Ray et al.; licensee BioMed Central Ltd.

Table C.1 Parameters defined in the model of Ray et. al. (2013). This table is adopted from Ray et. al. (2013) (Ray et al., 2013), © 2013 Ray et al.; licensee BioMed Central Ltd.

Parameter	Definition	Value	Reference
Synthesis, dimension =/hour			
s_{ime1}	Synthesis rate of Ime1	10	[15,43-45]
s_{ime2}	Synthesis rate of Ime2	10	[39]
s'_{ime2}	The maximum rate of auto-regulation-dependent Ime2 synthesis	3	Estimated
Degradation, dimension =/hour			
d_{ime1}	Degradation rate of Ime1	1	[3]
d'_{ime1}	The maximum rate of Ime2-activated Ime1 degradation	1	[3]
d_{pime1}	Degradation rate of pIme1	1	[3]
d_{ime2}	Degradation rate of Ime2	8	[3]
Phosphorylation, dimension =/hour			
p_{rim11}	Phosphorylation rate of Rim11	0.01	[2], Estimated
u_{rim11}	Dephosphorylation rate of Rim11	0.1	[2], Estimated
p_{ume6}	Phosphorylation rate of Ume6	0.3	[18], Estimated
u_{ume6}	Dephosphorylation rate of Ume6	0.01	[18], Estimated
p_{sok2}	Phosphorylation rate of Sok2	0.7	[6], Estimated
u_{sok2}	Dephosphorylation rate of Sok2	1	[6], Estimated
p_{ime1}	Phosphorylation rate of Ime1	2	Estimated
Constant, dimensionless			
c_{sok2}	Constant measuring half-maximum inhibition of Sok2 phosphorylation by Ime1	0.05	Estimated
c_{ime1}	Constant measuring half-maximum inhibition of Ime1 synthesis by pSok2	0.01	Estimated
c_1	Constant measuring half-maximum activation of Ime1 degradation by Ime2	0.01	Estimated
c_2	Constant measuring half-maximum activation of Ime2 synthesis through auto-regulation	1.4	Estimated
c_3	Constant measuring half-maximum activation of Ime2 degradation	2	Estimated

Appendix D

Cumulative Frequency Distributions of Behaviour and Non-behaviour Sets of the Sensitive Parameters

We plot the cumulative frequency distributions of the behaviour and non-behaviour sets resulting from global sensitivity analysis for each of the fifteen sensitive parameters at each three states: meiosis-only state at the nitrogen level of 0.06, transition state at the nitrogen level of 0.083 and mitosis-only state at the nitrogen level of 0.98. Cumulative distributions are given in the following three pages.

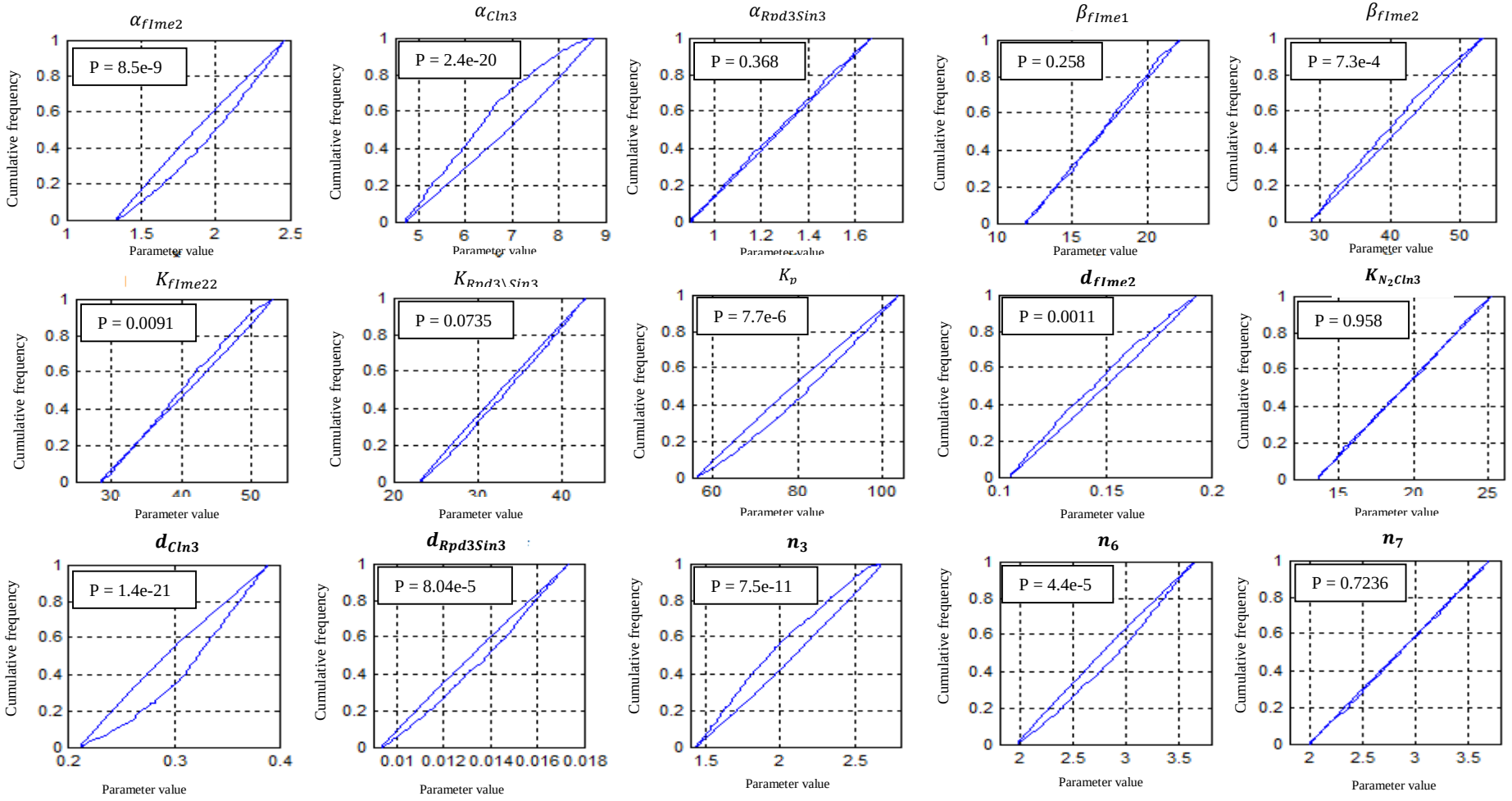

Figure D.1: Cumulative frequency distributions of the fifteen sensitive parameters in the meiosis-only state at nitrogen level of 0.06.The two blue curves represent the cumulative frequencies for the behaviour and non-behaviour sets. Parameters with similar cumulative distributions for the behaviour and non-behaviour sets indicate that changes to that variable have a small influence on the output. Parameters with significantly different cumulative distributions are sensitive and variation of these parameters results in distinguishing behaviour of the system output.

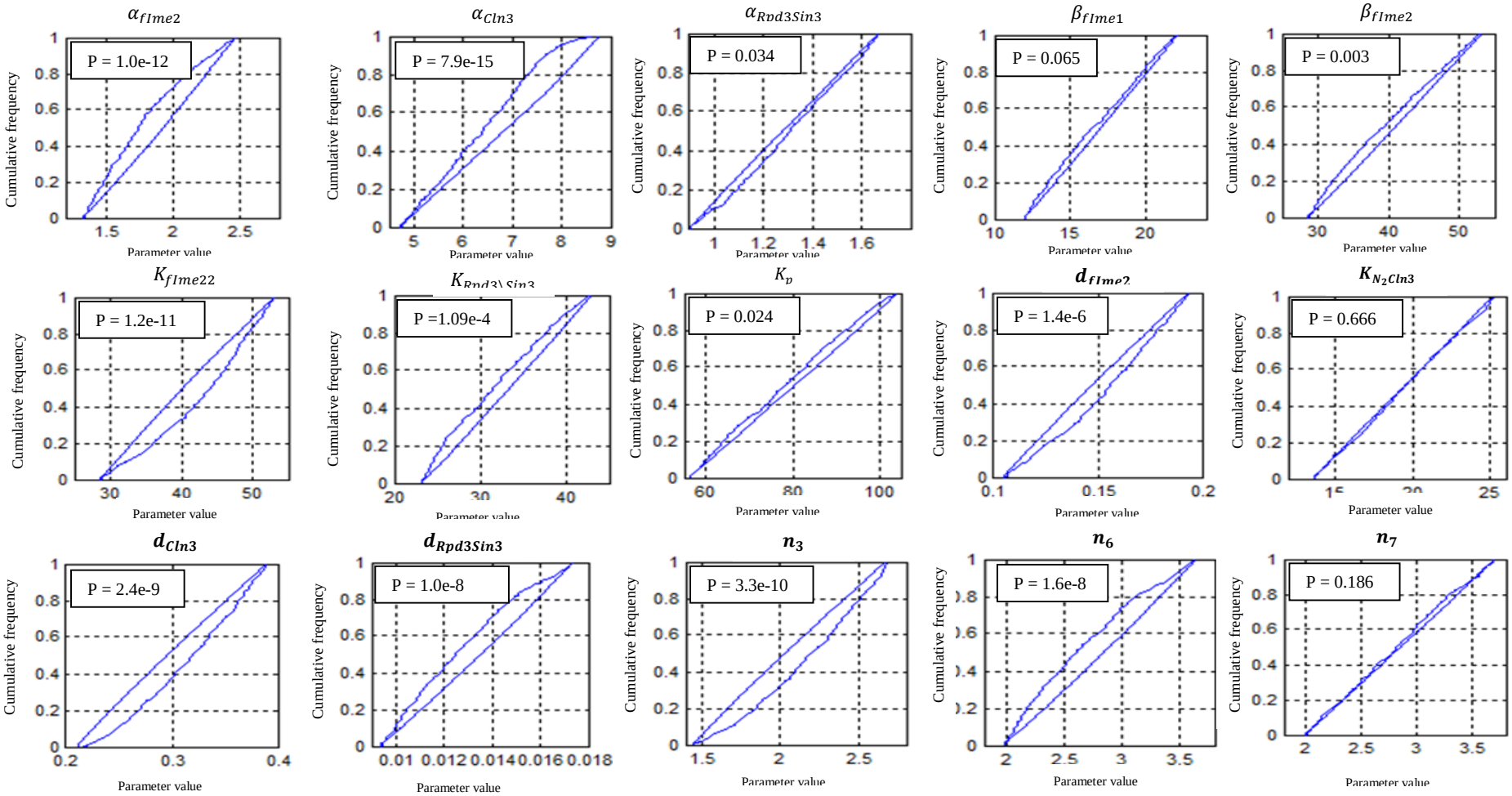

Figure D.2: Cumulative frequency distributions of the fifteen sensitive parameters in the transition state at nitrogen level of 0.083.The two blue curves represent the cumulative frequencies for the behaviour and non-behaviour sets. Parameters with similar cumulative distributions for the behaviour and non-behaviour sets indicate that changes to that variable have a small influence on the output. Parameters with significantly different cumulative distributions are sensitive and variation of these parameters results distinguishing behaviour of the system output.

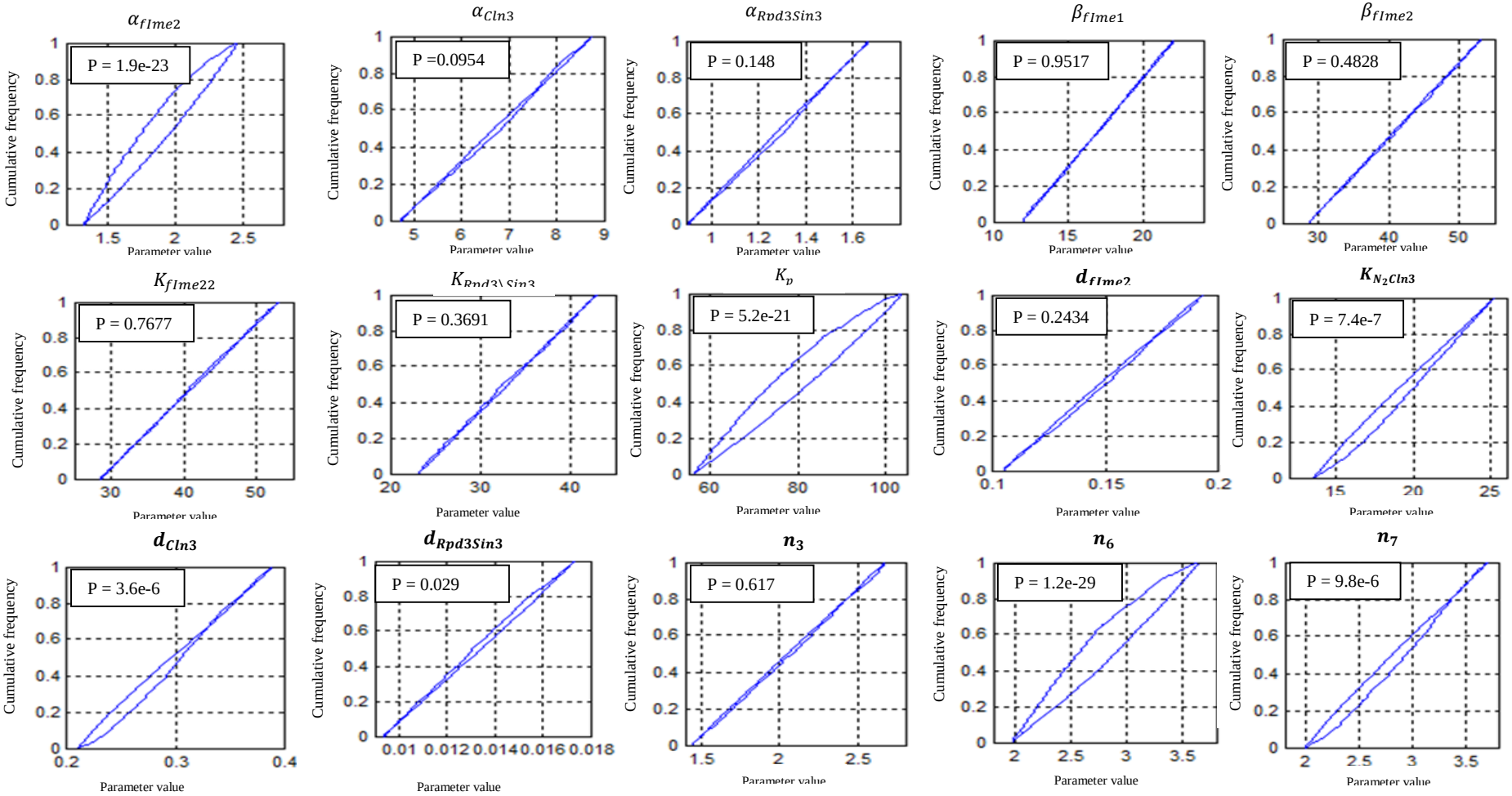

Figure D.3: Cumulative frequency distributions of the fifteen sensitive parameters in the mitosis state at nitrogen level of 0.98.The two blue curves represent the cumulative frequencies for the behaviour and non-behaviour sets. Parameters with similar cumulative distributions for the behaviour and non-behaviour sets indicate that changes to that variable have a small influence on the output. Parameters with significantly different cumulative distributions are sensitive and variation of these parameters results distinguishing behaviour of the system output.

Appendix E

Programming

E.1 The Mathematical Model of Meiosis Initiation

Main.m

```
% This is the main program of the mathematical model of meiosis initiation.
% The current simulation output is meiosis initiation at low nitrogen level
% (N2=0.06).

% other files are needed to be put in the same folder to run this script

      % parameters.m:defines the parameters
      % eqn1.m : defines the differential equations

clear all;

% simulation time
Tend=30;

% initial conditions of Ime1, Ime2, Cdk1/Cl3 and Rpd3/Sin3
Xo = [0.1 0 0.1 0.6];

% defining some initial values for parameters useful for the while loop
DD=0; % An element of the time matrix 'tt'
dtt=.1; % An element of the time matrix 'tt'
j=2; % pointer to be used in the while loop
SOlX=Xo; % SOlX is the final solution matrix
soltime=DD; % soltime is the final time matrix

% solving the ODE at each time step in a while loop, to checking whether
%the protein values are getting negative values. We impose a positive
%basal value for any negative protein value observed.

while(DD<Tend) % starting the while loop

% timespan
tt = DD:dtt:DD+dtt;

% calling the solver
[T X] = ode45(@eqn1,tt,Xo);

% imposing positive basal levels, if negative protein levels observed
if((X(length(T),1))<0),X((length(T)),1)=0.0001;end
if((X(length(T),2))<0),X((length(T)),2)=0.0001;end
if((X(length(T),3))<0),X((length(T)),3)=0.0001;end
if((X(length(T),4))<0),X((length(T)),4)=0.0001;end

% updating the initial condition matrix for the next step
Xo = [X(length(T),1);X(length(T),2);X(length(T),3);X(length(T),4)];

% Adding the solution to the final solution array
SOlX(j,1)=X(length(T),1);
SOlX(j,2)=X(length(T),2);
SOlX(j,3)=X(length(T),3);
SOlX(j,4)=X(length(T),4);
```

```
DD=DD+dtt; % Updating the element(DD) of the time matrix(tt) for the next
%step
soltime(j)=DD; % Updating the final time matrix
j=j+1; % Updating the pointer for the next step

end % end of the while loop

% Defining the experimental data to be compared with the simulation output
% Ime1 data extracted from experiments
Ime1Prot=[ 1.8 2.9 4.1 5.9 9.15 11.8];
Ime1Pro=[ 1.66/10 3.61/10 6/10 6.18/10 4.6/10 3.8/10 ];
ER=[5.733 7.0428 4.8298 4.025 5.0281 4.5236];

% Ime2 data extracted from experiments
Ime2Prot=[0 5 11.3 13.5 15.6 18.2 20];
Ime2Pro=[0/10 .8/10 3.2/10 4.8/10 4.7/10 4.1/10 3.3/10];

% Rpd3 data extracted from experiments
Rpd3X = [0 1 3 5 12];
Rpd3Y = [9 2.5081 1.1400 1.1400 1.5635]./10;

% Cln3 data extracted from experiments
CLn3IX = [0 0.5054 1.007 1.5036 1.9831 2.990];
CLn3IY = [1 3.1644 3.7505 5.7943 7.1281 10.430];
CLn3DX = [0 0.5139 1.0124 1.5057 1.9919 2.9940];
CLn3DY = [1 1.8188 1.5448 1.4204 1.8195 1.4207];


% plotting the experimental and in-silico protein levels
h1 = figure(1); % Defining a new figure and a header to access the figure

% Setting the position and size of the figure
set(h1, 'Position', [200 200 500 250]);

% plotting the Ime1 experimental data with error bars.
errorbar(Ime1Prot,Ime1Pro,ER/100,'ro');hold on;
plot(Ime2Prot,Ime2Pro,'k*');hold on;

% plotting the scaled Rpd3 data at low nutrients
plot(Rpd3X,(((Rpd3Y./0.9).*0.6)),'bs'); hold on;

% Scaled experimental Cln3 at high nutrients
% plot(CLn3IX,((CLn3IY)./9*(0.14)+.1),'b*'); hold on;
% Scaled experimental Cln3 at low nutrients
plot(CLn3DX,((CLn3DY)./10),'g*'); hold on;

% plotting the in-silico protein levels
plot(soltime,SOlX(:,1),'r','LineWidth',2),hold on;
plot(soltime,SOlX(:,2),'k.','LineWidth',2,'MarkerSize',4),hold on;
plot(soltime,SOlX(:,3),'g-.','LineWidth',2),hold on;
plot(soltime,SOlX(:,4),'b--','LineWidth',2),hold on;

% defining the axis limits for a better representation of the output
axis([0 30 0 0.7])
% defining the axis lables
xlabel('Time (hours)');
ylabel('Relative protein level');
```

parameters.m

```
% Parameters of the model and their values, as defined in Table 4.1

AlpaIme1=0.0004;   % α_fIme1
AlpaIme2=1.90;   % α_fIme2
AlpaCln3=6.74;   % α_Cln3
AlpaRpd3Sin3=1.2859; % α_Rpd3Sin3
BetaIme1=17; % β_fIme1
BetaIme2=40.92; % β_fIme2
BetaCln3=106.612;% β_Cdk1\Cln3
KIme11=10; % K_fIme11
KN2=2.550; % K_N2
dIme1=0.02800;% d_fIme1
n1=2.8; % n_1
n2=2.8; % n_2

KIme22=40.8; % K_fIme22
KIme12=4.65; % K_fIme12
KRpd3=33.0; % K_Rpd3\Sin3
KCln3Ime1=70.3250; % K_Cdk1\Cln3
KRpd3Ime1=105.3; % K_Rpd3SIme1

GammaPIme2=20.76; % γ_PIme2
KPIme2=80.1408; % K_p

n3=2.06; % n_3
n4=0.5679; % n_4
n5=2.8; % n_5
n6=2.80308; % n_6
dIme2=0.1490; % d_fIme2
KN2Cln3=19.4; % K_N2Cln3
n7=2.846; % n_7
GammaPCdk1=50.1; % γ_PCdk1Cln3
GammaPIme1Cln3=1.1384; % γ_PIme1Cln3
KPIme2Cdk1=100.9868; % K_PIme2Cdk1
KPIme1Cln3=125.9868; % K_PIme1Cdk1\Cln3
n8=2.8; % n_8
n9=2.8; % n_9
n10=2.0; % n_10
n11=2.8; % n_11
n12=0.8; % n_12
n13=37; % n_13
n14=0.06; % n_14
n15=0.01; % n_15
dCln3=0.2999078; % d_Cln3
dRpd3=0.05348; % d_Rpd3Sin3
xo=100; % fIme1_o
yo=100; % fIme2_o
no=6; % N_2o
zo=100; % Sin3/Rpd3_o
po=100; % Cdk1/Cln3_o

N2=0.06; % nitrogen level for meiosis initation
```

eqn1.m

```
%defines the differential equations
function [dx_dt]= eqn1(t,x)

parameters

%equation of Ime1 protein
dx_dt(1) =
(AlpaIme1/xo)+(BetaIme1/xo)*(((x(1))^n1)/((KIme11/xo)^n1+(x(1))^n1))*(KN2^(
n2)/(KN2^n2+(N2*no)^n2))*((KCln3Ime1^(n9))/(KCln3Ime1^n9+(x(3)*zo)^n9))*((K
Rpd3Ime1^(n11))/(KRpd3Ime1^n11+((n12-(n12/(1+exp(t-6))))*po)^n11))-
(GammaPIme1Cln3/xo)*(((x(3))^n10)/((KPIme1Cln3/zo)^n10+(x(3))^n10))-
(dIme1*x(2)*yo*x(1)) ;

%equation of Ime2 protein
dx_dt(2) =
(AlpaIme2/yo)+(BetaIme2/yo)*((((x(2))^n3)/((KIme22/yo)^n3+(x(2))^n3))*(((x(
1))^n4)/((KIme12/xo)^n4+(x(1))^n4))*(((KRpd3)^n5)/((KRpd3)^n5+(x(4)*po)^n5)
))-(GammaPIme2/yo)*(((x(3))^n6)/((KPIme2/zo)^n6+(x(3))^n6))-dIme2*x(2);

%equation of Cdk1/Cln3 complex
dx_dt(3) =
(AlpaCln3/zo)+(BetaCln3/zo)*((N2))^(n7)/((KN2Cln3/no)^n7+(N2)^n7)-
(GammaPCdk1/zo)*(((x(2))^n8)/((KPIme2Cdk1/yo)^n8+(x(2))^n8))-dCln3*x(3);

%equation of Rpd3/Sin3 complex
dx_dt(4) = (AlpaRpd3Sin3/po)-
dRpd3*((x(1)*xo)*1/po)*((1/(N2*no))*((n13)/(n15+(exp((1.6*t))))+n14));

dx_dt = dx_dt';
```

References

Adamah, D. J. B., Gokhale, P. J., Eastwood, D. J., Rajpert De-Meyts, E., Goepel, J., Walsh, J. R., Moore, H. D., Andrews, P. W., 2005. Dysfunction of the mitotic: meiotic switch as a potential cause of neoplastic conversion of primordial germ cells. International Journal of Andrology 29, 219-227.

Alberghina, L., Westerhoff, H. V., 2007. Systems biology: definitions and perspectives. Springer.

Alon, U., 2007. An introduction to systems biology: design principles of biological circuits. CRC press.

Angeli, D., Ferrell, J. E., Sontag, E. D., 2004. Detection of multistability, bifurcations, and hysteresis in a large class of biological positive-feedback systems. Proceedings of the National Academy of Sciences of the United States of America 101, 1822, doi:10.1073/pnas.0308265100

Arkin, A., Ross, J., 1994. Computational functions in biochemical reaction networks. Biophysical Journal 67, 560-578.

Barik, D., Baumann, W. T., Paul, M. R., Novak, B., Tyson, J. J., 2010. A model of yeast cell-cycle regulation based on multisite phosphorylation. Molecular Systems Biology 6.

Belle, A., Tanay, A., Bitincka, L., Shamir, R., O'Shea, E. K., 2006. Quantification of protein half-lives in the budding yeast proteome. Proceedings of the National Academy of Sciences 103, 13004-13009.

Black, D. L., 2003. Mechanisms of alternative pre-messenger RNA splicing. Annual Review of Biochemistry 72, 291-336.

Boogerd, F., Bruggeman, F. J., Hofmeyr, J.-H. S., Westerhoff, H. V., 2007. Systems biology: philosophical foundations. Elsevier.

Bowdish, K., Mitchell, A., 1993. Bipartite structure of an early meiotic upstream activation sequence from *Saccharomyces cerevisiae*. Molecular and Cellular Biology 13, 2172-2181.

Bowdish, K. S., Yuan, H. E., Mitchell, A. P., 1994. Analysis of RIM11, a yeast protein kinase that phosphorylates the meiotic activator IME1. Molecular and Cellular Biology 14, 7909-7919.

Butler, D., 1999. Computing 2010: from black holes to biology. Nature 402, C67-C70.

Cao, Y., Li, H., Petzold, L., 2004. Efficient formulation of the stochastic simulation algorithm for chemically reacting systems. The Journal of Chemical Physics 121, 4059.

Cao, Y., Gillespie, D. T., Petzold, L. R., 2006. Efficient step size selection for the tau-leaping simulation method. The Journal of Chemical Physics 124, 044109.

Champion, M. D., Hawley, R. S., 2002. Playing for half the deck: the molecular biology of meiosis. nature medicine 8, 50-56.

Chen, K. C., Csikasz-Nagy, A., Gyorffy, B., Val, J., Novak, B., Tyson, J. J., 2000. Kinetic analysis of a molecular model of the budding yeast cell cycle. Molecular Biology of the Cell 11, 369.

Chen, K. C., Calzone, L., Csikasz-Nagy, A., Cross, F. R., Novak, B., Tyson, J. J., 2004. Integrative analysis of cell cycle control in budding yeast. Molecular Biology of the Cell 15, 3841, doi:10.1091/mbc.E03-11-0794

Cho, R. J., Campbell, M. J., Winzeler, E. A., Steinmetz, L., Conway, A., Wodicka, L., Wolfsberg, T. G., Gabrielian, A. E., Landsman, D., Lockhart, D. J., 1998. A genome-wide transcriptional analysis of the mitotic cell cycle. Molecular Cell 2, 65-73.

Chu, S., Herskowitz, I., 1998. Gametogenesis in yeast is regulated by a transcriptional cascade dependent on Ndt80. Molecular Cell 1, 685-696.

Chu, S., DeRisi, J., Eisen, M., Mulholland, J., Botstein, D., Brown, P. O., Herskowitz, I., 1998. The transcriptional program of sporulation in budding yeast. Science 282, 699, doi:10.1126/science.282.5389.699

Colomina, N., Garí, E., Gallego, C., Herrero, E., Aldea, M., 1999. G1 cyclins block the Ime1 pathway to make mitosis and meiosis incompatible in budding yeast. The EMBO Journal 18, 320-329, doi:10.1093/emboj/18.2.320.

Covitz, P., Herskowitz, I., Mitchell, A., 1991. The yeast RME1 gene encodes a putative zinc finger protein that is directly repressed by a1-alpha 2. Genes & Development 5, 1982-1989.

Crick, F., 1988. What Mad Pursuit: A Personal View of Scientific Discovery. United State of America.

Danaie, P., Altmann, M., Hall, M. N., Trachsel, H., Helliwell, S. B., 1999. CLN3 expression is sufficient to restore G1-to-S-phase progression in *Saccharomyces cerevisiae* mutants defective in translation initiation factor eIF4E. Biochemical Journal 340, 135, doi:10.1042/0264-6021:3400135.

Dayani, Y., Simchen, G., Lichten, M., 2011. Meiotic recombination intermediates are resolved with minimal crossover formation during return-to-growth, an analogue of the mitotic cell cycle. PLoS GENETICS 7, e1002083.

Dennis, P. B., Fumagalli, S., Thomas, G., 1999. Target of rapamycin (TOR): balancing the opposing forces of protein synthesis and degradation. Current Opinion in Genetics & Development 9, 49-54.

Deutschbauer, A. M., Williams, R. M., Chu, A. M., Davis, R. W., 2002. Parallel phenotypic analysis of sporulation and postgermination growth in *Saccharomyces cerevisiae*. Proceedings of the National Academy of Sciences 99, 15530-15535.

Dorsman, J. C., Van Heeswijk, W. C., Grivell, L. A., 1990. Yeast general transcription factor GFI: sequence requirements for binding to DNA and evolutionary conservation. Nucleic Acids Research 18, 2769-2776.

Duntze, W., MacKay, V., Manney, T. R., 1970. *Saccharomyces cerevisiae*: a diffusible sex factor. Science 168, 1472-1473.

Dushek, O., vanáderáMerwe, P. A., Shahrezaei, V., 2011. Ultrasensitivity in Multisite Phosphorylation of Membrane-Anchored Proteins. Biophysical Journal 100, 1189-1197, doi:10.1016/j.bpj.2011.01.060.

Eckmann, C. R., Crittenden, S. L., Suh, N., Kimble, J., 2004. GLD-3 and control of the mitosis/meiosis decision in the germline of Caenorhabditis elegans. Genetics 168, 147-160.

Ermentrout, B., 2012. Xppaut. Computational Systems Neurobiology. Springer, pp. 519-531.

Esposito, M. S., Esposito, R. E., 1974. Genes controlling meiosis and spore formation in yeast. Genetics 78, 215.

Fall, C. P., Marland, E. S., Wagle, U., Tyson, J. J., 2002. Computational cell biology Springer.

Ferrell, J. E., 2002. Self-perpetuating states in signal transduction: positive feedback, double-negative feedback and bistability. Current Opinion in Cell Biology 14, 140-148, doi:10.1016/S0955-0674(02)00314-9.

Ferrell, J. E., 2008. Feedback regulation of opposing enzymes generates robust, all-or-none bistable responses. Current Biology 18, R244-R245, doi:10.1016/j.cub.2008.02.035.

Ferrell Jr, J. E., Machleder, E. M., 1998. The biochemical basis of an all-or-none cell fate switch in Xenopus oocytes. Science 280, 895-898, doi:10.1126/science.280.5365.895

Foiani, M., Nadjar-Boger, E., Capone, R., Sagee, S., Hashimshoni, T., Kassir, Y., 1996. A meiosis-specific protein kinase, Ime2, is required for the correct timing of DNA replication and for spore formation in yeast meiosis. Molecular and General Genetics MGG 253, 278-288.

Forsburg, S. L., Nurse, P., 1991. Cell cycle regulation in the yeasts *Saccharomyces cerevisiae* and *Schizosaccharomyces pombe*. Annual Review of Cell Biology 7, 227-256, doi:10.1146/annurev.cb.07.110191.001303.

Fraser, D., Kærn, M., 2009. A chance at survival: gene expression noise and phenotypic diversification strategies. Molecular Microbiology 71, 1333-1340, doi:10.1111/j.1365-2958.2009.06605.x.

Friedlander, G., Joseph-Strauss, D., Carmi, M., Zenvirth, D., Simchen, G., Barkai, N., 2006. Modulation of the transcription regulatory program in yeast cells committed to sporulation. Genome Biology 7, R20, doi:10.1186/gb-2006-7-3-r20.

G, D. V., T, H., M, L., J, M., B, S., 2006. A course in mathematical biology: quantitative modeling with mathematical and computational methods. Society for Industrial Mathematics, Philadelphia.

Gallego, C., Gari, E., Colomina, N., Herrero, E., Aldea, M., 1997. The Cln3 cyclin is down-regulated by translational repression and degradation during the G1 arrest caused by nitrogen deprivation in budding yeast. The EMBO Journal 16, 7196-7206, doi:10.1093/emboj/16.23.7196.

Gibson, M. A., Bruck, J., 2000. Efficient exact stochastic simulation of chemical systems with many species and many channels. The Journal of Physical Chemistry A 104, 1876-1889.

Gillespie, D. T., 1976. A general method for numerically simulating the stochastic time evolution of coupled chemical reactions. Journal of Computational Physics 22, 403-434.

Gillespie, D. T., 1977. Exact stochastic simulation of coupled chemical reactions. The Journal of Physical Chemistry 81, 2340-2361.

Gillespie, D. T., 2000. The chemical Langevin equation. The Journal of Chemical Physics 113, 297.

Gillespie, D. T., 2001. Approximate accelerated stochastic simulation of chemically reacting systems. The Journal of Chemical Physics 115, 1716.

Gillespie, D. T., 2002. The chemical Langevin and Fokker-Planck equations for the reversible isomerization reaction. The Journal of Physical Chemistry A 106, 5063-5071.

Gillespie, D. T., Petzold, L. R., 2003. Improved leap-size selection for accelerated stochastic simulation. The Journal of Chemical Physics 119, 8229.

Gimeno, C. J., Ljungdahl, P. O., Styles, C. A., Fink, G. R., 1992. Unipolar cell divisions in the yeast *S. cerevisiae* lead to filamentous growth: Regulation by starvation and RAS. Cell 68, 1077-1090.

Glansdorff, P., Prigogine, I., 1971. Thermodynamic theory of structure, stability and fluctuations. John Wiley & Sons Ltd

Goldbeter, A., Koshland, D., 1984. Ultrasensitivity in biochemical systems controlled by covalent modification. Interplay between zero-order and multistep effects. Journal of Biological Chemistry 259, 14441-14447.

Goldmark, J. P., Fazzio, T. G., Estep, P. W., Church, G. M., Tsukiyama, T., 2000. The Isw2 Chromatin Remodeling Complex Represses Early Meiotic Genes upon Recruitment by Ume6p. Cell 103, 423-433, doi:10.1016/S0092-8674(00)00134-3.

Görner, W., Durchschlag, E., Martinez-Pastor, M. T., Estruch, F., Ammerer, G., Hamilton, B., Ruis, H., Schüller, C., 1998. Nuclear localization of the C2H2 zinc finger protein Msn2p is regulated by stress and protein kinase A activity. Genes & Development 12, 586-597.

Graña, X., Reddy, E. P., 1995. Cell cycle control in mammalian cells: role of cyclins, cyclin dependent kinases (CDKs), growth suppressor genes and cyclin-dependent kinase inhibitors (CKIs). Oncogene 11, 211.

Granot, D., Margolskee, J. P., Simchen, G., 1989. A long region upstream of the IME1 gene regulates meiosis in yeast. Molecular and General Genetics MGG 218, 308-314.

Gunawardena, J., 2010. Models in systems biology: the parameter problem and the meanings of robustness. Elements of Computational Systems Biology, Vol. 1.
Gupta, P. K., 2009. Cell and Molecular Biology. Global Media, Meerut, IND.
Gurevich, V., Kassir, Y., Idnurm, A., 2010. A switch from a gradient to a threshold mode in the regulation of a transcriptional cascade promotes robust execution of meiosis in budding yeast. PLoS ONE 5, e11005, doi:10.1371/journal.pone.0011005
Guttmann-Raviv, N., Martin, S., Kassir, Y., 2002. Ime2, a meiosis-specific kinase in yeast, is required for destabilization of its transcriptional activator, Ime1. Molecular and Cellular Biology 22, 2047, doi:10.1128/MCB.22.7.2047-2056.2002.
Hao, N., Nayak, S., Behar, M., Shanks, R. H., Nagiec, M. J., Errede, B., Hasty, J., Elston, T. C., Dohlman, H. G., 2008. Regulation of cell signaling dynamics by the protein kinase-scaffold Ste5. Molecular Cell 30, 649.
Harvey Lodish, A. B., Paul Matsudaira, S. Lawrence Zipursky, David Baltimore, James Darnell, 1995. Molecular Cell Biology. Scientific American Books.
Hepworth, S. R., Friesen, H., Segall, J., 1998. NDT80 and the meiotic recombination checkpoint regulate expression of middle sporulation-specific genes in *Saccharomyces cerevisiae*. Molecular and Cellular Biology 18, 5750-5761.
Herskowitz, I., 1988. Life cycle of the budding yeast *Saccharomyces cerevisiae*. Microbiological Reviews 52, 536.
Herskowitz, I., Oshima, Y., 1981. Control of cell type in *Saccharomyces cerevisiae*: mating type and mating-type interconversion. Cold Spring Harbor Monograph Archive 11, 181-209.
Hill, A. V., 1910. The possible effects of the aggregation of the molecules of haemoglobin on its dissociation curves. The Journal of Physiology 40, 4-8.
Hodgkin, A. L., Huxley, A. F., 1952. A quantitative description of membrane current and its application to conduction and excitation in nerve. The Journal of Physiology 117, 500.
Holt, L. J., Hutti, J. E., Cantley, L. C., Morgan, D. O., 2007. Evolution of Ime2 phosphorylation sites on Cdk1 substrates provides a mechanism to limit the effects of the phosphatase Cdc14 in meiosis. Molecular Cell 25, 689-702, doi:10.1016/j.molcel.2007.02.012.
Hong, C., Lee, M., Kim, D., Kim, D., Cho, K.-H., Shin, I., 2012. A checkpoints capturing timing-robust Boolean model of the budding yeast cell cycle regulatory network. BMC Systems Biology 6, 129.
Honigberg, S. M., Purnapatre, K., 2003. Signal pathway integration in the switch from the mitotic cell cycle to meiosis in yeast. Journal of Cell Science 116, 2137, doi:10.1242/jcs.00460.
Hoops, S., Sahle, S., Gauges, R., Lee, C., Pahle, J., Simus, N., Singhal, M., Xu, L., Mendes, P., Kummer, U., 2006. COPASI—a complex pathway simulator. Bioinformatics 22, 3067-3074.
Huang, C.-Y., Ferrell, J. E., 1996. Ultrasensitivity in the mitogen-activated protein kinase cascade. Proceedings of the National Academy of Sciences 93, 10078-10083.
Jacob, F., Monod, J., 1961. Genetic regulatory mechanisms in the synthesis of proteins. Journal of Molecular Biology 3, 318-356.
Jeoung, D. I., Oehlen, L., Cross, F. R., 1998. Cln3-Associated Kinase Activity in *Saccharomyces cerevisiae* is Regulated by the Mating Factor Pathway. Molecular and Cellular Biology 18, 433-441.
Jørgensen, A., Nielsen, J. E., Almstrup, K., Toft, B. G., Petersen, B. L., Meyts, E. R. D., 2013. Dysregulation of the mitosis–meiosis switch in testicular carcinoma *in-situ.* The Journal of Pathology.
Kadosh, D., Struhl, K., 1997. Repression by Ume6 involves recruitment of a complex containing Sin3 corepressor and Rpd3 histone deacetylase to target promoters. Cell 89, 365-371.

Kahana, S., Pnueli, L., Kainth, P., Sassi, H. E., Andrews, B., Kassir, Y., 2010. Functional Dissection of IME1 Transcription Using Quantitative Promoter–Reporter Screening. Genetics 186, 829.
Kaizu, K., Ghosh, S., Matsuoka, Y., Moriya, H., Shimizu-Yoshida, Y., Kitano, H., 2010. A comprehensive molecular interaction map of the budding yeast cell cycle. Molecular Systems Biology 6.
Kassir, Y., Granot, D., Simchen, G., 1988. IME 1, a positive regulator gene of meiosis in *S. cerevisiae*. Cell 52, 853-862.
Kassir, Y., Adir, N., Boger-Nadjar, E., Raviv, N. G., Rubin-Bejerano, I., Sagee, S., Shenhar, G., 2003. Transcriptional regulation of meiosis in budding yeast. International Review of Cytology 224, 111-171, doi:10.1016/S0074-7696(05)24004-4.
Kasten, M. M., Dorland, S., Stillman, D. J., 1997. A large protein complex containing the yeast Sin3p and Rpd3p transcriptional regulators. Molecular and Cellular Biology 17, 4852.
Kavanagh, K., 2011. Fungi: Biology and Applications. Wiley.
Keizer, J., 1979. Nonequilibrium thermodynamics and the stability of states far from equilibrium. Accounts of Chemical Research 12, 243-249, doi:10.1021/ar50139a004.
Keizer, J., 1987. Statistical thermodynamics of nonequilibrium processes. Springer.
Kilfoil, M. L., Lasko, P., Abouheif, E., 2009. Stochastic variation: from single cells to superorganisms. HFSP Journal 3, 379-385.
Kimble, J., 2011. Molecular regulation of the mitosis/meiosis decision in multicellular organisms. Cold Spring Harbor Perspectives in Biology 3.
Kitano, H., 2001. Foundations of systems biology. MIT press Cambridge, MA.
Kitano, H., 2004. Biological robustness. Nature Reviews Genetics 5, 826-837.
Kitano, H., 2007. Towards a theory of biological robustness. Molecular Systems Biology 3.
Klipp, E., Herwig, R., Kowald, A., Wierling, C., Lehrach, H., 2008. Systems biology in practice: concepts, implementation and application. John Wiley & Sons.
Kominami, K., Sakata, Y., Sakai, M., Yamashita, I., 1993. Protein kinase activity associated with the IME2 gene product, a meiotic inducer in the yeast *Saccharomyces cerevisiae*. Bioscience, Biotechnology, and Biochemistry 57, 1731, doi:10.1271/bbb.57.1731.
Kristensen, A. R., Gsponer, J., Foster, L. J., 2013. Protein synthesis rate is the predominant regulator of protein expression during differentiation. Molecular Systems Biology 9.
Kulasiri, D., 2011. Computing molecular fluctuations in biochemical reaction systems based on a mechanistic, statistical theory of irreversible processes. Methods in Enzymology 487, 253.
Kulasiri, D., Nguyen, L. K., Samarasinghe, S., Xie, Z., 2008. A Review of Systems Biology Perspective on Genetic Regulatory Networks with Examples. Current Bioinformatics 3, 197-225.
Kurtz, S., Lindquist, S., 1984. Changing patterns of gene expression during sporulation in yeast. Proceedings of the National Academy of Sciences 81, 7323-7327.
Lackner, D. H., Bähler, J., 2008. Translational Control of Gene Expression: From Transcripts to Transcriptomes. International Review of Cell and Molecular Biology 271, 199-251.
Le Bouffant, R., Guerquin, M. J., Duquenne, C., Frydman, N., Coffigny, H., Rouiller-Fabre, V., Frydman, R., Habert, R., Livera, G., 2010. Meiosis initiation in the human ovary requires intrinsic retinoic acid synthesis. Human Reproduction 25, 2579-2590.
Leloup, J. C., Goldbeter, A., 1998. A model for circadian rhythms in Drosophila incorporating the formation of a complex between the PER and TIM proteins. Journal of Biological Rhythms 13, 70.
Levi, J., 1956. Mating reaction in yeast. Nature 177, 753-754.
Li, Y., Ray, D., Ye, P., 2013. Identification of germ cell-specific genes in mammalian meiotic prophase. BMC Bioinformatics 14, 1-13.

Li, Y., Lam, K.-s., Dasgupta, N., Ye, P., 2010. A yeast's eye view of mammalian reproduction: cross-species gene co-expression in meiotic prophase. BMC Systems Biology 4, 125.
Lodish, H., Berk, A., Kaiser, C., Krieger, M., Bretscher, A., Ploegh, H., Amon, A., Scott, M., 2013. Molecular cell biology. Macmillan, New York.
Lotka, A., 1924. Elements of physical biology: Reprinted (1956) as Elements of mathematical biology. Dover Publishers, New York.
Lu, C., Xu, M., Wang, Y., Qin, Y., Du, G., Wu, W., Han, X., Ji, C., Yang, Y., Gu, A., 2013. Genetic Variants in Meiotic Program Initiation Pathway Genes Are Associated with Spermatogenic Impairment in a Han Chinese Population. PloS ONE 8, e53443.
Lu, P., Vogel, C., Wang, R., Yao, X., Marcotte, E. M., 2006. Absolute protein expression profiling estimates the relative contributions of transcriptional and translational regulation. Nature Biotechnology 25, 117-124, doi:10.1038/nbt1270.
Maamar, H., Dubnau, D., 2005. Bistability in the Bacillus subtilis K-state (competence) system requires a positive feedback loop. Molecular Microbiology 56, 615-624, doi:10.1111/j.1365-2958.2005.04592.x.
Maamar, H., Raj, A., Dubnau, D., 2007. Noise in gene expression determines cell fate in Bacillus subtilis. Science 317, 526.
Mallavarapu, A., Thomson, M., Ullian, B., Gunawardena, J., 2009. Programming with models: modularity and abstraction provide powerful capabilities for systems biology. Journal of the Royal Society Interface 6, 257-270.
Manning, G., Plowman, G. D., Hunter, T., Sudarsanam, S., 2002. Evolution of protein kinase signaling from yeast to man. Trends in Biochemical Sciences 27, 514-520.
Mario, P., 2007. A brief history of SSA implementations.
Matsuura, A., Treinin, M., Mitsuzawa, H., Kassir, Y., Uno, I., Simchen, G., 1990. The adenylate cyclase/protein kinase cascade regulates entry into meiosis in *Saccharomyces cerevisiae* through the gene IME1. The EMBO Journal 9, 3225.
McCollum, J. M., Peterson, G. D., Cox, C. D., Simpson, M. L., Samatova, N. F., 2006. The sorting direct method for stochastic simulation of biochemical systems with varying reaction execution behavior. Computational Biology and Chemistry 30, 39-49.
McKay, M. D., Beckman, R. J., Conover, W. J., 1979. Comparison of three methods for selecting values of input variables in the analysis of output from a computer code. Technometrics 21, 239-245.
Mehta, P., Mukhopadhyay, R., Wingreen, N. S., 2008. Exponential sensitivity of noise-driven switching in genetic networks. Physical Biology 5, 026005, doi:10.1088/1478-3975/5/2/026005.
Mettetal, J. T., van Oudenaarden, A., 2007. Necessary noise. Science 317, 463.
Miller, M. E., Cross, F. R., 2001. Cyclin specificity: how many wheels do you need on a unicycle? Journal of Cell Science 114, 1811-1820.
Miller, M. E., Cross, F. R., Groeger, A. L., Jameson, K. L., 2005. Identification of novel and conserved functional and structural elements of the G1 cyclin Cln3 important for interactions with the CDK Cdc28 in *Saccharomyces cerevisiae*. Yeast 22, 1021-1036.
Mitchell, A. P., 1994. Control of meiotic gene expression in *Saccharomyces cerevisiae*. Microbiology and Molecular Biology Reviews 58, 56.
Morbidelli, M., Wu, H., 2005. Parametric sensitivity in chemical systems. Cambridge University Press.
Morgan, D., 2006. The Cell Cycle: Principles of Control (Primers in Biology Series).
Morgan, D. O., 1997. Cyclin-dependent kinases: engines, clocks, and microprocessors. Annual Review of Cell and Developmental Biology 13, 261-291.
Murray, J. D., 2002. Mathematical biology. Springer.
Nachman, I., Regev, A., Ramanathan, S., 2007. Dissecting Timing Variability in Yeast Meiosis. Cell 131, 544-556, doi:10.1016/j.cell.2007.09.044.

Naqib, F., Farah, C. A., Pack, C. C., Sossin, W. S., 2011. The rates of protein synthesis and degradation account for the differential response of neurons to spaced and massed training protocols. PLoS Computational Biology 7, e1002324.
Nevins, J. R., 2001. The Rb/E2F pathway and cancer. Human Molecular Genetics 10, 699.
Nguyen, L. K., 2009. Dynamical modelling of feedback gene regulatory networks. Vol. PhD. Lincoln University, New Zealand, Lincoln, New Zealand.
Nicolis, G., Prigogine, I., 1971. Fluctuations in nonequilibrium systems. Proceedings of the National Academy of Sciences 68, 2102.
Ninomiya-Tsuji, J., Nomoto, S., Yasuda, H., Reed, S. I., Matsumoto, K., 1991. Cloning of a human cDNA encoding a CDC2-related kinase by complementation of a budding yeast cdc28 mutation. Proceedings of the National Academy of Sciences 88, 9006-9010.
Noble, D., 2008. The music of life: biology beyond genes. Oxford University Press.
Novak, B., Tyson, J. J., 2004. A model for restriction point control of the mammalian cell cycle. Journal of Theoretical Biology 230, 563-579, doi:10.1016/j.jtbi.2004.04.039.
Novick, A., Weiner, M., 1957. Enzyme induction as an all-or-none phenomenon. Proceedings of the National Academy of Sciences of the United States of America 43, 553.
Nurse, P., 2000. A long twentieth century of the cell cycle and beyond. Cell 100, 71-78.
Onsager, L., Machlup, S., 1953. Fluctuations and irreversible processes. Physical Review 91, 1505-1512.
Pak, J., Segall, J., 2002. Regulation of the premiddle and middle phases of expression of the NDT80 gene during sporulation of *Saccharomyces cerevisiae*. Molecular and Cellular Biology 22, 6417-6429.
Palsson, B., 2006. Properties of Reconstructed Networks. Cambridge: Systems Biology.
Palsson, B. Ø., 2011. Systems biology: simulation of dynamic network states. Cambridge University Press.
Parviz, F., Heideman, W., 1998. Growth-Independent Regulation of CLN3 mRNA Levels by Nutrients in *Saccharomyces cerevisiae*. Journal of Bacteriology 180, 225-230.
Paulsson, J., 2004. Summing up the noise. Nature 427, 415–418.
Paulsson, J., 2005. Models of stochastic gene expression. Physics of Life Reviews 2, 157-175.
Pelechano, V., Chávez, S., Pérez-Ortín, J. E., 2010. A complete set of nascent transcription rates for yeast genes. PloS ONE 5, e15442.
Pierce, M., Benjamin, K. R., Montano, S. P., Georgiadis, M. M., Winter, E., Vershon, A. K., 2003. Sum1 and Ndt80 proteins compete for binding to middle sporulation element sequences that control meiotic gene expression. Molecular and Cellular Biology 23, 4814-4825.
Pnueli, L., Edry, I., Cohen, M., Kassir, Y., 2004. Glucose and nitrogen regulate the switch from histone deacetylation to acetylation for expression of early meiosis-specific genes in budding yeast. Molecular and Cellular Biology 24, 5197, doi:10.1128/MCB.24.12.5197-5208.2004
Pramila, T., Miles, S., GuhaThakurta, D., Jemiolo, D., Breeden, L. L., 2002. Conserved homeodomain proteins interact with MADS box protein Mcm1 to restrict ECB-dependent transcription to the M/G1 phase of the cell cycle. Genes & Development 16, 3034-3045, doi:10.1101/gad.1034302
Prigogine, I., 1978. Time, structure, and fluctuations. Science 201, 777.
Qian, H., 2006. Open-system nonequilibrium steady state: Statistical thermodynamics, fluctuations, and chemical oscillations. The Journal of Physical Chemistry B 110, 15063-15074.
Qian, H., 2007. Phosphorylation energy hypothesis: open chemical systems and their biological functions. Annual Review of Physical Chemistry 58, 113-142.
Qian, H., Qian, M., 2000. Pumped biochemical reactions, nonequilibrium circulation, and stochastic resonance. Physical Review Letters 84, 2271-2274.

Qian, H., Beard, D. A., 2005. Thermodynamics of stoichiometric biochemical networks in living systems far from equilibrium. Biophysical Chemistry 114, 213-220.
Qian, H., Reluga, T. C., 2005. Nonequilibrium thermodynamics and nonlinear kinetics in a cellular signaling switch. Physical Review Letters 94, 28101.
Qian, H., Saffarian, S., Elson, E. L., 2002. Concentration fluctuations in a mesoscopic oscillating chemical reaction system. Proceedings of the National Academy of Sciences of the United States of America 99, 10376.
Qian, H., Shi, P. Z., Xing, J., 2009. Stochastic bifurcation, slow fluctuations, and bistability as an origin of biochemical complexity. Physical Chemistry Chemical Physics 11, 4861-4870.
Qu, Z., MacLellan, W. R., Weiss, J. N., 2003. Dynamics of the cell cycle: checkpoints, sizers, and timers. Biophysical Journal 85, 3600-3611.
Rand, D. A., 2008. Mapping global sensitivity of cellular network dynamics: sensitivity heat maps and a global summation law. Journal of the Royal Society Interface 5, S59-S69.
Ray, D., Su, Y., Ye, P., 2013. Dynamic modeling of yeast meiotic initiation. BMC Systems Biology 7, 37.
Roeder, G. S., 1995. Sex and the single cell: meiosis in yeast. Proceedings of the National Academy of Sciences 92, 10450.
Rosenfeld, N., Young, J. W., Alon, U., Swain, P. S., Elowitz, M. B., 2005. Gene regulation at the single-cell level. Science 307, 1962, doi:10.1126/science.1106914.
Ross, J., Berry, R. S., 2008. Thermodynamics and fluctuations far from equilibrium. Springer Verlag.
Ross, J., Villaverde, A. F., 2010. Thermodynamics and Fluctuations Far From Equilibrium. Entropy 12, 2199-2243.
Rubinstein, A., Gurevich, V., Kasulin-Boneh, Z., Pnueli, L., Kassir, Y., Pinter, R. Y., 2007. Faithful modeling of transient expression and its application to elucidating negative feedback regulation. Proceedings of the National Academy of Sciences 104, 6241, doi:10.1073/pnas.0611168104
Sagee, S., Sherman, A., Shenhar, G., Robzyk, K., Ben-Doy, N., Simchen, G., Kassir, Y., 1998. Multiple and distinct activation and repression sequences mediate the regulated transcription of IME1, a transcriptional activator of meiosis-specific genes in *Saccharomyces cerevisiae*. Molecular and Cellular Biology 18, 1985.
Sánchez, I., Dynlacht, B. D., 2005. New insights into cyclins, CDKs, and cell cycle control. Vol. 16. Elsevier, pp. 311-321.
Sargsyan, K., 2005. Fluctuations in chemical reactions in a large volume. GFD Program Proceedings.
Schaechter, M., 2011. Eukaryotic Microbes. Academic Press.
Schindler, K., Winter, E., 2006. Phosphorylation of Ime2 regulates meiotic progression in *Saccharomyces cerevisiae*. Journal of Biological Chemistry 281, 18307.
Schindler, K., Benjamin, K. R., Martin, A., Boglioli, A., Herskowitz, I., Winter, E., 2003. The Cdk-activating kinase Cak1p promotes meiotic S phase through Ime2p. Molecular and Cellular Biology 23, 8718-8728, doi:10.1128/MCB.23.23.8718-8728.2003
Schlögl, F., 1972. Chemical reaction models for non-equilibrium phase transitions. Zeitschrift für Physik A Hadrons and Nuclei 253, 147-161.
Shefer-Vaida, M., Sherman, A., Ashkenazi, T., Robzyk, K., Kassir, Y., 1995. Positive and negative feedback loops affect the transcription of IME1, a positive regulator of meiosis in *Saccharomyces cerevisiae*. Developmental Genetics 16, 219-228, doi:10.1002/dvg.1020160302.
Shen, L., Chepelev, I., Liu, J., Wang, W., 2010. Prediction of quantitative phenotypes based on genetic networks: a case study in yeast sporulation. BMC Systems Biology 4, 128.

Shenhar, G., Kassir, Y., 2001. A positive regulator of mitosis, Sok2, functions as a negative regulator of meiosis in *Saccharomyces cerevisiae*. Molecular and Cellular Biology 21, 1603, doi:10.1128/MCB.21.5.1603-1612.2001.

Sherman, A., Shefer, M., Sagee, S., Kassir, Y., 1993. Post-transcriptional regulation of IME1 determines initiation of meiosis in *Saccharomyces cerevisiae*. Molecular and General Genetics MGG 237, 375-384, doi:10.1007/BF00279441

Shimizu, M., Li, W., Covitz, P. A., Hara, M., Shindo, H., Mitchell, A. P., 1998. Genomic footprinting of the yeast zinc finger protein Rme1p and its roles in repression of the meiotic activator IME1. Nucleic Acids Research 26, 2329-2336.

Shuster, E. O., Byers, B., 1989. Pachytene arrest and other meiotic effects of the start mutations in *Saccharomyces cerevisiae*. Genetics 123, 29-43.

Simchen, G., 2009. Commitment to meiosis: what determines the mode of division in budding yeast? BioEssays 31, 169-177, doi:10.1002/bies.200800124.

Smith, H. E., Mitchell, A. P., 1989. A transcriptional cascade governs entry into meiosis in *Saccharomyces cerevisiae*. Molecular and Cellular Biology 9, 2142-2152.

Smith, H. E., Su, S., Neigeborn, L., Driscoll, S. E., Mitchell, A., 1990. Role of IME1 expression in regulation of meiosis in *Saccharomyces cerevisiae*. Molecular and Cellular Biology 10, 6103-6113.

Stephens, M. A., 1970. Use of the Kolmogorov-Smirnov, Cramér-Von Mises and related statistics without extensive tables. Journal of the Royal Statistical Society. Series B (Methodological), 115-122.

Steven, J., 2009. The Knight Signet.

Strathern, J., Hicks, J., Herskowitz, I., 1981. Control of cell type in yeast by the mating type locus: The α1-α2 hypothesis. Journal of Molecular Biology 147, 357-372, doi:http://dx.doi.org/10.1016/0022-2836(81)90488-5.

Strogatz, S. H., 2001. Nonlinear dynamics and chaos: with applications to physics, biology, chemistry, and engineering (studies in nonlinearity). Westview Press.

Süel, G. M., Garcia-Ojalvo, J., Liberman, L. M., Elowitz, M. B., 2006. An excitable gene regulatory circuit induces transient cellular differentiation. Nature 440, 545-550, doi:10.1038/nature04588.

Swat, M., Kel, A., Herzel, H., 2004. Bifurcation analysis of the regulatory modules of the mammalian G1/S transition. Bioinformatics 20, 1506.

Szwarcwort-Cohen, M., Kasulin-Boneh, Z., Sagee, S., Kassir, Y., 2009. Human Cdk2 is a functional homolog of budding yeast Ime2, the meiosis-specific Cdk-like kinase. Cell Cycle 8, 647-654.

Szwarcwort-Cohen, M., Gurevich, V., Sagee, S., Kassir, Y., 2010. Ectopic expression of human Cdk2 and its yeast homolog, Ime2, is deleterious to *Saccharomyces cerevisiae*. Cell Cycle 9, 4711-4719, doi:10.4161/cc.9.23.14088.

Thron, C. D., 1997. Bistable biochemical switching and the control of the events of the cell cycle. Oncogene 15, 317.

Tóth, A., Queralt, E., Uhlmann, F., Novák, B., 2007. Mitotic exit in two dimensions. Journal of Theoretical Biology 248, 560-573, doi:10.1016/j.jtbi.2007.06.014

Toth Attila, N. B., Csikasz-Nagy Attila, 2004. Modelling the regulation of the transition between mitosis and meiosis of fission yeast Department of Applied Biotechnology and Food Science, Vol. PhD. Budapest University of Technology and Economics, Hungary.

Tuck, C., Zhang, T., Potapova, T., Malumbres, M., Novák, B., 2013. Robust mitotic entry is ensured by a latching switch. Biology Open 2, 924-931.

Tyson, J. J., 2007. Bringing cartoons to life. Nature 445, 823-823.

Tyson, J. J., Novak, B., 2008. Temporal organization of the cell cycle. Current Biology 18, R759-R768.

Tyson, J. J., Albert, R., Goldbeter, A., Ruoff, P., Sible, J., 2008. Biological switches and clocks. Journal of The Royal Society Interface 5, S1-S8.
Tyson, J. J., Baumann, W. T., Chen, C., Verdugo, A., Tavassoly, I., Wang, Y., Weiner, L. M., Clarke, R., 2011. Dynamic modelling of oestrogen signalling and cell fate in breast cancer cells. Nature Reviews Cancer 11, 523-532.
Ullah, M., Wolkenhauer, O., 2010. Stochastic approaches in systems biology. Wiley Interdisciplinary Reviews: Systems Biology and Medicine 2, 385-397.
Umbarger, H. E., 1961. Feedback control by endproduct inhibition. Cold Spring Harbor Symposia on Quantitative Biology, Vol. 26. Cold Spring Harbor Laboratory Press, pp. 301-312.
van Oudenaarden, A., Pedraza, J. M., 2005. Signal and noise propagation in genetic circuits. Massachusetts Institute of Technology.
Vellela, M., Qian, H., 2009. Stochastic dynamics and non-equilibrium thermodynamics of a bistable chemical system: the Schlögl model revisited. Journal of the Royal Society Interface 6, 925.
Venkatesh, S., Workman, J. L., 2012. Non-coding transcription SETs up regulation. Cell Research.
Verdugo, A., Vinod, P. K., Tyson, J. J., Novak, B., 2013. Molecular mechanisms creating bistable switches at cell cycle.
Vershon, A. K., Pierce, M., 2000. Transcriptional regulation of meiosis in yeast. Current Opinion in Cell Biology 12, 334-339, doi:10.1016/S0955-0674(00)00104-6.
Vidan, S., Mitchell, A. P., 1997. Stimulation of yeast meiotic gene expression by the glucose-repressible protein kinase Rim15p. Molecular and Cellular Biology 17, 2688-2697.
Vinod, P. K., Freire, P., Rattani, A., Ciliberto, A., Uhlmann, F., Novak, B., 2011. Computational modelling of mitotic exit in budding yeast: the role of separase and Cdc14 endocycles. Journal of the Royal Society Interface 8, 1128-1141, doi:10.1098/rsif.2010.0649
Voet, D., Voet, J. G., Pratt, C. W., 2006. Fundamentals of biochemistry: life at the molecular level. John Wiley & Sons, NewYork, 99-100.
Volterra, V., Brelot, M., 1931. Leçons sur la théorie mathématique de la lutte pour la vie. Gauthier-Villars Paris.
Walhout, M., Vidal, M., Dekker, J., 2012. Handbook of Systems Biology: Concepts and Insights. Academic Press.
Wannige, C., Kulasiri, D., Samarasinghe, S., 2014. A Nutrient Dependant Switch Explains Mutually Exclusive Existence of Meiosis and Mitosis Initiation in Budding Yeast. Journal of Theoretical Biology.
Wannige, T., Kulasiri, D., Samarasinghe, S., 2013. Modelling Stochasticity in Multi-stable and Oscillatory Biological Networks far from Equilibrium. In: WenJun, Z., (Ed.), Network Biology: Theories, Methods and Applications. Nova publishers, pp. 163-193.
Wiener, N., 1948. Cybernetics; or control and communication in the animal and the machine. John Wiley, Oxford, England.
Winter, E., 2012. The Sum1/Ndt80 Transcriptional Switch and Commitment to Meiosis in *Saccharomyces cerevisiae*. Microbiology and Molecular Biology Reviews 76, 1-15, doi:10.1128/MMBR.05010-11
Wolf, D. M., Arkin, A. P., 2003. Motifs, modules and games in bacteria. Current Opinion in Microbiology 6, 125-134, doi:http://dx.doi.org/10.1016/S1369-5274(03)00033-X.
Xie, J., Pierce, M., Gailus-Durner, V., Wagner, M., Winter, E., Vershon, A. K., 1999. Sum1 and Hst1 repress middle sporulation-specific gene expression during mitosis in *Saccharomyces cerevisiae*. The EMBO Journal 18, 6448-6454.
Xie, Z., Kulasiri, D., Samarasinghe, S., Qian, J., 2010. An unbiased sensitivity analysis reveals important parameters controlling periodicity of circadian clock. Biotechnology and Bioengineering 105, 250-259, doi:10.1002/bit.22540.

Xu, L., Ajimura, M., Padmore, R., Klein, C., Kleckner, N., 1995. NDT80, a meiosis-specific gene required for exit from pachytene in *Saccharomyces cerevisiae*. Molecular and Cellular Biology 15, 6572-6581.

Yaglom, J., Linskens, M., Sadis, S., Rubin, D. M., Futcher, B., Finley, D., 1995. p34Cdc28-mediated control of Cln3 cyclin degradation. Molecular and Cellular Biology 15, 731-741.

Yao, G., Lee, T. J., Mori, S., Nevins, J. R., You, L., 2008. A bistable Rb–E2F switch underlies the restriction point. Nature Cell Biology 10, 476-482.

Yao, G., Tan, C., West, M., Nevins, J. R., You, L., 2011. Origin of bistability underlying mammalian cell cycle entry. Molecular Systems Biology 7.

Yi, T.-M., Huang, Y., Simon, M. I., Doyle, J., 2000. Robust perfect adaptation in bacterial chemotaxis through integral feedback control. Proceedings of the National Academy of Sciences 97, 4649-4653.

Zi, Z., Liebermeister, W., Klipp, E., 2010. A quantitative study of the Hog1 MAPK response to fluctuating osmotic stress in *Saccharomyces cerevisiae*. PloS ONE 5, e9522, doi:10.1371/journal.pone.0009522.